DOCTORAL THESIS

Land-Ocean Interactions in Arctic Coastal Waters: Ocean Colour Remote Sensing and Current Carbon Fluxes to the Arctic Ocean

DISSERTATION

zur Erlangung des akademischen Grades
eines Doktors der Naturwissenschaften
am Fachbereich für Geowissenschaften
der Freien Universität Berlin

vorgelegt von

Bennet Juhls

Berlin, 2020

Erstgutachter: Prof. Dr. Jürgen Fischer

Zweitgutachter: Prof. Dr. Guido Grosse

Tag der Disputation: December 18, 2020

Bennet Juhls

Land-Ocean Interactions in Arctic Coastal Waters: Ocean Colour Remote Sensing and Current Carbon Fluxes to the Arctic Ocean

Dissertation, 31.07.2020

Freie Universität Berlin

Institute for Space Sciences

Department of Earth Sciences

Carl-Heinrich-Becker-Weg 6-10

12165 Berlin

Selbstständigkeitserklärung

Hiermit erkläre ich an Eides statt, dass ich die vorliegende Arbeit selbstständig und ohne fremde Hilfe angefertigt, keine anderen als die angegebenen Quellen und Hilfsmittel benutzt und die den benutzen Quellen wörtlich oder inhaltlich entnommenen Stellen als solche kenntlich gemacht habe. Diese Arbeit hat in gleicher oder ähnlicher Form noch keiner Prüfungsbehörde vorgelegen.

Berlin, den 31. Juli 2020 _____

Bennet Juhls

Erklärung zu inhaltlichen Beiträgen der Co-Autoren an verschiedenen Publikationen innerhalb der kumulativen Dissertation

Alle folgend gelisteten Publikationen, die Teil dieser kumulativen Dissertation sind, enthalten Beiträge von Co-Autoren. Insgesamt wurde für die Konzeption, Durchführung und Berichtsabfassung qualitativ und quantitativ der Großteil von mir beigetragen.

Juhls, B., Stedmon, C. A., Morgenstern, A., Meyer, H., Hölemann, J., Heim, B., Povazhnyi, V., and Overduin, P. P. (2020). Identifying Drivers of Seasonality in Lena River Biogeochemistry and Dissolved Organic Matter Fluxes. ***Frontiers in Environmental Science, 8, 53.***

Das Monitoring Programm, welches die Grundlage dieser Studie ist, wurde ausschlaggebend von mir initiiert und betreut. Die Idee für die Arbeit stammt von mir und ich schrieb das Manuskript. Dr. Pier Paul Overduin unterstützte die Konzeption der Studie und half zusammen mit den anderen Co-Autoren bei der Finalisierung des Manuskripts mittels kritischer Anmerkungen und Kommentaren. Prof. Jürgen Fischer stellte notwendige Rechen-Ressourcen bereit. Probennahmen und Probenanalysen wurden ebenfalls teilweise von mir durchgeführt. Die aufwendige Logistik hinter dem Monitoring Programm wurde durch mich, Dr. Anne Morgenstern und Dr. Pier Paul Overduin geleistet.

Juhls, B., Overduin, P. P., Hölemann, J., Hieronymi, M., Matsuoka, A., Heim, B., and Fischer, J. (2019). Dissolved organic matter at the fluvial–marine transition in the Laptev Sea using in situ data and ocean colour remote sensing. ***Biogeosciences, 16, 2693-2713.***

Die Idee dieser Arbeit stammt von mir. Die Studie wurde von mir mit Zuhilfe von Dr. Pier Paul Overduin, Dr. Birgit Heim und Prof. Jürgen Fischer konzipiert. Ich verfasste das Manuskript und alle Co-Autoren trugen mittels Vorschlägen und Kommentaren zur Verbesserung des Manuskripts bei. Probennahmen wurden vor und während der Bearbeitungszeit dieser Arbeit zu einem Großteil von mir im Verbund mit vielen weiteren Expeditionsteilnehmern geleistet.

Juhls B., Matsuoka, A., Lizotte, M., Bécu, G., Devred, E., Doxaran, D., El Kassar, J. R., Ferland, J., Forget, M. H., Hilborn, A., Maury, J., Overduin, P. P., Oziel, L., Babin, M. (in preparation) Seasonal dynamics of dissolved organic matter in the Mackenzie Delta, Canadian Arctic waters: implications for ocean colour remote sensing.

Diese Studie wurde von mir, zusammen mit Dr. Atsushi Matusoka und Dr. Pier Paul Overduin konzipiert. Das Manuskript wurde ausschließlich von mir verfasst. Alle Co-Autoren haben durch Diskussionen, Kommentare und Vorschläge zu dem Manuskript beigetragen. Probennahmen und Analysen wurden durch ein großes Team geleistet, an dem ich jedoch einen großen Anteil habe (Teilnahme an drei von vier Expeditionen, sowie umfangreiche logistische Zuarbeit). Prozessierungen von Satellitendaten wurden durch Dr. Atsushi Matsuoka, Jan Riad El Kassar und Dr. Martin Hieronymi unterstützt. Prof. Jürgen Fischer stellte notwendige Rechen-Ressourcen für die Datenanalyse dieser Arbeit bereit.

Berlin, den 31. Juli 2020 _____

Bennet Juhls

Abstract

Arctic rivers carry about 40 Tg of organic carbon per year into the Arctic Ocean, enough to change the colour of the surface water over entire shelf seas. Ongoing permafrost thaw mobilizes ancient organic matter in the Arctic Ocean's watershed and, in particular, organic carbon that was previously preserved in the perennially frozen soils. Whereas the particulate fraction of organic matter is prone to settling and subsequent burial, the dissolved fraction of organic matter (DOM) can be transported over large distances and is quickly integrated and cycled within the aquatic environment. Therefore, monitoring of DOM and its carbon (DOC) in terms of fluxes, quality, transport routes and ultimate fate in the Arctic Ocean, is one of the goals of current polar research. In situ observations in the Arctic are challenging and costly and hold tremendous scientific value. Ocean Colour Remote Sensing (OCRS) is a powerful tool that can complement in situ observations by providing frequent and synoptic estimates of surface water DOM and DOC concentration via the coloured fraction of DOM (CDOM). However, use of OCRS in Arctic organic-rich waters is hampered by uncertainties and needs further evaluation and development. The goal of this thesis is to advance our knowledge of the quantity, origin, seasonal variability and fate of DOM and carbon transported from land to sea in the Arctic. Biogeochemical and bio-optical parameters of water across the fluvial and marine zones in two Arctic regions were collected. These in situ datasets include: 1) Lena River DOM measured at least bi-weekly for one full year, 2) Lena River and Laptev Sea Shelf DOM and optical parameters measured intermittently over 11 years and 3) a suite of water column optical, radiometric, and biogeochemical measurements from spring to fall in the Mackenzie River Delta and on the Beaufort Sea Shelf. These data are a unique and novel resource for testing OCRS atmospheric correction and CDOM retrieval algorithms and for improving satellite-derived DOC estimates across the fluvial-marine transition zone. Frequent monitoring of the Lena River revealed that three source water types determine the strong seasonality of fluvial DOM: 1) melt water, 2) rain water and 3) subsurface water. The improved estimation of annual Lena River DOC flux was 6.79 Tg C, most of which (84%) was transported into the Lena River by melt and rain water. Optical properties of the DOM indicated that, in spring, the Lena River dominantly transports young carbon originating from degrading vegetation from land surfaces. With rising air temperatures in summer and fall, optical properties indicated an increasing fraction of older DOM originating from

deeper soil horizons and thawing permafrost deposits. Salinity and DOM were strongly correlated (r^2>0.8) in both shelf regions, indicating a dominant terrigenous source of DOM and a conservative mixing of DOM-rich river water with DOM-poor water from the Arctic Ocean. Both in situ and space-borne observations of surface waters revealed a strong seasonal variability of river plume propagation and DOC distribution on both shelves. The evaluation of several OCRS algorithms with in situ data showed that the OLCI (Ocean and Land Colour Instrument) neural network swarm (ONNS) algorithm performed best for the retrieval of CDOM in the Lena – Laptev Sea region (r^2=0.72, mean percentage error=58.4%), whereas the semi-analytical algorithm "gsmA" performed best in the Mackenzie – Beaufort Sea region (r^2=0.52, mean percentage error=24.1%). Furthermore, the Polymer atmospheric correction algorithm resulted in better match-up correlations than either the WFR or the C2RCC atmospheric corrections. For both regions, new DOC – CDOM models, based on the in situ observations, expand the applicability of OCRS to monitor DOC in surface waters to the entire fluvial-marine transition zone and improve the accuracy of DOC retrieval. Overall, the studies of this thesis demonstrated the capability of OCRS to monitor the propagation and distribution of DOM on Arctic shelves on large spatial and temporal scales. In the future, high frequency sampling in combination with OCRS of major Arctic rivers have the potential to improve quantification of DOC export into the Arctic Ocean and reduce current uncertainties due to the lack of data. Long-term OCRS time series merged from multiple satellites can help in identifying trends of land-sea carbon fluxes and their impact on the global carbon cycle and climate in a rapidly changing Arctic.

Zusammenfassung

Arktische Flüsse exportieren etwa 40 Tg organischen Kohlenstoff pro Jahr in den Arktischen Ozean - genug um die Farbe des Oberflächenwassers über ganze Schelfmeere zu verändern. Das durch den Klimawandel verstärkte Auftauen der Permafrostböden mobilisiert altes organisches Material, insbesondere organischen Kohlestoff, der zuvor im durchgehend gefrorenen Boden konserviert wurde. Während der partikuläre Teil der organischen Stoffe schnell absinkt und sedimentiert, kann der gelöste Teil der organischen Stoffe (dissolved organic matter - DOM) über große Entfernungen transportiert und schnell in das aquatische System integriert und umgesetzt werden. Daher ist die Bestimmung der Exportmengen und der Qualität des DOM und des gelösten organischen Kohlenstoffes (dissolved organic carbon - DOC), sowie deren Transportwege und endgültigen Schicksal, ein zentrales Ziel der aktuellen Polarforschung. Auch wenn in situ Beobachtungen in der Arktis mit enormen Herausforderungen und Kosten verbunden sind, haben sie einen enormen wissenschaftlichen Wert. Die Fernerkundung der Ozeanfarbe (Ocean Colour Remote Sensing - OCRS) ist ein leistungsstarkes wissenschaftliches Werkzeug, das in situ Beobachtungen ergänzen kann, indem es häufige und synoptische Abschätzungen der DOM- und DOC-Konzentrationen des Oberflächenwassers liefert. Für diese Abschätzung wird der färbende Anteil von DOM (coloured dissolved organic matter - CDOM) verwendet, der einen Proxy für DOC darstellt. Die Verwendung von OCRS in arktischen, organikreichen und optisch komplexen Gewässern birgt jedoch große Unsicherheiten und muss daher zunächst evaluiert und weiterentwickelt werden. Das Ziel dieser Arbeit ist es, unser Wissen über die Menge, Herkunft, saisonale Variabilität und den Verbleib von DOM und DOC, welche vom Land zum Meer transportiert werden, zu erweitern. Dazu wurden große in situ Datensätze mit biogeochemischen und biooptischen Parametern in der Übergangszone von Fluss- zu Meerwasser in zwei Flüssen, der Lena und dem Mackenzie, gesammelt. Diese Datensätze umfassen: 1) DOM Messungen in der Lena mindestens zweimal pro Woche über ein gesamtes Jahr; 2) DOM und biooptische Messungen in der Lena und auf dem Laptewsee Schelf von Expeditionen von 11 Jahren; sowie 3) eine Reihe an optischen, radiometrischen und biogeochemischen Messungen von Frühling bis Herbst in den Küstengewässern der Beaufortsee nördlich des Mackenzie Deltas. Diese Daten sind eine einzigartige und neuartige Ressource zum Testen von OCRS-Algorithmen für die Atmosphärenkorrektur und zur satelliten-basierenden Abschätzung von CDOM. Die regelmäßige und hochfrequentierte Beprobung des Lena-Wassers ergab, dass die

Abwechslung von drei Wassertypen die starke Saisonalität der DOM Konzentration und den Export bestimmen: 1) Schmelzwasser, 2) Regenwasser, und 3) Grundwasser. Die verbesserte Abschätzung des jährlichen DOC Exportes der Lena wurde auf 6.79 Tg C geschätzt, von denen ein Großteil (84%) durch Schmelz- und Regenwasser in die Lena transportiert wurde. Die optischen Eigenschaften des DOM zeigten, dass die Lena im Frühjahr vorwiegend jungen organischen Kohlenstoff transportiert, der aus dem Abbau von Oberflächenvegetation stammt. Bei höheren Lufttemperaturen im Sommer und Herbst zeigte sich hingegen ein zunehmender Anteil von älterem DOM, der aus tieferen Bodenhorizonten und auftauenden Permafrostböden stammen könnte. Die Salinität und die DOM-Konzentration waren in beiden Schelfregionen stark korreliert ($r^2>0.8$), was auf eine dominante terrigene DOM-Quelle und eine konservative Mischung von DOM-reichem Flusswasser mit niedrig-DOM Wasser aus dem Arktischen Ozean hindeutet. Sowohl in situ als auch satellitengestützte Beobachtungen von Oberflächenwasser zeigten eine starke saisonale Variabilität der Flusswasserausbreitung und der DOC-Verteilung auf beiden Schelfmeeren. Die Auswertung mehrerer OCRS-Algorithmen mithilfe von in situ Daten zeigten, dass der „ONNS“ (OLCI (Ocean and Land Colour Instrument) neural network swarm) Algorithmus für die Abschätzung von CDOM in der Lena – Laptewsee Region am besten geeignet ist ($r^2=0.72$, mittlerer prozentualer Fehler: 58.4%), während in der Mackenzie – Beaufortsee Region der semi-analytische Algorithmus „gsmA“ am besten abschneidet ($r^2=0.52$, mittlerer prozentualer Fehler=24.1%). Darüber hinaus führt die Polymer Atmosphärenkorrektur zu besseren Übereinstimmungskorrelationen als die „WFR“ oder die „C2RCC“ Atmosphärenkorrektur. Für beide Regionen erweitern neue DOC-CDOM Modelle, die auf in situ Beobachtungen basieren, die Anwendbarkeit von OCRS zur Langzeituntersuchung von DOC in Oberflächenwasser über die gesamte Übergangszone vom Fluss- zum Meerwasser. Zudem wurde die Genauigkeit der satelliten-basierenden Abschätzungen der DOC-Konzentration deutlich gesteigert. Insgesamt haben die Studien dieser Arbeit gezeigt, dass OCRS die Ausbreitung und Verteilung von DOM in arktischen Schelfmeeren auf großen räumlichen und zeitlichen Skalen verfolgen kann. In Zukunft können hochfrequentierte Probennahmen in Kombination mit OCRS die Quantifizierung des DOC-Exports in den Arktischen Ozean verbessern und die aktuellen Unsicherheiten aufgrund fehlender Daten verringern. Langzeit-OCRS Zeitreihen, die durch Zusammenführung der Daten mehrerer Satelliten entstehen, können dazu beitragen, Veränderungen der Kohlenstoffflüsse und ihre Auswirkungen auf den globalen

Kohlenstoffkreislauf und das Klima in einer sich schnell verändernden Arktis zu identifizieren.

Table of Contents

List of Figures

List of Tables

List of Abbreviations

AC	Atmospheric correction
AOPs	Apparent optical properties
ArcticGRO	Arctic Great Rivers Observatory
C2RCC	Case 2 Regional CoastColour
C2X	Case 2 extreme
CDOM	Coloured dissolved organic matter
CTD	Conductivity-Temperature-Depth probe
DOC	Dissolved organic carbon
DOM	Dissolved organic matter
EAO	Eastern Arctic Ocean
EC	Electrical conductivity
FDOM	Fluorescent dissolved organic matter
FUB/WEW	Freie Univsersität Berlin, Insitut für Weltraumwissenschaften
GSM	Garver, Siegel, Maritorena model
gsmA	Garver, Siegel, Maritorena model for the Arctic
IOPs	Inherent optical properties
MERIS	Medium Resolution Imaging Spectrometer
MODIS	Moderate-resolution Imaging Spectroradiometer
MPE	Mean percentage error
NAP	Non-algal particles
NCEP	National Centers for Environmental Prediction
NIR	Near infrared spectrum
NN	Neural network
OCRS	Ocean Colour Remote Sensing
OLCI	Ocean and Land Colour Instrument
OM	Organic matter
ONNS	OLCI Neural Network Swarm
PARTNERS	Pan-Arctic River Transport of Nutrients, Organic Matter, and Suspended Sediments
POC	Particulate organic carbon
QSSA	Quasi-Single-Scattering Approximation
RMSE	Root mean square error
SUVA	Specific ultraviolet absorbance
TOA	Top of atmosphere
TSM	Total suspended sediment
VIS	Visible wavelengths spectrum
WAO	Western Arctic Ocean

List of Publications

Table 1.1: Publication Summary.

	Publication
Chapter 3 (published)	Juhls, B., Stedmon, C. A., Morgenstern, A., Meyer, H., Hölemann, J., Heim, B., ... & Overduin, P. P. (2020). Identifying Drivers of Seasonality in Lena River Biogeochemistry and Dissolved Organic Matter Fluxes. Frontiers in Environmental Science, 8, 53. https://doi.org/10.3389/fenvs.2020.00053
Chapter 4 (published)	Juhls, B., Overduin, P. P., Hölemann, J., Hieronymi, M., Matsuoka, A., Heim, B., & Fischer, J. (2019). Dissolved organic matter at the fluvial–marine transition in the Laptev Sea using in situ data and ocean colour remote sensing. Biogeosciences, 16, 2693-2713. https://doi.org/10.5194/bg-16-2693-2019
Chapter 5 (in preparation)	Juhls B., Matsuoka, A., Lizotte, M., Bécu, G., Devred, E., Doxaran, D.,El Kassar, J. R., Ferland, J., Forget, M. H., Hilborn, A., Maury, J., Overduin, P. P., Oziel, L., Babin, M. Seasonal dynamics of dissolved organic matter of the Mackenzie Delta, Canadian Arctic waters: implications for ocean colour remote sensing
Complementary (in review)	Bussmann, I., Fedorova, I., Juhls, B., Overduin, P. P., and Winkel, M.: Seasonal methane dynamics in three different Siberian water bodies, Biogeosciences Discuss., https://doi.org/10.5194/bg-2020-106, in review, 2020.
Complementary (published)	Coch, C., Juhls, B., Lamoureux, S., Lafrenière, M., Fritz, M., Heim, B., & Lantuit, H. (2019). Comparisons of dissolved organic matter and its optical characteristics in small low and high Arctic catchments. Biogeosciences, 16, 4535-4553.
Complementary (published)	Heim, B., Juhls, B., Abramova, E., Bracher, A., Doerffer, R., Gonçalves-Araujo, R., ... & Overduin, P. (2019). Ocean colour remote sensing in the Laptev Sea. In Remote Sensing of the Asian Seas (pp. 123-138). Springer, Cham.
Complementary (published)	Kohnert, K., Juhls, B., Muster, S., Antonova, S., Serafimovich, A., Metzger, S., ... & Sachs, T. (2018). Toward understanding the contribution of waterbodies to the methane emissions of a permafrost landscape on a regional scale—A case study from the Mackenzie Delta, Canada. Global change biology, 24(9), 3976-3989.
Complementary (published)	Overduin, P. P., Schneider von Deimling, T., Miesner, F., Grigoriev, M. N., Ruppel, C., Vasiliev, A., Lantuit, H., Juhls, B., Westermann, S. (2019). Submarine Permafrost Map in the Arctic Modeled Using 1-D Transient Heat Flux (SuPerMAP). Journal of Geophysical Research: Oceans, 124(6), 3490-3507.
Complementary (in preparation)	Hölemann, J., Juhls, B., Bauch, D., Koch, B., Janout, M., Heim, B. (in preparation) The importance of fast ice formation and melt for the distribution of terrestrial derived dissolved organic matter in Siberian Arctic shelf seas
Complementary (in preparation)	Fritz, M., Gonçalves-Araujo, R., Juhls, B., Tanski, G., Heim, B., Koch, B., Foerster, S., Lantuit, H. (in preparation) Collapsing permafrost coasts as source of dissolved organic matter to Arctic coastal waters

Chapter I

Introduction

1 Introduction

1.1 Scientific motivation

The climate is warming in the Arctic and sea ice cover is shrinking in Arctic coastal and shelf regions (Farquharson et al., 2018; Chan et al., 2019). Geochemical and biological interactions between ocean and land drive the carbon cycle in these regions. On land, permafrost temperatures are rising (Biskaborn et al., 2019) and permafrost is consequently thawing, a process that is expected to mobilize ancient frozen carbon (Frey and Smith, 2005; Frey and McClelland, 2009; McGuire et al., 2009). Additionally, terrestrial biological productivity is currently increasing in Arctic river catchments as a response to climate warming (Gorham, 1991). This can lead to a growing accumulation of organic carbon in plants, part of which, after decomposition, drains into the Arctic Ocean. Increasing export of organic carbon into the Arctic Ocean changes the carbon cycle, which may exacerbate global climate warming through the release of greenhouse gases into the atmosphere. To improve future climate forecast scenarios, numerous recent studies focus on the sources, budget and fate of organic carbon in the Arctic (e.g. Kaiser et al., 2017; Vonk et al., 2019). The fate of organic carbon, once it is released to the Arctic estuarine and coastal waters (those waters that are directly influenced by riverine input, coastal erosion or resuspension in shallow waters), in particular, is intensely debated (Bauer et al., 2013; Fichot and Benner, 2014; Bröder et al., 2018). While the burial of organic carbon in the seafloor sediments can act as a carbon sink, the degradation of organic carbon in the water columns and its partially conversion to CO_2 is potentially a large source of carbon release to the atmosphere (Alling et al., 2010). More organic carbon in the Arctic Ocean may also shift the air-sea carbon equilibrium towards an increased CO_2 uptake by the atmosphere, causing a positive feedback loop to climate warming. Another positive feedback is the enhanced absorption of sunlight caused by increasing concentrations of dark organic matter in ocean surface water. Absorption by this organic matter intensifies radiative heating of the surface waters (Soppa et al., 2019), and therefore sea ice melt (Hill, 2008), and potentially leads to a warming of the seabed near the coast (Dmitrenko et al., 2011).

Unprecedented changes are currently underway in the Arctic that have the potential to affect the global climate system. Therefore, this thesis focuses on the current carbon transfer interactions between land and ocean in the Arctic.

1.1.1 Impact of climate warming on the Arctic

Air temperature in the Arctic is rising twice as fast as the global mean temperature (Polyakov et al., 2002; Serreze and Barry, 2011). The Arctic Ocean, its coastlines and the catchments of the rivers that drain into it, are currently experiencing drastic changes. Satellite data has revealed a dramatic and ongoing decrease in sea ice extent and thickness during the last two decades (Screen and Francis, 2016; Stroeve and Notz, 2018). It is expected that the Arctic Ocean will become completely ice-free in summer within the next few decades (Wang and Overland, 2009, 2012). Ice is thinning most rapidly near the coast and winter landfast sea ice protects the coastline from erosion for shorter and shorter periods (Overeem et al., 2011; Günther et al., 2013).

In Arctic rivers, ice thickness is also decreasing (Pavelsky and Zarnetske, 2017) and the open water periods are lengthening due to earlier ice break-up and later freeze-up (Shiklomanov and Lammers, 2014; Park et al., 2016). Over the last decades, water discharge from all Arctic rivers has increased, and most drastically for the Siberian rivers (Peterson, 2002; McClelland et al., 2006; Serreze et al., 2006) (**Figure 1.1**). These changes affect the seasonality of the river discharge and the Arctic freshwater cycle (Rawlins et al., 2010). Increasing export of freshwater can influence water mass stratification and circulation in the Arctic Ocean (Carmack and Aagaard, 1973; Clarke and Gascard, 1983; Peterson et al., 2006).

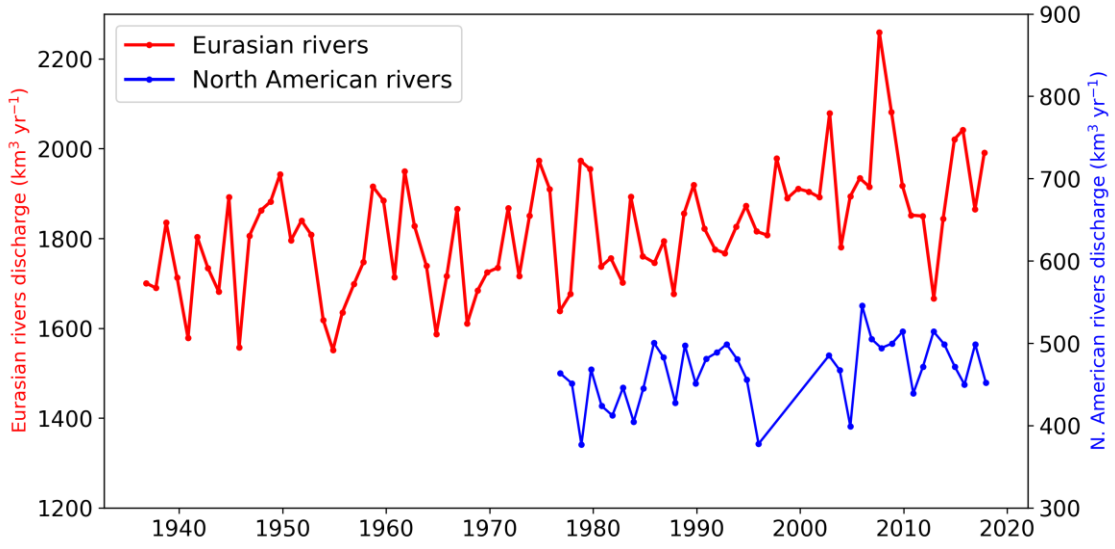

Figure 1.1: Long-term records of the annual discharge of large Eurasian and North American rivers flowing into the Arctic Ocean (data from Holmes et al. (2018c).

1.1.2 Dissolved organic matter from land to the Arctic Ocean: sources, fluxes and fate

Export of dissolved organic matter (DOM) and carbon (DOC) into the Arctic Ocean inevitably increases with increasing river discharge. The mobilization of DOC from degrading permafrost (Vonk et al., 2012; Dubinenkov et al., 2015) and the release of DOC by coastal erosion (Tanski et al., 2016, 2017) modify the cycling of carbon in ways that remain unknown and unquantified in the Arctic (MacGilchrist et al., 2014). Therefore, monitoring fluxes of organic matter from land to sea and understanding the fate of DOM after it is released into the Arctic Ocean have recently become a particular focus of research interest.

River discharge, its chemical composition and constituent concentrations, at any point in space and time, integrate environmental processes over a definable upstream area of the river watershed (Holmes et al., 2012a). Therefore, biogeochemical parameters of the river water are powerful indicators of the impacts of climate change. In 2002, a sampling program "Pan-Arctic River Transport of Nutrients, Organic Matter, and Suspended Sediments" (PARTNERS) was established to monitor fluvial matter fluxes to the Arctic Ocean. Its successor, the "Arctic Great Rivers Observatory" (ArcticGRO), continues the pan-Arctic sampling of the largest Arctic rivers. These sampling programs resulted in the first estimates of organic matter fluxes into the Arctic Ocean (Raymond et al., 2007; Stedmon et al., 2011; Holmes et al., 2012b; Wild et al., 2019). However, these estimates are typically based on a few (<10) samples per year. To compensate for periods without samples, load models are used to calculate annual fluxes. These load models assume a direct dependency of organic matter (OM) concentration on the discharge, which gauge stations provide on a daily basis. Changes to fluxes may be smaller than the errors that are generated using such assumed relationships between concentration and discharge. Thus, an accurate baseline is needed to observe flux changes in Arctic rivers.

Studies of the fate of DOM after it enters the Arctic Ocean are even scarcer than those focusing on its export to the ocean. Little is known about the transport pathways in shelf waters, or about the export and removal of the terrestrial organic matter in the Arctic Ocean. How these processes may be shifting with climate change is also uncertain (Morison et al., 2012; Fichot et al., 2013). While some studies report rapid and extensive removal of up to 70% of organic carbon from the water column (Alling et al., 2010; Letscher et al., 2011),

other studies report a conservative mixing across the Arctic shelves (Kattner et al., 1999; Semiletov et al., 2013; Tanaka et al., 2016; Pugach et al., 2018).

To address the knowledge gap in the transport and fate of organic-rich waters, synoptic and frequent monitoring of the fluvial-marine transition zones is needed. In situ monitoring and tracking of organic-rich Arctic river plumes is challenging as these areas are hard to reach and they impose severe constraints on sampling. Furthermore, in situ sampling captures a snapshot during expeditions, which usually take place from August to September, when sea ice conditions are the most favourable for navigation. In most cases, in situ datasets overlook the winter and shoulder seasons, which can be the most important for OM transport (McGuire et al., 2009). Thus, in situ sampling can hardly address potential long-term changes in the coastal waters on a pan-Arctic scale.

This thesis mainly focuses on the dissolved fraction of organic matter (DOM) and its carbon (DOC). DOM and DOC are bulk parameters for total amounts of groups of substances found in water solution. DOM refers to the total amount of organic matter (e.g. carbohydrates and lignins), whereas DOC refers to the concentration of organic carbon only. The "D" in both abbreviations refers to the dissolved species only. In practice, however, analytical observations of DOM and DOC are defined by the mean pore size of the filter (commonly between 0.2 µm and 0.7 µm) used to prepare the samples.

1.1.3 Ocean Colour Remote Sensing

Ocean Colour Remote Sensing (OCRS) is a powerful tool to complement in situ sampling. Optical satellite sensors can detect and monitor constituents, such as DOC in surface waters. Polar orbiting satellites can provide several images per day if cloud and light conditions are favourable. Moreover, a number of optical sensors offer high enough spatial resolution (<1 km) to observe Arctic river plumes carrying DOM onto the shelf. High spatial and temporal resolution make OCRS an invaluable tool to study land-river-ocean interactions in the Arctic shelf regions (**Figure 1.2**).

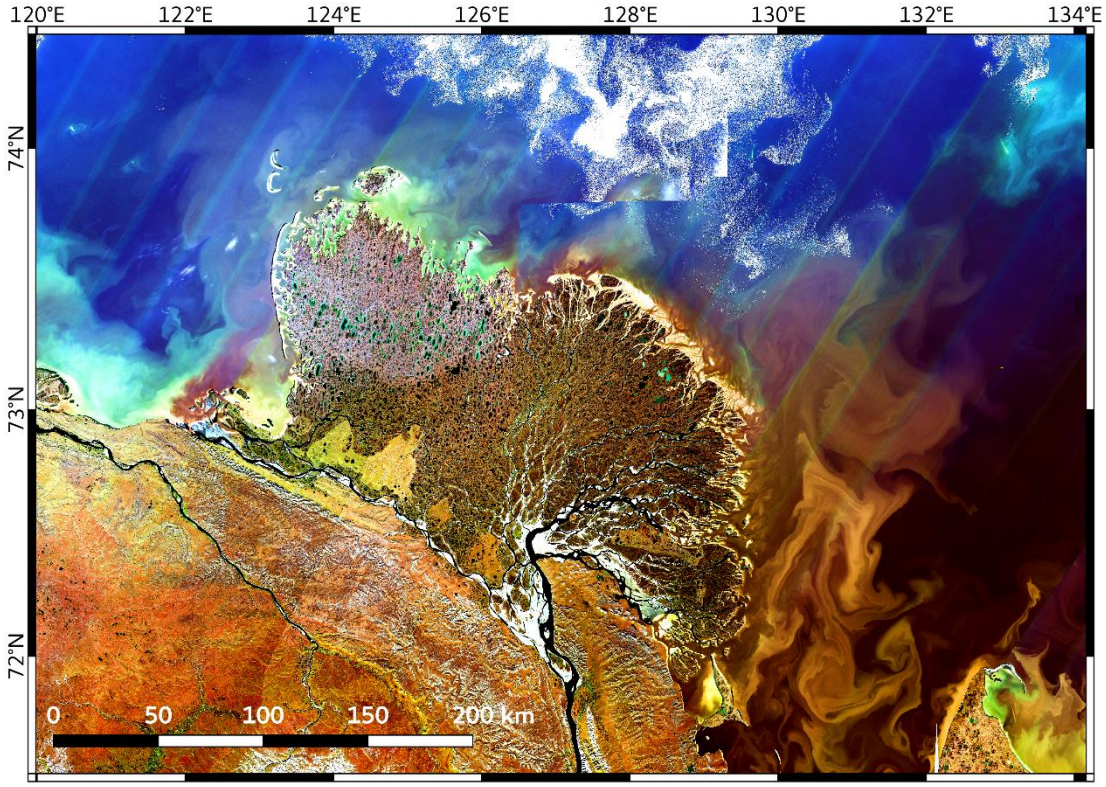

Figure 1.2: Sentinel 2a Multi Spectral Imager (MSI) true colour (RGB bands 2-3-4) mosaic image of the Lena River Delta and surrounding coastal waters from September 1 and 2, 2016. In-water structures show export fluxes of sentiment (bright and yellowish colours) and organic matter (dark and black colours). Reflectance values were stretched for land and water separately to make in-water structures visible.

Satellite-borne tracking of organic-rich river waters can reveal changes in freshwater pathways (Fichot et al., 2013) and can aid in understanding current shifts in the hydrological cycle of the Arctic Ocean under the effects of ocean currents, sea ice dynamics, and weather. Terrigenous DOM is frequently used to track freshwater in surface waters of the Arctic Ocean (e.g. Stedmon and Markager, 2001; Granskog et al., 2012; Stedmon et al., 2015). The coloured fraction of DOM (CDOM) can be measured by OCRS techniques. In river-influenced Arctic waters, the absorption of light by CDOM can be directly related to the concentration of DOC in the water. Under favourable cloud conditions, frequent satellite acquisitions can help to monitor carbon export and transport during the entire open water season. Furthermore, satellite observations can provide a better understanding of shifts in river seasonality, and how it affects the distribution of organic matter on Arctic shelves in the long term.

However, the performance and accuracy of OCRS products in Arctic coastal waters are generally not well constrained, mainly due to a lack of validation through in situ data. Few studies evaluate or validate OCRS-derived DOC concentrations in Arctic rivers or river-influenced Arctic Ocean waters (Matsuoka et al., 2013, 2017; Griffin et al., 2018; Huang

et al., 2019). The performance and accuracy of OCRS for the estimation of DOC depends primarily on three factors: (1) the performance of the atmospheric correction algorithms, which minimize interferences from the atmosphere with the signal received by the satellite; (2) the performance of a retrieval algorithm, which converts the satellite reflectance to absorption intensity of CDOM; and (3) the robustness of a relationship between DOC and CDOM, which is used to estimate DOC concentration from CDOM absorption.

To determine and improve the quality of OCRS and address all three of these factors, extensive in situ sampling is needed. For that, high spatial and temporal coverage as well as the capture of a wide range of water constituent concentrations in various combinations would be beneficial. In situ radiometric measurements of the water provide the ground truth for the atmospherically corrected signal from a satellite sensor. Besides, in situ sampling of both DOC concentration and CDOM absorption aids to improve retrieval of CDOM and to establish robust relationships between DOC and CDOM.

1.2 Objectives, thesis organization and author contributions

This thesis aims to expand our current knowledge of land-to-sea DOM and the associated carbon fluxes in the Arctic and to improve the methods of their quantification with satellite-borne Ocean Colour sensors. Two Arctic land-sea systems were extensively studied in the scope of the thesis. They include the near-mouth region of the Lena and Mackenzie rivers as well as fluvial-marine transition zones and the coastal waters of the Laptev and Beaufort Seas. Variety of in situ and remote sensing platforms were used to acquire the data over the entire spatial extent of the two systems and over different seasons (**Figure 1.3**). For the Lena River – Laptev Sea system, a long-term in situ sampling program for the river water monitoring was established in the frame of the work on this thesis. The chapters of this thesis answer the following specific objectives at various temporal and spatial scales:

- Improving accuracy of DOM flux estimation by increasing sampling frequency and including ice-covered and shoulder seasons.
- Describing seasonal variability of DOM flux with high temporal resolution and linking the variability to the seasonally changing dominant water sources.
- Estimating sources and quality (e.g. chemical characteristics and age) of DOM in in the Lena River and in the receiving coastal waters of the Laptev Sea and the Mackenzie mouth region. For that, in situ optical properties from multi annual and multi seasonal field campaigns were used.

- Evaluating OCRS algorithms at regional scale in the Laptev Sea and Beaufort Sea and improving accuracy and applicability of OCRS for the monitoring of DOC concentrations in surface water on Arctic shelves.

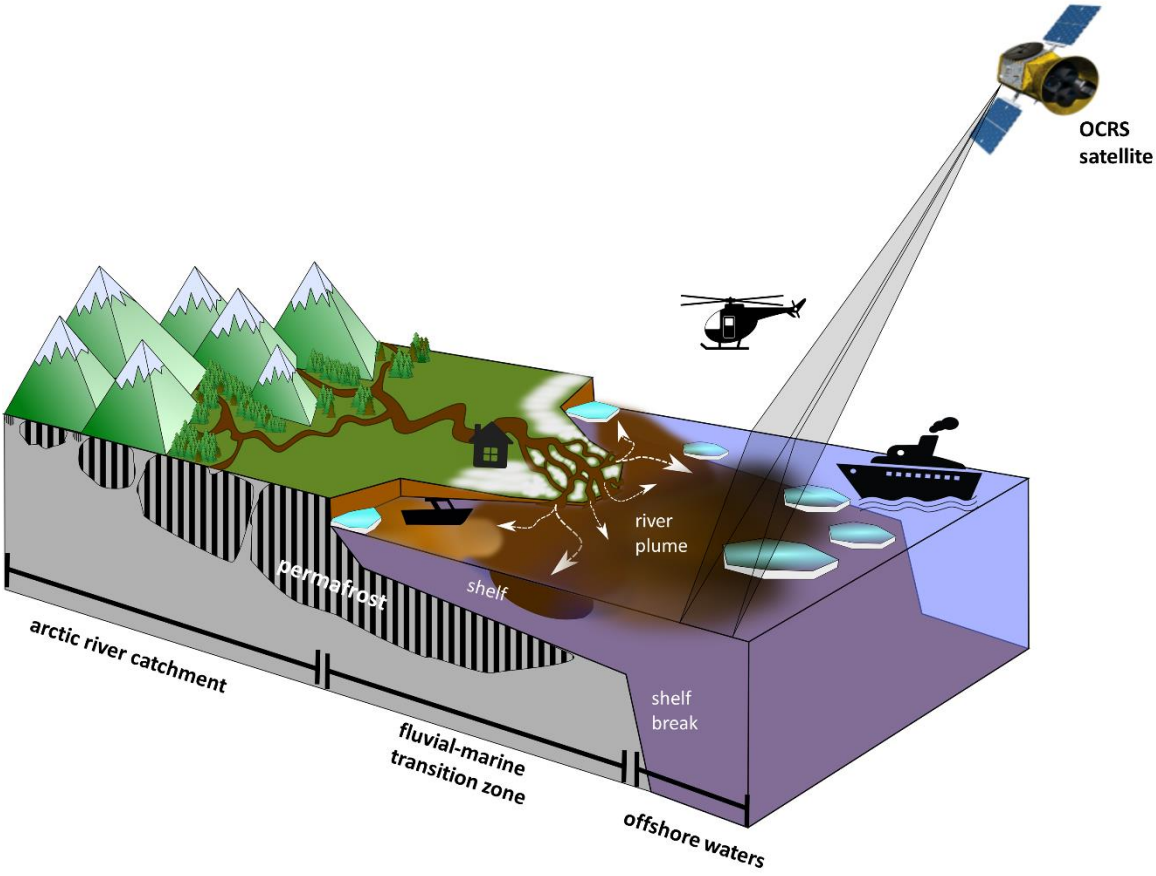

Figure 1.3: Schematic illustration of the Arctic land, coastal and ocean systems studied and observational platforms used in this thesis. Dissolved constituents of river, coastal and shelf waters and ice were measured and estimated in situ and remotely. Various in situ sampling platforms such as boats, ships, helicopter, and Arctic research stations as well as Ocean Colour satellites were used to study the organic matter fluxes from land to sea.

The organization and structure of the thesis is following:

Chapter 2 provides the scientific background and a short review of the state of knowledge about organic matter in the Arctic Ocean. Moreover, this chapter guides through the fundamentals, feasibility, and limitations of OCRS in Arctic coastal waters.

Chapter 3 presents the first results of the sampling program near the mouth of the Lena River. Observed biogeochemical parameters provide a baseline for the estimation of the DOM fluxes and characterization of seasonality drivers of the Lena River water properties. The study is published in Frontiers of Environmental Science (Juhls et al., 2020). The thesis' author together with a small team initiated, developed and maintained this sampling program as well as the analysis of samples.

Chapter 4 synthesizes data from eleven ship-based campaigns to river, coastal and offshore waters in the Laptev Sea and Lena River Delta region. Sampled DOC and CDOM data were used to develop a new model for the OCRS-quantification of DOC from optical absorption measurements for this region. Furthermore, OCRS products were evaluated for the retrieval of DOC concentration. The study is published in Biogeosciences (Juhls et al., 2019). The author of the thesis participated in most of the expeditions and performed some of the water sample analyses.

Chapter 5 presents the results of a series of sampling campaigns to the Mackenzie Delta region in 2019. Combined biogeochemical, biooptical and radiometric in situ measurements were used to evaluate performance of atmospheric correction and CDOM retrieval algorithms. The best performing combination of algorithms was then used to monitor the river water plume propagation on a large spatial and temporal scale with OCRS. This chapter is a manuscript in preparation.

Chapter 6 provides major outcomes and the concluding summary of this thesis with a brief outlook.

Chapter II

Scientific background

2 Scientific background

Although the Arctic Ocean constitutes only about 1% of the global ocean volume (Opsahl et al., 1999), it receives about 10% of the global river discharge (Aagaard and Carmack, 1989; McClelland et al., 2012). This strong impact of freshwater from the surrounding landmasses distinguishes the Arctic Ocean from the other oceans (e.g. the Southern Ocean). While numerous rivers drain into the Arctic Ocean, the six biggest Arctic rivers (Yukon, Mackenzie, Ob', Yenisey, Lena, and Kolyma) contribute about 65% (3913 km^3 yr^{-1}) to the total annual discharge into the Arctic Ocean (Holmes et al., 2012b). The fluxes of terrestrial material carried by river waters to the sea exert a strong influence on the Arctic Ocean, particularly on its surface waters.

Following, background information on the organic matter and the Arctic carbon cycle is provided. This thesis focuses on the dissolved fraction of organic material and organic carbon for a number of reasons. The dissolved fraction is readily labile making it more bioavailable as compared to the particulate fraction. Furthermore, the particulate fraction is prone to settling and, thus, less relevant for pan-Arctic transport processes. Large areas are affected by terrigenous dissolved organic matter due to the large volume that drains into the Arctic Ocean and propagated over large spatial scales.

2.1 Dissolved organic carbon in the Arctic carbon cycle

Arctic aquatic systems play key roles in the global carbon cycle. They can, for instance, serve as a significant pool for particulate and dissolved inorganic and organic carbon and may exert considerable influence on the turnover and sinking of organic carbon. About 50% of the global soil organic carbon is stored in Arctic permafrost soils (Gorham, 1991; Tarnocai et al., 2009), making the cycle of organic carbon in the Arctic an essential part of the global carbon cycle. Recent estimates report that 1035 ± 150 Pg of organic carbon is stored in the surface layer (top 3 m) of the northern permafrost regions (Hugelius et al., 2014; Schuur et al., 2015). Ice-rich Pleistocene permafrost (Yedoma) is an important stock of organic carbon storing about 500 Pg of organic carbon (Grosse, 2013), which is highly vulnerable to climate change. It can potentially generate large fluxes of old carbon that was previously inactive in the carbon cycle (Vonk et al., 2012).

Soils, rich in organic carbon, release it as carbon dioxide (CO_2) or methane (CH_4) into the atmosphere and as particulate organic carbon (POC) and DOC into the aquatic systems.

About 94 Tg of dissolved and particulate inorganic and organic carbon is transported annually from land into the Arctic Ocean via rivers and coastal erosion (McGuire et al., 2009). Altogether, the Arctic carbon cycle is complex and many of its pathways remain poorly quantified (**Figure 2.1**). For example, little attention has been paid to the inorganic fraction of carbon fluxes (McGuire et al., 2009), although they might be substantial (Striegl et al., 2007).

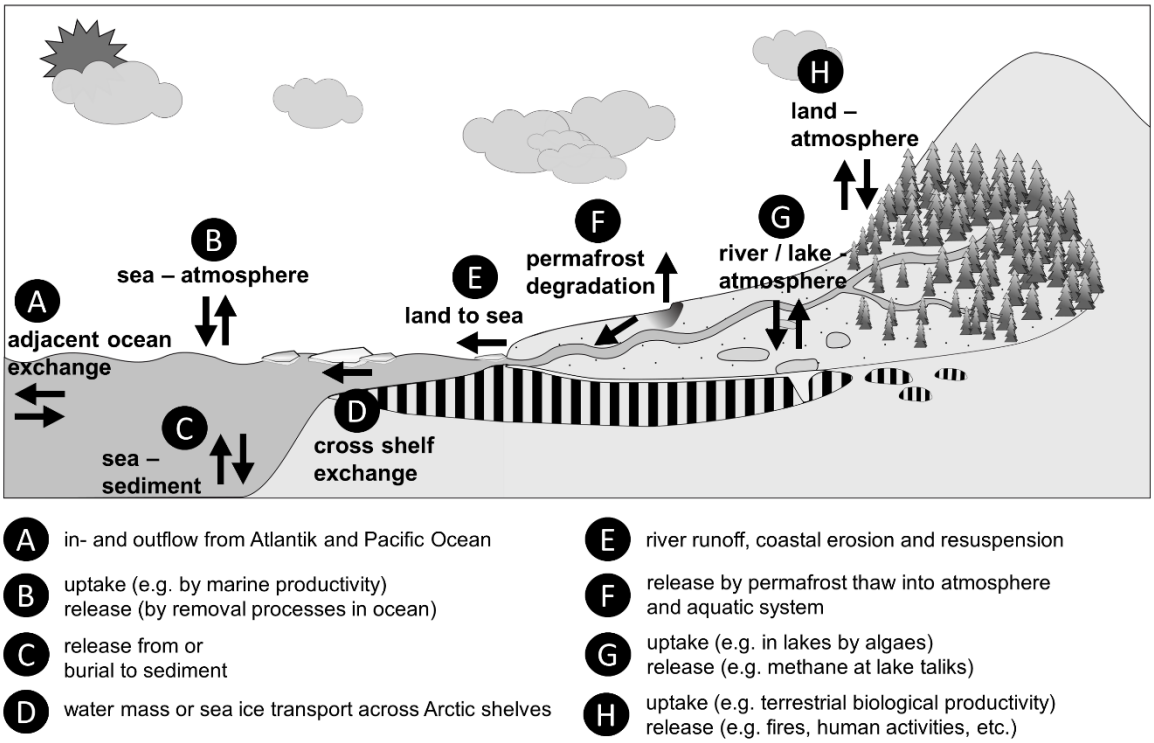

Figure 2.1: Carbon pathways, sources and trigger release and modification processes (A to H) in and between different compartments (land, shelf seas, central basins) of the Arctic.

The DOC makes up about 38% of the total Arctic carbon flux from land to sea (McGuire et al., 2009). It constitutes about 10 - 17% of the global DOC flux from land to sea (Raymond et al., 2007). The six major Arctic rivers transport 7.5 - 9.5% (Raymond et al., 2007; Stedmon et al., 2011; Holmes et al., 2012b) of the global annual riverine DOC to the Arctic Ocean (210 to 240 Tg C yr^{-1}; Ludwig et al. (1996); Cauwet (2002)). While substantial effort has been spent on quantifying fluxes of DOM into the Arctic Ocean, only some studies provide information about the composition of the DOM. Arctic DOM is composed of a wide and variable range of compounds. Most frequent of them are lipids, amino acids, proteins, pigments, tannins, and lignins. Lignin phenols, that are found in river runoff and in the surface waters of the Arctic Ocean (Lobbes et al., 2000; Benner et al., 2004; Amon et al., 2012), contain large amounts of aromatic carbon (Lebo et al., 2001) and

exclusively originate from vascular plants. They are identified as the humic fraction of the DOM (Kattner et al., 1999). Therefore, lignin is often used to trace the terrestrial fraction of DOM (e.g. Mann et al., 2016). Studies report that the lignin-rich terrigenous DOM in Arctic surface waters is rather refractory (Hansell et al., 2004; Holmes et al., 2008; Alling et al., 2010; Letscher et al., 2011), but also, contradictory, report a rather short DOC half-life (<3 years) on the Siberian shelves (Alling et al., 2010; Letscher et al., 2011).

Non-humic components of DOM that are found in the Arctic, such as amino acids and proteins, are typically related to autochthonous production and primarily originate from microbial communities (Coble, 2007). A fraction of DOM, which absorbs light predominantly in the ultraviolet (UV), is termed coloured dissolved organic matter (CDOM). CDOM is often used as a tracer for DOC in Arctic river and shelf waters and can be measured by optical sensors due to its specific optical absorption properties (**chapter 2.2.2**).

2.1.1 Sources of dissolved organic matter in the Arctic Ocean

There are multiple sources of organic matter in the Arctic Ocean: (1) terrestrial organic matter, released via rivers and coastal erosion, (2) release of organic matter from sea ice, (3) freshly produced organic matter by biological activity in the water column, and (4) laterally transported organic matter from other water masses such as Atlantic water. Terrestrial DOM from rivers and eroding coastlines constitutes the dominant source and fraction of organic carbon in Arctic coastal and shelf waters.

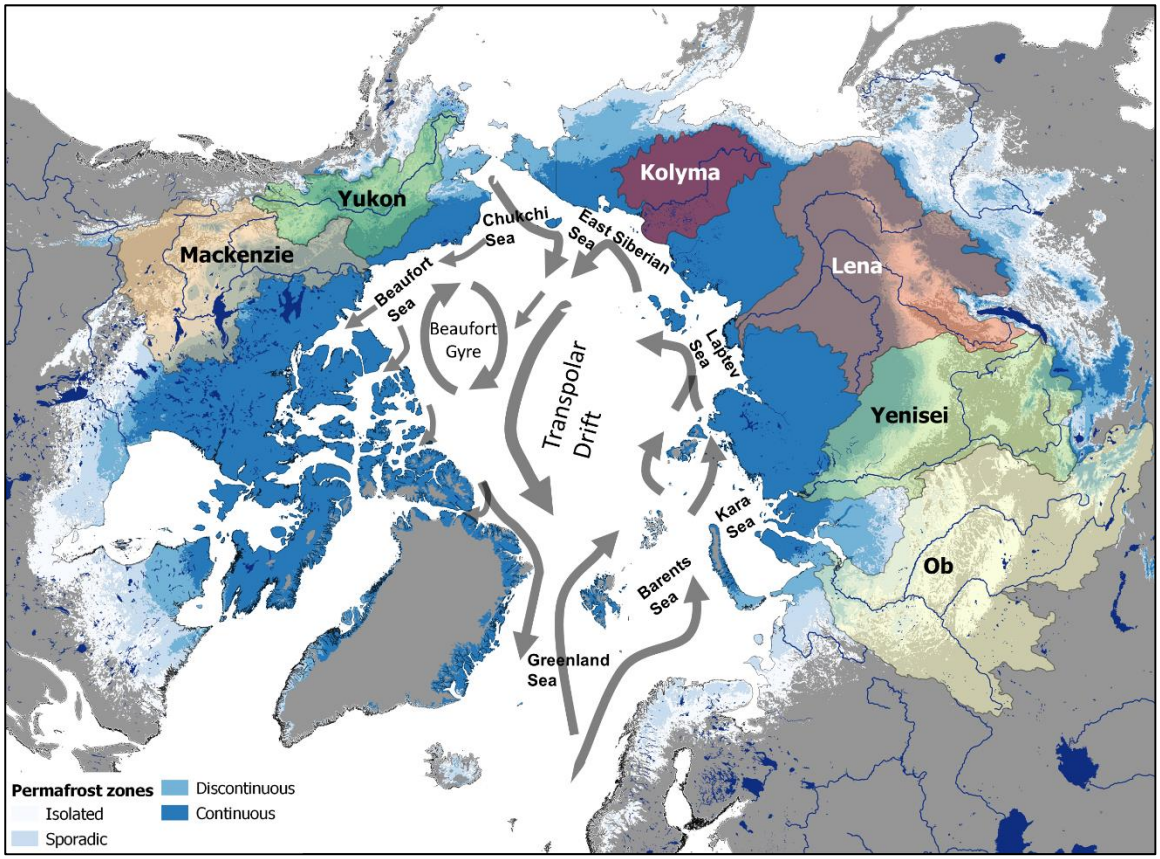

Figure 2.2: Pan-Arctic map of permafrost zones (Obu et al., 2019), and catchments of the six largest Arctic rivers (GRDC, 2020) and the Arctic Seas. Arrows display major oceanic currents.

The largest in situ source of DOM and carbon produced in the Arctic Ocean is primary production that varies on seasonal and interannual scales (Davis and Benner, 2005; Mathis et al., 2007). Arrigo and Van Dijken (2011) estimated net primary productivity rates ranging from 441 to 585 Tg C yr^{-1} in the Arctic Ocean. According to their estimates, productivity may have increased by 20% between 1998 and 2009 due to an increase in the spatial and temporal extent of open waters. These same authors project a 65% productivity increase under conditions of ice-free summers in the Arctic Ocean. Besides the decline of sea ice, the increase of nutrients influx drives the increase of primary production in the Arctic (Babin, 2020; Lewis et al., 2020). While phytoplankton growth can result in elevated concentrations of particulate organic matter for limited areas and periods, the concentration of particulate matter in the offshore and central waters of Arctic Ocean waters is generally low. The major fraction of the total organic carbon there is DOC (Anderson and Amon, 2015).

The highest DOC concentrations from biological activity are found in sea ice attributed to ice algae production. Extensive algae blooming occurs in spring at the ice-water interface

in the bottom ice. There, Smith et al. (1997) and Riedel et al. (2008) observed DOC concentrations higher than 30 mg L^{-1}. While pack ice generally holds low concentrations of DOC (<0.3 mg L^{-1}; Mathis et al (2007)), land-fast ice can contain significant amounts of DOC (>4.8 mg L^{-1}; Hölemann et al., in prep.), which is likely accounted to inclusion of DOC from river water or coastal erosion.

Another source of DOM in the Arctic Ocean is the lateral transport of inflowing Atlantic and Pacific waters (**Figure 2.2**). Atlantic water that enters the Arctic Ocean through the Fram Strait and the Barents Sea was found to have DOC concentrations varying between 0.6 and 1.3 mg L^{-1} (Børsheim and Myklestad, 1997; Opsahl et al., 1999; Amon et al., 2003; Engbrodt and Kattner, 2005). Mean DOC concentrations of Pacific water flowing through the Bering Strait equal about 0.9 mg L^{-1} (Hansell et al., 2004).

Erosion along Arctic coasts is an additional source of terrigenous organic matter. The supply of organic matter to the Arctic Ocean by coastal erosion is strongly limited to the open water period when wave energy, tides and currents, in combination with increased air and water temperatures and thawing permafrost, result in significant loss of coastline (up to 25 m yr^{-1}; Jones et al., (2009), Günther et al. (2015)) and release of organic matter that is stored in the soils. Coastal Yedoma and ice-rich coasts, in particular, show the most rapid retreat rates and the highest vulnerability to climate warming. Coastal erosion is predominantly important as a source for the particulate fraction of carbon fluxes to the Arctic Ocean (6-7 Tg C yr^{-1}), whereas the flux of the dissolved fraction is relatively small (0.07 Tg C yr^{-1}) (McGuire et al., 2009). The release of POC through coastal erosion is in the same order of magnitude as the release of POC by Arctic rivers (Stein et al., 2004).

The largest source of the dissolved fraction of terrigenous organic matter are the Arctic rivers. Coastal waters receive particularly high concentrations of DOM and DOC through the rivers. Thawing permafrost in Arctic river watersheds is expected to drastically increase the fluxes of DOM into the Arctic coastal waters. Altogether, the catchments of the Yukon, Mackenzie, Ob', Yenisey, Lena and Kolyma rivers make up 53% of the total pan-Arctic watershed (Holmes et al., 2012b). However, these six rivers alone contribute 50-80% to the total terrestrial DOC export (25–36 Tg C yr^{-1}; Raymond et al. (2007)) into the Arctic Ocean. The discharge of ~673 km^3 yr^{-1} of water (Holmes et al., 2012b) from the Yenisey River makes it's input into the Arctic Ocean the largest of all Arctic rivers. Although the Lena River has a lower discharge (588 km^3 yr^{-1}), it exhibits the highest DOC concentration (up

to 19.2 mg L^{-1}) and the highest flux of DOC (7.3 Tg C yr^{-1}; Stedmon et al. (2011)) of all Arctic rivers. Overall, the Siberian rivers in the eastern Arctic exceed North American rivers that flow into the western Arctic in terms of discharge and DOC fluxes. The combined discharge flux of Ob', Yenisey, Lena and Kolyma (1824 km^3 yr^{-1}) is ~3.5 times larger compared to the combined flux from the Mackenzie and Yukon River (524 km^3 yr^{-1}). The DOC flux from the Siberian rivers (17 Tg C yr^{-1}) is ~13 times higher compared to the two North American rivers (1.3 Tg C yr^{-1}). Thus, DOC concentrations in the coastal waters of the Siberian Arctic (Kara, Laptev and East-Siberian Sea) are substantially higher than in the Beaufort and Chukchi seas in the western Arctic (Holmes et al., 2012a). **Figure 2.3** provides an overview of discharge and DOC fluxes of the six biggest Arctic rivers, reported from multiple studies.

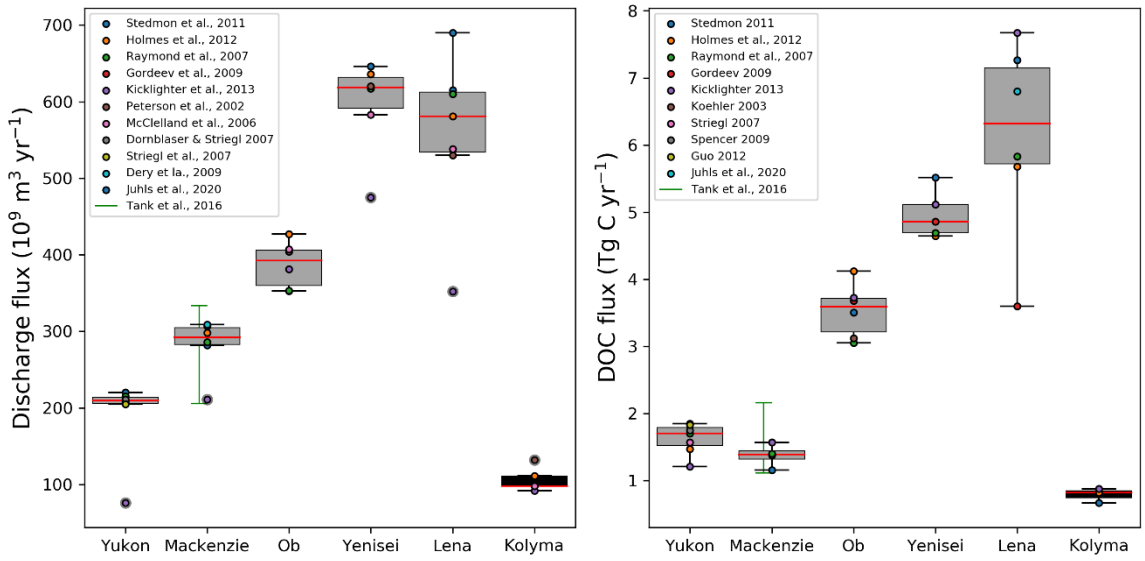

Figure 2.3: Published discharge (a) and DOC flux (b) of the six largest Arctic Rivers. Boxplots show the main statistics across all studies and single coloured points show the values reported in each study. The study by Tank et al. (2016) reports a series discharge and DOC fluxes for the Mackenzie over a 39-year period, which is displayed by the green bar. Periods of record for each study differed.

Arctic rivers export of DOC is not constant throughout the year but closely tied to the variability in discharge rates (Holmes et al., 2012b). The hydrograph of Arctic rivers is characterized by a strongly nival (snowmelt dominated) discharge regime (Woo, 1986), with a spring peak between the middle of May (North American rivers) and the middle of June (East Siberian rivers) (**Figure 2.4**). In the Lena River, up to 70% of the annual DOC flux is exported during the spring freshet (Raymond et al., 2007). During summer and fall, the discharge strongly depends on the precipitation within the catchment and varies between years. In winter, the discharge of Arctic rivers is generally low.

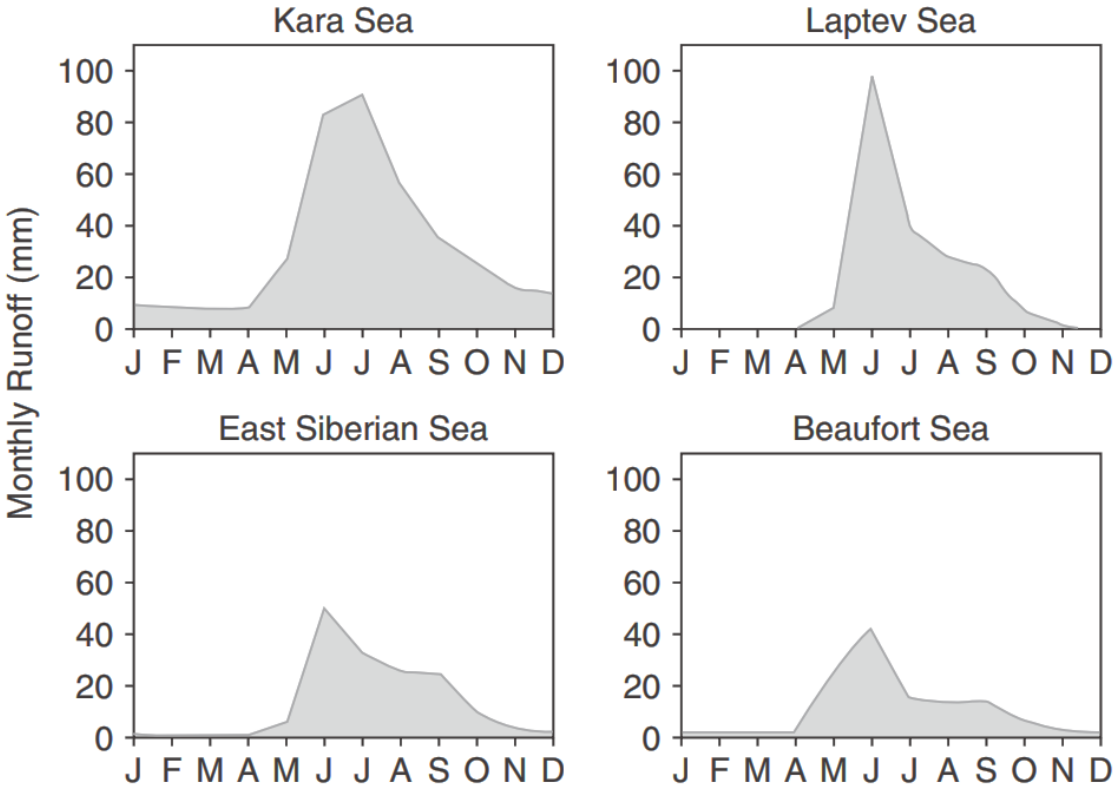

Figure 2.4: Monthly averaged runoff (1990-1999) for four regions of the pan-Arctic domain: Kara Sea with the rivers Norilka, Ob', Pur, Yenisey; Laptev Sea with the Anabar, Lena, Olenyok and Yana rivers; East Siberian Sea with the Alazeya, Indigirka and Kolyma rivers, and the Beaufort Sea with the Anderson, Kaparuk and the Mackenzie rivers. Figure from Holmes et al. (2012a).

2.1.2 Removal, transport pathways and export of terrigenous organic matter

Recent studies show that freshwater transport in surface waters (polar mixed layer and upper halocline waters), as well as sea ice formation and melt, play major roles in the fate of organic matter in the Arctic Ocean (Granskog et al., 2012; Fichot and Benner, 2014). In the shallow Arctic shelf seas, terrigenous organic carbon can either be mineralized in the water column and in the upper layer of sediments, or it can be buried unmodified into deeper sediments (Bröder et al., 2018). A number of processes that remove DOM from the water column may perturb its conservative behaviour across Arctic shelves. This often-reported behaviour expects mixing of DOM-poor marine water with DOM-rich river water without significant losses and gains along the salinity gradient of DOM.

Amon and Meon (2004) report low removal rates of DOM from the Yenisey River waters during short-term experiments. Similarly, Osburn et al. (2009) conclude that removal of DOM in fluvial-marine transition zone of the coastal Beaufort Sea is negligible. In contrast, Hansell et al. (2004) and Granskog et al. (2012) report that about 30 to 70% of the

terrigenous DOC is removed from the water column before it is exported from the Arctic Ocean. For the East Siberian and Laptev Sea shelves, Schlosser et al. (1994) report a DOM residence time of 3.5 years which was later used to compute removal rates for the Laptev Sea (0.3 yr^{-1}; Alling et al. (2010)) and for the Makarov and Eurasian Basins (0.24 ± 0.07 yr^{-1}; Letscher et al. (2011)). To calculate removal rates, observations from the major rivers were used to extrapolate zero salinity DOM end member values and compare them. However, estimating removal rates of DOM using this method is challenging because of the variable intensity of a number of different processes such as microbial degradation, flocculation and mineralization by photobleaching, all of which may be responsible for the removal of DOM and its carbon to various degrees.

A number of studies focus on the contributions of these processes to DOM removal. Amon and Meon (2004) as well as Benner et al. (2004) consider degradation of DOM by photobleaching to be generally low in the Arctic due to the low sun elevations and shielding by frequent cloud cover and long-term ice cover. However, with the ongoing decline in sea ice extent and shortening of the ice cover period, photobleaching is expected to increase in the coming decades (Bélanger et al., 2006). Using an optical-photochemical-coupled model, Bélanger et al. (2006) showed that photomineralization of DOC in the south-eastern Beaufort Sea is not a major process of removal of terrigenous DOC in the Arctic. However, photomineralization could become more important in response to declining sea ice. In the Hudson Bay, where sun elevation is higher and ice cover is shorter compared to higher latitudes, Granskog et al. (2009) showed that photobleaching is likely the major driver for the removal of terrigenous DOM. Furthermore, this process could help to explain the high CO_2 concentrations observed in the coastal waters of the Hudson Bay.

Coagulation and flocculation are processes that remove organic carbon from the water column by reallocating it from the dissolved (DOC) to the particulate (POC) fraction, which is prone to settle to the sediments of the sea floor. Besides the composition of DOM and variability in salinity, water temperature, concentration of suspended solids and bacterial abundance are major controlling factors of flocculation in the fluvial-marine transition zone (Droppo et al., 1998). However, the importance of flocculation for riverine DOC removal in the fluvial-marine transition zone and the seasonal dependency of changes in the composition and quality of DOM are not well studied (Vetrov et al., 2004; Lasareva et al., 2019).

The alteration of the conservative behaviour of DOM in the Arctic Ocean by numerous processes limits the use of DOM as a tracer for river water. However, in the estuarine mixing zone no or very little removal of DOM has been found (Granskog et al., 2012). While earlier studies show that the lignin-rich Arctic riverine DOM is highly recalcitrant to bacterial consumption and flocculation (Köhler et al., 2003), Holmes et al. (2008) show that DOM, exported by Arctic rivers during spring, is more labile than DOM, exported during summer. Conclusions from these earlier studies may, however, be biased by a dominance of summer sampling (Holmes et al., 2008).

The time it takes for the cross-shelf transport and degradation of remineralized or buried terrigenous organic carbon is another major factor for the fate of organic carbon on Arctic shelves (Bröder et al., 2018). Bröder et al. (2016) report, that across the Siberian shelf sediments, most terrigenous organic carbon degrades before it reaches the continental slope.

The transport of DOM from the Beaufort Sea Shelf towards the Beaufort Gyre (Fichot et al., 2013) as well as the transport from the East Siberian Arctic shelves to the Transpolar Drift are the dominant routes of terrigenous DOM in the Arctic Ocean (Guay et al., 2001; Charette et al., 2020). River water, predominantly from the Siberian shelves, enters the Transpolar Drift and thereby becomes a major source of DOM in the central Arctic. Charette et al. (2020) report a DOC flux of 37 ± 22 Tg C yr^{-1} in the Transpolar Drift, a large fraction of which can be attributed to terrigenous DOC from the Arctic rivers. Another important transport pathway of terrigenous DOM released by the Eurasian rivers follows the predominantly eastward coastal current system and does not directly enter the Transpolar Drift (Guay et al., 2001; Fichot et al., 2013; Anderson and Amon, 2015). Inter-annual variations in the direction of transport pathways can be linked to atmospheric circulation patterns such as the Arctic Oscillation Index and the Arctic Dipole. When the Arctic Oscillation Index is negative, a state, which is characterized by low surface pressure in the Arctic, the Siberian river water quickly enters the Transpolar Drift and flows towards the Fram Strait. When the Arctic Oscillation Index is positive, resulting in high surface pressure in the Arctic, large volumes of river water from the Siberian shelves are transported towards the Canadian Basin and enter the Beaufort Gyre (Mauritzen, 2012; Morison et al., 2012). The exchange rate of terrigenous DOM between Canadian Arctic and Siberian shelves is mostly unknown (Granskog et al., 2012). On a regional scale,

Thibodeau et al. (2014) show the connection between the direction of the Lena River plume propagation and interannual variations of the Arctic Dipole.

Sea ice drift is also a major pathway for the transarctic transport of riverine DOM (Dmitrenko et al., 1999). Its role may increase with the strengthening of the sea ice drift (Spreen et al., 2011). On the other hand, the amount of DOM transported by sea ice drift can decrease due to stronger ice melt in the marginal zones, lower ice survival rates and earlier ice-melt release of DOM in the northern Arctic shelves or in the central Arctic Ocean (Krumpen et al., 2019).

Most of the DOM export from the Arctic Ocean to adjacent oceans is observed in the Fram Strait with the East Greenland Current (Granskog et al., 2012) and in the Canadian Archipelago (Walker et al., 2009). A high-resolution ocean-sea ice model revealed a net southward export through the Fram Strait that accounted for about 50% of the total Arctic riverine DOM input, highlighting that the DOM export is a major removal pathway of Arctic DOM (Fahrbach et al., 2001; Granskog et al., 2012). The best guess of terrigenous DOM export flux via the Canadian Archipelago, based on elevated CDOM levels in the North Water Polynya (Scully and Miller, 2000) and reported volumes of water transport (Lundberg and Haugan, 1996), indicates fluxes of similar magnitude between Canadian Archipelago and East Greenland Current (Amon, 2004).

Presently, observations suggest that the Arctic Ocean acts as an overall carbon sink. Improving the quantification of present-day carbon fluxes will provide the grounds for predictive values under climate change. Because they play significant roles in the cycling of carbon at local to global scales and are likely most vulnerable to increasing temperatures, Arctic shelves represent areas of key interest to acquire current-day observations and anticipate future changes.

2.2 Ocean Colour Remote Sensing - Fundamentals and limitations

OCRS detects the light that leaves the surface of a water body, typically within the visible (VIS, wavelength 400-700 nm) and the near-infrared (NIR, wavelength 700-1000 nm) part of the spectrum. Ocean Colour sensors measure the intensity of received light at a number of channels (defined by central wavelengths) across the VIS and NIR. The colour of the water is in direct relation to its constituents and their optical properties (absorption by organic matter, scattering by particles, etc.), also called inherent optical properties (IOPs). The ultimate goal of OCRS is to estimate the concentration of these constituents in water

from its colour, which is directly dependent on the type and the concentration of the constituents.

The early development of OCRS is associated with the launch of the satellite NIMBUS-7 in 1978, which carried the Coastal Zone Colour Scanner (CZCS) (Hovis et al., 1980). CZCS was the first satellite sensor that was specifically built to sense the ocean surface waters and retrieve optically active constituents from them. Multiple studies based on the data from CZCS were able to demonstrate the potential of OCRS to observe such water constituents and to monitor their spatial and temporal variability as well as their long-term trends (Bricaud et al., 1987; Yoder et al., 1987). Currently, there are a number of optical sensors in space, which are used for OCRS. **Table 2.1** shows the characteristics of a few optical sensors that were used in the frame of this thesis. Modern optical satellite programs aim to cover the globe with multiple satellites that are identical by their parameters but orbit with a shift relative to each other for a faster and fuller coverage of the Earth's surface. Polar regions are scanned more frequently than other regions on Earth due to polar orbits and overlapping wide swaths of most optical satellite sensors. Variety in the spatial, spectral, and temporal resolutions of different sensors enables users of OCRS to choose the data that are optimal for the subject of their study. While studying small-scale features (tens of meters) requires high spatial resolution, large patterns that appear on a pan-Arctic scale might not require such a high spatial resolution but could benefit from higher spectral and temporal resolutions. Higher spatial resolution often comes with lower spectral resolution, imposing a compromise that is contingent on the objectives of the study.

Table 2.1: List of optical satellite sensors and their properties that are used in this thesis.

Satellite (Sensor)	Duration (operational)	Spatial resolution (m)	Spectral resolution (no. of bands in VIS - NIR)	Revisit time
Sentinel 2 a & b (MSI)	S2a since 2015, S2b since 2017	10, 20, 60 (depends on band)	12 (442.7 to 2202.4 nm)	daily (a & b combined)
Sentinel 3 a & b (OLCI)	S3a since 2016, S3b since 2018	~300	21 (400 to 1020 nm)	5-10 per day (a & b combined)
Aqua, Terra (MODIS)	Aqua since 2002, Terra since 1999	250, 500, 1000 (depends on band)	19 (405 to 2155 nm)	5-10 per day (Aqua & Terra combined)
Envisat (MERIS)	2002 to 2012	~300	15 (412.5 to 900 nm)	~5 per day

However, the use of OCRS in Arctic waters, particularly in coastal waters, is challenging. Ice and cloud cover significantly reduce the availability of data. Extreme optical complexity of the water due to the interaction of several highly concentrated and optically active constituents, requires the cautious use of OCRS data and an inevitable priori evaluation or validation. Limitations and challenges of OCRS are further described and discussed in

chapter 2.2.4 and **chapter 6.4**. Despite these challenges, OCRS remains a powerful tool for monitoring DOM runoff and its fate in the Arctic Ocean. The principle and measurement processes for monitoring DOM with OCRS are based on the influence of the atmosphere and water on natural sunlight. Natural sunlight enters the water, where it is altered by the absorption or scattering from the water constituents. The type and intensity of this alteration depends on the type and concentration of the constituents in the water. While dissolved matter dominantly absorbs photons, particles mostly scatter them. Absorbing and scattering properties of many water constituents are empirically and theoretically known. Therefore, the signal of altered light received by a satellite sensor can be used to identify the constituents and their concentrations. However, the signal that is received by the satellite sensor is a mixture of light scattered and absorbed in the atmosphere and in the water body (**Figure 2.5**). Understanding and quantifying the alteration of the pathways and light properties in the atmosphere is a major challenge of OCRS.

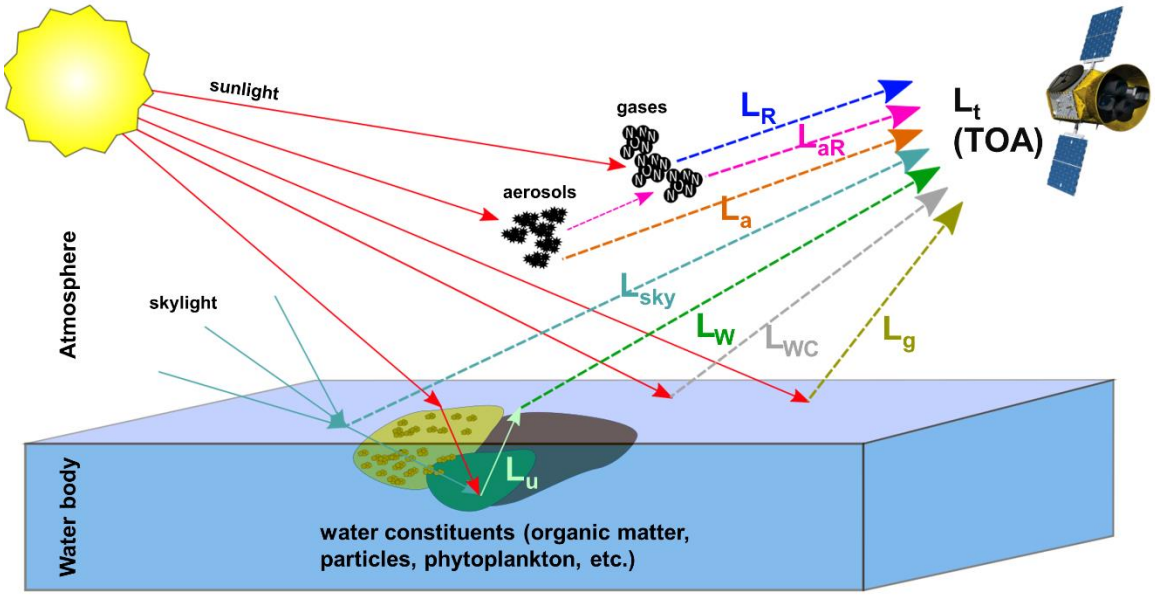

Figure 2.5: Schematic illustration of radiance pathways and alterations in water and atmosphere that contribute to the total radiance at the top of atmosphere (L_t^{TOA}) received by a satellite sensor. Abbreviations are further explained in **chapter 2.2.1**.

To retrieve information about the water constituents, OCRS usually consist of three major steps: (1) Atmospheric correction – quantifying and eliminating the atmosphere-related distortion in the signal received by the satellite; (2) Retrieving inherent optical properties (IOPs) of the water constituents from the atmosphere-corrected signal; (3) Relating the

IOPs to absolute concentrations of the water constituents. The next chapter describes these steps in more details including basic techniques, challenges and recent advances.

2.2.1 Atmospheric correction

The total radiance at the top of the atmosphere (L_t^{TOA}) consists of contributions from multiple radiance pathways. The water leaving radiance (L_w) is the part, which exits the water and contains the information needed for OCRS. However, L_w often only represents a minor fraction of L_t^{TOA} (Antoine and Morel, 1999). The main goal of the atmospheric correction is to "eliminate" the other path radiances (than L_w) that are contributing to L_t^{TOA}. The importance of atmospheric correction is crucial considering the level of accuracy that is needed. Direct reflected radiance from sun glint on the water surface (L_g), background radiance from the sky that is reflected by the water surface (L_{sky}), and both sun and sky radiance reflected by wave-induced whitecaps or foam at the surface of the water (L_{wc}) as well as absorption and scattering by aerosols (L_a) and atmospheric gases (also known as Rayleigh radiance L_R), including multiple scattering between them (L_{aR}) are the other factors controlling the alteration of L_t^{TOA}. The total radiance (L_t), which is detected by the satellite sensor at the top of the atmosphere (TOA), can thus be described as:

$$L_t = L_R + L_a + L_{aR} + L_g + L_{sky} + L_{wc} + L_w. \qquad \text{(Equation 2.1)}$$

This is a simplified model which can be expanded or described differently (Wang and Bailey, 2001; Wang, 2002; Franz et al., 2007). For example, L_g, L_{sky}, L_{wc} and L_w can be altered further in the atmosphere, and the radiance depends on the viewing direction and the wavelength. For the brevity, these are not included here. To calculate the fraction of the water-leaving radiance (L_w) from the measured total TOA radiance (L_t^{TOA}), all other terms in L_t (Equation 2.1) need to be quantified and eliminated from L_t.

Various methods and schemes for atmospheric correction are currently used, and some of them are evaluated in this thesis. One common approach relies on the assumption that water in the NIR part of the spectrum fully absorbs the light and thus appears black (Gordon and Clark, 1981). This so-called "black pixel assumption" can determine aerosol properties and their effect on the radiance (Siegel et al., 2000). The type of aerosol present in the atmosphere can be determined using spectral bands in the NIR, which are not affected by gas absorption and the correction of Rayleigh scattering. The spectral properties of the various types of aerosol are then used to correct all satellite sensor bands. An alternative

approach for atmospheric correction uses artificial neural networks that are trained with radiances and their pathways simulated by radiative transfer. A third approach is the iterative spectral optimisation method that applies all spectral bands to make the atmospheric and sun glint correction.

In situ measurements of L_w that are not influenced by the atmosphere can be compared with L_t at the satellite and thus used to evaluate and validate atmospheric correction algorithms. A spectral imaging radiometer can measure the radiance and irradiance right above or below the water surface. For above water measurements, commonly, the above surface ($^+$) upwelling radiance (L_u^+), the sky radiance (L_{sky}^+) and the downwelling irradiance (E_d^+) are measured. For measurements below the water surface, these can be extrapolated to the water surface to obtain an independent estimate of water-leaving radiance. In this case, measurements at different water depths (z) of $L_u(z^-)$ and $E_d(z^-)$ are extrapolated to $z=0^-$, normalized with E_d^+ and transferred to above water. Both above water and below water measurements can then be used to calculate the normalized water leaving radiance or the remote sensing reflectance (R_{rs}, more in **chapter 2.2.3**) which then can be compared to the signal at the satellite.

2.2.2 IOPs and their spectral characteristics

Atmospherically corrected spectral radiances can be used to retrieve IOPs, which are the wavelength-dependent optical properties of the water constituents. IOPs are those properties that are only dependent on the type and the concentration of the water constituents but independent of the intensity and geometry of the incident light. Coefficients of absorption $a(\lambda)$ and scatter $b(\lambda)$ of water constituents are IOPs that can be measured in situ and are also retrieved by OCRS. The total absorption $a_{Tot}(\lambda)$ of water is the sum of the absorption by the constituents and by pure water:

$$a_{Tot}(\lambda) = a_w(\lambda) + a_{CDOM}(\lambda) + a_{Ph}(\lambda) + a_{NAP}(\lambda), \qquad \text{(Equation 2.2)}$$

where $a_W(\lambda)$ is the absorption by pure water, $a_{CDOM}(\lambda)$ the absorption by CDOM, $a_{Ph}(\lambda)$ the absorption by phytoplankton and $a_{NAP}(\lambda)$ absorption by non-algal particles.

Similarly, the total scattering $b_{Tot}(\lambda)$ of water is the sum of the scattering by the constituents and by pure water:

$$b_{Tot}(\lambda) = b_w(\lambda) + b_{Ph}(\lambda) + b_{NAP}(\lambda), \qquad \text{(Equation 2.3)}$$

where $b_W(\lambda)$ is the scattering by pure water, $b_{Ph}(\lambda)$ scattering by phytoplankton and $b_{NAP}(\lambda)$ scattering by non-algal particles. Currently, the contribution of CDOM to scattering is usually neglected and thus left out here.

The most important optically-active constituents are described below in more detail. In the context of this thesis' focus on DOM and DOC, the following analysis emphasizes $a_{CDOM}(\lambda)$ since it is one of the dominant optically-active constituents of river-influenced Arctic coastal water and a key parameter for OCRS monitoring of the fluxes and fate of organic carbon.

Coloured dissolved organic matter (CDOM)

Coloured (or chromophoric) dissolved organic matter (CDOM) is the coloured and, thus, the optically-measurable fraction of DOM. CDOM colours the water yellowish-brownish (**Figure 2.6**) which is also reflected in the earlier term "yellow substance" (Jerlov, 1953) or the German term "Gelbstoff" (Kalle, 1937). It is a complex mixture of chromophores from various compounds of DOM (Stedmon and Nelson, 2015).

Figure 2.6: Filtered water sample (filtered through 0.22 µm pore size) from a creek runoff draining organic-rich permafrost. The strong yellow colour indicates a high concentration of DOM (Photo: Bennet Juhls).

In surface waters of the Arctic shelves and even in the central Arctic Ocean, CDOM absorption is high (Gonçalves-Araujo et al., 2018) due to the high river input, which impacts the availability of light and the energy budget in the water (Soppa et al., 2019). Generally in the Arctic Ocean, CDOM absorbs more light than other water constituents such as chlorophyll, for instance (Gonçalves-Araujo et al., 2018). Only during short periods, and within limited nutrient-rich regions, phytoplankton blooms with high chlorophyll concentrations optically dominate over CDOM. In sea water influenced by river runoff, CDOM absorption can be used as a proxy for DOC and, therefore, for the quantification of land-to-ocean carbon fluxes (Mannino et al., 2008). OCRS (see also **chapter 2.2.3**) uses an empirical relationship between CDOM absorption and DOC

concentration, which are simultaneously measured in situ. However, this relationship needs to be adapted to regional and temporal settings (a topic further discussed in **chapter 3**, **chapter 4** and **chapter 5**).

Most commonly, CDOM absorption is defined through an absorbance $A(\lambda)$ term, which is measured by a spectrophotometer. The absorbance is the ratio of incident to transmitted spectral radiant power through a sample across the path length L and can be used to calculate the Napierian (natural logarithm) absorption coefficient $a_{CDOM}(\lambda)$:

$$a_{CDOM}(\lambda) = \frac{2.303 * A(\lambda)}{L}. \qquad \text{(Equation 2.4)}$$

Depending on the expected concentration of organic matter or the transparency of the sample, usually 1, 5 or 10 cm quartz cuvettes are used to measure CDOM absorbance. The spectral shape of $a_{CDOM}(\lambda)$ is most commonly described by an exponential model:

$$a_{CDOM}(\lambda) = a_{CDOM}(\lambda_0) * e^{-S(\lambda-\lambda_0)}, \qquad \text{(Equation 2.5)}$$

where $a_{CDOM}(\lambda_0)$ is the absorption coefficient at reference wavelength λ_0 and S is the spectral slope of $a_{CDOM}(\lambda)$ for the chosen wavelength range (**Figure 2.7**).

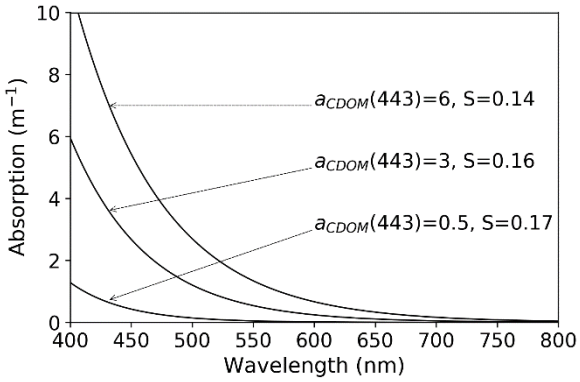

Figure 2.7: Three examples of $a_{CDOM}(\lambda)$ spectra that are modelled using Equation 2.5 and given $a_{CDOM}(443)$ and S.

Chemical characteristics of terrestrial DOM are distinctively different from the characteristics of DOM produced by aquatic organisms (Stedmon and Nelson, 2015). These differences allow the use of various parameters of CDOM absorption (such as the spectral slope of $a_{CDOM}(\lambda)$ at different wavelengths, the ratio of spectral slopes, and DOC-normalized absorbance (specific ultraviolet absorbance - SUVA)) to derive the chemical characteristics, the origin of DOM and degradation processes that have altered it (Weishaar et al., 2003; Helms et al., 2008; Fichot and Benner, 2012). Parameters of CDOM absorption are further discussed in **chapter 3** and **chapter 4**. CDOM not only absorbs but also emits

light as fluorescence, which can be used to detect different fluorophores and, thus, sources of DOM. Using Parallel Factor Analysis (PARAFAC), independent DOM components can be differentiated with a spectrophotometric measured excitation-emission matrix (EEM) of DOM fluorescence (FDOM) (Stedmon et al., 2003; Stedmon and Bro, 2008). Besides CDOM absorption, a number of other IOPs contribute to the total scatter and absorption (Equation 2.3 and Equation 2.4) that control the propagation of light in the water and changes its intensity and spectral composition (Werdell et al., 2018). The absorption by Non-Algal Particles (NAP) is spectrally very similar to CDOM absorption (**Figure 2.8**) and is often described in combination with CDOM. This combination is termed absorption by detrital particulate matter and CDOM: $a_{dg}(\lambda) = a_{NAP}(\lambda) + a_{CDOM}(\lambda)$. Phytoplankton absorption is determined by the composition and concentration of pigments from major algal groups. The dominant group of pigments is composed of the chlorophylls which are typically characterized by absorption peaks in the blue and red parts of the spectrum (**Figure 2.8**). Depending on the relative contributions of the pigment groups, the absorption properties of phytoplankton can vary. Similar to CDOM, chlorophyll has a specific fluorescence peak around 683 nm that offers alternative methods to measure it. Pure water without any of the above-mentioned constituents strongly absorbs light in the UV and NIR parts of the spectrum (**Figure 2.8**).

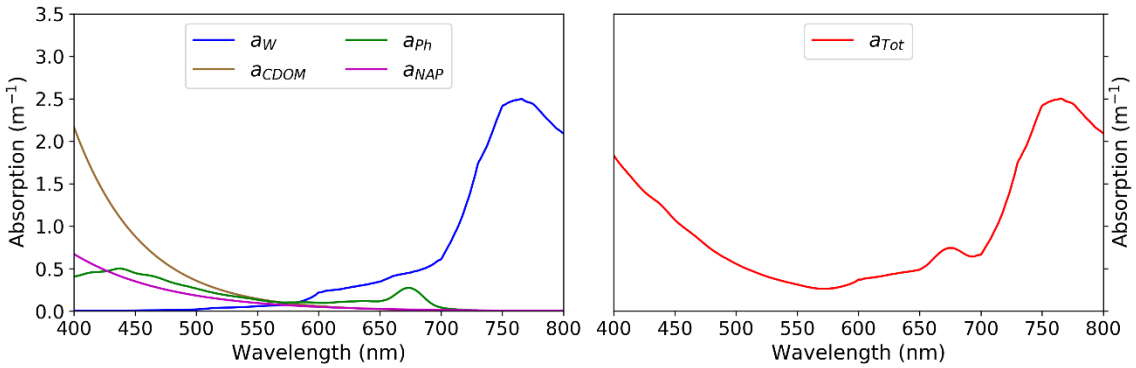

Figure 2.8: Spectral characteristics of absorbing components. Left: Absorption spectra of a_w with temperature=0 °C and salinity=0, $a_{CDOM}(\lambda)$ with $a_{CDOM}(443)$=1 m^{-1} and S=0.018, $a_{Ph}(\lambda)$ with $a_{Ph}(443)$=0.5 m^{-1} and $a_{NAP}(\lambda)$ with $a_{NAP}(443)$=0.4 m^{-1} and S=0.013. Right: Total absorption spectra using Equation 2.2. Concentrations were chosen to agree with a range that is typical of Arctic coastal waters.

The spectral shape of particle scattering (phytoplankton and Non-Algal Particles, that are often combined due to their similar spectral shape to $b_p(\lambda)$) varies depending on particle type, shape and size. However, in forward models the spectral dependency of scattering is commonly described as:

$$b_p(\lambda) = \lambda^{-S_{bp}}. \qquad \text{(Equation 2.6)}$$

Spectral scattering by pure water $b_w(\lambda)$ is known from lab experiments and often further estimated as a function of physical properties of ocean water: temperature and salinity.

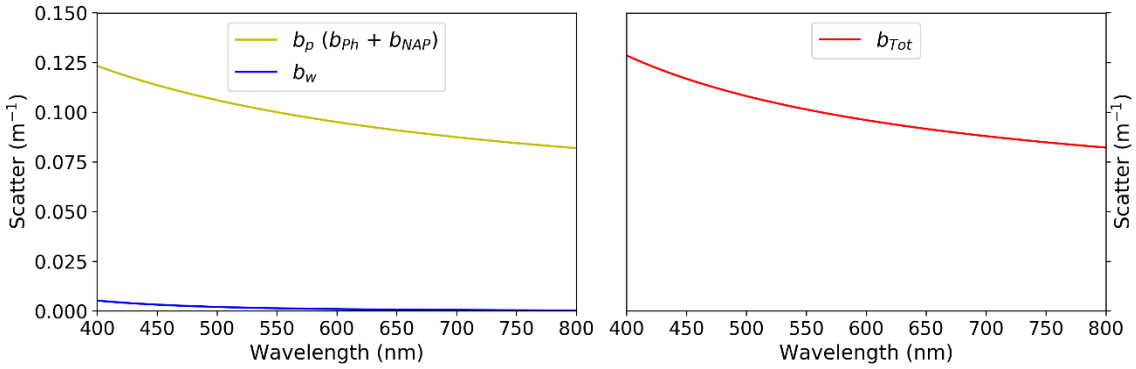

Figure 2.9: Spectral characteristics of scattering components. Left: Scattering by particles (yellow) that is a combination of 50% spectrally flat scatterer and 50% blue scatterer with *bp*(555)=0.05 m^{-1} and S=1.2 and by pure water (blue, temperature=0 °C, salinity=0). Right: Total scattering as the sum of *bp*(λ) and *bw*(λ) (Equation 2.3). Concentrations were chosen to agree with a range that is typical of Arctic coastal waters.

The angular distribution of light scattering depends on the volume scattering function (VSF). The first widely used VSF measurements were described by (Petzold et al., 1972). During the last decade, prototype sensors have been capable of measuring the VSF over broad angular ranges (Slade and Boss, 2006; Zhang et al., 2013; Hu et al., 2019).

2.2.3 From AOPs to IOPs

OCRS measures Apparent Optical Properties (AOPs), which depend on the medium (IOPs, **chapter 2.2.2**) and the surrounding light field, which can be measured. The AOP remote sensing reflectance R_{rs} (λ; sr^{-1}) contains the spectral colour information of the water. It is defined as the ratio between water-leaving radiance (L_w) and downwelling irradiance (E_d). R_{rs} is the most common AOP used for the retrieval of IOPs.

To detect in-water optically-active constituents with a satellite sensor, the inverse problem of relating the observed quantity (R_{rs}) to a set of unknown variables of interest (IOPs) needs to be solved with an appropriate forward model. Multiple combinations of IOPs with varying intensities can result in the same R_{rs} spectrum, imposing a major challenge to solving the inverse problem (Sydor et al., 2004; Defoin-Platel and Chami, 2007). The choice of a forward model and the methodology to solve the inverse problem strongly depends on the water type. Historically, water types in OCRS are often divided into “Case 1” and “Case 2” waters. Case 1 waters are primarily determined by the optical properties of phytoplankton and minor CDOM and NAP products related to it. Case 2 waters are optically-complex waters which combine all other types of waters, in which optical

properties are determined by other constituents. Case 1 and Case 2 waters differ in their optical complexities and require different methodologies to achieve the best results.

There are two main forward modelling approaches to relate R_{rs} to IOPs: 1) quasi-single scattering approximations (QSSA) (Gordon, 1973) and (2) radiative transfer simulations (Fischer and Grassl, 1984; Mobley et al., 1993). While radiative transfer quantifies the fate of the incident downwelling photon flux and its interaction with optically active constituents (such as CDOM, chlorophyll, etc.), the quasi-single scattering approximation is a simplified analytical model that relates R_{rs} to a function of IOPs. Further, three most common solution methods are used to quantify the IOPs: 1) Semi-analytical inversion approaches that use a combination of empirical assumptions and relations known from radiative transfer; 2) Look-up-table approaches that use a forward modelled databases of R_{rs} based on specific IOPs, which are then used to retrieve IOPs from remotely sensed R_{rs}; 3) empirical approaches that use large sets of in situ or simulated databases and apply statistical methods (e.g. regressions, machine learning algorithms or neural networks) to relate R_{rs} to IOPs. Until recently, computational power was a crucial limiting factor for the application of these methods on big data volumes. Therefore, most commonly used OCRS retrieval algorithms are semi analytical approaches, such as the "GSM" (Maritorena et al., 2002), "gsmA" (Matsuoka et al., 2013) and "QAA" (Lee et al., 2002) employed the QSSA (Werdell et al., 2018) described as:

$$u(\lambda) = \frac{b_{Tot}(\lambda)}{a_{Tot}(\lambda) + b_{Tot}(\lambda)}, \qquad \text{(Equation 2.7)}$$

where $u(\lambda)$ can then be related to $r_{rs}(\lambda)$ with a formula by (Gordon et al., 1988):

$$r_{rs}(\lambda) = \sum_{i=1}^{2} G_i(\lambda) * [u(\lambda)]^i, \qquad \text{(Equation 2.8)}$$

where G_i are coefficients that represent the illumination conditions, geometry, sea surface properties, and the shape of the marine VSF (e.g. Gordon et al., 1988; Lee et al., 2002).

Further, $r_{rs}(\lambda)$ can be calculated from $R_{rs}(\lambda)$, observed by a satellite instrument, using the relationship by (Lee et al., 2002):

$$r_{rs}(\lambda) = \frac{R_{rs}(\lambda)}{0.52 + 1.7 R_{rs}(\lambda)}, \qquad \text{(Equation 2.9)}$$

where the numerical coefficient 0.52 accounts for the changes of radiance and irradiance transmittance from below to above the water surface including the refractive index of water. The coefficient 1.7 accounts for the ratio of upwelling irradiance to upwelling radiance

evaluated below the surface (Lee et al., 2002). **Figure 2.10** shows three examples of $R_{rs}(\lambda)$ that are representative of river, coastal and offshore waters in the Arctic. The three $R_{rs}(\lambda)$ were simulated using QSSA, Equation 2.7 to Equation 2.9, and given IOPs.

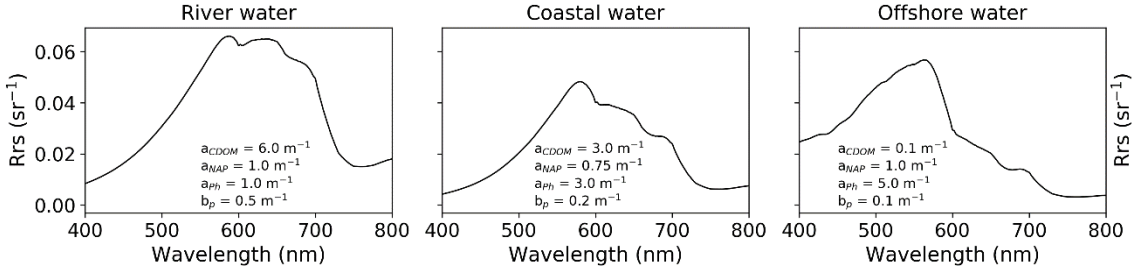

Figure 2.10: Remote Sensing Reflectance for three different water types that are relevant for this thesis. The spectra were simulated using the IOP forward model using Equation 2.7 to 2.9. IOP input values are displayed within the graphs.

Recently, an increasing amount of methodologies, other than QSSA, have been developed to retrieve IOPs. Retrieval algorithms such as the MERIS Case-2 water algorithms (Doerffer and Schiller, 2007), C2RCC (Brockmann et al., 2016) or ONNS (Hieronymi et al., 2017) apply neural networks. The use of neural network algorithms has recently increased and proven to produce reasonable approximations of IOPs in optically complex (Case-2) waters (D'Alimonte and Zibordi, 2003; Bricaud et al., 2007; Jamet et al., 2012; D'Alimonte et al., 2016). Artificial neural networks represent a regression technique to parameterize the relationship between the reflectance and the IOPs.

To retrieve the concentration of biogeochemical constituents, empirical relationships between IOPs and concentration of biogeochemical parameters, both measured in situ, are used. Particulate backscatter ($b_p(\lambda)$, m^{-1}), for example, is often used to determine the concentration of suspended particle matter in the water column (SPM, mg L^{-1}) and phytoplankton absorption (a_{Ph}, m^{-1}) is used to estimate chlorophyll concentration (mg L^{-1}). The relationship between CDOM absorption (a_{CDOM}) and DOC concentration (mg L^{-1}) can be applied in river-influenced waters. Robustness of the relationship and its regional variations, as well as factors influencing these variations, are discussed in **chapter 3**, **chapter 4** and **chapter 5** of this thesis.

2.2.4 Limitations of Ocean Colour Remote Sensing

Even though the application of OCRS holds great advantages compared to solely in situ sampling, it has a number of limitations, that are, in part, specific to polar regions. A general limitation of passive optical OCRS is the penetration depth of the natural sunlight in water, which is especially low in turbid waters. The penetration depth of light defines the water

depth to which the satellite sensor effectively “sees”. For turbid Arctic coastal waters, the depth layer that is captured by optical satellite sensors is often less than one meter. Properties of deeper water masses cannot be retrieved with classical OCRS. Active remote sensing techniques such as LiDAR remote sensing show potential for detection of subsurface water properties (Lu et al., 2014; Schulien et al., 2017). Polar night is another limitation for passive optical remote sensing, which requires sunlight. Even during the summer, sun elevation in polar regions is often too low for the application of the developed atmospheric correction algorithms, which are also often not evaluated for low sun elevation. Another major OCRS limitation is the presence of clouds, fog and ice cover. In Arctic seas, cloud cover can be widespread and persistent, especially in the summer months. The presence of clouds generally increases with rising temperatures in the Arctic (Schweiger, 2004; He et al., 2019). Fog often develops during the ice melt period when cold open water directly comes into contact with the atmosphere. Sea ice shields the water surface and, therefore, impedes the use of OCRS. Furthermore, near sea ice, OCRS often suffers from the so-called adjacency effect, which is a radiance contamination from neighbouring ice and water with distinctly different reflectance. Whereas sea ice covers the central Arctic Ocean throughout the entire year, coastal waters are typically ice-free between June and October. With progressing sea ice decline, OCRS will likely become applicable in more areas of the Arctic Ocean and during longer periods. Furthermore, increasing frequency of satellite acquisitions raise the chance to overcome cloud and ice cover limitations (**Figure 2.11**).

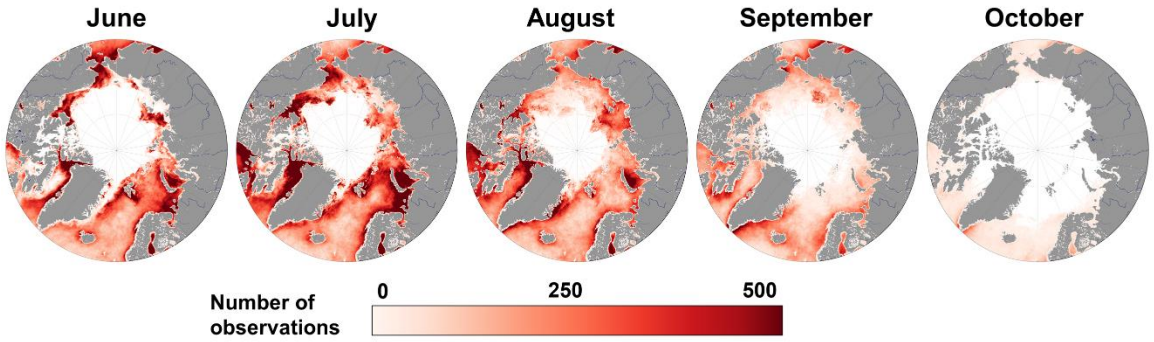

Figure 2.11: Mean number of cloud and ice-free observations from June to October between 2009 and 2019 acquired by four polar orbiting optical satellite sensors (MERIS, Aqua-MODIS, SeaWiFS and VIIRS). Large white areas in the central part of the Arctic Ocean are sea ice. Data from globally merged Ocean Colour CCI v. 4.2 (https://esa-oceancolour-cci.org/).

The use of OCRS in coastal waters of the Arctic Ocean is fraught with pitfalls, due to the optical complexity and spatially and temporally changing applicability of OCRS algorithms. Turbulent and complex combinations of different optically-active constituents

strongly complicate the discrimination of the individual IOPs. Optical dominance of one constituent can hide and superpose the optical properties of other constituents (**Figure 2.12**).

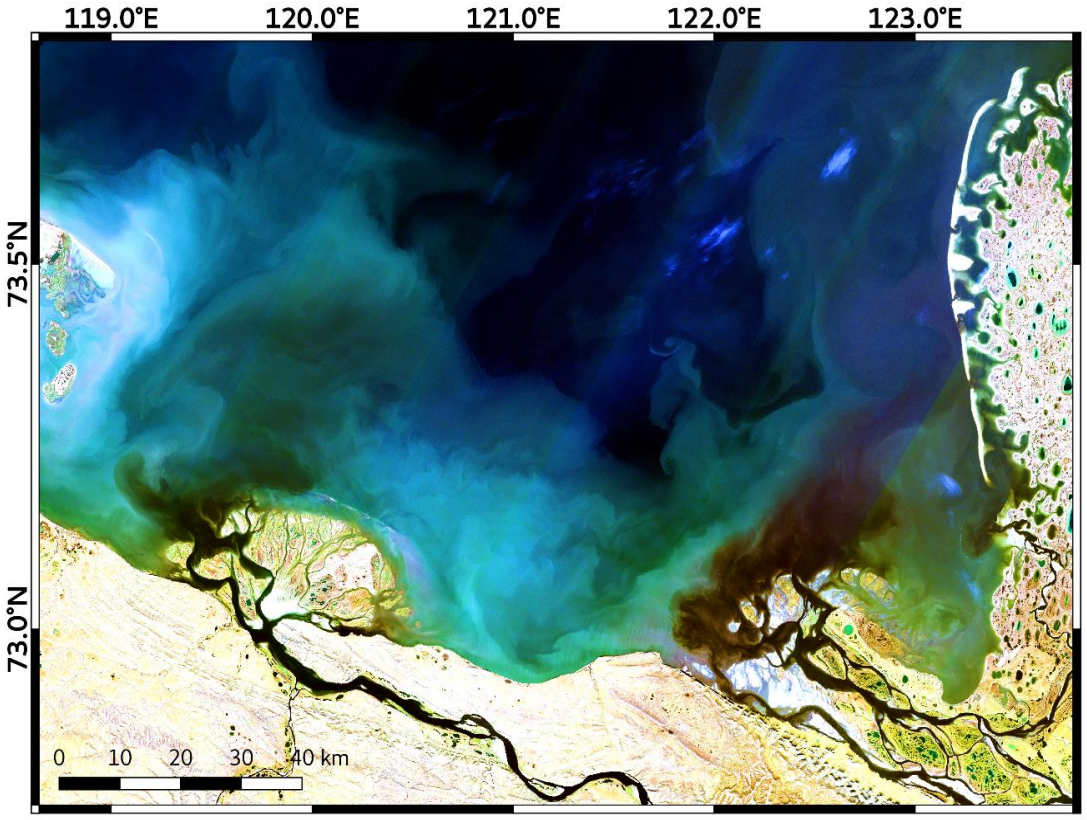

Figure 2.12: True colour satellite image (Sentinel 2 MSI) of the Olenek Delta (left) and the western part of the Lena River Delta (right) showing the export of dark organic matter rich waters to the Arctic Ocean. River channels are clearly visible by their black colour. Bright lighter colours indicate waters where backscattering from sediment particles dominate over absorption by organic matter.

Compared to the global ocean, Arctic coastal waters near river mouths are characterized by extreme ranges of IOPs. Specific algorithms developed and validated for different water types can fail in these extreme ranges. Often, atmosphere correction algorithms fail or provide false results in extremely turbid waters. Turbid waters also can be erroneously masked as clouds. Therefore, atmospheric corrections and in-water retrieval algorithms, which are perfectly functional in the open ocean waters require careful evaluation before being applied in coastal and river-influenced waters

Chapter III

Identifying drivers of seasonality in Lena River biogeochemistry and dissolved organic matter fluxes

https://doi.org/10.3389/fenvs.2020.00053

3 Identifying drivers of seasonality in Lena River biogeochemistry and dissolved organic matter fluxes

B. Juhls[1], C. A. Stedmon[2], A. Morgenstern[3], H. Meyer[3], J. Hölemann[4], B. Heim[2], V. Povazhnyi[5], P. P. Overduin[3]

[1]Institute for Space Sciences, Department of Earth Sciences, Freie Universität Berlin, Berlin, Germany

[2]National Institute of Aquatic Resources, Technical University of Denmark, Copenhagen, Denmark

[3]Alfred Wegener Institute, Helmholtz Centre for Polar and Marine Research, Potsdam, Germany

[4]Alfred Wegener Institute, Helmholtz Centre for Polar and Marine Research, Bremerhaven, Germany

[5]Otto Schmidt Laboratory for Polar and Marine Research, Arctic and Antarctic Research Institute, St. Petersburg, Russia

Citation: Juhls, B., Stedmon, C. A., Morgenstern, A., Meyer, H., Hölemann, J., Heim, B., Povazhnyi, V., and Overduin, P. P. (2020). Identifying Drivers of Seasonality in Lena River Biogeochemistry and Dissolved Organic Matter Fluxes. *Frontiers in Environmental Science, 8, 53.*

3.1 Abstract

Warming air temperatures, shifting hydrological regimes and accelerating permafrost thaw in the catchments of the Arctic rivers is affecting their biogeochemistry. Arctic rivers monitoring is necessary to observe changes in the mobilization of dissolved organic matter (DOM) from permafrost. The Lena River is the second largest Arctic river and 71% of its catchment is continuous permafrost. Biogeochemical parameters, including temperature, electrical conductivity (EC), stable water isotopes, dissolved organic carbon (DOC) and absorption by coloured dissolved organic matter (a_{CDOM}) have been measured as part of a new high-frequency sampling program in the central Lena River Delta. The results show strong seasonal variations of all biogeochemical parameters that generally follow seasonal patterns of the hydrograph. Optical indices of DOM indicate a trend of decreasing aromaticity and molecular weight from spring to winter. High-frequency sampling improved our estimated fluvial flux of annual dissolved organic carbon flux (6.79 Tg C).

EC and stable isotope data were used to distinguish three different source water types which explain most of the seasonal variation in the biogeochemistry of the Lena River. These water types match signatures of (1) melt water, (2) rain water and (3) subsurface water. Melt water and rain water accounted for 84% of the discharge flux and 86% of the DOC flux. The optical properties of melt water DOM were characteristic of fresh organic matter. In contrast, the optical properties of DOM in subsurface water revealed lower aromaticity and lower molecular weights, which indicate a shift towards older organic matter source mobilized from deeper soil horizons or permafrost deposits. The first year of this new sampling program sets a new baseline for flux calculations of dissolved matter and has enabled the identification and characterization of water types that drive the seasonality of the Lena River water properties.

3.2 Introduction

The current warming of the Siberian Arctic (Richter-Menge et al., 2019) is causing intense changes in atmospheric forcing, precipitation, subsurface water storage and runoff from rivers to the Arctic Ocean (Yang et al., 2002; Velicogna et al., 2012; Bintanja and Selten, 2014; Niederdrenk et al., 2016). A number of studies report an increase of runoff from the Eurasian Arctic rivers (Peterson, 2002; McClelland et al., 2006; Shiklomanov and Lammers, 2009). Of all Arctic rivers, the Lena River is the second largest in annual discharge. Its annual discharge increased by 15.6% since 1936 (Ye et al., 2003; Shiklomanov, 2010), which may primarily be due to a winter discharge increase by 93% (Tananaev et al., 2016). Furthermore, increasing Lena River temperature (Yang et al., 2002; Liu et al., 2005) leads to more intense thermal erosion along the river shores and the coast of the Laptev Sea (Aré, 1988; Bareiss and Görgen, 2005), warms the surface waters of the central Laptev Sea, and accelerates thawing of newly formed subsea permafrost (Angelopoulos et al., 2019). A change of the river discharge, as well as changes of temperature and biogeochemical properties of river water, can strongly affect the physical state of the Arctic Ocean and marine ecosystems, especially in coastal waters. Increased export of dark, organic-rich river water leads to stronger absorption of sunlight and an increased heat flux, which can, in turn, contribute to sea ice decline (Pegau, 2002; Hill, 2008).

The carbon reservoirs of Arctic river watersheds are currently in transition. Thawing permafrost is releasing previously stored carbon (Schuur et al., 2015; Plaza et al., 2019; Turetsky et al., 2019) and increasing seasonal growth of vegetation (Schuur et al., 2009;

Keuper et al., 2012). Both of these processes will increase the particulate and dissolved organic matter flux into rivers and the fluvial flux to coastal waters (Frey and Smith, 2005). Hydrological flow paths will shift towards increased groundwater flow and affect the source and composition of dissolved organic matter (DOM) (Amon et al., 2012). While particulate material is mostly deposited in shelf sea sediments to become mineralised or buried (Charkin et al., 2011; Wegner et al., 2013), dissolved organic matter is exported offshore into the open Arctic Ocean (i.e. Juhls et al., 2019) and approximately 50% is thought to be exported onwards to the Atlantic (Granskog et al., 2012). Most of the DOM transported by the Lena River originates from leaching of surface soils of dominantly boreal forest vegetation (Amon et al., 2012; Kaiser et al., 2017b). However, the effect of ongoing permafrost thaw on hydrological pathways will affect DOM fluxes (Freeman et al., 2001; Frey and Smith, 2005). In addition to the amount of DOM, its composition, source and age in the Lena River are expected to change (Amon et al., 2012; Walker et al., 2013; Mann et al., 2016; Wild et al., 2019).

Initiation of the pan-Arctic River sampling programs PARTNERS (2003-2007), Student Partners (2004-2009) and ArcticGRO (since 2009), have provided invaluable insights into the quantitative and qualitative properties of dissolved and particulate matter exported into the Arctic Ocean (Raymond et al., 2007; Holmes et al., 2008; Stedmon et al., 2011; Amon et al., 2012; Mann et al., 2016). Results of PARTNERS and ArcticGRO (Raymond et al., 2007) show that the Lena River contributes 20 - 29% of the total circumpolar fluvial dissolved organic carbon (DOC) export to the Arctic Ocean. However, reported estimates of annual Lena River DOC fluxes span a wide range between 3.6 Tg C (Gordeev and Kravchishina, 2009) and 7.67 Tg C (Kicklighter et al., 2013). This is likely because the calculation of annual flux is based on a few water samples per year, which are usually taken during open water season (Raymond et al., 2007; Stedmon et al., 2011; Holmes et al., 2012b). Such estimates are susceptible to systematic biases: limited sampling can miss seasonal peaks of DOC concentration and lead to subsequent underestimation of the DOC flux (Jollymore et al., 2012). Furthermore, samples from the Lena River are mostly taken in Zhigansk, which is located ~800 km upstream of the river mouth (**Figure 3.1**). Little is known about DOM transformation, mineralisation and release to the atmosphere on the way from Zhigansk to the river mouth (Amon et al., 2012). In order to identify a trend in DOC flux, it is crucial to reduce uncertainty in the calculated annual flux to below the interannual variability. While most research attention has focussed on potential long-term

trends of river DOC export (Kicklighter et al., 2013; Tank et al., 2016), seasonal variations of ice break-up and freeze-up timing and the associated discharge, material load and biogeochemistry are also affected by the changing climate and require research attention. Earlier spring ice break-up and later freeze-up in fall result in longer open water and shorter winter flow periods and will have an impact on the annual organic matter flux. Monitoring river water biogeochemistry may provide insights into the progress of this change, since the river water chemistry, measured near its mouth, integrates the changes occurring in the catchment as a whole. DOM fluxes and composition can be expected to change and this will also ultimately influence the fate of terrestrial carbon in the Arctic, including that carbon stored in shelf sediments, mineralised in the Arctic, and exported to the north Atlantic Ocean.

To accurately capture short-term variability and understand how changing climate influences in-river processes that affect organic matter quality and its function in the fluvial ecosystem, it is necessary to monitor water constituents with a high temporal resolution and throughout the whole season (including both open water and ice-covered periods). To characterize fluxes from land to sea, this should be done as close as possible to the river mouth. Such sampling, carried out over multiple years, can enable prediction of future responses of river flux to projected change. The Research Station Samoylov Island provides an opportunity to meet these criteria in the central Lena River Delta as it serves as the basis for regular, frequent and year-round sampling for major biogeochemical parameters. The goal of this study is to better understand and decipher seasonal variations of hydrochemical characteristics and organic matter and its optical properties of the Lena River. We aim to identify how changing water sources drive seasonal changes in fluvial biogeochemistry by putting such a sampling program into place over one year at the Research Station Samoylov Island. With this, we provide a basis for future trend analyses and remote sensing studies that may be used to upscale observations from the hydrographic point scale.

3.3 Material and methods

3.3.1 Study area and sample collection

The Lena watershed area (2.61×10^6 km^2) extends ~2400 km from north to south and is underlain by all types of permafrost: continuous (70.5%), discontinuous (10.6%), sporadic (6.0%) and isolated (7.3%). 5.6% of the watershed, on the northern side of the Lake Baikal, is free of permafrost (numbers calculated using permafrost zones by Obu et al. (2019). The

catchment is dominantly covered by forest (72.1%) and shrubland (12.5%) (Amon et al., 2012).

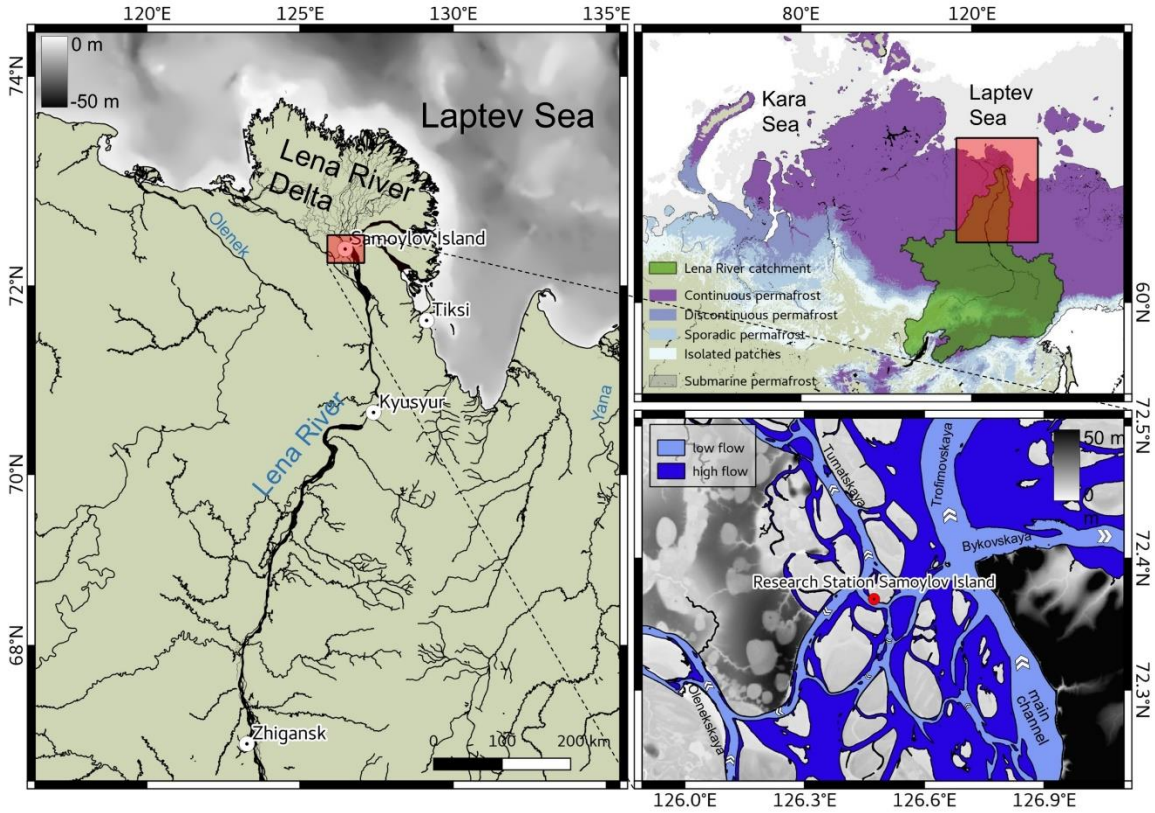

Figure 3.1: Lena River Delta region. The upper right panel shows an overview map of the study area with permafrost zones (Obu et al., 2019; Overduin et al., 2019). The left panel shows the northern part of the Lena River catchment with the Lena River Delta at the coast of the Laptev Sea. The lower right panel the central Lena River Delta with the location of the Research Station Samoylov Island and the Lena River channels (blue) and flow directions; DEM is based on ArcticDEM (Porter et al., 2018). Dark blue indicates Lena River channels during high flow right after spring ice break-up and light blue indicates Lena River channels during low flow in late summer (based on Sentinel 2 imagery, (Copernicus Open Access Hub)).

We collected water samples from the river surface in the centre of the Olenekskaya Channel near Samoylov Island using a pre-rinsed HDPE 1 L bottle (in summer) or a UWITEC 1 L water sampler (under ice) for one year beginning in April 2018 (**Figure 3.1**). The island is located in the central Lena River Delta and hosts a permanently staffed research station (Research Station Samoylov Island), which has been operating since 2013. Additional sample sets with higher temporal resolution, from different years and from Lena River ice, are listed in **Table 3.1**. During the open water period (May 28, 2018 to October 22, 2018), water was sampled from a small boat, and during ice-covered period (until May 27, 2018 and from October 23, 2018), through a hole drilled through the river ice. Two samples during the river ice break-up as well as four samples during the ice freeze-up in October were taken from the shore due to the inaccessibility of a more centered location on the river

channel. Water samples were subsampled, filtered and conserved at the research station directly after sampling.

Table 3.1: Sampling period, frequency, sample type and measured parameters of datasets used in this study.

Dataset	Location	Period	Type	Frequency	No. of samples	Parameters
This study	Samoylov Island	April 20, 2018 - April 6, 2019	water samples	~ every 4 days	75	DOC, a_{CDOM}, stable H_2O isotopes, cations & anions, EC
This study	Samoylov Island	July 4, 2018 - July, 15 2018	water samples	2 times per day	23	DOC and a_{CDOM} (using different filter types and filter pore sizes), stable H_2O isotopes, EC
This study	Samoylov Island	May 4, 2018	ice core samples	1 time	1 ice core with 57 subsamples	DOC, a_{CDOM}, stable H_2O isotopes, cations & anions, EC
(Eulenburg et al., 2019)	Samoylov Island	May 22, 2014 – June 19, 2014	water samples	1 to 2 times per day	43	DOC, a_{CDOM}, stable H_2O isotopes, EC
ArcticGRO & Partners (Holmes et al., 2018a, b)	Zhigansk	2002 – 2019	water samples	up to 6 per year	64	DOC, a_{CDOM}, stable H_2O isotopes

Sampling started on April 20, 2018 at a frequency of ~4 days and is ongoing. For this study, we use a dataset of almost one complete year (until April 6, 2019). For each sample, in situ temperature and electrical conductivity (EC) were measured using a hand-held conductivity meter (WTW COND 340I, accuracy ± 0.5%). For all samples, a series of biogeochemical parameters were analysed (**Table 3.1**). The EC was additionally re-measured on each sample in the lab using a hand-held conductivity meter (WTW Multilab 540, accuracy ± 0.5%) after transport to Germany. For 11 days, from July 4, 2018 to July 15, 2018, samples were taken at a higher frequency and for additional parameters (**Table 3.1**). The data sets used here are available online (https://doi.org/10.1594/PANGAEA.913196, https://doi.org/10.1594/PANGAEA.913279).

3.3.2 Discharge

The discharge of the Lena River is monitored by the Russian Federal Service for Hydrometeorology and Environmental Monitoring (Roshydromet) and data are available at www.r-arcticnet.sr.unh.edu (Shiklomanov, 2010, 1936 to 2009) and www.arcticgreatrivers.org (Shiklomanov et al., 2018, 1999 to present). All discharge data shown in this study were corrected for the distance difference between the gauge station at

Kyusyur and water sampling station at Samoylov Island (~220 km) using a Lena River propagation speed estimate (88 km d^{-1}) from Smith and Pavelsky (2008).

3.3.3 Biogeochemical parameters

For each sample of the Lena River monitoring program, 1 L of surface river water was collected and subsequently subsampled. For DOC and CDOM absorption (a_{CDOM}), the sample was filtered through a 0.45 µm cellulose acetate filter which had been rinsed with 20 mL sample water. Over 10 days in July 2018, additional filter type and pore size tests for DOC and a_{CDOM} were carried out (**Appendix Figure 1**). DOC samples were filled into a pre-rinsed 20 mL glass vial and acidified with 25 µL HCl Suprapur (10 M) and stored in the dark at 4 °C. After transport, DOC samples were analysed at the Alfred Wegener Institute Helmholtz Centre for Polar and Marine Research (AWI), Potsdam, Germany. DOC concentrations were analysed using high temperature catalytic oxidation (TOC-VCPH, Shimadzu). Three replicate measurements of each sample were averaged. After every ten samples, a blank (Milli-Q water) and a standard was measured. Eight different commercially available certified standards cover a range between 0.49 mg L^{-1} (DWNSVW-15) and 100 mg L^{-1} (Std. US-QC). The results of standards provide an accuracy better than ± 5%.

a_{CDOM} samples were collected in pre-rinsed 50 mL amber glass bottles that were stored in the dark at 4 °C until analysis. a_{CDOM} was measured at the Otto Schmidt Laboratory for Polar and Marine Research (OSL), Saint Petersburg, Russia using a SPECORD 200 spectrophotometer (Analytik Jena) and at the German Research Centre for Geosciences (GFZ), Potsdam, Germany using a LAMBDA 950 UV/Vis (PerkinElmer). The median absorbance (A_λ) of three replicate measurements was used to calculate the $a_{CDOM}(\lambda)$:

$$a_{CDOM}(\lambda) = \frac{2.303 * A_\lambda}{l}, \qquad \text{(Equation 3.10)}$$

where l is the path length (length of cuvette). Fresh Milli-Q water was used as reference. To detect chemical composition and molecular structure of the DOM, two optical indices, SUVA and S275-295, were used. Both indices correlate with aromaticity and molecular weight of bulk DOC (Weishaar et al., 2003; Helms et al., 2008). SUVA (m^2 g C^{-1}) was calculated by dividing the decadal absorption A/l (m^{-1}) at 254 nm by DOC concentration (mg L^{-1}). The spectral slope of $a_{CDOM}(\lambda)$ between 275 and 295 nm (S275-295) is an index

for photodegradation (Helms et al., 2008). S275-295 was calculated by fitting a regression for the wavelength ranges 275 to 295 nm to the exponential function (Helms et al., 2008):

$$a_{\mathrm{CDOM}}(\lambda) = a_{\mathrm{CDOM}}(\lambda_0) * e^{-S(\lambda-\lambda_0)}, \qquad \text{(Equation 3.11)}$$

where $a_{\mathrm{CDOM}}(\lambda_0)$ is the absorption coefficient at reference wavelength λ_0 and S is the spectral slope of $a_{\mathrm{CDOM}}(\lambda)$ for the chosen wavelength range.

Water samples for stable isotopes were collected untreated in 10 mL HDPE vials, sealed tightly, stored in the dark at 4 °C. Measurements were conducted at the laboratory facility for stable isotopes at AWI Potsdam using a Finnigan MAT Delta-S mass spectrometer equipped with equilibration units for the online determination of hydrogen and oxygen isotopic composition. The data is given as δD and $\delta^{18}O$ values, which is the per mille difference to standard V-SMOW. The deuterium excess (d-excess) is calculated by:

$$\text{d-excess} = \delta D - 8.* \delta^{18}O. \qquad \text{(Equation 3.12)}$$

The measurement accuracy for hydrogen and oxygen isotopes was better than ±0.8 ‰ and ±0.1 ‰, respectively (Meyer et al., 2000).

Water samples for concentrations of major dissolved components were filtered using a syringe-mounted 0.45 µm CA filter and kept cool and dark until analysis. Concentrations of major anions (SO_4^{2-}, Cl^-, Br^-, F^-, NO^{3-} and PO_4^{3-}) were determined using ion chromatography (Thermo-Fischer ICS 2100; Weiss, 2001). Total dissolved elemental concentrations (for Al, Ba, Ca, Fe, K, Mg, Mn, Na, P, Si and Sr) were measured with inductively coupled plasma optical emission spectroscopy (ICP-OES; Perkin Elmer Optima 8300DV; Boss and Fredeen, 1997).

In addition, one ice core (LE08) was drilled on the river channel at Samoylov Island on 4 May 2018 (**Figure 3.1**). The core was drilled using a Kovacs Mark III and wrapped in HDPE plastic sleeves and stored frozen for transport to AWI Potsdam where further subsampling and analysis were done. The core was retrieved in 5 pieces with a total length of 144 cm, which was close to the ice thickness measured in the borehole. The ice core was cut into 3 cm slices and analysed for DOC, $a_{\mathrm{CDOM}}(\lambda)$, stable oxygen isotopes, cations and anions following the methods described above.

3.3.4 Flux calculations

For visualization, concentrations (C_d) between sampling dates were linearly interpolated. Then, daily fluxes were calculated by multiplying daily concentrations and the daily discharge (Q_d):

$$\text{Flux}_d = C_d \text{ (mg L}^{-1}\text{) x } Q_d \text{ (m}^3 \text{ s}^{-1}\text{) x 86400 s.} \quad \text{(Equation 3.13)}$$

Daily fluxes (Flux_d) were summed for individual periods. The annual heat flux was calculated as in (Liu et al., 2005; Yang et al., 2013) to enable inter-annual comparisons. Negative river water temperatures were set to 0 °C and the specific heat capacity of water was set constant to 4.184 J g^{-1} $°C^{-1}$.

3.3.5 Water source endmember calculation

98% of the variability of all measured parameter can be explained by three components (**Appendix Table 1**). We distinguished three water source fractions using EC and water $\delta^{18}O$ by solving the mass balance equation:

$$f_{EM1} + f_{EM2} + f_{EM3} = 1, \quad \text{(Equation 3.14)}$$

$$f_{EM1}EC_{EM1} + f_{EM2}EC_{EM2} + f_{EM3}EC_{EM3} = EC, \quad \text{(Equation 3.15)}$$

$$f_{EM1}\delta^{18}O_{EM1} + f_{EM2}\delta^{18}O_{EM2} + f_{EM3}\delta^{18}O_{EM3} = \delta^{18}O, \quad \text{(Equation 3.16)}$$

for unknowns, where $f \in [0; 1]$ is the fraction of each water source. We chose endmember for EC and $\delta^{18}O$ values that encompass the overall variability of observed EC and $\delta^{18}O$ (**Table 3.2**).

Table 3.2: Electrical conductivity (EC) and $\delta^{18}O$ for water source endmember

Endmember	EC (µS cm^{-1})	$\delta^{18}O$ (‰)
EM1	80	-25
EM2	100	-16
EM3	600	-22

3.4 Results

The Lena River discharge shows strong seasonality, with low discharge during the ice-covered winter, a spring peak maximum and a moderate summer discharge (**Figure 3.2**). In some years, additional discharge peaks in late summer and fall occur. Over the period from 1936 to 2018, the Lena River's annual discharge increased (1.44 x 10^9 m^3 yr^{-1}), to a large part driven by the increasing winter (November to April) discharge flux

(0.41 x 10^9 m^3 yr^{-1}; **Figure 3.2** inset). Furthermore, trends are clearly visible in the colours of **Figure 3.2**, indicating that river ice breaks up earlier and freezes later in the year.

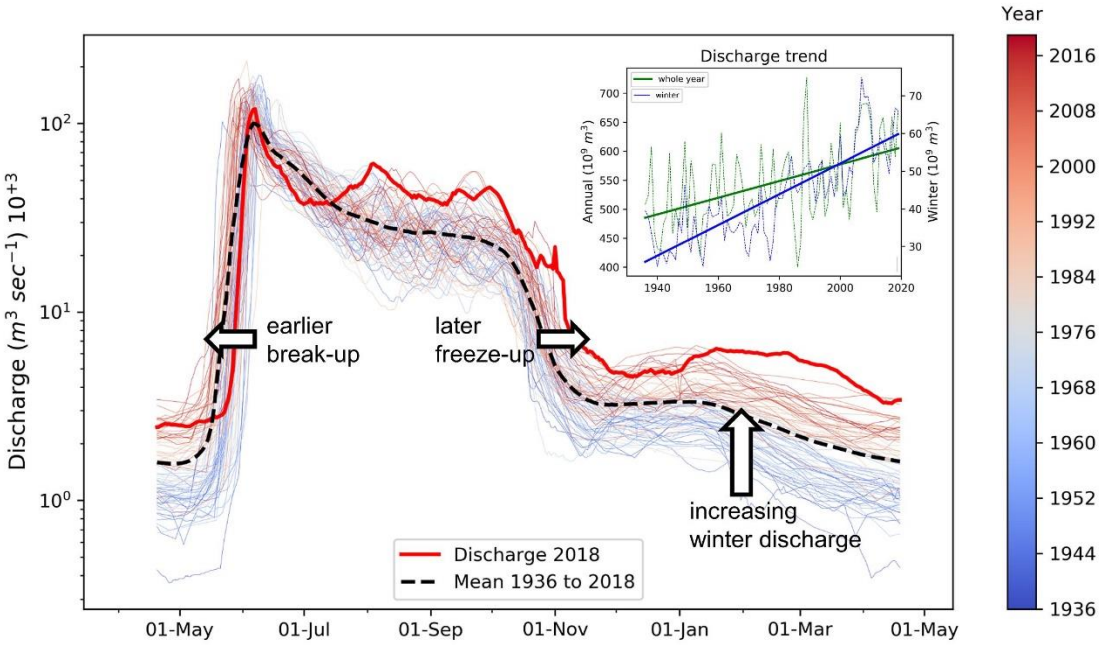

Figure 3.2: Discharge data from Kyusyur station from 1936 to 2018. Colours from blue to red indicate the year from 1936 to 2018. The red thick solid line shows the year 2018 and the black thick dashed shows the mean of the period from 1936 to 2018. The inset figure show the discharge flux for the whole year (green) and for November to April (blue). Discharge data: A.I. Shiklomanov (2010) 1939-2008, ArcticGRO 2009-2019.

Putting the year 2018 into the long-term context, the winter (November to April) and late summer (August to October) discharge were significantly higher than their 1938-2018 means. The timing and intensity of the 2018 spring discharge peak was close to the long-term median. Summer 2018 was also characterized by multiple higher discharge events, which rise above the long-term mean. The elevated discharge continues into the first 3 months of 2019 (dashed line in **Figure 3.3**B and C).

3.4.1 Lena River temperature and chemistry

During the period when the Lena River is ice-covered, the mean river water temperature below the ice is slightly below 0 °C (-0.2 to -0.01 °C; **Figure 3.3**A). During the first days of spring peak discharge, the temperature only marginally increases to 1.5 °C. About 2 weeks after the start of spring peak discharge, the temperature rises within 1 week to a relatively stable summer level around 16 °C. With decreasing air temperatures in fall, the river temperature gradually decreases and reaches 0 °C in mid-October when the Lena River starts to freeze. The highest river water temperature (17.6 °C) was recorded on August 15, 2018. The EC drops almost simultaneously with the onset of the spring peak

discharge from its annual maximum of 490 µS/cm to its annual minimum of 99 µS/cm. The EC is generally low in summer, and gradually increases during the ice-covered period. The summer discharge peaks coincide with decreases in the EC.

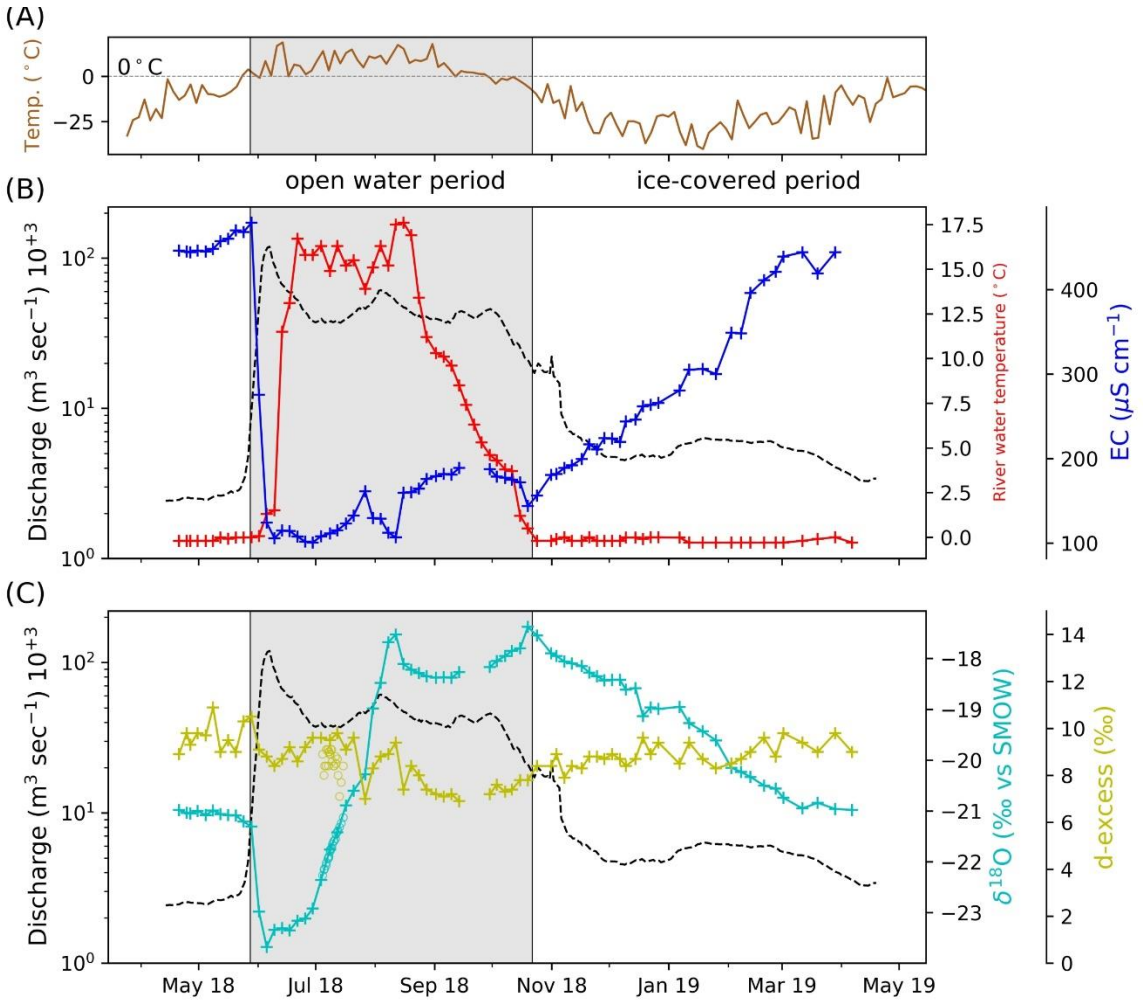

Figure 3.3: Air temperature, measured in Tiksi (A), discharge (black dashed line) (B & C), river water temperature and EC (B) and $\delta^{18}O$ and d-excess (C). The grey area indicates the period where the Lena River channels around Samoylov Island were not ice covered (dates are based on optical satellite imagery). The EC values are those from measurements made in the laboratory following sampling

A strong seasonality in river water $\delta^{18}O$ values was observed, ranging between -17.4 ‰ and -23.7 ‰ in the sampling period. During late winter, when the Lena River ice thickness reached its maximum (March-April), $\delta^{18}O$ was stable at around -21 ‰. The lowest $\delta^{18}O$ values (-23.7 ‰) occurred during the spring freshet in the first days of June, coinciding with the highest discharge. The highest $\delta^{18}O$ (-17.4 ‰) occurred shortly before freeze-up at the end of October. Similarly high $\delta^{18}O$ (-17.5 ‰) occurred during the mid-summer discharge peak. With decreasing discharge and freezing of the Lena River and its catchment, $\delta^{18}O$ gradually decreased towards -21 ‰. d-excess values were highest (+10.9 ‰) during late winter and lowest (+6.9 ‰) in late summer. The d-excess of the

measurements in July 2018 were about 0.5 ‰ lower than long-term values. Additional measurements of $\delta^{18}O$ in July 2018 agreed with the long-term measurements.

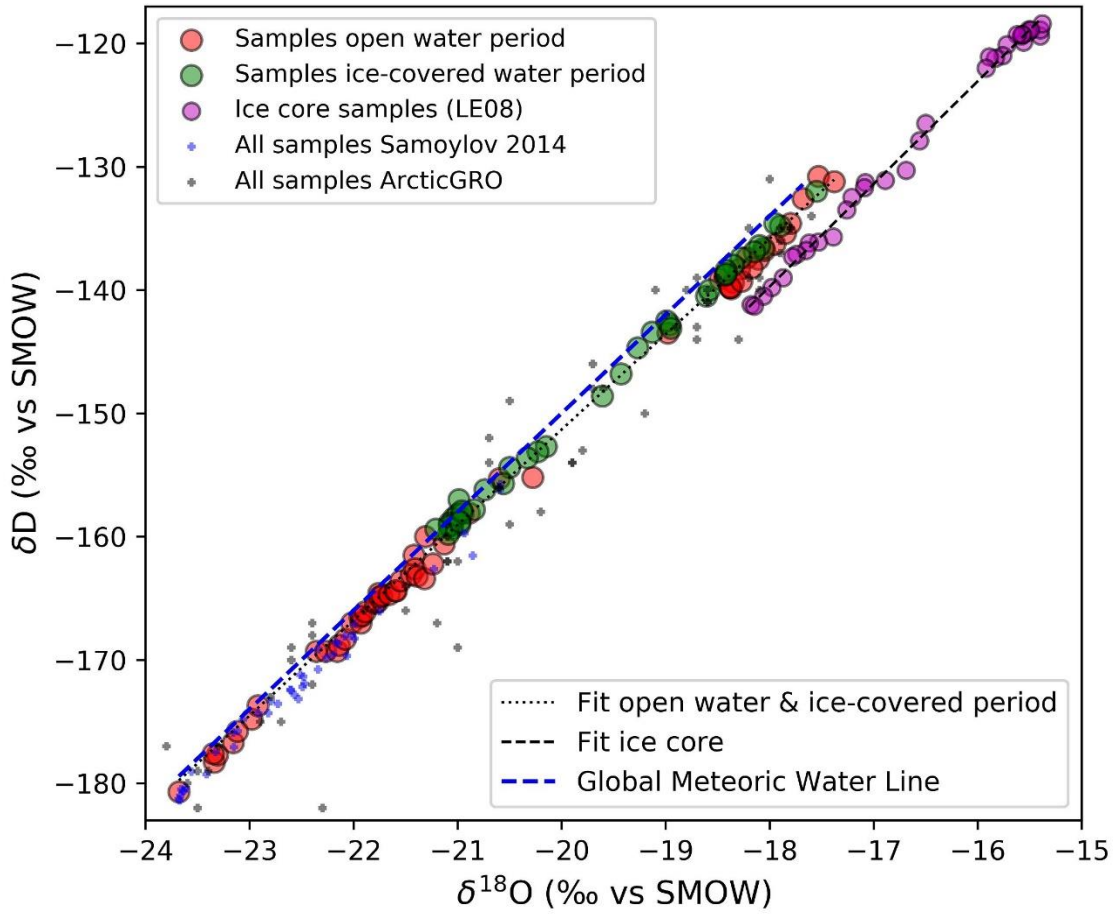

Figure 3.4: Relationship between $\delta^{18}O$ and δD for open water (red) and ice-covered (green) samples. The black dotted line shows the linear regression of samples from open water period (May 28, 2018 to October 22, 2018) and ice-covered period (until May 27, 2018 and from October 23, 2018) combined ($\delta D = 7.73 \times \delta^{18}O + 3.36$). The black dashed line shows the linear regression of ice core samples ($\delta D = 8.33 \times \delta^{18}O + 10.14$). The blue dashed line shows the global meteoric water line after (Craig, 1961). Additional samples from Samoylov 2014 (blue crosses) and ArcticGRO (grey crosses) including samples from the ice-covered period as well as open water period.

For all samples in the Lena River dataset, we observed a very strong relationship (r^2=0.996) between $\delta^{18}O$ and δD (**Figure 3.4**). The slope of the linear regression is lower (7.73) than the Global Meteoric Water Line (slope GMWL=8.0), but almost identical to the Local Meteoric Water Line (the slope of the LMWL is 7.6 for 381 event-based samples, and 7.7 for 41 monthly means; (Spors, 2018)). Lena River ice core samples (LE08) showed overall higher $\delta^{18}O$ and δD than water samples and the regression line showed a clear offset compared to river water samples (**Figure 3.4**). The slope of the linear regression of ice core samples (8.32) was higher than that of Lena River water. Lena River water samples from 2014 were similarly strongly correlated (r^2=0.987) and had a similar slope (7.6) compared

to the Lena River samples from 2018. Both slopes, from 2014 and 2018, are lower, compared to the GMWL. Ice core samples had higher mean $\delta^{18}O$ and δD values, but with a shift to lower δD for similar $\delta^{18}O$.

The concentrations of most of the major cations and anions correlated with the seasonal variability in EC (**Appendix Figure 3**). Whereas concentrations of all ions increased during the ice-covered period, the concentration of K behaved differently, with lower values during January and February 2019. During the ice-covered period, Na and Cl^- dominated, while in summer and during the spring discharge peak, Ca and Cl^- and SO_4^{2-} dominated. Whereas concentrations for some species regained over 50% of their late winter concentration during summer (F^-, Si), others did not increase until mid-winter (Na, Ba, Cl^-, Br^-). The end of the open water period was marked by a small decrease in concentration that lasts for almost 2 weeks for all species. Si concentration was hardly affected by precipitation events during the open water period, in contrast to all other measured concentration (for example, the precipitation peak centered at August 20, 2018). Annual fluxes of major ions are presented in **Table 3.3**. Note that some concentrations fell below analytical detection limits and this prevented a meaningful flux calculation.

3.4.2 Dissolved Organic Carbon (DOC) and Coloured Dissolved Organic Matter (CDOM)

Dissolved organic matter in the Lena River varied with the hydrograph, with DOC concentrations ranging from 4.9 to 18.2 mg L^{-1} and $a_{CDOM}(254)$ ranging from 40.8 to 150.92 m^{-1} (**Figure 3.5**A). Lowest values were observed at the end of winter, right before or with the onset of the spring ice break-up, whereas highest values occurred only a few days later during the spring ice break-up. In summer (July to October) both DOC and $a_{CDOM}(254)$ returned to values near pre-break-up (~6 to 7 mg L^{-1} DOC and ~44 to 50 m^{-1} $a_{CDOM}(254)$) but then increased during the mid-summer discharge peak from 6.2 to 10.2 mg L^{-1} and from 45.3 to 85.6 m^{-1} $a_{CDOM}(254)$. High frequency sampling during July 2018 agreed closely with the overall pattern from the annual sampling (circles in **Figure 3.5**).

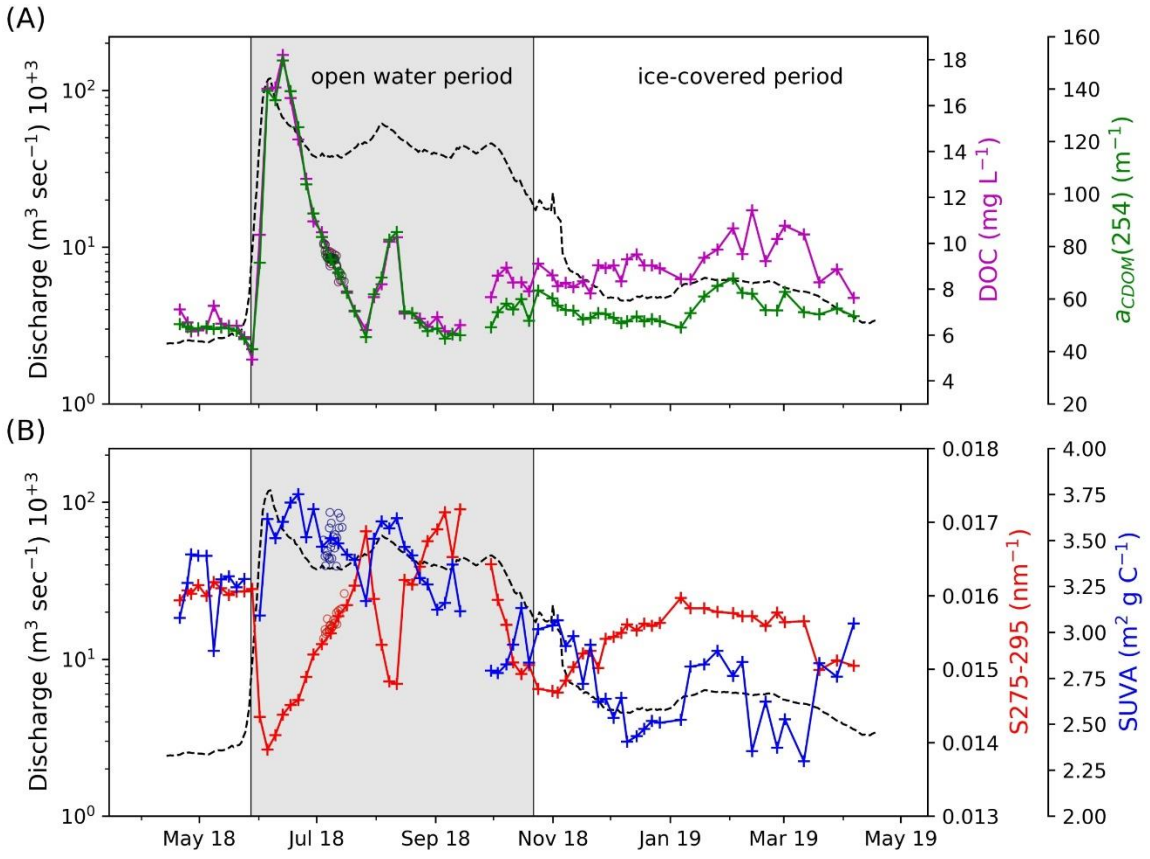

Figure 3.5: Seasonal variation of DOC and $a_{CDOM}(254)$ (A) and S275-295 and SUVA (B). Black dashed line shows the discharge. Circles in respective colours show high frequency measurements from July 2018.

In winter, DOC and $a_{CDOM}(254)$ increased in response to comparatively minor fluctuations in discharge, with winter maximums of 11.4 mg L^{-1} and 67.8 m^{-1}, respectively. DOC and $a_{CDOM}(254)$ in the river ice had means of 1.04 mg L^{-1} DOC and 0.96 m^{-1} $a_{CDOM}(254)$, with no clear systematic vertical trend down core (**Appendix Figure 4**).

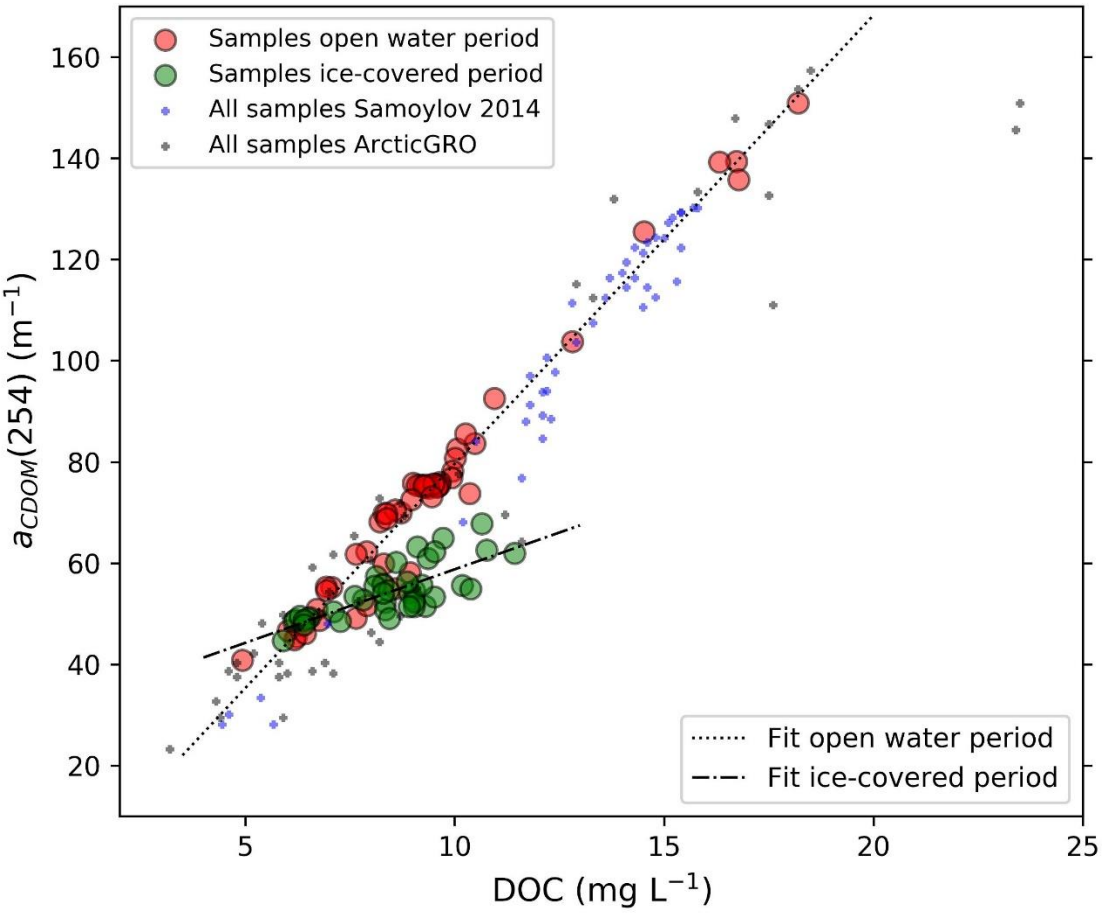

Figure 3.6: Relationship of Lena River DOC and $a_{CDOM}(254)$ samples. Samples from 2018/19 are shown as circles. Samples from the open water period (May 28, 2018 to October 22, 2018) are displayed as red circles, r^2: 0.97, samples from the ice covered period (until May 27, 2018 and from October 23, 2018) as green circles, r^2: 0.59). ArcticGRO data (grey crosses) sampled near Zhigansk (r^2=0.89, Holmes et al., 2018b) and monitoring data from the 2014 freshet (blue crosses) sampled near Samoylov Island (Samoylov 2014, r^2=0.96, Eulenburg et al., 2019) are added for comparison. The dotted black line shows the linear regression of the samples from the open water period ($a_{CDOM}(254)$ = 8.86 x DOC - 8.98) and the dashed-dotted black line shows the linear regression of the samples from the ice-covered period ($a_{CDOM}(254)$ = 2.91 x DOC + 29.74).

Two periods with clear correlations between DOC and $a_{CDOM}(254)$ were apparent: one for the open water period (May 28, 2018 to Oct. 22, 2018), and another for the rest of the time series, with ice cover. These separation indicates qualitative differences in the river DOM (**Figure 3.6**). The slope for the $a_{CDOM}(254)$ vs DOC regression was significantly steeper for the open water period (8.86 m^2 g^{-1}) while the ice covered period had a low slope (2.91 m^2 g^{-1}) and greater intercept. These seasonal qualitative changes were also reflected in S275-295 and SUVA. The lowest slopes (0.0139 nm^{-1}) were measured during the spring ice break-up and the highest during late summer (0.172 nm^{-1}). In winter, during the ice-covered period, S275-295 varied between 0.0147 and 0.0162 nm^{-1}. The SUVA peaked during the spring ice break-up (3.75 m^2 g C^{-1}) and during the early summer discharge peak (3.62 m^2 g C^{-1}) and reached a minimum in late winter (2.3 m^2 g C^{-1}). Beginning at spring

ice break-up, SUVA decreased until late winter. In April 2019, almost 2 months before the return of the spring ice break-up, SUVA increased from 2.2 to 3.1 m^2 g C^{-1}.

3.4.3 DOC flux

We calculated an annual DOC flux of 6.79 Tg C and a discharge flux of 690.2 x 10^9 m^3 for the considered period of one year starting April 20, 2019, during which 2.78 Tg C (41% of annual flux) were transported in spring, 3.26 Tg C (48% of annual flux) in summer and 0.75 Tg C in winter (11% of annual flux) (**Appendix Figure 5**).

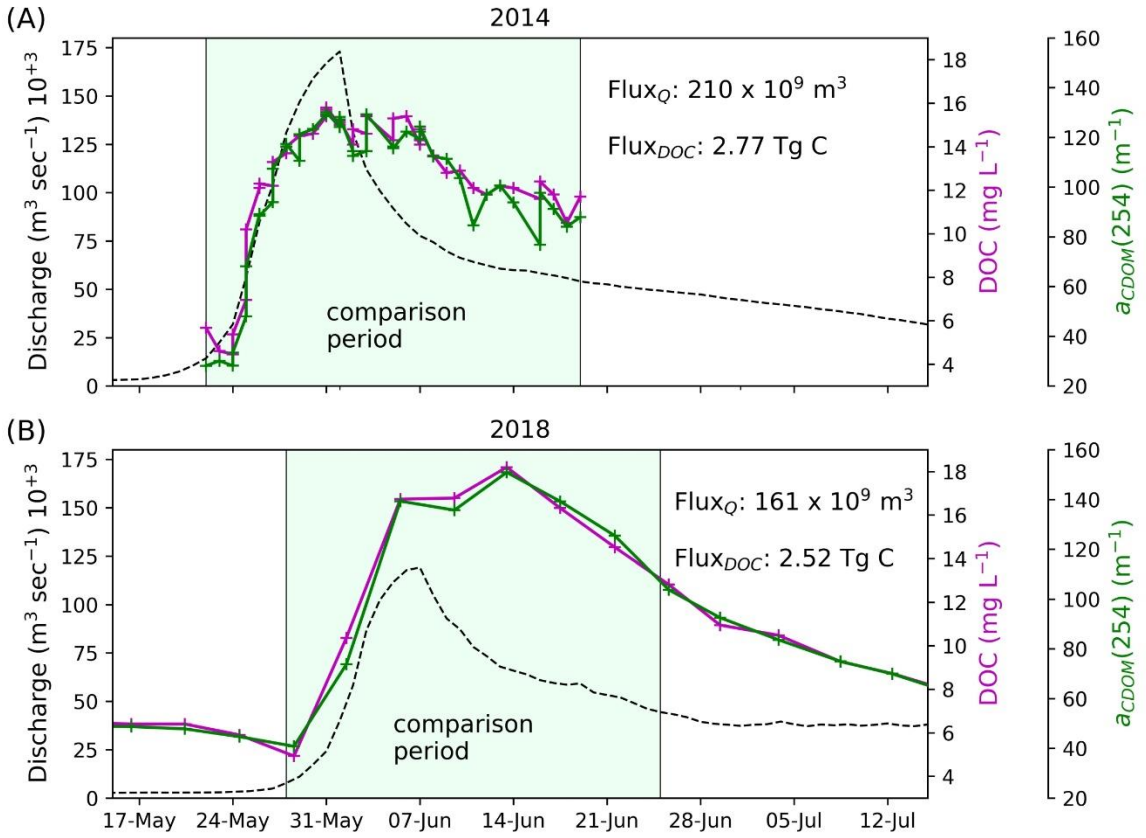

Figure 3.7: DOC and $a_{CDOM}(254)$ concentrations in 2014 (A) and 2018 (B). The 2014 sampling period, was compared to the hydrologically same period in 2018. The flux of discharge (Q) and DOC for the period (29 days) is presented in each panel.

Table 3.3: Annual mean values and annual fluxes of Lena River biogeochemical parameter.

	Discharge	**Temperature**	**EC**	**Heat flux**	**DOC**	**a_{CDOM}(254)**			
Annual mean	21173.8 $m^3 s^{-1}$	4.74 °C	250.6 µS cm^{-1}	6.95 x 10^{16} J d^{-1}	8.85 mg L^{-1}	62.8 m^{-1}			
Annual flux	690.2 x 10^9 m^3	-	-	25.3 EJ	6.79 Tg	52.1 x 10^{12} m^2			
	Ca	K	Mg	Na	Si	Sr	Fl	Cl	SO4
Annual mean	22.5 mg L^{-1}	0.83 mg L^{-1}	6.69 mg L^{-1}	18.0 mg L^{-1}	3.02 mg L^{-1}	0.19 mg L^{-1}	0.12 mg L^{-1}	26.5 mg L^{-1}	19.2 mg L^{-1}
Annual flux	11.8 Tg	0.45 Tg	3.29 Tg	6.95 Tg	1.59 Tg	0.09 Tg	0.07 Tg	10.2 Tg	8.76 Tg

Next, we compare the DOC concentration, a_{CDOM}(254) and calculated fluxes of the spring period in 2014 (**Figure 3.7**A) with the hydrologically aligned similar period in 2018 (**Figure 3.7**B). In 2014, the spring ice break-up discharge peak occurred 6 days earlier than in 2018. Thus, we compare period of similar length in 2018 (29 days) which is shifted 6 days later. In 2014, the discharge flux was 23.3% higher than in 2018, whereas the DOC flux was only 9% higher. This was due to the maximum DOC concentrations being slightly lower in 2014. Both years showed a similar pattern of decreasing DOM concentrations right before the start of the discharge peak followed by a rapid increase of DOM. Right after the discharge reached its maximum, it decreased again rapidly, whereas the DOM concentration remained high and decreased slowly.

3.5 Discussion

3.5.1 Drivers of seasonal variability in hydrochemistry and DOM

The Lena River is characterized by a strong seasonality in discharge and its water biogeochemistry and the hydrograph can generally be divided into three periods: the spring ice break-up, summer to fall, and winter. Hence, we compare and contrast these three hydrologically and biogeochemically distinct periods and speculate about the shifts in the provenance of the water and its dissolved load.

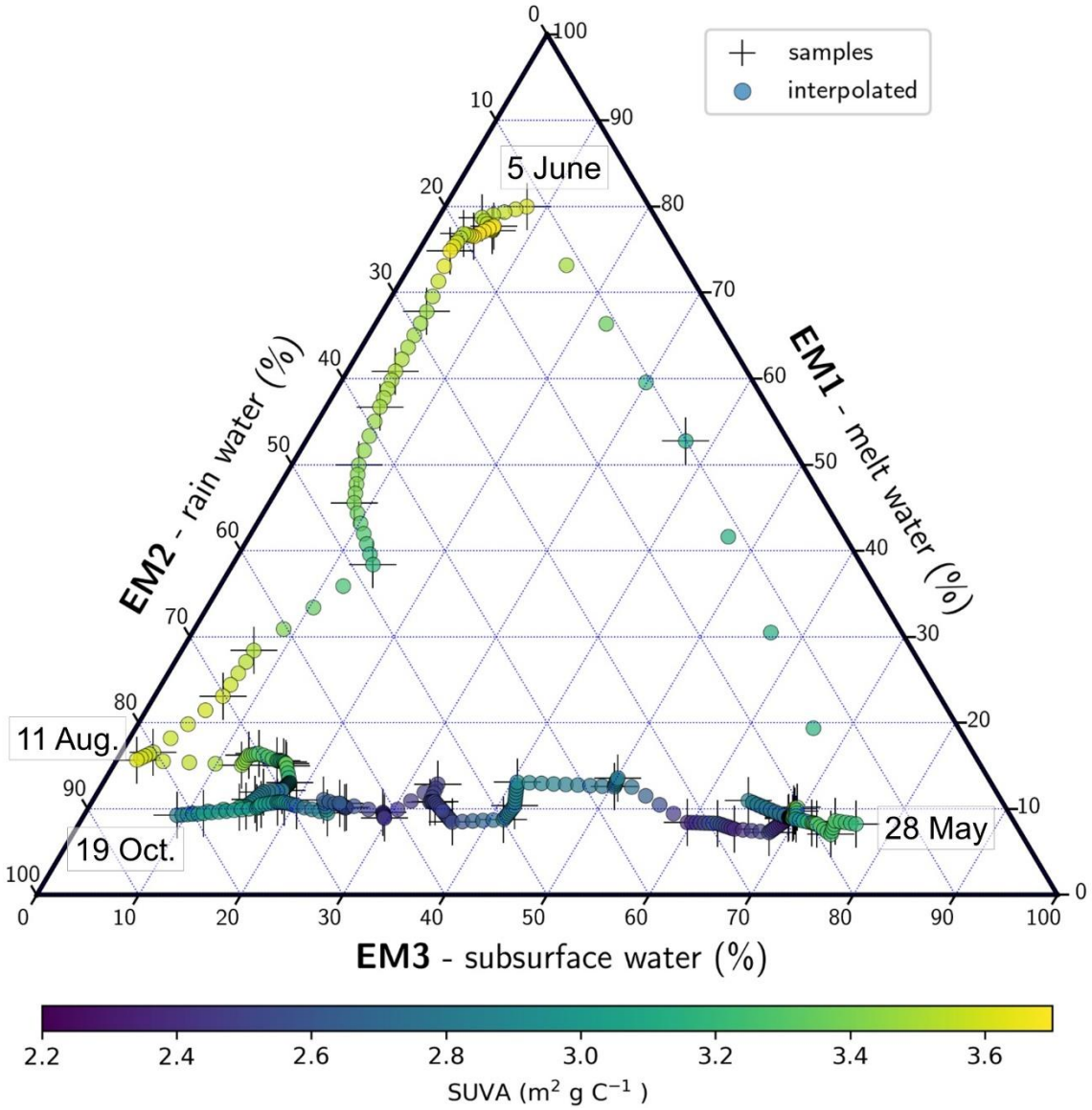

Figure 3.8: Water source fractions for each sample (cross) and each interpolated day (coloured circle) based on EC and stable isotope endmember calculations; Colour shows the SUVA. The extreme values of the water source fractions are indicated by dates.

1) **Spring ice break-up** is the period when air temperatures are consistently positive in most of the catchment and major parts of the winter-accumulated snow and ice melt. Snowmelt does not occur simultaneously across the whole catchment, but begins in the south and moves northward. About 4 days after the ice break-up of the Lena River, the annual discharge maximum (~120000 m^3 s^{-1}) is reached. River water temperatures during the first days of the spring discharge peak remain around 0 °C, resulting in an export of large volumes of cold water to the Laptev Sea. Simultaneously with the discharge maximum, the water source endmember EM1 peaks (80% on June 5) and remains the dominant water source until mid-July (**Figure 3.8**). We identified this endmember as melt water due to the sudden drop of EC (**Figure 3.3**B), major ions (**Appendix Figure 3**) as

well as $\delta^{18}O$ values (**Figure 3.3**C). Chosen endmember values for EM1 with low EC (80 µS cm^{-1}) and low $\delta^{18}O$ (-25 ‰) are characteristic for snow melt water and agree well to reported values (Sugimoto and Maximov, 2012; Spors, 2018; Bonne et al., 2020). With regards to the DOM results it is clear that this pulse has two portions associated with it. The initial input of snow meltwater has low DOM and likely reflects snow not in contact with soil. This results in an initial decrease in DOM in the river which lasts on the order of a week, captured by the high temporal resolution of sampling. This interpretation is supported by the fact that the qualitative measures of DOM (SUVA and S275-295) do not change, essentially reflecting dilution of river water. This is then followed by the discharge maximum, where DOC reaches highest annual concentrations (18.2 mg L^{-1}). In only two months (between June 2, 2018 and August 2, 2018), 53.2% (3.62 Tg C) of the total annual DOC flux (6.79 Tg C) is exported to the Laptev Sea. By applying water source fractions, we estimate that 43.3% (2.9 Tg C) of the annual DOC flux is transported with melt water into the river (**Figure 3.9**). Moreover, melt water accounts for 35% (242 x 10^9 m^3) of the total annual discharge flux (690.18 x 10^9 m^3). This volume agrees well with the accumulated snow volume in the Lena River catchment. Using a mean (1988 to 2000) winter peak value of 120 mm as the snow water equivalent in the catchment (Yang et al., 2007), we derive a snow to water equivalent volume of (295.2 x 10^9 m^3).

With the discharge peak and high DOM concentrations, the quality of the organic matter also changes. Optical indices of DOM (SUVA and S275-295) were comparable to reported values (Walker et al., 2013). The changes occurring during the freshet indicate an organic matter source with high molecular weight and aromaticity (**Figure 3.5**B) (Weishaar et al., 2003; Helms et al., 2008) which is likely young DOM (Amon et al., 2012). During this period, the frozen ground beneath the snowpack during melt limits infiltration, confining most flow to a thin desiccated organic layer and to overland or snowpack flow. The DOM thus likely originates from modern plant litter, which is washed into the Lena River by the rapid and extensive snowmelt (Amon et al., 2012). Very low S275-295 during the spring ice break-up also suggests the input of fresh DOM.

2) **Open water period in summer and fall** is the period during which Lena River water temperatures reach the annual maximum. In this period, the discharge decreases to about half of the spring peak values (40000 to 60000 m^3 s^{-1}). The fraction of EM1 (melt-water) decreases and another water source endmember - EM2 - becomes dominant. f_{EM2} peaks during the discharge events in summer (82.3% on August 11, and 81.6% on October 19)

(**Figure 3.8**). At the same time, $\delta^{18}O$ reaches its highest annual values and the EC is dropping. Such high $\delta^{18}O$ and low EC suggest that this end member is meteoric in origin. For these rain-induced discharge maxima, $\delta^{18}O$ and d-excess co-vary. This is likely related to less evaporative fractionation (and thus a higher d-excess), when more moisture is transported to the catchment. On the other hand, the highest evaporative fractionation is observed during the late summer (lowest d-excess). When discharge in summer is low, DOM concentrations are likewise low (~6 mg L^{-1}). During these periods, little DOM is mobilized and transported into the Lena River. In total, rain water accounts for 49.3% (340 x 10^9 m^3) of annual discharge. 42.6% (2.9 Tg C) of DOC is transported by rain water into the Lena River (**Figure 3.9**).

During the summer period the quality of the DOM changes (lower SUVA, higher S275-295). This could reflect the progress of soil thawing and a deepening active layer. Percolation and the leaching of older and more degraded DOM from deeper in the soil would explain both observations. Changes in SUVA can be linked to changes in source and age of DOM (Stedmon et al., 2011; O'Donnell et al., 2014; Coch et al., 2019) and can indicate the intensity of permafrost degradation within the catchment (Abbott et al., 2014). Furthermore, direct relationships are found between dissolved organic $\delta^{14}C$ and SUVA (Neff et al., 2006; Butman et al., 2012; O'Donnell et al., 2014). Annual maxima in S275-295 during low discharge in summer points towards a higher degree of (photo)-degradation in the river, which can be a result of longer transport time from its source to the sampling station and an exposure of DOM to photodegradation.

There are peaks in DOM concentrations during the distinct rain-induced discharge peaks in summer and fall (**Figure 3.2**). During these periods, that are likely caused by precipitation events over a large area, more DOM is mobilized from the catchment and transported into the Lena River. The general trend towards older and more degraded DOM is interrupted for those events and DOM similar to that transported by the spring snow melt enters the river. However, during the second strong rain event with peak values of rain water fraction (October 19), higher SUVA values compared to the first summer rain event (August 11) point towards a smaller fraction of young organic material. We suggest that reservoirs of young organic material on the land surface of the Lena River catchment are continuously washed out throughout the summer and thus higher relative fractions of older DOM from deeper soil horizons or permafrost become visible in the water samples. Additionally, rain events cause higher water levels in the Lena River that can re-connect

isolated waterbodies and flush lakes, ponds and wetlands. In this way, DOM from phytoplankton production and bleached DOM from standing water bodies can be introduced to the Lena River.

Generally, during the open water period a trend towards lower SUVA and higher S275-295 values is present and continues into the early winter along with a decreasing fraction of rain water. Thus, the amount of fresh and young DOM transported with rain water from the Lena River catchment decreases.

3) **Winter** is the period when the Lena River is entirely covered with ice and the discharge is low (< 6000 m^3 s^{-1}) compared to the other seasons and to the annual mean of 21885 m^3 s^{-1}. During this period, most precipitation in the Lena River catchment accumulates as snow on land and the water level is gradually lowered. The remaining rain water is removed from the hydrological system of the Lena River catchment and the rain water fraction decreases gradually during the first half of the winter (**Figure 3.8**).

In early March, $\delta^{18}O$ and EC reach a stable level. At this time, the third endmember (EM3) becomes the dominant water source (76.1% on May 28) (**Figure 3.8**). We suggest that this water source endmember represents subsurface water such as groundwater, soil and pore water (Abbott et al., 2014), which are the only significant natural water sources in winter, when air temperatures are permanently below 0 °C. Subsurface water represents 15.7% (105 x 10^9 m^3) of the annual Lena River water flux. 14.1% (1 Tg C) of the DOC flux was transported with this water during our year of observation (**Figure 3.9**).

Optical DOM characteristics in winter continue the trend of summer and fall towards older and more degraded DOM until January 2019 when DOM concentrations and SUVA values begin to increase, coincident with a small increase in discharge. During low discharge in winter, a substantial part of the basin outlet discharge originates from the Vilui reservoir (Tananaev et al., 2016), which is regulated by a dam (Viluyskaya HPS) constructed in the 1970s. Changes of DOM concentration and composition may be caused by the higher relative fraction of reservoir water that is released through the Vilui dam. In reservoir water all water sources are pooled throughout the year, leading to DOC concentrations elevated above the otherwise low winter levels. The major increase in long term winter discharge of the Lena River in the late 1970s (**Figure 3.2**) coincides with the completion of Vilui dam construction and its reaching full capacity (Ye et al., 2003; Tananaev et al., 2016). In late winter, before the spring ice break-up, SUVA increases which likely coincides with first

input of fresh DOM from the southern most parts of the catchment, where temperatures begin to rise above 0 °C during the day.

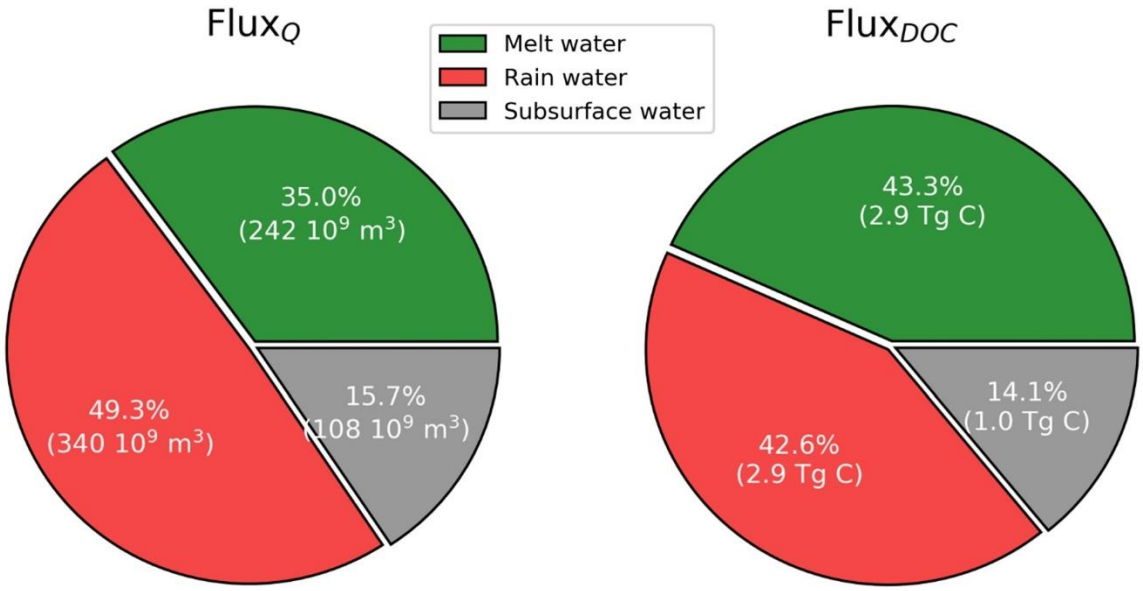

Figure 3.9: Percentage and absolute fractions of discharge flux ($Flux_Q$) and DOC flux ($Flux_{DOC}$) for each endmember water source.

Data from the ice core samples suggest that only low concentrations of DOM are incorporated into the river ice. Once the river ice is exported to the Laptev Sea Shelf after spring ice break-up, it tends to dilute the shelf waters rather than act as a source of high DOM (Amon et al., 2012). However, patches of high sediment load on the Lena River ice (Fedorova et al., 2015) and the erosion of shorelines during ice jams (van Huissteden, 2020) contribute to the particulate organic matter flux to the Laptev Sea. There is likely a contribution to DOM from dissolution of the transported POM but this is quantitatively to be expected low in comparison to the river load of DOM.

The results presented here show that high frequency sampling reveals subtle changes in water chemistry reflecting the seasonal changes in the hydrology of the Lena River catchment. Most of the intra-annual variation in the Lena River water biogeochemistry can be captured by the 3-component endmember analysis presented here. However, river water at the basin outlet represents an integrated signal from the entire catchment and geographical and temporal variations of biogeochemical signals within the catchment cannot be detected by sampling.

3.5.2 Comparison of reported DOM values and fluxes for the Lena River

Overall, our observed ranges of DOC concentrations and $a_{CDOM}(254)$ agree well with reported values from sampling programs of shorter duration or substantial lower sampling frequency (ArcticGRO and PARTNERS (Holmes et al., 2018a, 2018b); Lena River freshet 2014 (Eulenburg et al., 2019)). ArcticGRO and PARTNERS samples have significantly higher DOC concentrations compared to samples from Samoylov Island in 2014 and 2018. Generally, these samples show a lower r^2 (0.89) of their DOC to $a_{CDOM}(275)$ regression, compared to the dataset shown in this study (r^2=0.97). This may indicate either a prominent local influence of anomalous DOM or the impact of analytical differences and different sampling protocols.

Table 3.4: Previously published discharge and DOC fluxes and type of sampling and calculation

Study	Type	Year(s)	Annual discharge flux (10^9 m^3)	Annual DOC flux (Tg C)
Opsahl et al. (1999)	In situ	1999	n.a.	4.7
Raymond et al. (2007)	In situ + load model	2004	566	5.26
		2005	654	6.39
Gordeev and Kravchishina (2009)	In situ	n.a.	n.a.	3.6
Stedmon et al. (2011)	In situ + load model	2004 & 2005	615.1	7.27
Holmes et al. (2012)	In situ + load model	1999-2008	581	5.68 (varied between 4.1 to 7.4 Tg C yr^{-1})
Kicklighter et al. (2013)	Terrestrial ecosystem model	1990 - 2006	352	7.67
Wild et al. (2019)	In situ + load model	2003 - 2013	n.a.	5.71
This study	In situ, long period, high frequency	2018/19	690.18	6.8

A number of studies have reported annual organic carbon fluxes of the Lena River (**Table 3.4**). Reported values range between 3.6 Tg C (Gordeev and Kravchishina, 2009) and 7.67 Tg C (Kicklighter et al., 2013). Variability in DOC flux estimates is likely not only the result of inter-annual variability, but probably also results from differences in sampling frequency, sampling strategy and methods of calculating flux. All of the reported studies are based on a lower number of samples per year and/or on statistical models that are used to pair discharge measurements with concentration (**Table 3.4**). With statistical models, such as LOADEST (Runkel et al., 2004), estimated daily concentrations can be generated, with which seasonal or annual fluxes can be calculated. Although seasonal changes for the relation of discharge to concentration are taken into account in such models, the very low number of samples is critical and simplifying assumptions can cause systematic biases in flux estimates. Our dataset improves sample frequency and reveals that there is no clear relationship between discharge and DOC concentration. A relationship only persists during

spring (r^2=0.87, not shown). The impact of methodological differences for flux calculations becomes clear when comparing reported DOC flux values for 2004 and 2005 from Raymond et al. (2007) and Stedmon et al. (2011), that are based on precisely the same data but differ by 22.3% (1.46 Tg C). Furthermore, the reported fluxes that used models to relate discharge and DOC concentration tacitly assume that variations in DOC concentration are driven by processes changing the discharge, which is equivalent to a one-component system. Thus, the expected increase of DOC mobilization from degrading and thawing permafrost, which does not significantly affect discharge, cannot be reflected by such models.

The identification of seasonal fluxes by selecting certain time periods (Stedmon et al., 2011; Holmes et al., 2012b) throughout different years is a method of addressing this shortcoming but prevents meaningful direct comparisons. The timing of seasonal changes such as the spring ice break-up varies between years and thus influence flux calculations for time periods defined by the calendar. Differences in seasonal fluxes between years (**Appendix Figure 5**) thus are more likely to show shifts in seasonal timing than in water or dissolved load provenance.

We compared DOC fluxes during the spring discharge peak of two years (2014 and 2018). Although the discharge flux between both years differs by 26.4% (4.9 km^3), the difference in DOC flux is not as severe (9.4%). At least for the spring discharge peak, lower discharge is compensated by higher concentrations, which results in a similar flux. This is, however, not the case for summer and fall rain events where high DOC concentrations are triggered by rain that washes organic matter from land surfaces into the Lena River. Thus, recurrences intervals and the intensity of such rain events dominate inter-annual variability in DOC fluxes.

The high temporal resolution of the sampling program presented in this study improves our ability to capture all seasonal events relevant to organic carbon fluxes, without assuming a relationship between DOC concentration and discharge. Thus, we are confident that our flux calculation can be used as a baseline for future trend analysis of Lena River DOC fluxes and, in particular, for the identification of changing seasonality. Little is known about changes in biogeochemistry between sampling locations further upstream (e.g. Zhigansk) and Samoylov Island. Continuous sampling of both programs (Samoylov sampling and ArcticGRO) will, however, enable future comparative studies.

3.6 Conclusion

In a warming Arctic, we expect permafrost landscapes to change dramatically. One result will be the remobilization of dissolved matter from permafrost. In particular, the release of dissolved organic carbon is under immense research attention due to its strong potential feedbacks for the climate. By monitoring the biogeochemistry of Arctic river water at the river mouth, we can observe ongoing changes that reflects change at the catchment scale.

In this study, we present one year of biogeochemical data from the Lena River, one of the largest Arctic rivers. We improve on existing studies by sampling at high temporal frequency throughout the whole year. The main drivers that are responsible for the strong seasonality of water discharge and DOC flux were ascribed to three water sources – melt water, rain water and subsurface water. Melt and rain water were found to be the prevailing water sources that transport together 5.8 Tg C dissolved organic matter (85% of annual flux) into the Lena River. Optical DOM indices revealed changing composition and sources of DOM throughout the year. The high resolution sampling also revealed two phases of melt water introduction, with an initial phase of approximately one week, during which melt water carries little or no DOM and dilutes river DOM concentrations without altering DOM character, followed by large pulse of fresher organic matter from the catchment that substantially changes the river DOM characteristics. Future studies including $\delta^{14}C$ measurements of the age of the DOM will enable direct relation of optical DOM indices to the DOM age and the contribution of permafrost thaw as shown in Neff et al. (2006).

The results of this sampling program provide a baseline for future shifts in seasonal variations as well as inter-annual variation of DOM and the chemistry of the Lena River. The annual flux of 6.8 Tg C was calculated without recourse to load models, which are probably the source of discrepancies between existing estimates. Continuous under-ice sampling revealed that high winter DOM concentrations are probably related to the discharge of reservoir water from the Vilui tributary.

This dataset represents the first year of a planned long-term monitoring program at the Research Station Samoylov Island and provides a reference data set against which future change of this large integrative system may be measured. Continuous sampling of Arctic River water will facilitate identification of intra and inter-annual trends during ongoing climate change.

3.7 Funding and acknowledgements

This research has been supported by the by Geo.X, the Research Network for Geosciences in Berlin and Potsdam (grant no. SO_087_GeoX). The author V. Povazhnyi was supported from the Ministry of Higher Education and Science of the Russian Federation project RFMEFI61617X0076. Support with instrumentation in the field was provided by the project Modular Observation Solutions for Earth Systems – MOSES.

We acknowledge support from the Open Access Publication Initiative of Freie Universität Berlin.

We are grateful to Andrey Astapov, Sergey Volkov and Ekaterina Abramova who were involved in continuous sampling. We are eminently thankful to Antje Eulenburg for her massive efforts to support this sampling program and the analysis of several parameter shown in this study. Furthermore, we thank the Trofimuk Institute of Petroleum Geology and Geophysics, Siberian Branch of the Russian Academy of Sciences (IPGG SB RAS), Novosibirsk, Russia, for their efforts to run the Research Station Samoylov Island and the team of the Otto Schmidt Laboratory for Polar and Marine Research in St. Petersburg for support in logistics and sample analysis. Furthermore, we thank the logistics of the Alfred Wegener Institute, Potsdam, Germany, specifically Waldemar Schneider and Volkmar Aßmann as well as Luidmila Pestryakova from the Northeastern Federal University (NEFU), Yakutsk, Russia.

Projects from the EU Horizon 2020 programme (Nunataryuk, grant no. 773421) and from BMBF-NERC's Changing Arctic Ocean programme (CACOON, NERC grant no. NE/R012806/1, BMBF grant no. 03F0806A) supported discussions within a larger group of experts.

Chapter IV

Dissolved Organic Matter at the Fluvial-Marine Transition in the Laptev Sea Using in situ Data and Ocean Colour Remote Sensing

https://doi.org/10.5194/bg-16-2693-2019

4 Dissolved Organic Matter at the Fluvial-Marine Transition in the Laptev Sea Using in situ Data and Ocean Colour Remote Sensing

B. Juhls[1], P. P. Overduin[2], J. Hölemann[3], M. Hieronymi[4], A. Matsuoka[5], B. Heim[2], J. Fischer[1]

[1]Institute for Space Sciences, Department of Earth Sciences, Freie Universität Berlin, Berlin, Germany

[2]Alfred Wegener Institute Helmholtz Centre for Polar and Marine Research, Potsdam, Germany

[3]Alfred Wegener Institute Helmholtz Centre for Polar and Marine Research, Bremerhaven, Germany

[4]Institute of Coastal Research, Helmholtz-Zentrum Geesthacht, Geesthacht, Germany

[5]Takuvik Joint International Laboratory, Département de Biologie, Université Laval, Canada

Citation: Juhls, B., Overduin, P. P., Hölemann, J., Hieronymi, M., Matsuoka, A., Heim, B., and Fischer, J. (2019). Dissolved organic matter at the fluvial–marine transition in the Laptev Sea using in situ data and ocean colour remote sensing. *Biogeosciences, 16, 2693-2713.*

4.1 Abstract

River water is the main source of dissolved organic carbon (DOC) in the Arctic Ocean. DOC plays an important role in the Arctic carbon cycle and its export from land to sea is expected to increase as ongoing climate change accelerates permafrost thaw. However, transport pathways and transformation of DOC in the land-to-ocean transition are mostly unknown. We collected DOC and $a_{CDOM}(\lambda)$ samples from 11 expeditions to river, coastal and offshore waters and present a new DOC-$a_{CDOM}(\lambda)$ model for the fluvial-marine transition zone in the Laptev Sea. The $a_{CDOM}(\lambda)$ characteristics revealed that the dissolved organic matter (DOM) in samples of this dataset are primarily of terrigenous origin. Observed changes in $a_{CDOM}(443)$ and its spectral slopes indicate that DOM is modified by microbial- and photo-degradation. Ocean Colour Remote Sensing (OCRS) provides the absorption coefficient of coloured dissolved organic matter ($a_{CDOM}(\lambda)^{sat}$) at λ=440 or 443 nm, which can be used to estimate DOC concentration at high temporal and spatial

resolution over large regions. We tested the statistical performance of five OCRS algorithms and evaluated the plausibility of the spatial distribution of derived $a_{CDOM}(\lambda)^{sat}$. The ONNS algorithm showed the best performance compared to in situ $a_{CDOM}(440)$ (r^2=0.72). Additionally, we found ONNS-derived $a_{CDOM}(440)$, in contrast to other algorithms, to be partly independent of sediment concentration, making ONNS the most suitable $a_{CDOM}(\lambda)^{sat}$ algorithm for the Laptev Sea region. The DOC-$a_{CDOM}(\lambda)$ model was applied to ONNS-derived $a_{CDOM}(440)$ and retrieved DOC concentration maps showed moderate agreement to in situ data (r^2=0.53). The in situ and satellite-retrieved data were offset by up to several days, which may partly explain the weak correlation for this dynamic region. Satellite-derived surface water DOC concentration maps from MERIS satellite data demonstrate rapid removal of DOC within short time periods in coastal waters of the Laptev Sea, which is likely caused by physical mixing and different types of degradation processes. Using samples from all occurring water types leads to a more robust DOC-$a_{CDOM}(\lambda)$ model for the retrievals of DOC in Arctic shelf and river waters.

4.2 Introduction

Large volumes of fresh water (3588 ± 257 km^3 yr^{-1}) (Syed et al., 2007) and DOM (25–36 Tg C yr^{-1}) (Raymond et al., 2007) are discharged by Arctic rivers into the Arctic Ocean (Dittmar and Kattner, 2003; Cooper et al., 2005; Stedmon et al., 2011). Recent studies predict an increase of DOM flux to the Arctic Ocean with continued climate warming and permafrost thawing (Freeman et al., 2001; Camill, 2005; Frey and Smith, 2005). This will lead to a cascade of effects on the physical, chemical and biological environment of Arctic shelf waters (Stedmon et al., 2011). These include an increase of radiative heat transfer into surface waters, changes in carbon sequestration, and reductions of sea ice extent and thickness (Hill, 2008; Matsuoka et al., 2011).

The Laptev Sea is a wide shelf sea in the eastern Arctic, characterized by fresh surface waters from the Lena River, which delivers around one fifth (609.5 ± 59 km^3 yr^{-1}) of all river water to the Arctic Ocean (Stedmon et al., 2011; Bauch et al., 2013; Fedorova et al., 2015). River water is the main source of DOM and thus of DOC and coloured dissolved organic matter (CDOM) to the Laptev Sea Shelf (Cauwet and Sidorov, 1996; Kattner et al., 1999; Lobbes et al., 2000; Thibodeau et al., 2014; Gonçalves-Araujo et al., 2015; Vantrepotte et al., 2015). Moreover, the Lena River has the highest peak concentrations of DOC of up to 1600 µmol L^{-1} (Stedmon et al., 2011) of all Arctic rivers. The fate and transformation of DOM as it is discharged to the Arctic Ocean, however, are not well

known. Physical and biological processes, such as photodegradation (Opsahl and Benner, 1997; Helms et al., 2008, 2014; Gonçalves-Araujo et al., 2015) and microbial degradation (Benner and Kaiser, 2011; Matsuoka et al., 2012, 2015; Fichot and Benner, 2014; Fasching et al., 2015), as well as mineralization (Kaiser et al., 2017a) and flocculation (Guo et al., 2007; Asmala et al., 2014), are responsible for the modification and removal of DOM from river-influenced surface waters. Given the strong seasonality of Lena River runoff (Yang et al., 2002), DOC concentration varies greatly in time and space (Cauwet and Sidorov, 1996; Raymond et al., 2007; Stedmon et al., 2011; Amon et al., 2012). Once exported to the sea, rapid transport of water masses and dislocation of fronts cause rapid changes in concentrations of surface water constituents at any given location.

Therefore, DOC sampling at high temporal and spatial resolutions over long periods is necessary to understand these changes. Discrete in situ sampling of DOC during expeditions provides point measurements at the time of sampling and is complicated by the difficulty of accessing shallow water for ocean-going vessels. The resulting inadequacy of sample coverage in space and time can be overcome by using OCRS data. The absorption coefficient of CDOM ($a_{CDOM}(\lambda)$) at a reference wavelength λ (usually λ=443 nm or λ=440 nm is used) is an optical property of the water and can also be derived with OCRS during ice and cloud-free periods. Hereinafter, we refer to satellite derived $a_{CDOM}(\lambda)$ as $a_{CDOM}(\lambda)^{sat}$. CDOM absorbs light in the ultraviolet and visible wavelengths (Green and Blough, 1994) and can be used to estimate DOC concentration (Nelson and Siegel, 2002). Thus, OCRS provides an alternative to discrete water sampling (Matsuoka et al., 2017). DOC concentration maps with high spatial and temporal resolution will improve our understanding of DOC dynamics in fluvial-marine transition zones and better quantify carbon cycling. However, most OCRS retrieval algorithms have focused on optically deep (Case 1) waters, which usually correspond to open ocean where all optical water constituents are coupled to chlorophyll concentration (Morel and Prieur, 1977; Mobley et al., 2004; Antoine et al., 2014). Generally, the Laptev Sea coastal to central-shelf waters and Lena River water can be classified as extreme-absorbing and high-scattering waters with high optical complexity (Case 2) (Heim et al., 2014). Algorithms for Case 1 water do not provide reasonable estimates of water constituents in optically complex waters (Antoine et al., 2013). Hieronymi et al. (2017) use a novel algorithm for the retrieval of OCRS products such as $a_{CDOM}(440)$. This algorithm is specifically designed for a broad range of

concentrations of different water constituents including extremely high absorbing waters with $a_{CDOM}(440)$ of up to 20 m^{-1}.

In order to estimate DOC concentration from $a_{CDOM}(\lambda)$, a number of empirical relationships between in situ DOC and $a_{CDOM}(\lambda)$ for Arctic regions (Spencer et al., 2009; Fichot and Benner, 2011; Matsuoka et al., 2012; Örek et al., 2013; Walker et al., 2013; Gonçalves-Araujo et al., 2015; Mann et al., 2016), as well as global (Massicotte et al., 2017), are presented in recent studies. However, the DOC-$a_{CDOM}(\lambda)$ relationship can vary in different water types and can change between seasons and regions (Mannino et al., 2008; Vantrepotte et al., 2015). Furthermore, existing Arctic datasets of DOC and $a_{CDOM}(\lambda)$ taken in situ are almost all limited to either offshore, coastal or river waters, so that a DOC-$a_{CDOM}(\lambda)$ relationship has not been established for the range of water types in Arctic coastal waters. Samples from near-shore waters from Arctic shelves are under-represented in these datasets. In order to obtain synoptic DOC concentration maps that cover the fluvial-marine transition, a relationship valid for a combination of these different water types is required.

Spectral shapes of $a_{CDOM}(\lambda)$ can provide additional information on the DOM quality and about involved biogeochemical processes that modify the DOM (Carder et al., 1989; Nelson et al., 2004, 2007; Matsuoka et al., 2012). Various studies use the $a_{CDOM}(\lambda)$ slope in the UV domain (S275-295) as an indicator of the photodegradation history of the $a_{CDOM}(\lambda)$ (Del Vecchio and Blough, 2002; Helms et al., 2008; Fichot and Benner, 2012). Recent studies presented $a_{CDOM}(\lambda)$ slopes at different wavelengths ranges and their correlation to the DOC specific absorption coefficient ($a^*_{CDOM}(\lambda)$) at different wavelengths for the Eastern Arctic Ocean (EAO) (Makarewicz et al. (2018): S300-600 to $a^*_{CDOM}(350)$) and the Western Arctic Ocean (WAO) (Matsuoka et al. (2012): S350-500 to $a^*_{CDOM}(440)$). However, direct comparisons of published studies is made difficult by their use of different reference wavelengths.

In this study, we aim to better understand the transport of organic material from land to sea in the Arctic and improve its detection at regional scale in the Laptev Sea, where the Lena River provides a major source of DOM to the Arctic Ocean. For this, we compile a dataset of DOC and $a_{CDOM}(\lambda)$ samples collected during multiple expeditions to the Laptev Sea and Lena River region in order to investigate the optical characteristics and variability of $a_{CDOM}(\lambda)$. With this dataset we develop a new DOC-$a_{CDOM}(\lambda)$ relationship which we apply to OCRS data in order to estimate DOC concentration from space. We test and evaluate the

accuracy of different OCRS algorithms for the fluvial-marine transition zone in the Laptev Sea.

4.3 Material and methods

4.3.1 Study area and expeditions

The in situ data presented in this study are compiled from several, mostly unpublished datasets from Russian-German expeditions to the Lena River and Laptev Sea that took place from 2010 to 2017 (**Table 4.2**). Sampling locations of this dataset include large parts of the western and central Laptev Sea Shelf, coastal regions around the Lena River Delta and channels of the Lena River (**Figure 4.1**).

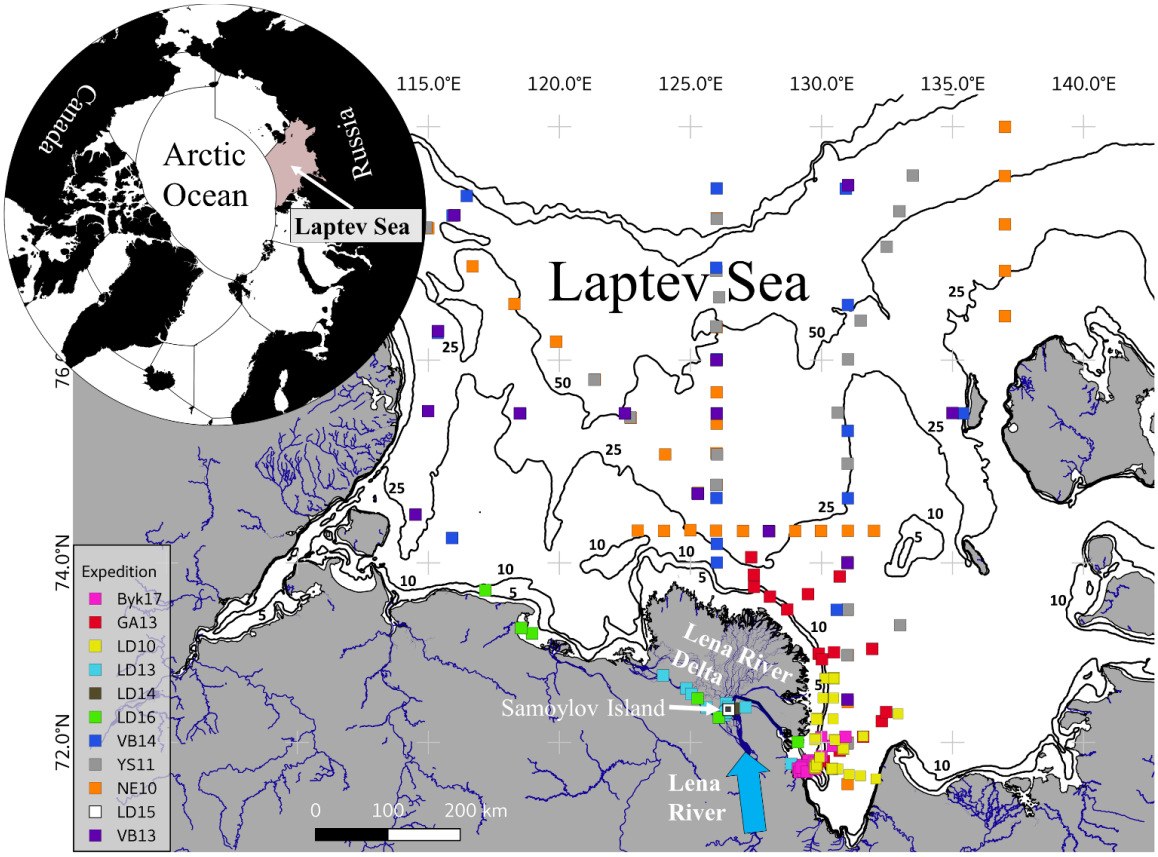

Figure 4.1: Map of the Laptev Sea and the Lena River Delta region with sample locations from 11 Russian-German expeditions; upper left map shows the Arctic Ocean and the location of the Laptev Sea on the Russian Arctic shelf. Bathymetry is shown by black contour lines and water depth in meters.

All ship- and land-based sampling took place during the ice-free period between the end of June and mid-September. Only one land-based sampling in the central Lena River Delta took place between the end of May and the end of June, during Lena River peak discharge after the ice break-up. The ship expeditions, which covered offshore shelf waters (NE10,

YS11, VB13 and VB14), were conducted on board RV *Nikolay Evgenov* (NE), RV *Jacob Smirnitsky* (YS) and RV *Viktor Buynitskiy* (VB), respectively. For the other ship expeditions, smaller boats were used for sampling in coastal waters or on the Lena River. Water sampling at the research station on Samoylov Island (LD14) was carried out from small boats or from the shore (**Figure 4.1**). **Table 4.2** shows a summary of sampling periods, water types and the sampled parameters of the individual expedition datasets.

4.3.2 Hydrographic characteristics and sample processing

For each sampling location included in this dataset, vertical profiles of the water column temperature and salinity were measured with a CTD (Sontek CastAway CTD for LD14, LD15, LD16, Byk17 and a Seabird 19+ for LD10, LD13, NE10, YS11, VB13, VB14, GA13). In this study we use the practical salinity unit (psu) to describe salinity. Aboard ships and boats, water samples were taken using Niskin bottles or an UWITEC water sampler at defined depths. Since this study focuses on improving satellite retrievals, only surface water samples (discrete samples from 2 and 5 m water depth) were included in the compiled dataset. Based on visual examination of the water column characteristics we also included samples from 10 m depth wherever a thick homogeneous upper mixed layer was present. During the expedition LD14, water samples were taken from the shore of Samoylov Island at around 0.5 m depth using 5-liter glass bottles

Water samples for DOC analysis were filtered through 0.7 µm GF/F filter and acidified with 25 µL HCl suprapur (10 M) after sampling. Samples were stored cool and dark for transport. DOC concentrations were measured using high temperature catalytic oxidation (TOC-VCPH, Shimadzu). Three measurements of each sample were averaged and after each 10 samples, a blank and a standard (*Battle-02*, *Mauri-09* or *Super-05* certified reference material from National Laboratory for Environmental Testing, Canada) were measured for quality control.

Samples for $a_{CDOM}(\lambda)$ analysis were filtered through 0.22 µm Millipore GSWP filters (GA13, LD16, Byk17) or 0.7 µm Whatman GF/F (LD10, YS11, VB13, VB14, LD14, LD15) after sampling. 100 ml filtrate was stored cool and dark in amber glass bottles until further analysis. $a_{CDOM}(\lambda)$ was measured with a spectrophotometer (SPECORD 200, Analytik Jena) by measuring the absorbance (A_λ) at 1 nm intervals between 200 and 750 nm. Absorption was calculated from the resulting absorbance measurements via:

$$a_{\mathrm{CDOM}}(\lambda) = \frac{2.303 * A_{\lambda}}{L}, \qquad \text{(Equation 4.17)}$$

where L is the path length (length of cuvette), to calculate the $a_{\mathrm{CDOM}}(\lambda)$. Fresh Milli-Q water was used as reference. The quartz cuvette length varied depending on the expected absorption in the sampled water (1 or 5 cm for river or coastal waters, 5 or 10 cm for offshore shelf waters). Resulting $a_{\mathrm{CDOM}}(\lambda)$ spectra were corrected for baseline offsets by subtracting the mean absorption between 680 and 700 nm, assuming zero absorption at >680 nm. We focussed on a_{CDOM} at 443 nm since most OCRS algorithms use this wavelength to retrieve $a_{\mathrm{CDOM}}(\lambda)$. This wavelength corresponds to one spectral band of most multispectral satellite sensors. Spectral slopes of $a_{\mathrm{CDOM}}(\lambda)$ were calculated by non-linearly fitting the following equation (Jerlov, 1969; Bricaud et al., 1981):

$$a_{\mathrm{CDOM}}(\lambda) = a_{\mathrm{CDOM}}(\lambda_0) * e^{-S(\lambda - \lambda_0)}, \qquad \text{(Equation 4.18)}$$

where $a_{\mathrm{CDOM}}(\lambda_0)$ is the absorption coefficient at reference wavelength λ_0 and S is the spectral slope of $a_{\mathrm{CDOM}}(\lambda)$ for the chosen wavelength range. Spectral slopes of $a_{\mathrm{CDOM}}(\lambda)$ were calculated fitting Equation 4.18 for the individual wavelength ranges (275 to 295 nm for S275-295 and 350 to 500 nm for S350-500). The DOC specific absorption coefficient at λ=440 nm was calculated with $a^*_{\mathrm{CDOM}}(440) = a_{\mathrm{CDOM}}(440)$ / DOC.

4.3.3 Satellite data

In order to monitor spatiotemporal variability of DOC in surface waters and test the applicability of the established DOC-$a_{\mathrm{CDOM}}(\lambda)$ model from this study, we used OCRS. We applied the DOC-$a_{\mathrm{CDOM}}(\lambda)$ model to calculate DOC concentration from satellite-retrieved $a_{\mathrm{CDOM}}(\lambda)$. For this study, we chose the Medium Resolution Imaging Spectrometer (MERIS) because of its high spectral resolution and spectroradiometric quality (Delwart et al., 2007). Many OCRS algorithms were developed specifically for this sensor and are designed for coastal waters. MERIS L1 satellite scenes at reduced resolutions (1 km spatial resolution) were obtained from the MERIS Catalogue and Inventory (MERCI). Scenes with reduced resolution were chosen because of their larger extent and thus better coverage of the in situ data stations. Furthermore, Hu et al. (2012) reported a better signal to noise ratio compared to MERIS full resolution data and recommended the use of MERIS reduced resolution data. We checked all expedition periods for cloud-free MERIS satellites scenes but only two expeditions from 2010 (LD10 and NE10 ship expeditions) could be used to evaluate the performance of the remote sensing retrieval of the surface water DOC concentration.

During those periods, we identified a few scenes with substantial cloud-free data coverage that were acquired during the 2010 expedition periods. **Table 4.1** lists MERIS scenes used in this study. In order to visualize satellite-derived results, we generated mosaic images containing the average of the overlap from multiple satellite scenes to extend the data coverage between cloud gaps. To compare in situ with satellite data, we used the median of three by three extracted pixel values from each single processed OCRS image. To discuss processes that cause differences between satellite images we extracted reanalysis surface wind data (4 times daily) from the National Centers for Environmental Prediction.

Table 4.1: List of MERIS scenes used in this study

Scene name	Date, Time (UTC)	Match-up with
MER_RR__1PRBCM20100803_020534_000005942091_00404_44045_0005	2010-08-03 02:05	LD10
MER_RR__1PRBCM20100804_031401_000005942091_00419_44060_0004	2010-08-04 03:14	LD10
MER_RR__1PRBCM20100805_024241_000005942091_00433_44074_0003	2010-08-05 02:42	LD10
MER_RR__1PRBCM20100907_034618_000005942092_00405_44547_0002	2010-09-07 03:46	NE10
MER_RR__1PRBCM20100918_030140_000005942093_00061_44704_0006	2010-09-18 03:01	NE10
MER_RR__1PRBCM20100919_023010_000005942093_00075_44718_0007	2010-09-19 02:30	NE10
MER_RR__1PRBCM20100920_033916_000005942093_00090_44733_0008	2010-09-20 03:39	NE10

Hieronymi et al. (2017) developed the OLCI (Sentinel-3 Ocean and Land Colour Instrument) Neural Network Swarm (ONNS) in-water algorithm for the retrieval of OCRS products, among them $a_{CDOM}(440)$. This algorithm is designed for broad concentration ranges of different water constituents, including extremely high absorbing waters. The algorithm differentiates 13 optical water types (OWT) and uses specific neural networks (NN) for each OWT. Every NN is trained for narrow concentration ranges. The values of $a_{CDOM}(440)$ used for the training of the NN's are up 20 m^{-1}. The final product is a weighted sum of all NNs depending on OWT membership. The standard atmospheric correction of ONNS, namely the C2RCC (Brockmann et al., 2016), is applied. ONNS makes use of 11 out of the 21 OLCI bands, including the 400 nm band, which is the only one not delivered by MERIS. In order to retrieve OCRS products with ONNS from MERIS imagery, a band adaptation NN-algorithm is utilized to extrapolate remote sensing reflectance at 400 nm, which is usually provided with an uncertainty <5% for these waters (Hieronymi, 2019). Note that the ONNS-algorithm uses the $a_{CDOM}(\lambda)$ wavelength 440 nm whereas all other algorithms use 443 nm.

Additionally, we tested the following open source OCRS algorithms: (1) FUB/WeW MERIS Case-2 Water properties processor (FUB/WeW) (Schroeder and Schaale, 2005) developed for $a_{CDOM}(443)$ up to 1 m^{-1}), MERIS Case 2 Water algorithm (C2R) (Doerffer and Schiller, 2007) ($a_{CDOM}(443)$ up to 1 m^{-1}) which is used for the MERIS 3rd Reprocessing

of ESA's distributed products, and the Case 2 Regional CoastColour (C2RCC) (Brockmann et al., 2016) with C2RCC ($a_{CDOM}(443)$ up to 1 m^{-1}) and C2X ($a_{CDOM}(443)$ up to 60 m^{-1}). All algorithms used in this study use neural networks trained with databases of radiative transfer simulations or in situ measurements or both to invert the satellite signal into inherent optical water properties such as $a_{CDOM}(\lambda)^{sat}$ and concentrations such as total suspended sediment (TSM). In this study the atmospheric correction from Case 2 Regional CoastColour processor (C2RCC) (Brockmann et al., 2016) was used to provide atmosphere corrected reflectances for the OCRS algorithms ONNS, C2R, C2RCC and C2X. For the FUB/WeW algorithm the atmospheric correction provided by the FUB/WeW processor (Schroeder and Schaale, 2005) was used.

Functions for satellite retrieval evaluation

In order to evaluate the retrieval of $a_{CDOM}(\lambda)^{sat}$ from the tested OCRS algorithms, we used a number of evaluation parameters suggested by Bailey and Werdell (2006) and Matsuoka et al. (2017). Among them, we use the median of satellite to in situ ratio (Rt), the semi-interquartile range (SIQR), the median absolute percent error (MPE), and root mean square error (RMSE). The evaluation parameters are defined as follows:

$$Rt = median(\frac{X_{sat}}{X_{in\ situ}}), \quad \text{(Equation 4.19)}$$

$$SIQR = \frac{Q_3 - Q_1}{2}, \quad \text{(Equation 4.20)}$$

$$MPE = median(100 * \left|\frac{X_{sat} - X_{in\ situ}}{X_{in\ situ}}\right|), \quad \text{(Equation 4.21)}$$

$$RMSE = \sqrt{\frac{\sum_{n=1}^{N}[X_{sat} - X_{in\ situ}]^2}{N}}, \quad \text{(Equation 4.22)}$$

where X_{sat} and $X_{in\ situ}$ are the satellite-derived and in situ measured $a_{CDOM}(443)$, respectively. Q1 represents the 25th ratio percentile and Q3 represent the 75th ratio percentile.

Table 4.2: Expedition focus regions, years and region. Mean and standard deviation of hydrographic and DOM parameters. The number of samples between DOC and $a_{CDOM}(443)$ differs for some expeditions and "n.a," indicates that no DOC measurements were made.

Expedition (Code)	Focus region	Year	Season	S (psu)	DOC (µmol L^{-1})	$a_{CDOM}(443)$ (m^{-1})	S275-295 (nm^{-1})	S350-500 (nm^{-1})
Lena 2010 (LD10)	Coastal	2010	Aug.	6.03 ± 6.59	563 ± 156 (n=29)[1]	3.39 ± 0.27 (n=9)	0.0152 ± 0.0006	0.0167 ± 0.0019
Transdrift XVIII (NE10)	Central shelf	2010	Sept.	23.6 ± 6.6	n.a.	0.66 ± 0.46 (n=107)	0.0196 ± 0.0016	0.0175 ± 0.0028
Transdrift XIX (YS11)	Central shelf	2011	Aug. & Sept.	19.6 ± 3.6	239 ± 55 (n=29)	0.75 ± 0.21 (n=26)	0.0193 ± 0.0009	0.0161 ± 0.0129
Lena 2013 (LD13)	Lena River	2013	July & Aug.	0.01 ± 0.05	695 ± 77 (n=28)[2]	3.25 ± 0.6 (n=28)	0.016 ± 0.0007	0.0166 ± 0.0006
Gonçalves-Araujo et al., (2015) (GA 13)	Coastal	2013	July & Aug.	14.2 ± 9.4	398 ± 155 (n=59)[4]	1.5 ± 0.86 (n=42)[3]	0.017 ± 0.0015	0.0181 ± 0.00158
Transdrift XXI (VB13)	Central shelf	2013	Aug. & Sept.	22.6 ± 6.9	n.a.	0.71 ± 0.55 (n=19)	0.0201 ± 0.0023	0.0184 ± 0.0017
Lena 2014 (LD14)	Lena River	2014	May & June	0.01 ± 0.05	1049 ± 248 (n=50)	5.66 ± 1.85 (n=44)	0.0145 ± 0.001	0.0159 ± 0.0005
Transdrift XXII (VB14)	Central shelf	2014	Sept.	28.3 ± 2.9	176 ± 53 (n=46)	0.36 ± 0.19 (n=47)	0.0208 ± 0.0021	0.0196 ± 0.00164
Lena 2015 (LD15)	Lena River	2015	July & Sept.	0.01 ± 0.05	n.a.	2.66 ± 0.72 (n=12)[5]	0.0167 ± 0.0009	0.0166 ± 0.0006
Lena 2016 (LD16)	Lena River & Coastal	2016	Aug. & Sept.	7.3 ± 9.5	499 ± 164 (n=17)	2.47 ± 1.22 (n=35)	0.0164 ± 0.001	0.0164 ± 0.0014
Bykovsky 2017 (Byk17)	Coastal	2017	June & July	1.3 ± 2.2	675 ± 61 (n=22)	2.6 ± 0.69 (n=22)	0.0161 ± 0.0009	0.019 ± 0.0013

[1]doi.org/10.1594/PANGAEA.842220

[2]doi.org/10.1594/PANGAEA.844928

[3]doi.org/10.1594/PANGAEA.875748

[4]doi.org/10.1594/PANGAEA.842221

[5]doi.org/10.1594/PANGAEA.875754

4.4 Results

4.4.1 Spatial and temporal variability of DOC and CDOM

To examine variability of DOC and CDOM optical properties along the land-ocean continuum of the Lena-Laptev system, we generated a large dataset that covers spring freshet through late summer from 2010 to 2017 (**Table 4.2**). Compared to previously published datasets (Matsuoka et al., 2012; Walker et al., 2013; Gonçalves-Araujo et al., 2015; Mann et al., 2016), this dataset compiles not only samples of one water type but covers river, coastal and offshore waters throughout the most variable portion of the open water season.

To better understand characteristics of DOC and $a_{CDOM}(\lambda)$ in freshwater-marine waters, the compiled dataset was first classified into three water types according to salinity: (1) fresh river water with salinities from 0-0.2, (2) mesohaline coastal water with salinities from 0.2-16 and (3) offshore waters with salinities >16.

Overall, DOC concentrations tended to decrease from river to offshore. The same trend was also observed in $a_{CDOM}(443)$. In river water, DOC concentrations and $a_{CDOM}(443)$ ranged from 370 to 1315 µmol L^{-1} (median=779 µmol L^{-1}) and 1.17 to 7.91 m^{-1} (median=3.61 m^{-1}), respectively (**Figure 4.2**a and b). DOC concentrations and $a_{CDOM}(443)$ in coastal waters ranged from 205 to 923 µmol L^{-1} (median=590 µmol L^{-1}) and 0.71 to 3.79 m^{-1} (median=2.05 m^{-1}), respectively. Values in offshore water were the least variable of all three water types with DOC concentrations from 91 to 606 µmol L^{-1} (median=234 µmol L^{-1}) and $a_{CDOM}(443)$ from 0.077 to 1.86 m^{-1} (median=0.5 m^{-1}). Generally, observed DOC and $a_{CDOM}(443)$ values were similar to reported findings from the Lena River and Laptev Sea regions (Cauwet and Sidorov, 1996; Raymond et al., 2007; Stedmon et al., 2011; Amon et al., 2012; Heim et al., 2014; Gonçalves-Araujo et al., 2015).

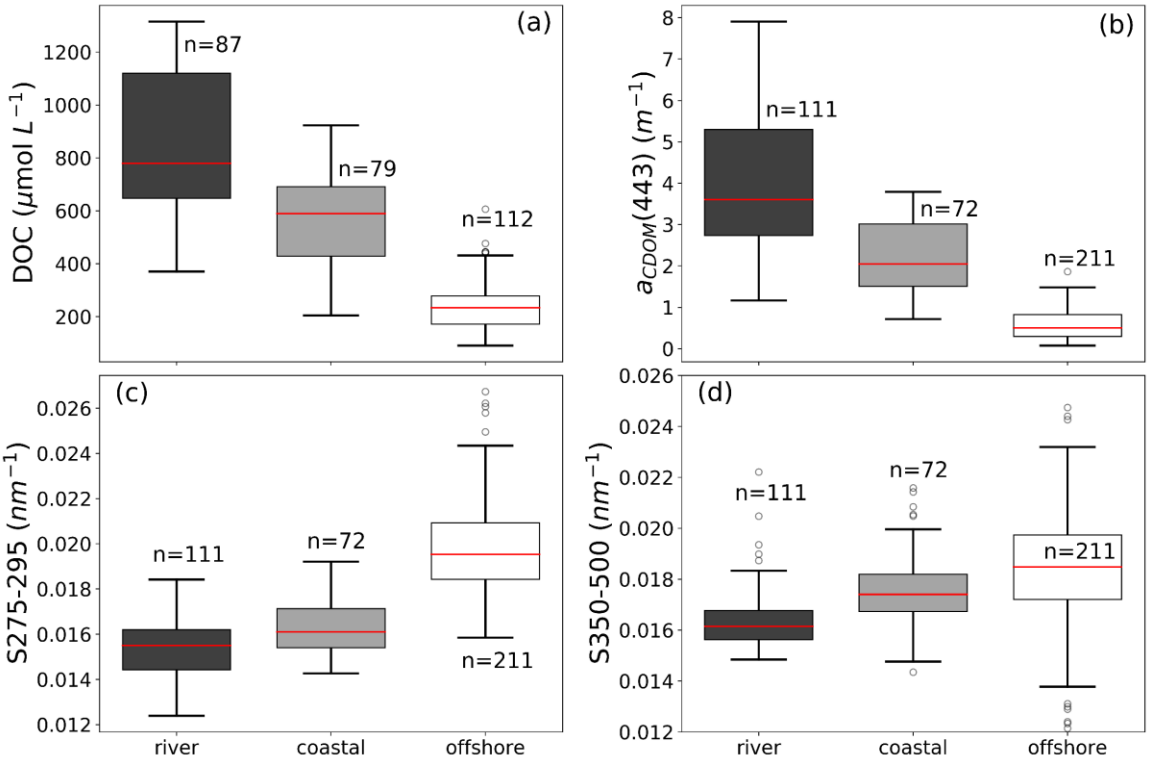

Figure 4.2: Boxplot of (a) DOC concentration, (b) $a_{CDOM}(443)$, (c) S275-295 and (d) S350-500 for the three water types clustered by salinity (river <0.2, coastal <16, offshore >16); the red line indicates median of each water type.

The spectral UV slope (S275-295) (**Figure 4.2**c) showed similar maximum and median values for river (max.=0.0184 nm^{-1}, median=0.0155 nm^{-1}) and coastal waters (max.=0.0192 nm^{-1}, median=0.0161 nm^{-1}). We observed the lowest S275-295 in the Lena River water during the spring freshet at the beginning of June (LD14, **Table 4.2**). Offshore water has significantly higher S275-295 values ranging from 0.0158 to 0.0267 nm^{-1} (median=0.195 nm^{-1}). For river and coastal water, S350-500 showed a similar variability as S275-295. The range of offshore water S350-500 however, showed substantially higher variation and covered a broad range (**Figure 4.2**d).

In contrast to trends in DOC concentrations and $a_{CDOM}(443)$, $a_{CDOM}(\lambda)$ spectral slopes in two distinct spectral domain (S275-295 and S350-500) tended to increase from river to offshore (**Figure 4.2**). While the spectral slopes between river (max.=0.0184 nm^{-1}, median=0.0155 nm^{-1}) and coastal waters (max.=0.0184 nm^{-1}, median=0.0158 nm^{-1}) were not substantially different, those between the river and offshore were significantly different (p-value $\leq 10^{-8}$).

4.4.2 CDOM absorption characteristics

We compared salinity and $a_{CDOM}(443)$ for the compiled dataset. As in other river-influenced waters, there was a strong linear relationship between $a_{CDOM}(443)$ and salinity (r^2=0.87, n=283) (**Figure 4.3**), suggesting that physical mixing prevails and plays a role in near-conservative behavior of $a_{CDOM}(\lambda)$. For this analysis, only coastal and offshore waters were included since river water was constant in salinity but varied seasonally in $a_{CDOM}(443)$ (LD14, **Table 4.2**). In coastal and offshore waters, $a_{CDOM}(443)$ decreased gradually with increasing salinity. The observed mixing line is similar to the reported mixing-line for Laptev Sea Shelf waters from Heim et al. (2014), which was developed using parts of this compiled dataset (LD10 & YS11). The reported relationship from Matsuoka et al. (2012), however, shows generally lower $a_{CDOM}(443)$ values in waters of the WAO along the salinity gradient. S350-500 was very variable along the mixing-line. However, low $a_{CDOM}(443)$ along the mixing line had high S350-500 and higher $a_{CDOM}(443)$ had low S350-500.

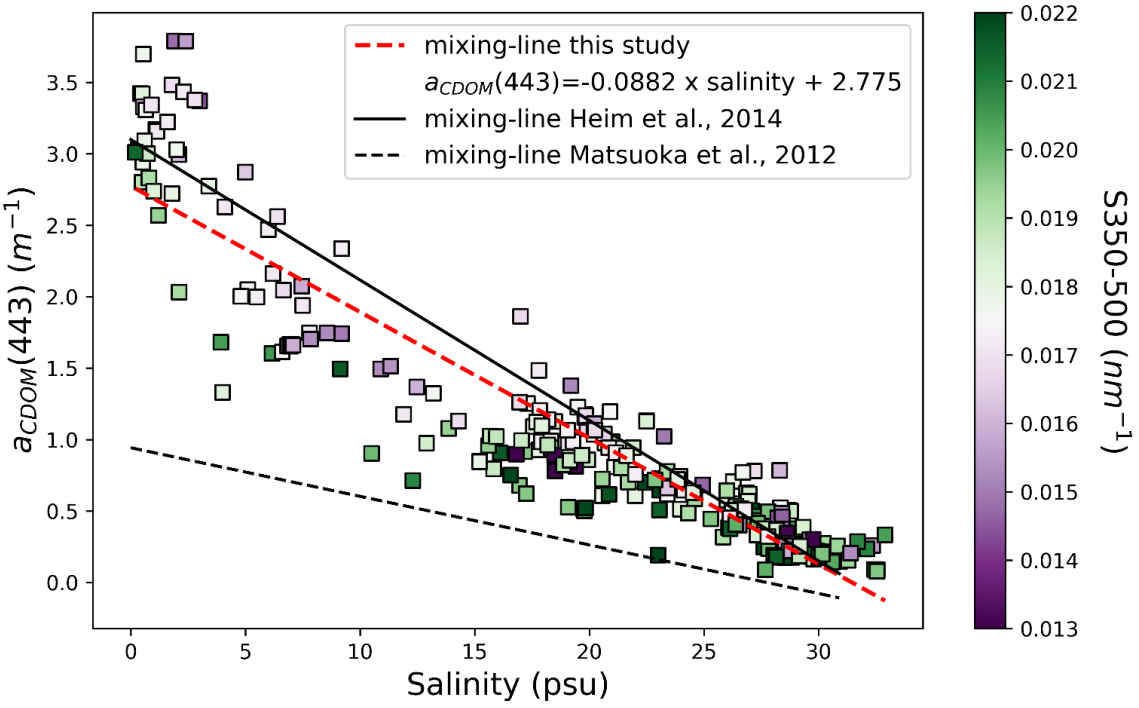

Figure 4.3: Relationship between $a_{CDOM}(443)$ and salinity (n=283, r^2=0.87) for all available water sampled from less than 10 m water depth and a salinity >0.2; colour of data-points indicates S350-500; red dashed line shows the linear fit representing the mixing line between Salinity and $a_{CDOM}(443)$ within this dataset. Solid black line shows the reported mixing-line from Heim et al. (2014) and dashed black line to one from Matsuoka et al. (2012) (adapted to $a_{CDOM}(443)$ using Equation 4.18 and a constant slope of 0.018.

Bulk information, combined use of magnitudes and spectral slopes of CDOM absorption are useful for understanding sources and/or processes involved in the modification of dissolved organic matter (e.g. Fichot and Benner (2012) and Helms et al. (2008)). The

strongest correlation was observed between $a_{CDOM}(443)$ and the UV slope S275-295 (**Figure 4.4**a, Pearson correlation coefficient (r) =-0.84). Similar strong correlations were reported by Fichot and Benner (2011) between $a_{CDOM}(350)$ and S275-295 for coastal waters of the Beaufort Sea in the WAO. Here, we used $a_{CDOM}(443)$ to make the findings useful for the OCRS community, which usually retrieves a_{CDOM} at 443 nm. The spectral slope S350-500 showed moderate correlation with $a_{CDOM}(443)$ (**Figure 4.4**b, r=-0.54). Furthermore, a high number of S350-500 values were located outside the range of observed S350-500 values for coastal waters of the western Arctic (dashed lines, **Figure 4.4**b).

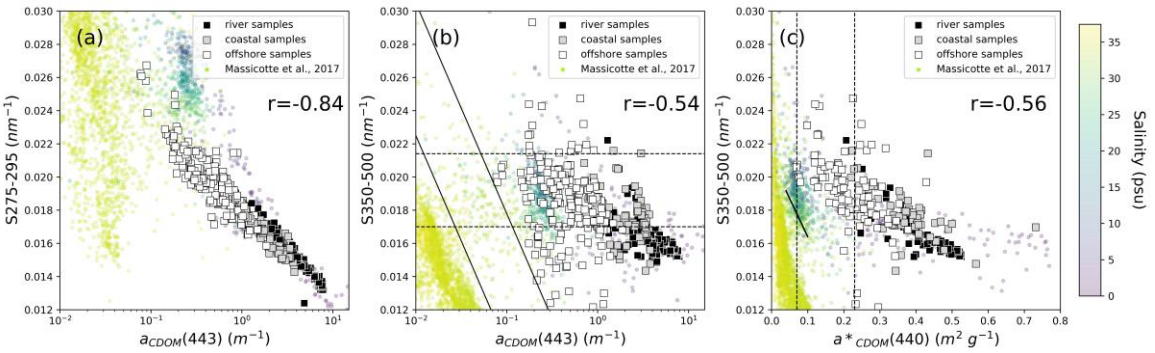

Figure 4.4: (a) Relationship between $a_{CDOM}(443)$ and S275-295; (b) $a_{CDOM}(443)$ vs. S350-500 with 95% confidence intervals of regressions of western Arctic coastal waters (dashed lines) and for western Arctic oceanic water (solid lines) reported by Matsuoka et al. (2011), (2012), (c) $a^*_{CDOM}(440)$ vs. S350-500 with dashed lines representing the borders of $a^*_{CDOM}(440)$ for oceanic waters report by Nelson and Siegel (2002) and solid line shows the reported relationship between $a^*_{CDOM}(440)$ and S350-500 from Matsuoka et al. (2012). Circles show global data from Massicotte et al. (2017) where colours indicate the salinity.

We observed a moderate correlation between $a^*_{CDOM}(440)$ and S350-500 (**Figure 4.4**c, r=-0.56). Most samples from this study are located above the $a^*_{CDOM}(440)$ limits of oceanic water reported by Nelson and Siegel (2002), dashed lines in **Figure 4.4**c, indicating that water samples from this study are primarily river influenced with higher aromaticity (Weishaar et al., 2003; Helms et al., 2008; Granskog et al., 2012). The reported relationship between $a^*_{CDOM}(440)$ and S350-500 from Matsuoka et al. (2012), solid line in **Figure 4.4**c, deviates strongly in slope of the regression and range of $a^*_{CDOM}(440)$ values from this data from the fluvial-marine transition zone of the Laptev Sea.

Compared to the global CDOM absorption characteristics from Massicotte et al. (2017) (**Figure 4.4**a to c, coloured circles), samples from this study are within the range of freshwater influenced samples with lower salinities and clearly differentiate from high saline oceanic waters.

4.4.3 DOC – CDOM relationship

Generally, retrieval of optical water properties and water constituents such as DOC from satellite data consists of three steps: (1) atmospheric correction of the top of atmosphere radiance to the water-leaving or the in-water reflectance, which is needed as input for the OCRS algorithms, (2) the retrieval of $a_{CDOM}(\lambda)^{sat}$ from the atmospherically-corrected reflectance received by satellite, and (3) if $a_{CDOM}(\lambda)^{sat}$ is retrieved from OCRS, DOC can be calculated using an in situ DOC versus in situ $a_{CDOM}(\lambda)$ relationship. The direct validation and evaluation of different atmospheric corrections (1) is beyond the scope of this study. In the following, we present a new regional DOC-$a_{CDOM}(\lambda)$ relationship (3) from our compiled in situ dataset.

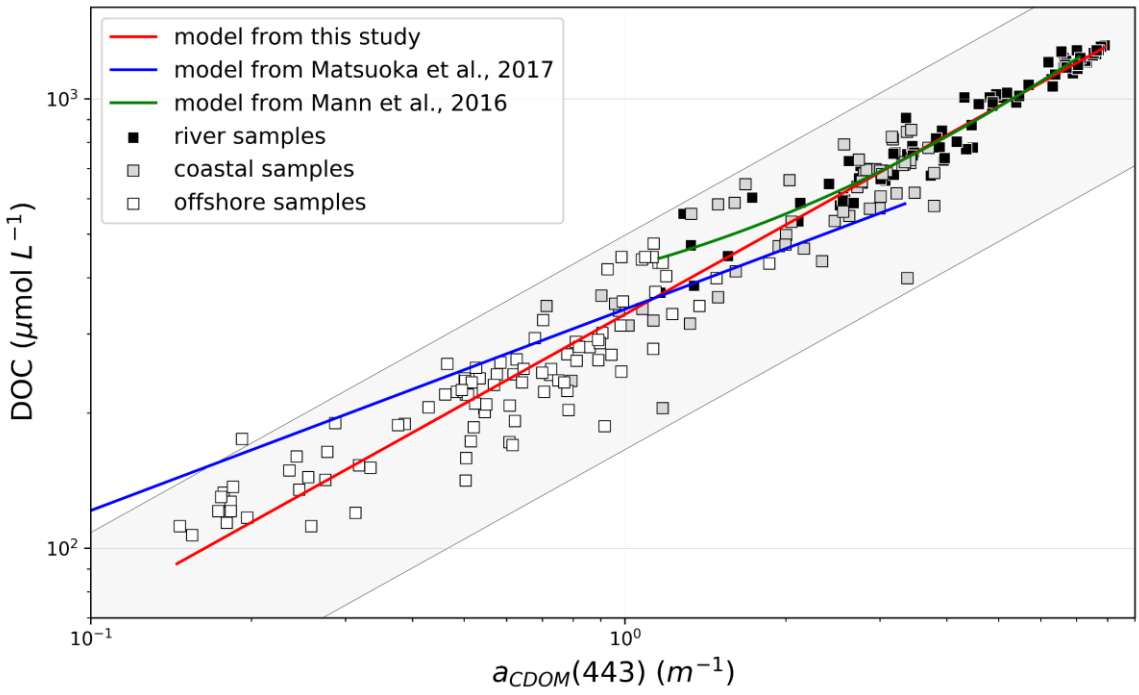

Figure 4.5: Relationship between $a_{CDOM}(443)$ and DOC (r^2=0.96). Red line shows the derived model from this dataset. The blue line shows the relationship from Matsuoka et al. (2017) for a pan-Arctic dataset for offshore and coastal waters. The green line shows the relationship for Lena River water from Mann et al. (2016). The filled grey area shows the 50% error range. Note that the axes are displayed in log-scale.

We observed a strong relationship between $a_{CDOM}(443)$ and DOC concentration for all water samples including river to marine waters (**Figure 4.5**). One order of magnitude variation in DOC corresponded to more than 2 orders of magnitude of variation in $a_{CDOM}(443)$ for this sample set, and corresponded to the range from moderately absorbing waters (0.1–1.0 m^{-1}) to highly absorbing waters (>1.0 m^{-1}). After testing different regression models, the best fit was derived with a power function (Equation 4.23, red line in **Figure 4.5**):

$$DOC\ (\mu mol * L^{-1}) = 10^{2.525} * a_{CDOM}(443)^{0.659}. \quad \text{(Equation 4.23)}$$

The agreement between model and data (r^2=0.96, n=227) allowed estimation of DOC by $a_{CDOM}(443)$ within a 50% error range. The highest deviations from the fitted line corresponded to the transition zone between offshore shelf waters and coastal waters ($a_{CDOM}(443)$=0.5–1.5 m^{-1}) and to the very low end of the $a_{CDOM}(443)$ range (<0.5 m^{-1}). It is noted that the fitting model of this dataset using only offshore or river water samples would result in a lower slope (exponent=0.617 for coastal and offshore water, 0.606 for offshore water only) in the resulting DOC-$a_{CDOM}(443)$ model. Including coastal and river samples substantially increased the slope of the fit, which results in higher DOC estimates for high $a_{CDOM}(443)$. The reported relationship from Mann et al. (2016) is similar for high-$a_{CDOM}(443)$ river water but deviates for low-$a_{CDOM}(443)$ river water and coastal and offshore water. The model presented by Matsuoka et al. (2017) (blue line in **Figure 4.5**) has a lower slope and results in highest differences for DOC estimation at high $a_{CDOM}(443)$.

Model coefficients for other selected $a_{CDOM}(\lambda)$ wavelengths are presented in **Appendix Table 2**. Furthermore, the relationship between S275-295 and DOC had a slightly weaker correlation with DOC (r^2=0.92) than $a_{CDOM}(443)$.

4.4.4 Satellite retrieved CDOM

To estimate the surface water DOC concentration with the presented DOC-$a_{CDOM}(\lambda)$ model (Equation 4.23, **Figure 4.5**) and generate DOC concentration maps for large scales, we need a robust and accurate retrieval of $a_{CDOM}(\lambda)^{sat}$.

Table 4.3: Performance of tested OCRS algorithms for $a_{CDOM}(\lambda)^{sat}$ with in situ $a_{CDOM}(443)$ or $a_{CDOM}(440)$. Note that not all OCRS algorithms are developed for the highly absorbing waters (high $a_{CDOM}(\lambda)$) found in the Arctic coastal region.

OCRS algorithm	n	slope	intercept	r^2	Rt	SIQR	%MPE	RMSE
ONNS	34	0.571	0.493	0.716	0.679	0.217	58.39	0.436
C2R	34	0.157	0.087	0.329	3.23	0.075	223.38	0.277
C2RCC	34	0.048	0.157	0.271	3.23	0.093	223.05	0.097
C2X	34	1.023	-0.212	0.652	1.09	0.224	100.0	0.919
FUB/WeW	34	0.178	0.013	0.545	3.76	0.057	276.49	0.2

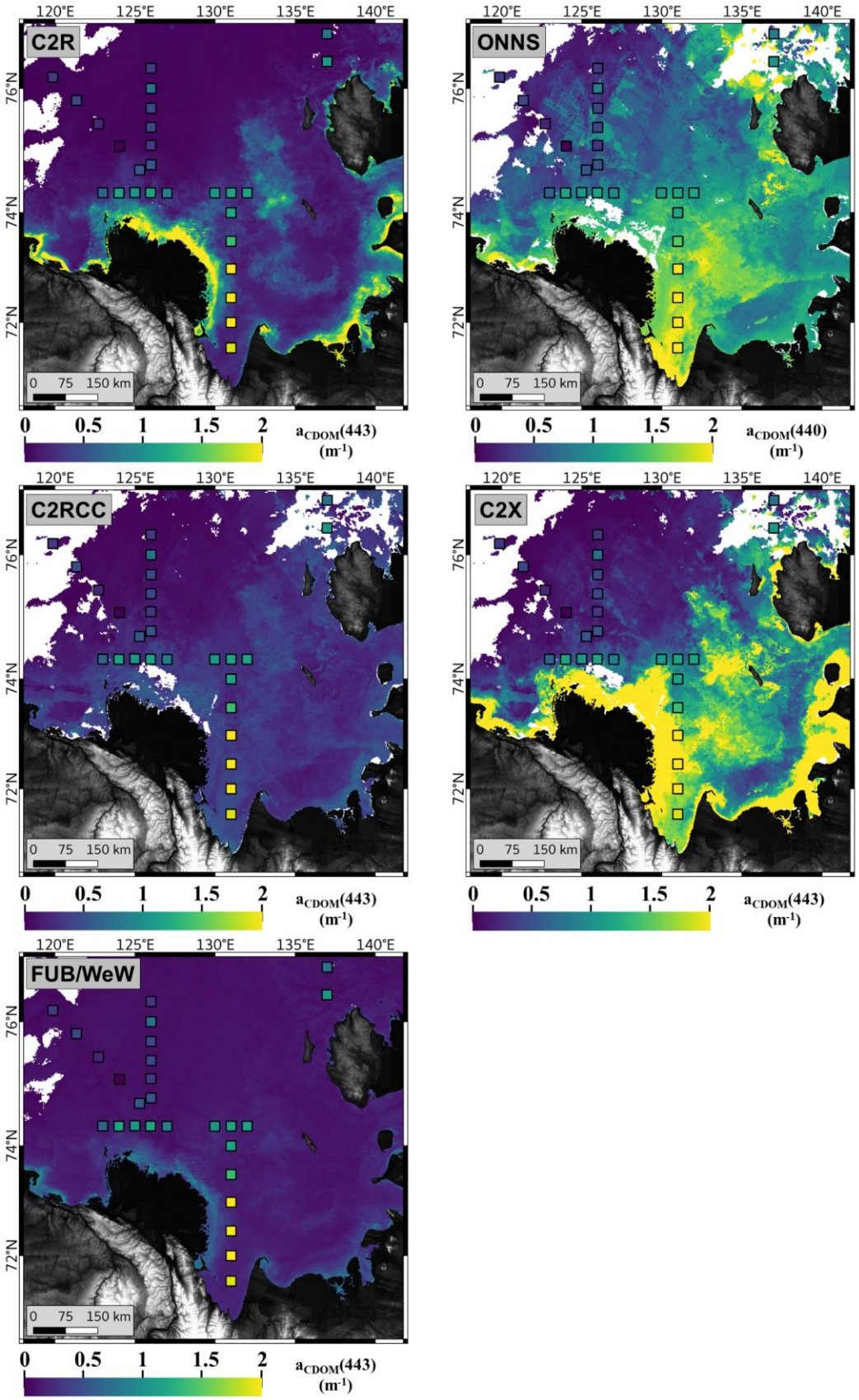

Figure 4.6: Surface water $a_{CDOM}(\lambda)^{sat}$ from MERIS mosaic from 5 scenes from September 2010 (scenes listed in **Table 4.1**) for all tested OCRS algorithms (C2R, ONNS, C2RCC, C2X, FUB/WeW). Squares show in situ $a_{CDOM}(443)$ ($a_{CDOM}(440)$ for ONNS) with colours according to same colour scale as satellite data.

We examined the performance of five OCRS algorithm in terms of $a_{CDOM}(443)^{sat}$ retrieval using Equation 4.19 to Equation 4.22. For this purpose, $a_{CDOM}(443)^{sat}$ retrievals were compared to in situ data from within 10 days of the satellite retrievals. Our comparisons showed highly varying results (**Figure 4.6**, **Appendix Figure 6**, **Table 4.3**) and strong under- or overestimation of $a_{CDOM}(\lambda)^{sat}$. Particularly in turbulent coastal waters, comparison of $a_{CDOM}(443)^{sat}$ with in situ $a_{CDOM}(443)$ is challenging, given the fact that the magnitude of CDOM absorption can vary greatly over a short time for the location of a given pixel. ONNS-derived $a_{CDOM}(\lambda)^{sat}$ performed best (r^2=0.716, Rt= 0.679, SIQR=0.217, %MPE=58.39, RMSE=0.436). The C2X algorithm performed similarly with a lower r^2 (0.65) and substantially higher %MPE (100.0) and RMSE (0.919). In addition to the comparison with in situ data, we evaluated the plausibility of the resulting spatial distributions and observed extremely high C2X-derived $a_{CDOM}(443)^{sat}$ values in the Lena River mouth (up to 10 m^{-1}). Such values of $a_{CDOM}(443)$ were not confirmed by any reported in situ data. ONNS-derived $a_{CDOM}(443)^{sat}$ showed values which are in the range of in situ observed $a_{CDOM}(443)$. Other algorithms show clear underestimations of $a_{CDOM}(443)^{sat}$ compared to in situ data (**Appendix Figure 5**). Thus, ONNS was the only algorithm that produced $a_{CDOM}(\lambda)$ values in a similar range to in situ measured $a_{CDOM}(440)$.

4.4.5 Surface water DOC concentrations in coastal waters of the Laptev Sea

Using the presented DOC-$a_{CDOM}(\lambda)$ model, we generated satellite-derived images of surface water DOC concentrations for the Lena-Laptev Sea region. All scenes were processed with the ONNS algorithm and $a_{CDOM}(440)$ was averaged for each mosaic. DOC concentrations for two mosaics (**Figure 4.7**b & d) were calculated by using the adapted model from Equation 4.23 with coefficients for $a_{CDOM}(440)$ instead of $a_{CDOM}(443)$. The mean time difference between the two mosaics is 31 days. The DOC mosaic from early August 2010 (**Figure 4.7**b) shows high DOC concentrations over large areas in the eastern Laptev Sea. Concentrations (>600 µmol L^{-1}) were highest in Buor Khaya Bay east of the Lena River Delta where the Lena River exports most of its water. The plume of the Lena River with high DOC concentrations (~500 µmol L^{-1}) had propagated northeastward in this scene. The DOC mosaic from September 2010 (**Figure 4.7**d) shows generally lower DOC concentrations compared to the earlier scene. Highest concentrations were found in the coastal areas in Buor Khaya Bay (east of the Lena River Delta) and around the Olenek

River Delta (west of the Lena River Delta) to the west of the Lena Delta. While ONNS performs well in river-influenced waters, we note that DOC concentrations at the northern edge can be influenced by cloud masking (patches of high DOC concentrations shown in northeast corner of **Figure 4.7**d).

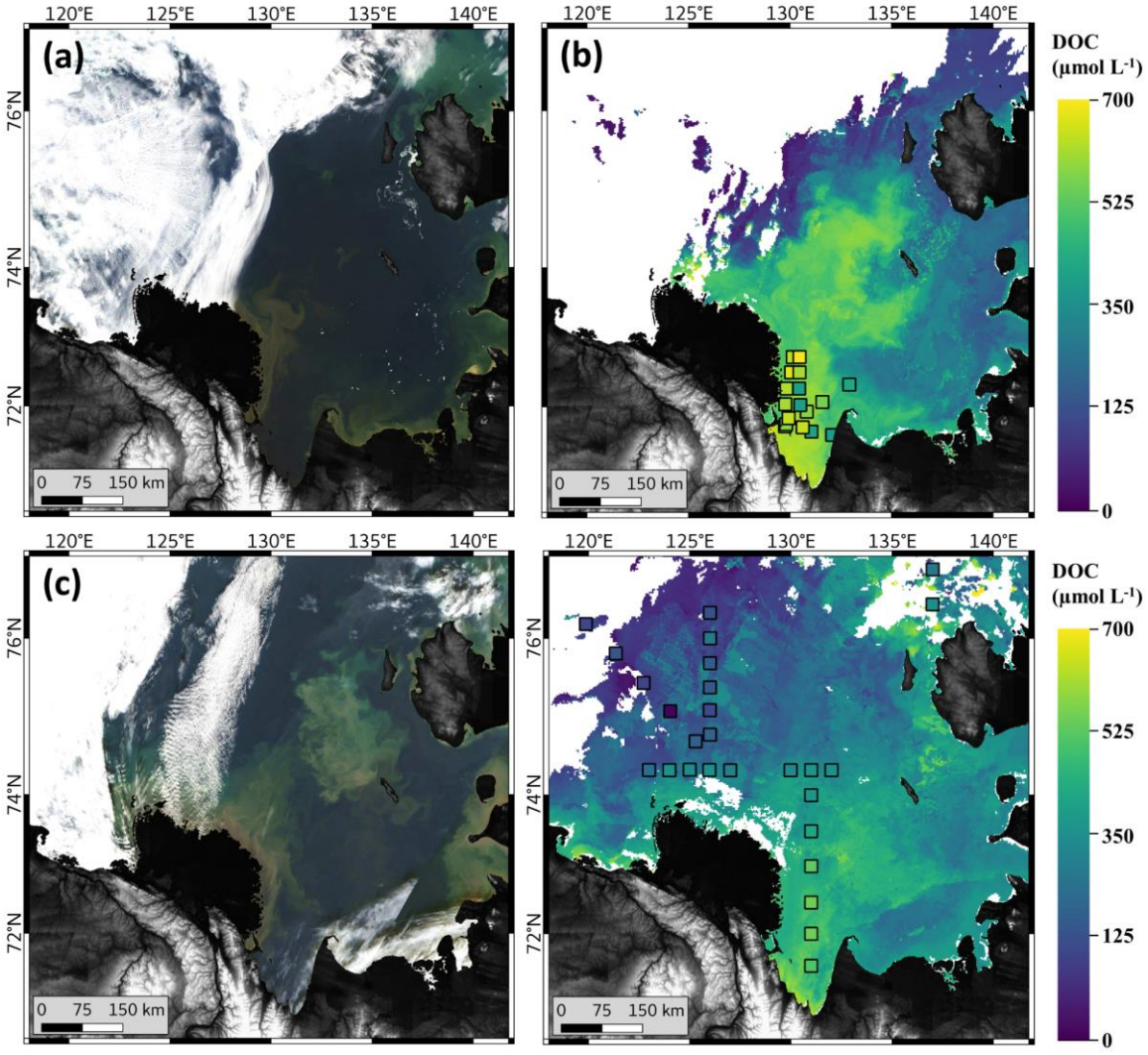

Figure 4.7: (a) Quasi-true colour image from August 5, 2010; (b) Surface water ONNS-DOC concentration from satellite mosaics from August 3, 2010 to August 5, 2010. (c) Quasi-true colour image from September 7, 2010. d) Surface water ONNS-DOC concentration from satellite mosaics from September 7, 2010 and September 18, 2010 to September 20, 2010. Squares in (b) and (d) squares indicate in situ concentrations with same colour scale as satellite data.

Both quasi-true colour satellite images (**Figure 4.7**a & c) show sediment-rich, strongly backscattering waters around the Lena River Delta resulting from fluvial transport. In the satellite image from September 7, 2010 (**Figure 4.7**c) there is also a large strongly backscattering area in the eastern Laptev Sea, where resuspension events in shallow water (5-10 m, **Figure 4.1**) occurred between both acquisition periods. These resuspension events are not visible in the calculated DOC concentration maps at right (**Figure 4.7**d).

In situ DOC vs. remotely-sensed DOC

To evaluate the satellite-retrieved DOC concentrations, we compared in situ and ONNS-retrieved DOC concentrations (**Figure 4.8**) using the presented DOC-$a_{CDOM}(\lambda)$ model (Equation 4.23) and investigated the plausibility of the DOC value ranges and the derived spatial patterns (**Figure 4.7**b & c). This evaluation revealed a moderate performance (r^2=0.53, slope=0.61) (**Figure 4.8**) despite several days difference in sampling times between satellite and in situ sampling. The use of MERIS full resolution data revealed a slightly better performance (r^2=0.68, slope=0.77). However, we preferred the use of reduced resolution data due to the reported better quality (Hu et al., 2012). This comparison constitutes an evaluation and not a direct validation of the method. The latter is hampered by the lack of matching data and the time offsets between satellite acquisition and in situ sampling dates. The DOC-$a_{CDOM}(\lambda)$ model presented in this study improved satellite-derived estimates of DOC concentration compared to estimates using the DOC-$a_{CDOM}(\lambda)$ relationship reported by Matsuoka et al. (2017) (r^2=0.46, **Figure 4.8**).

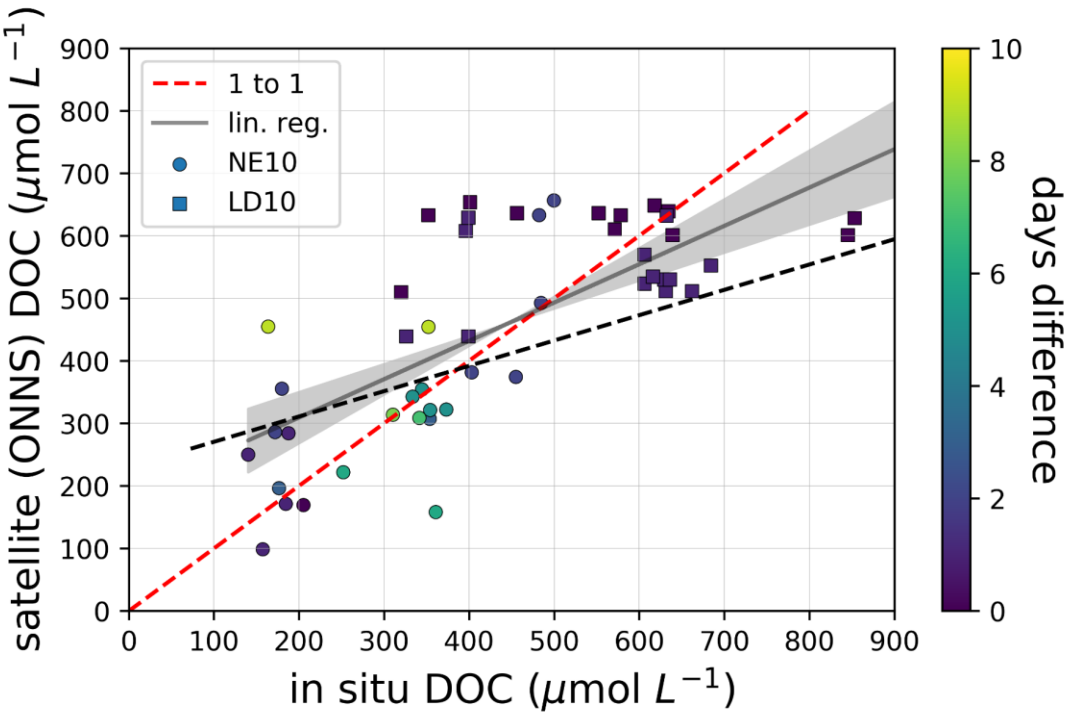

Figure 4.8: Comparison of in situ DOC and ONNS-derived DOC. The dark gray line shows a linear regression (r^2=0.53, slope=0.61, n=50). The gray area represents the 95% confidence interval. The red line indicates 1:1 correspondence. Days difference (symbol colour) shows the temporal offset between the satellite scene and in situ water sampling. The dashed black line shows the satellite DOC concentration calculated by using the DOC-$a_{CDOM}(443)$ relationship from Matsuoka et al. (2017).

To spare in situ data for this performance test, data from LD10 was not used to develop the DOC-$a_{CDOM}(\lambda)$ model (Equation 4.23). The DOC concentrations for NE10 were calculated

from in situ $a_{CDOM}(443)$ measurements using Equation 4.23, since no in situ DOC measurements were taken on NE10. These in situ DOC concentrations are therefore not independent, but were derived from the DOC-$a_{CDOM}(443)$ relationship for the entire dataset. However, samples from NE10 were not used for the development of the DOC-$a_{CDOM}(\lambda)$ relationship since in situ DOC was missing. We use the data to test the DOC retrieval for a wide range of concentrations. Further validation of the DOC retrieval will require additional in situ datasets collected simultaneously with cloud-free, open-water remote sensing acquisitions by using the MERIS successor OLCI.

4.5 Discussion

4.5.1 Sources and modification of DOM in the fluvial-marine transition

Our results showed that $a_{CDOM}(443)$ decreases as a function of salinity (**Figure 4.3**), indicating that river water is the main source of CDOM on the Laptev Sea Shelf waters and in coastal waters and thus that most CDOM is of terrigenous origin. Despite the tight relationship, some data points deviated from the mixing line in the salinity range from 2 to 24. Deviations from the mixing line can result from combined physical, chemical, and biological processes that modify CDOM optical properties (Asmala et al., 2014; Matsuoka et al., 2015, 2017). Helms et al. (2008) and Matsuoka et al. (2012) suggested that higher $a_{CDOM}(443)$ and lower S350-500 can be used as a proxy indicating that microbial degradation is more important than photodegradation. Indeed, we observed higher $a_{CDOM}(443)$ associated with lower S350-500 within a similar salinity range (**Figure 4.3**), pointing towards stronger microbial degradation than photodegradation.

Flocculation can also modify CDOM optical properties by removing larger molecules once the river water encounters saline water. However, given the fact that this process occurs at low salinities (0 to 3) (Asmala et al., 2014), flocculation alone cannot explain the deviation of $a_{CDOM}(443)$ values apart from the mixing line.

S275-295 was strongly correlated with $a_{CDOM}(443)$ (**Figure 4.4**a), which is mainly associated with the high content lignin chromophores in our samples (Fichot et al., 2013) and is partly explained by the long exposure of DOM to solar radiation and the resulting photodegradation (Helms et al., 2008; Hansen et al., 2016). Lena River water shows high lignin content and higher proportion of syringyl and vanyl phenols relative to p-hydrox phenols (Amon et al., 2012). Benner and Kaiser (2011) showed that this could make the

DOM more subject to photodegradation, which might supports why such a high correlation was observed.

Compared to the strong relationship between S275-295 and $a_{CDOM}(443)$, a moderate correlation was observed for S350-500 versus $a_{CDOM}(443)$ relationship (**Figure 4.4**b), suggesting different degradation mechanisms were involved during the transition from river to coastal and offshore waters. Here we use S350-500, which is often used in the OCRS community (Babin et al., 2003; Matsuoka et al., 2011, 2012), instead of S350-400, which is the wavelength range suggested by Helms et al. (2008). Note that the correlation between S350-500 and S350-400 is very high (r=0.98) and thus both slopes can be used. The mean river endmember value of S350-500 at salinity zero was 0.0163 nm^{-1}. This value tends to be lower in the EOA (including Lena river mouth) than in the WAO (Stedmon et al., 2011; Matsuoka et al., 2017). The higher $a_{CDOM}(443)$ associated with the lower spectral slope observed in our river and coastal waters suggested more aromaticity in waters obtained from Lena-Laptev region (Stedmon et al., 2011). This was further demonstrated by our higher $a^*_{CDOM}(443)$ (**Figure 4.4**c).

The S350-500 versus $a_{CDOM}(443)$ relationship showed a moderate but significant negative correlation and most samples were within a terrestrial range (dashed lines, **Figure 4.4**b). The fact that no samples were within the reported ranges of photodegradation for oceanic waters (solid lines, **Figure 4.4**b) suggest that CDOM in coastal waters of the Laptev Sea would have been highly influenced by terrestrial inputs but with least photodegradation effect compared to that in oceanic waters (Matsuoka et al., 2015, 2017). It is likely that high turbidity and thus less transparent water of coastal regions in the Laptev Sea protects DOM from photodegradation. Data points outside of the ranges might indicate either microbial degradation and/or sea ice melt (Matsuoka et al., 2017). Given the only minor influence of ice melt waters during most of our field campaigns, microbial degradation is more likely for some of our samples, which is consistent with our explanation for deviated samples shown in **Figure 4.3**.

The difference in optical properties of $a_{CDOM}(\lambda)$ observed between EAO and WAO is possibly caused by geological difference rather than climatic influences (Gordeev et al., 1996). This is partly supported by the chemical characterization of lignin phenols (Amon et al., 2012). Our results showed specificity of optical properties in the Lena and Laptev

Sea and underline the necessity of discussing spectral optical properties when $a_{CDOM}(443)$ and DOC concentration are estimated in this region.

4.5.2 Linking CDOM absorption to dissolved organic carbon concentration

Previous reported DOC-$a_{CDOM}(\lambda)$ models such as Walker et al. (2013), Örek et al. (2013) and Mann et al. (2016) for Arctic rivers, Matsuoka et al. (2012) for WAO and Gonçalves-Araujo et al. (2015) for coastal waters are restricted in their use to the water type of samples. Our presented DOC-$a_{CDOM}(\lambda)$ relationship improves reported models from Mann et al. (2016) and Matsuoka et al. (2017) for the estimation of DOC from $a_{CDOM}(443)$ in DOC-rich waters in transition zones of river and seawater of the Lena-Laptev region. Matsuoka et al. (2017) provided satellite-retrieved DOC concentration maps for coastal waters of the Lena River Delta region, retrieved with a DOC-$a_{CDOM}(443)$ relationship developed using a pan-Arctic in situ dataset. However, the retrieved DOC concentrations were likely underestimated compared to in situ measurements in the coastal regions of the Laptev Sea presented in this study. In coastal or $a_{CDOM}(443)$-rich, river-influenced water, the difference between the two relationships is expected to be highest. Applying the Matsuoka et al. (2017) relationship to $a_{CDOM}(443)$-rich waters outside its validity ranges (>3.3 m^{-1}) would result in underestimation of DOC compared to the relationship presented in this study. Taking mean Lena River $a_{CDOM}(443)$ of 4.1 m^{-1}, which is similar to the highest $a_{CDOM}(443)$ values in coastal waters, the difference in modelled DOC concentration between both relationships is 186.8 µmol L^{-1}. The main reason for this underestimation is likely the lack of near-coastal and river water samples with high DOC for the development of their relationship. This hypothesis was confirmed by testing the relationship of our dataset by removing coastal and river water. This decreased the slope of the fitting model and lead to an underestimation of DOC in coastal and river waters (without coastal and river water: slope=0.617). The slope of the reported fitting model from Matsuoka et al. (2017) is lower (0.448), compared to the fitting model from this study (all samples: slope=0.664). This difference highlights the importance of using a broad concentration range to develop such relationships.

The broad concentration range of the relationship presented here permits the generation of remotely sensed surface DOC concentration maps of the Laptev Sea across the fluvial-marine transition zone using $a_{CDOM}(443)$. The applicability of this relationship for other

Arctic fluvial-marine transition regions (e.g. Yenisei, Ob, Kolyma, Mackenzie) is untested and the relationship may need to be extended with regionally specific data.

Previous studies using $a_{CDOM}(443)$ often focused on different wavelengths for $a_{CDOM}(\lambda)$. The shape of the DOC-$a_{CDOM}(\lambda)$ relationship is strongly dependent on the chosen $a_{CDOM}(\lambda)$ wavelength: whereas DOC-$a_{CDOM}(350)$ shows a linear relationship, $a_{CDOM}(443)$ can be better described with a power function (see Equation 4.23). **Appendix Table 2** provides coefficients for selected $a_{CDOM}(\lambda)$ wavelengths. We encourage the data publication of all available wavelengths for $a_{CDOM}(\lambda)$ measurements in future studies to enable direct comparisons between studies and regions.

ONNS-derived DOC

The evaluation of ONNS-derived $a_{CDOM}(\lambda)^{sat}$ performed best when tested with in situ data (**Table 4.3**). Thus, we selected the ONNS-derived $a_{CDOM}(440)^{sat}$ to calculate DOC concentration based on the Equation 4.23. The evaluation of ONNS-derived DOC concentrations showed moderate performance (r^2=0.53). We suggest that the only moderate agreement likely results from rapid movement of near-coastal water fronts. Fluvial-marine transition zones, as in this study area, are characterized by rapidly moving water fronts with large variations in DOC concentration. A spatial shift of a plume between in situ sampling and the satellite acquisition can cause large errors in the match-up performance. All samples from LD10 expedition are located in the near-coastal areas east of the Lena River Delta where rapid movements of water fronts are likely. This could partly explain deviations comparing in situ measurements and the satellite derived DOC at a given pixel. Taking this into account, the observed agreement shows an adequate retrieval of DOC by satellite using the OCRS algorithm ONNS.

Using satellite-retrieved surface water DOC concentration maps (**Figure 4.7**b & d), we demonstrated rapid changes in DOC concentrations in the Laptev over 1 month in late summer. The rapid DOC decrease can result from a combination of vertical mixing, dilution, and microbial- and photodegradation of the organic material in the surface water (Holmes et al., 2008; Mann et al., 2012; Fichot et al., 2013). OCRS could potentially be used to monitor the rapid removal of DOM by degradation from surface waters on Arctic shelves.

4.5.3 OCRS algorithms in shallow Arctic fluvial-marine transition zones

We observed specific problems of $a_{CDOM}(\lambda)^{sat}$ retrievals for optically complex shallow shelf waters using different OCRS algorithms. The retrieved $a_{CDOM}(\lambda)^{sat}$ in shallow waters often shows a co-variation with high TSM, which is a result of high particle backscatter in the water such as sediments or some phytoplankton types. In our study, we observed that most OCRS algorithms show a strong coupling of $a_{CDOM}(\lambda)^{sat}$ and TSM in all areas of high sediment concentration (compare **Figure 4.7** and **Figure 4.9**b).

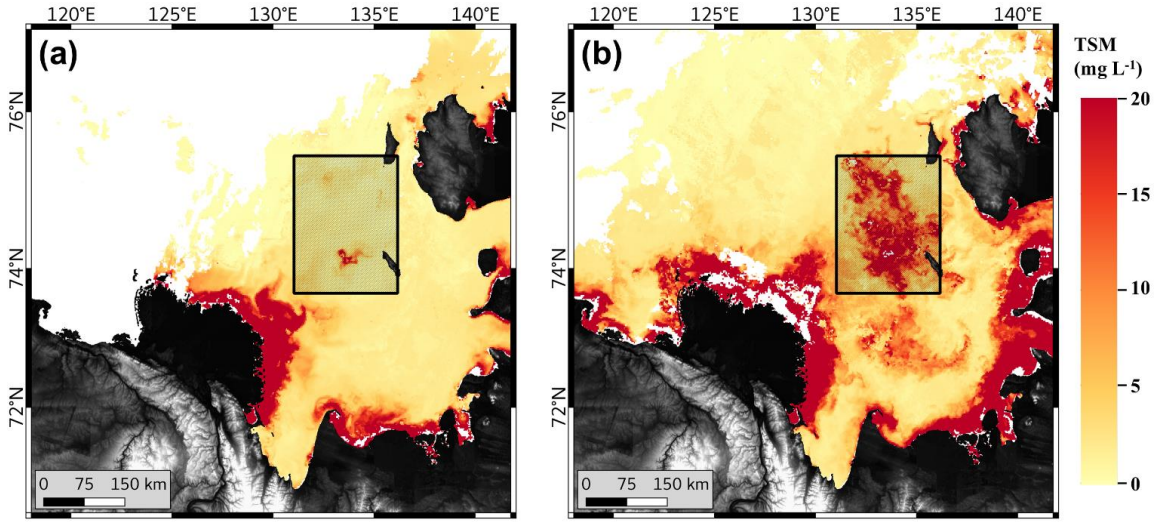

Figure 4.9: ONNS-derived TSM concentration for satellite mosaics from (a) August 2010 and (b) September 2010. Shallow water area is highlighted by black square.

Our study area, the Laptev Sea Shelf, is characterized by extremely shallow waters with frequent resuspension of sediments from the seafloor, for example during storm events. In the Lena River plume, close to the river mouth, where large amounts of TSM and organic matter are transported to the Arctic Ocean, we expect DOC and TSM to co-vary. Once exported by the Lena River, most particles quickly settle to the seafloor whereas DOM concentration gradually decreases with increasing physical mixing and ongoing degradation. In offshore resuspension areas with very high TSM concentration, DOC and TSM do not necessarily co-vary. Large amounts of terrigenous organic matter can be mineralized on short time scales (about 50% within a year, Kaiser et al. (2017)) and strongly degraded when deposited in sediments (Bröder et al., 2016, 2019; Brüchert et al., 2018).

We observe a strong increase of TSM concentrations in the eastern Laptev Sea in September (**Figure 4.9**b) compared to August (**Figure 4.9**a), which is likely caused by differences in wind speed and resulting wave energy leading to resuspension. During acquisitions in August, wind speeds were very low (NCEP reanalysis mean surface wind

speed of 2.06 m s^{-1} for 75 °N & 132.5 °E from August 1 to August 5, 2010) whereas in September winds were stronger (NCEP reanalysis mean surface wind speed of 6.54 m s^{-1} for 75 °N & 132.5 °E from September 4 to September 20, 2010). A high TSM concentration in the near-coastal regions around the Lena River Delta, caused by the sediment export by the Lena River, is similar in both mosaics.

The evaluation of OCRS algorithms with in situ data showed the generally good performance of the ONNS and the C2X algorithms (**Table 4.3**). However, shallow resuspension areas are not covered by in situ measurements. Thus, the performance of OCRS algorithms cannot be tested in these areas. Whereas the C2X algorithm derives high $a_{CDOM}(443)$ in the resuspension areas in the eastern Laptev Sea, the ONNS algorithm derives lower $a_{CDOM}(440)$ (**Figure 4.6**).

Including all pixels of each scene (**Figure 4.6**), the ONNS-derived $a_{CDOM}(440)$ does not show a linear relationship with TSM concentration (**Figure 4.10**a). However, using only pixels proximal to the Lena River Delta, we observe a correlation (r=0.68), which is caused by the co-variation of TSM and $a_{CDOM}(440)$ in river plume. The C2X-derived $a_{CDOM}(443)$ shows a linear relationship between $a_{CDOM}(443)$ and TSM (r=0.79). The correlation regimes of the $a_{CDOM}(443)$ and TSM from river mouth regions and resuspension areas are visible (**Figure 4.10**b). Thus, we show that C2X-derived $a_{CDOM}(443)$ might vary with TSM. Further confirmation of these satellite-based observations with in situ data is currently not possible due to a lack of in situ data in shallow areas. A partial independence between ONNS-retrieved $a_{CDOM}(440)$ and TSM is of high importance in shallow Arctic shelf waters, such as the Laptev Sea. Using C2X algorithm, resuspension events would result in erroneous estimation of $a_{CDOM}(443)$.

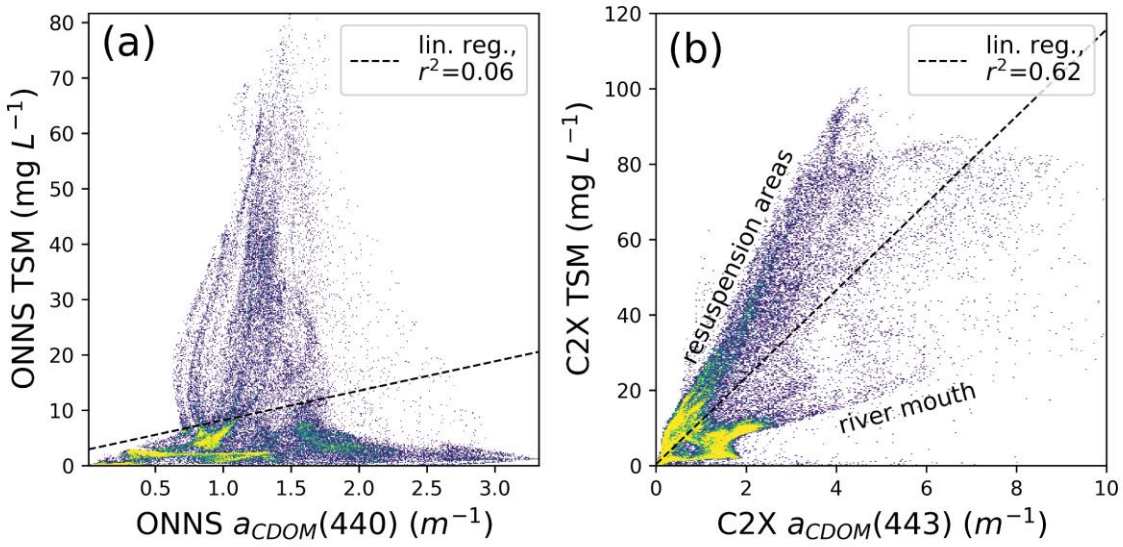

Figure 4.10: Relationship between (a) ONNS retrieved $a_{CDOM}(440)$ and TSM concentration and (b) C2X retrieved $a_{CDOM}(440)$ and TSM concentration for the MERIS scene from September 7, 2010. Relationship, using other scenes from September, is not varying significantly (September 18, 2010: ONNS r^2=0.22 and C2X r^2=0.55, 19.09.2010: ONNS r^2=0.23 and C2X r^2=0.67, September 20, 2010: ONNS r^2=0.03 and C2X r^2=0.66).

Furthermore, the C2X-derived TSM concentration is substantially higher compared to TSM concentration derived by ONNS (**Figure 4.10**). Örek et al. (2013) and Heim et al. (2014) report TSM concentrations between 10 and 70 mg L^{-1} for Lena River water and up to 18 mg L^{-1} in coastal water near the Lena River Delta measured in situ in August 2010. These values are similar to TSM concentrations derived by the ONNS algorithms but lower than C2X algorithm TSM. Considering overestimation of C2X derived $a_{CDOM}(443)$ and TSM compared to in situ data, the use of neural networks trained for a broad range of constituent concentration likely leads to inaccurate results. Combination of neural networks with narrow concentration ranges and a classification into distinct water types (results of classification shown in **Appendix Figure 7**), as used in ONNS-algorithm, provide more robust and accurate results in regions with a broad range of water types.

4.6 Conclusion

In this study, we demonstrate sources and modification of dissolved organic matter (DOM) by analysing $a_{CDOM}(\lambda)$ characteristics in the fluvial-marine transition zone where the Lena River meets the Laptev Sea. Our results suggest that the $a_{CDOM}(\lambda)$ spectral slope S350-500 could be useful to identify and distinguish processes that degrade DOM at this transition. Comparisons of $a_{CDOM}(\lambda)$ characteristics from this study with reported values from a global dataset and western Arctic waters identify DOM sources as primarily terrigenous.

We demonstrate the strength of a large in situ dataset that covers multiple water types for deriving the relationship between the optical DOM properties and DOC concentration in surface water of the Laptev Sea and Lena Delta region. The broad range of DOC concentrations and $a_{CDOM}(443)$ from river, coastal and offshore water used to develop this model enables the accurate estimation of DOC by $a_{CDOM}(\lambda)$ in the transition zone between river and seawater. Comparing satellite-retrieved $a_{CDOM}(440)$, using the OCRS ONNS algorithm, and in situ $a_{CDOM}(440)$ demonstrates the performance of the algorithm for these optically complex waters. DOC concentrations calculated from satellite data moderately agreed with in situ DOC measurements (r^2=0.53), demonstrating the applicability of the DOC-$a_{CDOM}(\lambda)$ relationship from our compiled dataset. ONNS-derived $a_{CDOM}(440)$ was found to be independent of the suspended sediment concentration. Thus, resuspension events and resulting sediment-rich backscattering waters seem to have no or little influence on the accuracy of ONNS-derived $a_{CDOM}(440)$.

The Arctic coastal waters of the Laptev Sea are a key region for the fate of terrestrial DOM and can be monitored synoptically using optical remote sensing with a reasonable accuracy. MERIS-retrieved DOC concentrations presented in this study provide a detailed picture of the spatial distribution of the DOC-rich Lena River water on the Laptev Sea Shelf and indicate the rapid changes in the magnitude of DOC concentrations in the surface waters within short time periods. If cloud distribution allows, optical remote sensing provides data of high spatial and temporal resolution to track freshwater pathways in the Arctic Ocean, which is of high interest to the oceanographic community.

4.7 Funding and acknowledgements

This work was financially supported by Geo.X, the Research Network for Geosciences in Berlin and Potsdam, (grant # SO_087_GeoX). Transdrift expedition data were obtained within the framework of the Laptev Sea System project, supported by the German Federal Ministry of Education and Research (BMBF grant # 03G0833) and the Ministry of Education and Science of the Russian Federation. Part of this study was funded by the Japan Aerospace Exploration Agency (JAXA) GCOM-C project (Contract #: 16RSTK-007867) to AM.

We thank the crews and colleagues on-board the research vessels involved in sampling. We are grateful to the colleagues of the Russian-German Otto-Schmidt-Laboratory in St. Petersburg for support and accessibility of laboratory instruments for sample analysis. We

are eminently thankful to Dr. Hajo Krasemann for processing MERIS scenes with the ONNS algorithm and the valuable discussion. NCEP-Reanalysis data were provided by the NOAA-CIRES Climate Diagnostics Center, Boulder, CO, USA at http://www.cdc.noaa.gov/. Furthermore, we thank Antje Eulenburg for laboratory analysis of several parameter datasets and Philippe Massicotte for sharing his dataset with us to compare our data. Projects from the EU Horizon 2020 programme (Nunataryuk, grant # 773421) and from the BMBF-NERC's Changing Arctic Ocean programme (CACOON, NERC: grant # NE/R012806/1, BMBF: grant # 03F0806A) supported discussions within a larger group of experts. The authors are grateful to Dr. Piotr Kowalczuk and one anonymous reviewer for their constructive comments, which helped to improve the manuscript.

Chapter V

Seasonal dynamics of dissolved organic matter in the Mackenzie Delta, Canadian Arctic waters: implications for ocean colour remote sensing

5 Seasonal dynamics of dissolved organic matter in the Mackenzie Delta, Canadian Arctic waters: implications for ocean colour remote sensing

B. Juhls[1], A. Matsuoka[2], M. Lizotte[2], G. Bécu[2], E. Devred[3], D. Doxaran[4], J. R. El Kassar[1], J. Ferland[2], M. H. Forget[2], A. Hilborn[3], J. Maury[4], P. P. Overduin[5], L. Oziel[2], M. Babin[2]

[1]Institute for Space Sciences, Freie Universität Berlin, Berlin, Germany

[2]Takuvik Joint International Laboratory, Département de Biologie, Université Laval, Québec City, Canada

[3]Laboratoire d'Océanographie de Villefranche, CNRS-UPMC, France

[4]Alfred Wegener Institute Helmholtz Centre for Polar and Marine Research, Potsdam, Germany

[5]Ocean and Ecosystem Sciences Division, Bedford Institute of Oceanography, Fisheries and Oceans Canada, Canada

Article in preparation: Juhls B., Matsuoka, A., Lizotte, M., Bécu, G., Devred, E., Doxaran, D., El Kassar, J. R., Ferland, J., Forget, M. H., Hilborn, A., Maury, J., Overduin, P. P., Oziel, L., Babin, M. (in preparation) Seasonal dynamics of dissolved organic matter in the Mackenzie Delta, Canadian Arctic waters: implications for ocean colour remote sensing.

5.1 Abstract

Rapid changes in the Arctic are affecting the aquatic environment. Increasing air temperatures and associated permafrost thaw in Arctic river catchments are expected to change the quantity and quality of organic matter (OM) in rivers and the coastal ocean. A significant amount of OM is delivered by river discharge into the Arctic Ocean. However, knowledge regarding the distribution and the fate of terrigenous organic matter and the carbon it contains when it is released to the coastal waters is remarkably lacking, particularly in permafrost regions. Sampling in Arctic regions comes with high logistical efforts and costs. In situ water sampling in Arctic regions is difficult due to harsh weather, dynamic ice conditions and remoteness. As a result, in situ observations in Arctic waters are mostly limited to short periods and small target areas. Ocean Colour Remote Sensing (OCRS) can overcome these challenges by providing synoptic and high frequency estimates of dissolved organic carbon (DOC) concentration in the surface water, if ice and

cloud conditions are favourable. OCRS can be a powerful tool to complement monitoring DOC fluxes, their potential changes under climate change, and deepen our understanding of their fate in the Arctic Ocean. However, the performance of OCRS in optically complex Arctic coastal waters is poorly evaluated. Empirical relationships between DOC and coloured dissolved organic matter (CDOM), required to estimate DOC concentrations from satellite-derived CDOM, are often limited in their validity to narrow concentration ranges for specific water types. The aim of this study is to capture the seasonal variability of the Mackenzie River plume and the DOC distribution on the Beaufort Sea Shelf. For that, extensive in situ sampling was carried out in the fluvial-marine transition zone, focusing on the strongly undersampled near-shore waters of the Mackenzie Delta region. The sampling started before spring ice break-up and ended in the fall 2019. Using the in situ dataset, existing OCRS atmospheric corrections (AC) and CDOM retrieval algorithms were evaluated. The evaluation of the three atmospheric correction algorithms showed that the Polymer AC yields the best performance (18.7% error). For the retrieval of CDOM, the gsmA algorithm showed better results (24.1% error) compared to the ONNS algorithm (54.1% error). The DOC-CDOM relationship based on merged datasets from this and the previous studies in the Mackenzie-Beaufort Sea region allowed the estimation of DOC concentrations from OCRS across the entire fluvial-marine transition zone which includes river, coastal, and offshore waters. Finally, the best performing combination of OCRS algorithms (Polymer AC and gsmA CDOM retrieval) was used to illustrate the seasonal variation of DOC in the surface waters of the Beaufort Sea on high spatial and temporal scales throughout the entire open water period. The results revealed a strong seasonal variability in size of the river plume and its DOC concentrations. The widest lateral extent of the plume was observed in June, early in the open-water period right after the spring freshet, indicating that the Mackenzie River runoff was the main driver of plume propagation and DOC distribution on the shelf. Later in the year when the Mackenzie discharge decreased, other processes such as currents and winds dominantly controlled the transport of the river water and the distribution of DOC on the shelf. Satellite-derived maps of surface water DOC concentration placed the in situ observations into a larger temporal and spatial context and revealed transport pathways, removal, and additional sources of DOC in the Mackenzie- Beaufort Sea region. Furthermore, they demonstrated the high capability of OCRS to monitor the seasonal variation of the river plume propagation and DOC distribution on the Beaufort Sea Shelf.

5.2 Introduction

Warming in the Arctic watersheds is expected to affect the biogeochemistry of riverine waters (Frey and McClelland, 2009; Holmes et al., 2012a). Particularly, the mobilization of organic carbon from thawing permafrost (Frey and Smith, 2005) accompanied by an increase in river discharge (Peterson, 2002; McClelland et al., 2006) are expected to affect the organic carbon flux from land to sea and its fate in the Arctic Ocean. Arctic rivers are characterized by a strong seasonal variation of dissolved organic carbon (DOC) export to the Arctic Ocean (Raymond et al., 2007; Stedmon et al., 2011; Holmes et al., 2012b; Le Fouest et al., 2013; Juhls et al., 2020). Monitoring the seasonality in the biogeochemistry of DOC in Arctic coastal waters, including its quantity and quality, can help us understand its impact on the global carbon cycle. Currently the seasonal variability of DOC-rich river water export, propagation, as well as its distribution and fate in Arctic coastal and shelf waters, is poorly understood. In situ sampling is often limited to a narrow period in time and restricted spatial scope. Especially near-shore coastal waters, which are the transition zones between river and ocean, are strongly undersampled due to their challenging accessibility. Ocean Colour Remote Sensing (OCRS) is a tool that enables the monitoring of surface water organic carbon concentration. The intensity of absorption by coloured dissolved organic matter (CDOM), which can be retrieved by satellite, can be related to DOC concentration using empirical relationships derived from in situ measurements. Increasingly, OCRS has been applied in Arctic shelf waters (Fichot et al., 2013; Matsuoka et al., 2016, 2017; Juhls et al., 2019) to observe dissolved organic matter (DOM) concentrations and distributions. Given the absence of clouds and ice, OCRS can provide a synoptic view and high temporal resolution. However, the performance of OCRS in near-shore Arctic coastal waters is poorly evaluated, mainly due to a lack of in situ observations. Furthermore, cross-compartment in situ datasets, covering river, coastal and offshore water, are needed to develop robust relationships between DOC and CDOM to extend the application of OCRS across the entire fluvial-marine transition zone.

The Mackenzie River is the fourth largest riverine freshwater source to the Arctic Ocean (Holmes et al., 2012b), releasing large amounts of organic matter and associated organic carbon to the Beaufort Sea. Most of its catchment area is underlain by zones of discontinuous permafrost, which are especially vulnerable to warming in the Arctic (Frey and McClelland, 2009). Tank et al. (2016) report a 39.3% increase in fluxes of DOC from the Mackenzie River over the last four decades and suggest permafrost thaw as an important

driver for that increase. While the monitoring of organic matter, its carbon fluxes, and their characteristics in Arctic rivers is steadily improving (Raymond et al., 2007; Cooper et al., 2008; Stedmon et al., 2011; Holmes et al., 2012b; Tank et al., 2016; Juhls et al., 2020), not much attention has been paid to the fluvial-marine transition zone, mostly due to the challenge it poses in terms of accessibility. These zones, which include estuarine, coastal, and near-shore waters, are suspected to be crucial for the fate of organic carbon in the Arctic Ocean and in the overall cycling of carbon in the Arctic (Vetrov et al., 2004; Granskog et al., 2009; Lasareva et al., 2019). Several studies suggest that fluvial fluxes are substantially altered in these zones before they reach the open Arctic Ocean (Emmerton et al., 2008; Holmes et al., 2012b; McClelland et al., 2012). However, distribution, transport behaviour, and removal rates of terrigenous organic matter on the shelf are ill-constrained. Although a few studies provided first insights into DOM fluxes and optical characteristics of the Mackenzie River (Raymond et al., 2007; Mann et al., 2016; Tank et al., 2016) and the offshore Beaufort Sea (Doxaran et al., 2012; Matsuoka et al., 2012, 2013; Antoine et al., 2013; Fichot et al., 2013), they focused on either the fluvial or marine system, leaving an understudied gap in the transition zone between both. During the ARDEX (2003), CASES (2002-2004), Circumpolar Flaw Lead (2008), and Malina (2009) expeditions, the fluvial-marine transition from the Mackenzie River water to the offshore Beaufort Sea was sampled for organic matter (Emmerton et al., 2008; Retamal et al., 2008; Vallières et al., 2008; Osburn et al., 2009; Shen et al., 2012; Forest et al., 2014). However, a low number of samples across a large region and limited seasonal coverage of the sampling could not resolve the spatial distribution and seasonal patterns of the Mackenzie River plume and its changing optical DOM characteristics.

To improve the use of OCRS in Arctic shelf waters, Matsuoka et al. (2013) designed a new algorithm for the retrieval of CDOM absorption using a semi-analytical approach, specifically adapted for Arctic waters. While the algorithm showed a reasonable accuracy (12% error) in offshore waters of the Arctic Ocean (Matsuoka et al., 2017), the performance in optically complex near-shore waters has not yet been comprehensively evaluated. Recently, another CDOM retrieval algorithm ONNS was designed by Hieronymi et al. (2017) for a broad range of water constituent concentrations, including extremely high absorbing and scattering waters such as the near-shore waters of the Beaufort Sea. The performance evaluation of the ONNS algorithm on the Laptev Sea Shelf, including coastal waters near the Lena River mouth, indicated reasonable accuracy for the OCRS retrieval of

CDOM absorption (Juhls et al., 2019). Besides testing the accuracy of CDOM retrievals, the performance of the atmospheric correction algorithms in Arctic near-shore coastal waters also requires thorough evaluation, hence the requirement for in situ radiometric measurements. Relationships between DOC and CDOM enable the monitoring of DOC from space. Matsuoka et al. (2012) established such a relationship for the Beaufort Sea region, which was, however, limited in its validity to mostly offshore waters due to the lack of samples from near-shore or river waters. Other reported relationships from varying Arctic regions (Matsuoka et al., 2012, 2017; Pugach et al., 2018; Juhls et al., 2019) indicate that substantial regional and seasonal variability of DOM characteristics can affect these relationships. In order to provide accurate estimates of DOC across the fluvial-marine transition zone using OCRS, DOC-CDOM relationships require inclusion of a wider range of water types across domains.

To understand the temporal and spatial influences of highly dynamic seasonal variations in Arctic river discharge and DOM flux on the composition of shallow shelf surface water, we investigate the seasonal and spatial variability of DOM in the fluvial-marine transition zone in the Mackenzie River – Beaufort Sea region using in situ and OCRS data. Therefore, we first evaluate the performance of multiple OCRS algorithms and develop a new DOC-CDOM relationship for monitoring of DOC concentrations from space. To achieve this goal, we use a unique dataset of in situ biogeochemical and bio-optical properties measured during an extensive field campaign in the Mackenzie Delta region from April to September 2019. Second, we use OCRS to illustrate the seasonal variability of DOC distribution on the Beaufort Sea Shelf on a large spatial and temporal scale.

5.3 Methods

5.3.1 Study area, sampling periods, and strategies

We carried out an extensive field campaign in the Mackenzie Delta region from April to September 2019. The goal was to capture the seasonal variability of DOM distribution and characteristics from before ice break-up in spring until before freeze-up in late fall. The repeated sampling focused on the two main outflow regions of the Mackenzie River: Shallow Bay and Mackenzie Bay in the west and Kugmallit Bay in the east, respectively, as well as on the river channels across the delta. Most sampling locations were revisited four times (**Figure 5.1**). Sampling during different seasons is extremely challenging in this region due to uncertain ice cover and broken ice fields during and after ice break-up.

Additionally, very shallow water (<5 m) mandates the use of small draught boats, which is challenging under frequently harsh weather conditions. To tackle these challenges, various sampling platforms were used (**Figure 5.2**). The efforts that were required for such a multi-platform operation are part of the value and uniqueness of the dataset presented in this study.

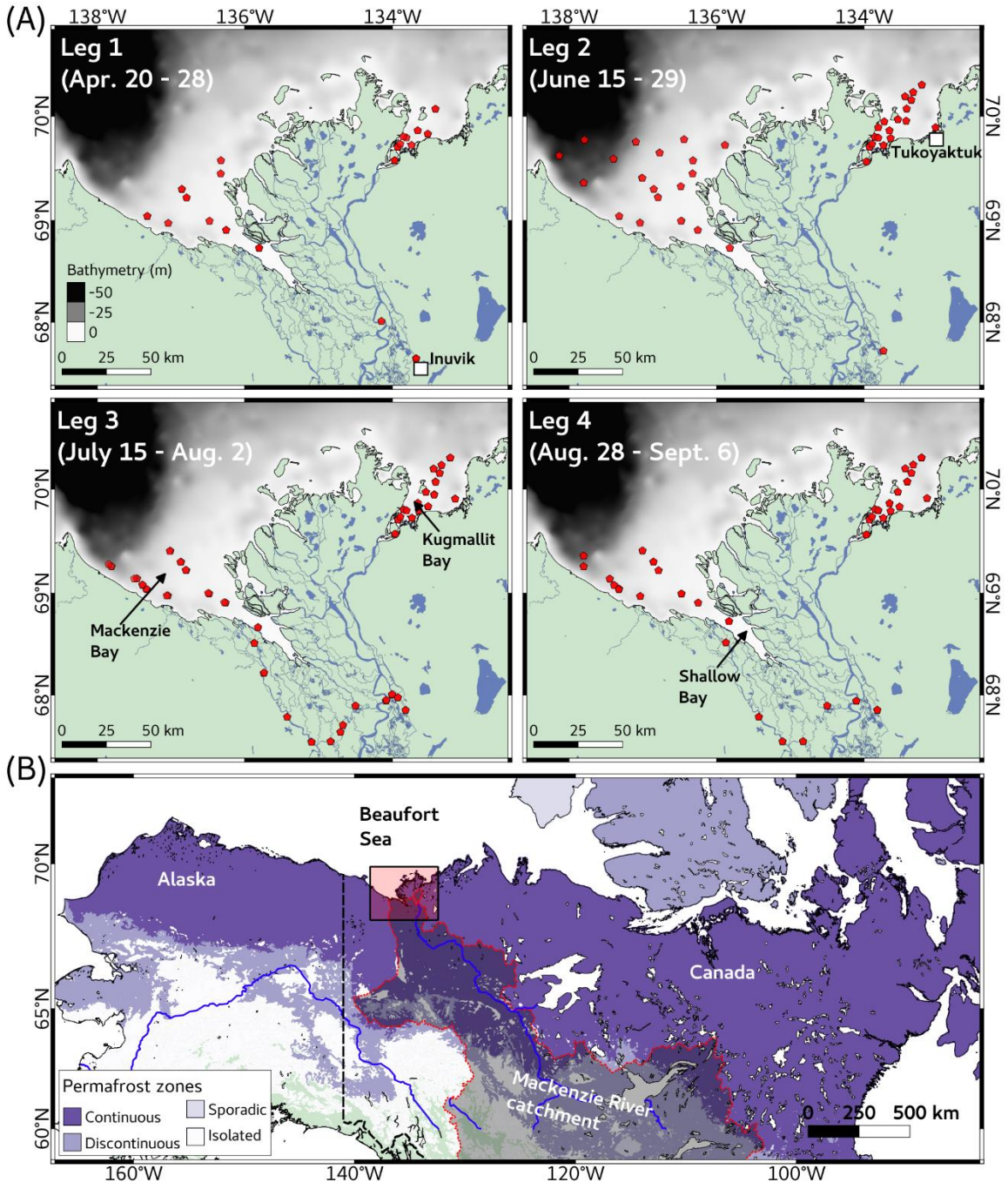

Figure 5.1: (A) Sampling locations (red points) for each of the four expedition legs. (B) Northern part of the Mackenzie River catchment and underlying permafrost zones (Obu et al., 2019).

During the first leg of the campaign (April 20-28, 2019), the Mackenzie River and the coastal Beaufort Sea had a consolidated ice cover. Sampling locations were reached by helicopter (Shallow and Mackenzie Bay) and snowmobiles (Kugmallit Bay). Water samples and CTD profiles were taken from holes drilled through the ice. During leg 2 (June 15-29, 2019), remnant ice fields were expected in Mackenzie and Shallow Bay in the early period of the open-water season, rendering the use of boats dangerous. Thus, water samples and CTD profiles were taken from a hovering helicopter, which had the advantage of allowing greater spatial coverage. In Kugmallit Bay, small motorboats (~6 m in length) were used. Similar boats were used during leg 3 (July 25 to August 2, 2019) and leg 4 (August 28 to September 6, 2019). The sampling area was located near the river mouth to capture a salinity gradient from 0 (river water) to >20 (marine-dominated water). Overall, sampling was carried out at 143 stations throughout the four expedition legs of which 14 stations have been revised during all four legs.

Figure 5.2: Sampling platforms used during the expedition. (A) Under-ice sampling in Shallow Bay in April 2019 (credit: Laurent Oziel). (B) In-flight helicopter sampling in Shallow Bay in June 2019 (credit: Bennet Juhls). (C) Typical small boat used for sampling in Mackenzie, Shallow, and Kugmallit Bays during the open water period (credit: Martine Lizotte).

The four sampling periods were chosen to cover the main variations of the Mackenzie River hydrograph. Leg 1 (April 20-28) captured the pre-freshet season, before the river and land-fast ice had broken up. This period represents typical winter conditions when the discharge of the Mackenzie River is low. Leg 2 (June 15-29) covered the period right after the break-up, when the Mackenzie River and the coastal Beaufort Sea became ice free and a maximum flux of freshwater flowed to the Beaufort Sea. Leg 3 (July 25 to August 2) and leg 4 (August 28 to September 6) were carried out during the Arctic middle and late summer, after air temperatures had reached their annual maximum and the sea ice extent on the Beaufort Sea had reached its annual minimum.

5.3.2 In situ hydrological, biogeochemical and radiometric data

Hydrological data of the water column were acquired with a conductivity-temperature-depth probe (CTD RBR Maestro during leg 1 and a CTD RBR Concerto during legs 2 to

4). During leg 1, the CTD was manually lowered in the water through an ice hole with a velocity of less than 0.3 m s^{-1} and an acquisition frequency of 6 Hz, yielding a vertical resolution of a few centimeters. During legs 2 to 4, the CTD was installed on a Seabird Scientific (formerly WETLabs) optical package frame, which was deployed with a velocity of 0.3 m s^{-1} and an acquisition frequency of 8 Hz. Only downcasts were used and poor quality profiles, that had been affected by iced sensors, were removed. Atmospheric pressure was used to tare the CTD pressure sensors. CTD profiles were smoothed and binned to a regular 0.01 m depth grid.

For DOC concentration, water samples were filtered through 0.7 µm GF/F filter, and acidified with 25 µL Suprapur HCl (10 M) on the same day of sampling. DOC samples were stored and kept at 4 °C in the dark during transport until further analysis. Concentration of DOC was measured using high-temperature catalytic oxidation (TOC-VCPH, Shimadzu) at the Alfred Wegener Institute (AWI) Potsdam, Germany. Blanks (Milli-Q water) and certified reference standards (Battle-02, Mauri-09 or Super-05 from the National Laboratory for Environmental Testing, Canada) were measured for quality control.

Measurement of CDOM absorption was conducted from a water sample using an UltraPath liquid waveguide system (World Precision Instruments, Inc.) over the wavelengths ranging from 200 to 722 nm (see also Matsuoka et al. (2012)). To minimize temperature effects, both the sample and the reference water were kept at 4 °C for at least 30 minutes prior to analysis. We followed the International Ocean Colour Coordinating Group (IOCCG) Ocean Optics and Biogeochemistry CDOM protocols (Mannino et al., 2019) with a few modifications: 1) reference water with salinity ±2 relative to the sample was prepared on site to minimize the effect of difference in refractive index between sample and reference; 2) CDOM was measured in flow mode (a measurement was made while water was running using a peristaltic pump) (Lefering et al., 2017). While the use of a long optical cell provides a good signal in the visible spectral domain essential to OCRS, it necessarily suffers from light saturation in the UV domain. To overcome this issue, an optimal length of a cell (i.e., 10 cm or 200 cm) was carefully selected following an empirical relationship between observed optical density at 350 nm and at 443 nm based on Matsuoka et al. (2012). For each sample, measurements were done in triplicates. A quality control was made by visual inspection for each spectrum.

CDOM measurements were fitted using following equation:

$$a_{CDOM}(\lambda) = a_{CDOM}(\lambda_0) * e^{-S(\lambda-\lambda_0)}, \quad \text{(Equation 5.24)}$$

where S is the spectral slope of $a_{CDOM}(\lambda)$ between 350 and 500 nm (Babin et al., 2003; Matsuoka et al., 2012). The specific ultraviolet absorbance (SUVA; m^2 g C^{-1}) was calculated by dividing the decadal absorption (A/l; m^{-1}) at 254 nm by DOC concentration (mg L^{-1}).

Radiometric C-OPS data

Vertical profiles of downwelling irradiance (E_d) and upwelling radiance (L_u) were measured during legs 2, 3, and 4 using a Compact-Optical Profiling System (C-OPS) in a ICEPRO frame from Biospherical Instruments, Inc. (a system description is available in Morrow et al. (2010)). Additionally, above-surface incident downward irradiance ($E_s(0^+)$) was measured at about two meters above sea level and was used to correct in-water E_d and L_u for changes in the incident light field (Zibordi et al., 2019). All radiometric quantities were measured at 19 wavelengths spanning from 380 to 875 nm. In-water profiles were obtained from the boat using a 3 m long pole, deployed towards the sun to avoid shading from the boat. The data that were acquired with a tilt of more than 5 degrees were discarded (Hooker et al., 2013). Subsurface downward irradiance and upward radiance $E_d(0\text{-})$ and $L_u(0\text{-})$ were estimated with an iterative least square fitting of the log-transformed $E_d(z)$ and $L_u(z)$ vs depth z. Fitting was applied to successively greater depths until the correlation coefficient (r^2) exceeded 0.99 or until the layer thickness reached 2.5 m (Bélanger et al., 2017). The Remote Sensing Reflectance (R_{rs}) was calculated following Mobley (1999) with:

$$Rrs\ (\lambda) = \frac{0.54 * L_u(0^-,\lambda)}{E_s(0^+,\lambda)}. \quad \text{(Equation 5.25)}$$

Note that C-OPS measurements were taken during leg 2 (only in Kugmallit Bay), leg 3 and leg 4. There were no under-ice measurements using the C-OPS during leg 1.

5.3.3 Remote Sensing data

Sentinel-3 OLCI a and b full resolution (FR) Level 1b (L1b) data were acquired from https://coda.eumetsat.int. We downloaded all available scenes acquired at the time of in situ sampling (±1 day) for the open water season (leg 2, 3 and 4). In this study, we tested three algorithms for atmospheric corrections: (1) The baseline atmospheric correction

BAC/BIAC, based on the black pixel assumption including bright pixel correction, downloaded as L2 product (further referred to as WFR) from https://coda.eumetsat.int; (2) The spectral optimization algorithm Polymer v.4.12 (Steinmetz et al., 2011), which models the atmospheric contribution through a polynomial function, processed in python using the L1b FR data; and (3) the neural network approach C2RCC v.2.1 (Brockmann et al., 2016), processed via GPT in SNAP v.7.0.3 using L1b FR. For Polymer and C2RCC, standard processing parameters were chosen and no ancillary data was used. The L1b data served as the basis for further processing for atmospheric corrections and retrieval algorithms. While bidirectional correction was applied for Polymer and C2RCC, it was not applied for WFR. Atmospherically corrected OLCI Remote Sensing Reflectance (R_{rs}) was then used as an input to two in-water retrieval algorithms: (1) the semi-analytical in-water algorithm gsmA (Matsuoka et al., 2013), which was specifically adapted for Arctic waters and adapted to OLCI bands for this study, and (2) the ONNS processor (Hieronymi et al., 2017; Hieronymi, 2019), which consists of several blended neural networks that are specialized for 13 different optical water classes including optically complex waters.

For match-up comparisons between in situ and satellite data, a three by three pixel matrix around each sampling location was extracted from all satellite images acquired within six hours of the in situ sampling period. All extracted pixels were filtered by removing pixels that were flagged by using a list of flags that are provided by the individual atmospheric corrections (**Appendix Table 3**). If less than four of nine pixels were valid following the flag filtration, the station was excluded from further analysis. When stations were covered by more than one satellite acquisition within the six hours surrounding the sampling time, all available pixels were included in the analysis, relaxing the recommended criterion of ± one hour (or ideally shorter for coastal waters). Finally, we calculated a median R_{rs} of the extracted pixels for each station.

5.3.4 Match-up statistics

To evaluate the performance of the match-ups we used the slope and the coefficient of determination (r^2) of the linear regression between in situ and remotely sensed R_{rs}. Furthermore, the mean percentage error (MPE) and the root mean square error (RMSE) (Bailey and Werdell, 2006; Matsuoka et al., 2017) were calculated as:

$$MPE\ (\%) = median(100 * \left|\frac{X_{sat} - X_{in\ situ}}{X_{in\ situ}}\right|), \qquad \text{(Equation 5.26)}$$

$$RMSE\ (sr^{-1}) = \sqrt{\frac{\sum_{n=1}^{N}[X_{sat} - X_{in\ situ}]^2}{N}}, \qquad \text{(Equation 5.27)}$$

where X_{sat} and $X_{in\ situ}$ are the satellite-derived and in situ measured $a_{CDOM}(443)$, respectively.

5.4 Results and discussion

5.4.1 Seasonality of Mackenzie River plume propagation observed in situ

The Mackenzie River, like all Arctic rivers, is characterized by a nival hydrographic regime (Yang et al., 2015): low water discharge in winter is followed by a very high discharge in spring during a short freshet. In summer, the discharge is variable and mostly depends on the intensity of rain events within the catchment. The extent of river plume propagation to the Beaufort Sea strongly depends on the volume of exported water, but also on other factors including wind and ocean currents.

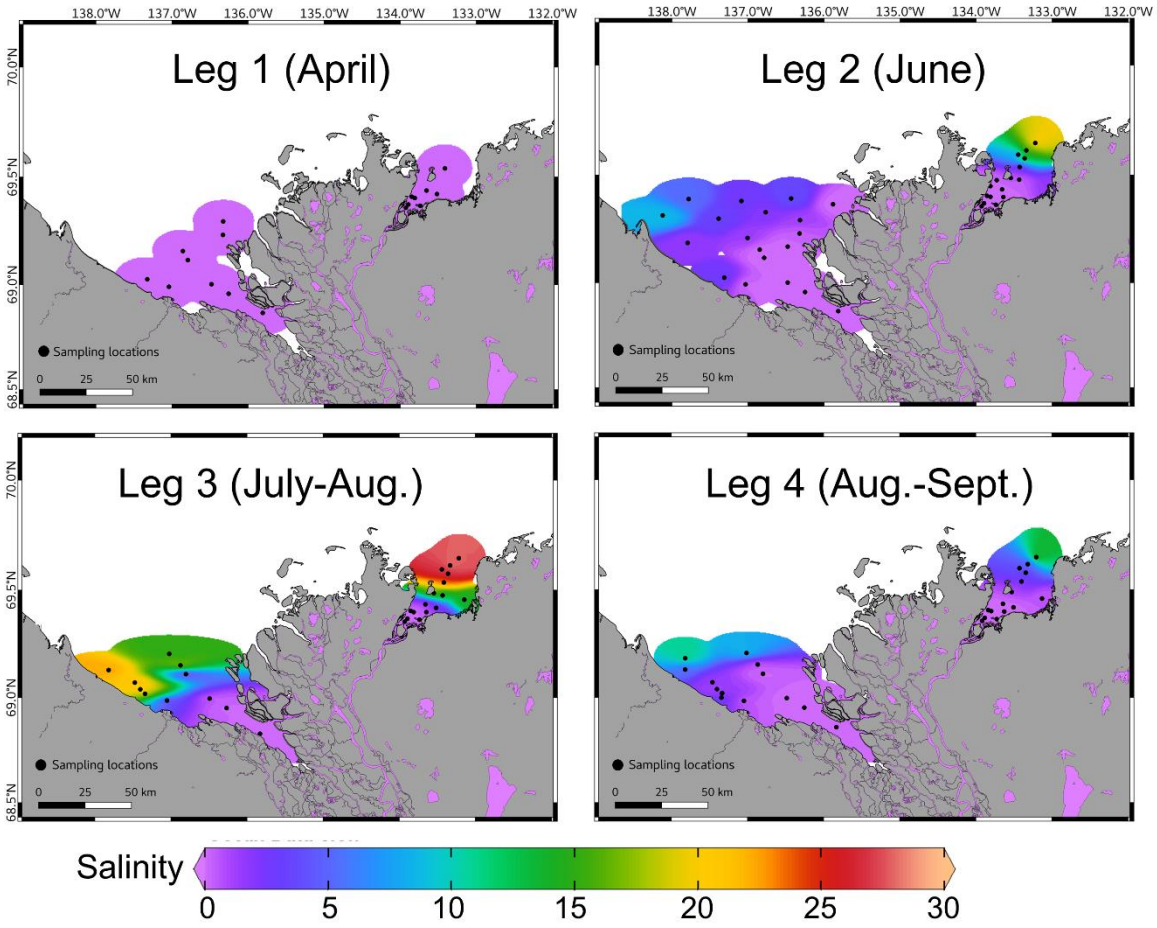

Figure 5.3: Spatial distribution of the in situ salinity in the surface water during the four expedition legs.

Figure 5.3 shows the in situ observed surface salinity distribution in the coastal Mackenzie Delta region during the four expedition legs in 2019. In April, during leg 1, solely fresh river water was found within the entire sampled area, with the salinity ranging between 0.11 and 0.17 in the surface waters right below the ice. Even at the distant offshore stations (>50 km from river mouth), no higher salinity water was observed. In leg 2, the fresh river water plume displayed the greatest extent of the three expedition legs during the open water period. Whereas in the western bay (Mackenzie and Shallow Bays), the river plume propagated over large areas with low salinities observed more than 100 km away from the river mouth, the plume extent in the eastern bay (Kugmallit Bay) was limited to only a few tens of kilometres from the mouth. The bigger plume size in the Mackenzie Bay (west) compared to the Kugmallit Bay (east) is likely a direct result of a larger freshwater reception in the Mackenzie Bay. In summer, during leg 3, the river plume extent was substantially smaller compared to leg 2. High salinity waters (>20) were found in the eastern sector of Mackenzie Bay and in the northern sector of Kugmallit Bay. At the end of August/ beginning of September, during leg 4, the plume extent with low salinity water once again increased and high salinity waters were found only in the most offshore stations.

5.4.2 Seasonal variability of dissolved organic matter in coastal surface water

Concentration of organic matter was measured by using the bulk optical parameters CDOM absorption at 443 nm ($a_{CDOM}(443)$). The carbon content of the dissolved organic matter was measured as DOC. **Figure 5.4** shows the observed ranges for a representative subset of stations that were revisited during all four expedition legs (n=14). Concentrations of DOC from under ice samples during leg 1 showed the highest range from 3.3 to 8.8 mg L^{-1} with a mean value of 5.7 mg L^{-1}. The mean DOC concentration for leg 2 (5.8 mg L^{-1}) was the highest among all legs, and the mean DOC concentration for leg 3 was the lowest (4.1 mg L^{-1}). During leg 1, $a_{CDOM}(443)$ was low and, unlike DOC concentrations, showed a very narrow range (0.39 to 0.73 m^{-1}). Seasonal patterns of DOC and $a_{CDOM}(443)$ were, however, similar with the lowest $a_{CDOM}(443)$ during leg 1 (mean of 0.55 m^{-1}) and the highest during leg 2 (mean of 1.41 m^{-1}). The changing ratio between DOC and CDOM is shown by SUVA, which can be a useful proxy for the molecular weight (Chowdhury, 2013) and the aromatic content (Weishaar et al., 2003) of DOM. The low SUVA (~1.6 m^2 g^{-1} C) during leg 1 points towards low molecular weight and aromaticity indicating a distinctly different source of

the DOM in winter. In contrast, high SUVA during leg 2 indicates high molecular weight and high aromatic content which is characteristic of young DOM with recently fixed carbon (Amon et al., 2012) likely originating from modern plant litter (Stedmon et al., 2011). During the open water period (leg 2 to 4), SUVA is generally higher compared to leg 1. The lower SUVA during leg 3, coinciding with a lower discharge (**Figure 5.11**) and consequent decreased land surface drainage, is feasibly related to increasing DOM source fractions from permafrost degradation (Abbott et al., 2014).

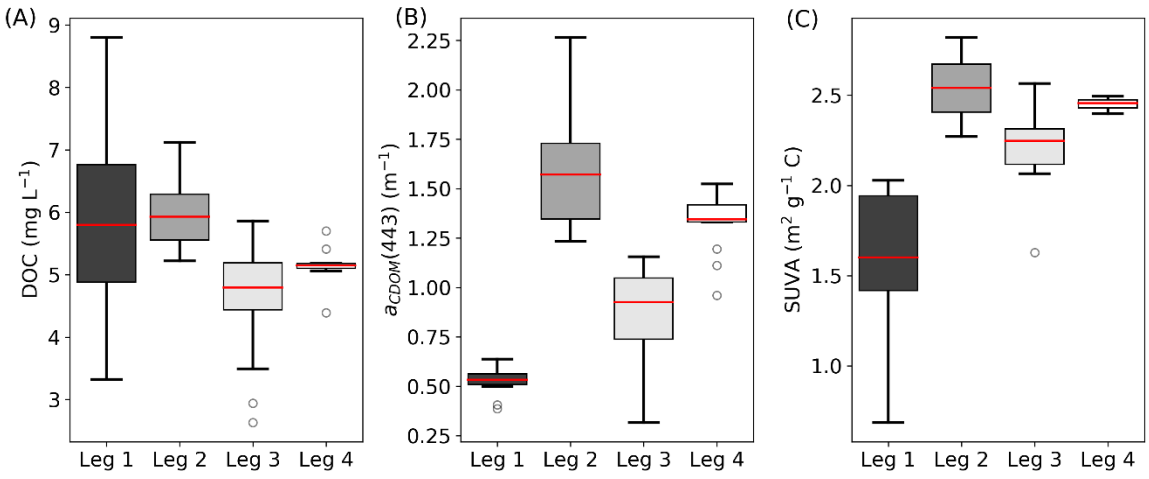

Figure 5.4: Main statistics of DOC concentration (A), CDOM absorption at 443 nm (B), and SUVA (C) for only the stations that were revisited during all four expedition legs (n=14).

Observed DOC concentrations and $a_{CDOM}(443)$ showed a strong relationship with salinity for all expedition legs during the open water period (**Figure 5.5**). The mixing line for both DOC and $a_{CDOM}(443)$, varied slightly between the expedition legs in slope and intercepts (represented by grey areas in **Figure 5.5**). Zero salinity intercept of the mixing lines (red symbols in **Figure 5.5**), including the variability between the legs, are within or close to the observed river concentrations. The highest DOC and $a_{CDOM}(443)$ along the salinity gradient were observed during leg 2, whereas the lowest DOC and $a_{CDOM}(443)$ were observed during leg 4.

The strong relationship of DOC and $a_{CDOM}(443)$ to salinity agrees to earlier studies that reported conservative mixing behaviour of DOM in the coastal Beaufort Sea (Emmerton et al., 2008; Osburn et al., 2009; Matsuoka et al., 2012) and clearly identifies terrigenous material as the dominant source of DOM. Larger amounts of autochthonously produced DOM from primary production or additional release of DOC by coastal erosion would be visible in deviations from the hypothetical mixing line (regression line in **Figure 5.5**). The main driver for the seasonal variability of the mixing line is likely the seasonal variation of

DOC and $a_{CDOM}(443)$ in the Mackenzie River, which defines the initial concentration at zero salinity. Only for leg 4, the mixing line is lower compared to leg 3 (not shown), although river DOC and $a_{CDOM}(443)$ was higher during leg 4. The found relationship between DOC and salinity (combined leg 2 to 4, red lines in **Figure 5.5**A and B) agrees well with the relationships reported in Osburn et al. (2009) and Matsuoka et al. (2012). The found relationship between $a_{CDOM}(443)$ and salinity, agrees well with Osburn et al. (2009) whereas the relationship reported by Matsuoka et al. (2012) is substantially different.

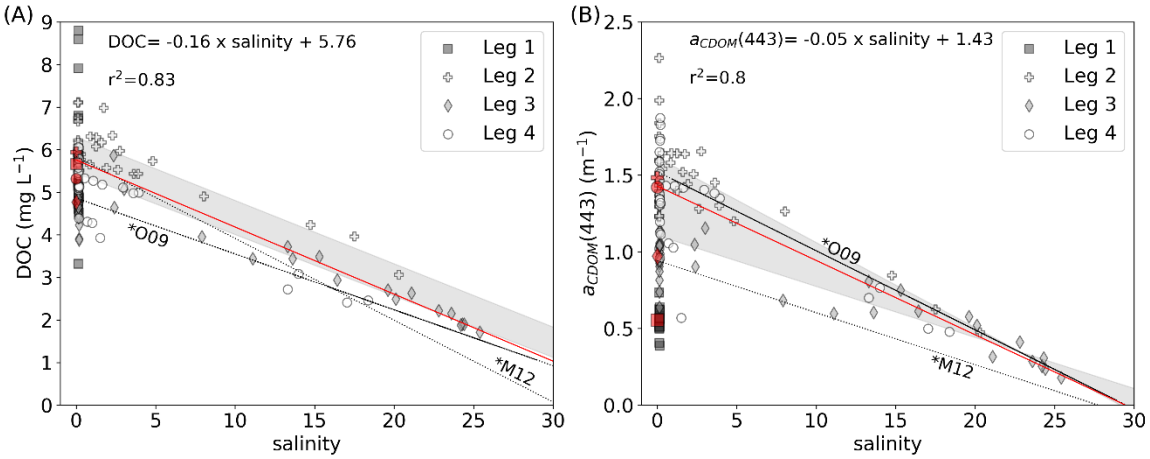

Figure 5.5: Relationships between DOC and salinity (A) and $a_{CDOM}(443)$ and salinity (B) for all samples from four expedition legs. The red lines show the regressions for the samples from legs 2, 3, and 4 (samples with salinity <0.5 are excluded). Red symbols show the mean DOC (A) and mean $a_{CDOM}(443)$ (B) for samples with salinities <0.5 (river water). The grey filled areas show the range of relationships, when calculated separately for each leg. Reported regression lines from Osburn et al. (2009) for the coastal Beaufort Sea (*O09) and from Matsuoka et al. (2012) for the offshore Beaufort Sea (*M12) are given for comparison. Note that for leg 1 no salinities >0.5 were observed and thus no regression line between salinity and DOC or $a_{CDOM}(443)$ was considered.

DOC-CDOM relationship

Concentrations of DOC in river-influenced water can be estimated from the absorption intensity of the coloured DOM fraction (CDOM). This is empirically based on the multiple studies reporting a strong relationship between DOC and CDOM on Arctic shelf seas (Matsuoka et al., 2012, 2017; Gonçalves-Araujo et al., 2015; Pugach et al., 2018; Juhls et al., 2019). For an accurate quantification of DOC from CDOM in the fluvial-marine transition, a robust relationship must be developed that addresses the knowledge gap associated with near-shore waters and changing seasons. We compared the relationships of the individual expedition legs of this study to previously reported DOC-CDOM relationships from other Arctic shelves. Variations of the DOC-CDOM relationship can be caused by geographical differences, different seasons when samples were collected or different concentration ranges that were used to develop the relationships. The

identification and characterization of this variability is necessary to define the validity of these relationships.

Figure 5.6 shows the relationship between DOC and $a_{CDOM}(443)$ for all the samples from the four expedition legs. We found a strong non-linear relationship for legs 2 to 4, but not for leg 1. Samples from leg 1 showed high variability in DOC but low variability in $a_{CDOM}(443)$. Thus, the relationship, developed from samples during the open water period, cannot be used to estimate DOC from CDOM during the ice cover period and may not be representative of the shoulder seasons in spring and fall. Generally, the DOC-CDOM relationship for the open water period (combined legs 2-4) is similar to previously reported relationships for the Lena River – Laptev Sea transitional zone (Juhls et al., 2019), offshore Beaufort Sea (Matsuoka et al., 2012), and pan-Arctic (Matsuoka et al., 2017). The relationships from Matsuoka et al. 2012 and 2017 differ substantially from the relationship from combined leg 2, 3 and 4 of this study in high concentration DOC ranges (>5 mg L^{-1}), which is likely caused by a lack of samples from the river mouth waters with high DOC concentration that were used by Matsuoka et al. (2012). This is confirmed by a close resemblance between the DOC–CDOM relationship from this study and the DOC–CDOM relationship from Juhls et al. (2019), which was developed using a large number of samples from river, coastal, and offshore waters in the Laptev Sea region. The comparison of reported relationships with the cross-domain coverage of the relationship from this study endorsed the use of non-linear models for an optimal fit. Seasonal differences in DOM characteristics that result in changing relationships between DOC and CDOM further complicate the development of a robust model. However, in order to consider seasonal variations of the relationship, more in situ data are needed.

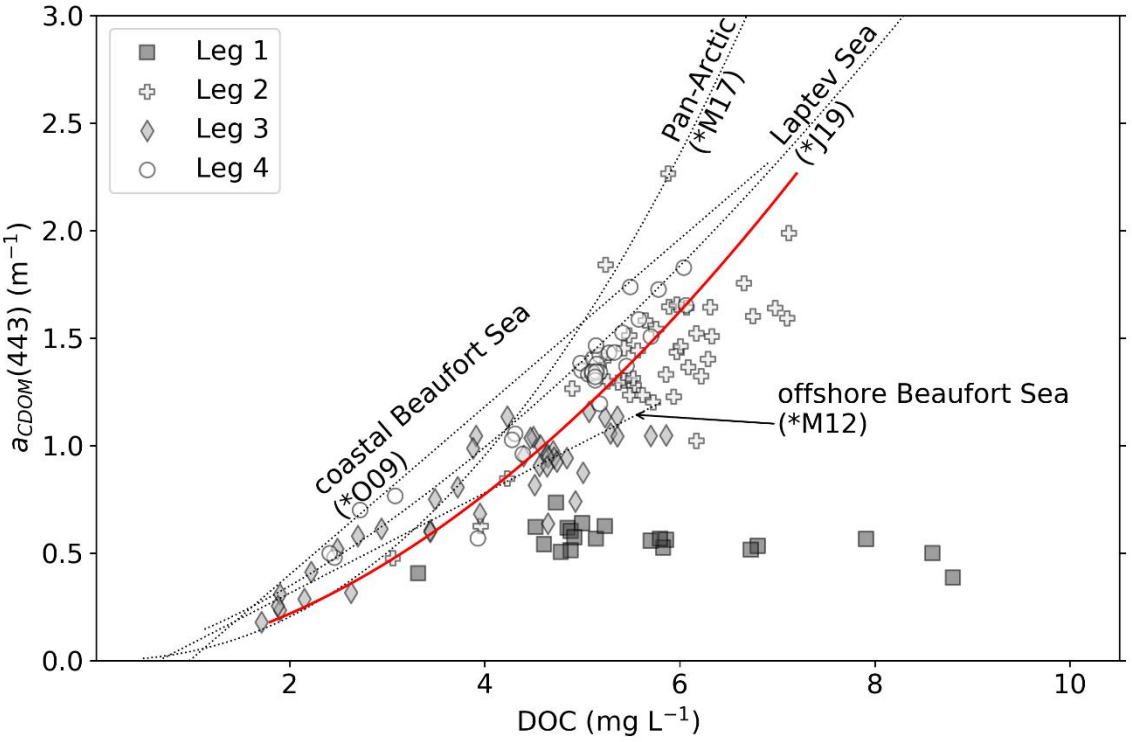

Figure 5.6: Relationships between DOC and $a_{CDOM}(443)$. The red solid line shows the regression for the open water samples from this study (leg 2, 3 and 4) (DOC = $10^{0.663}$ x $a_{CDOM}(443)^{0.519}$). The dashed black line shows the relationships reported by Osburn et al. (2009) for the coastal Beaufort Sea (*O09), Matsuoka et al. (2012) for the offshore Beaufort Sea (*M12), Matsuoka et al. (2017) for the pan-Arctic (*M17), and Juhls et al. (2019) for the Laptev Sea (*J19).

5.4.3 Evaluation of Ocean Colour Remote Sensing data

To evaluate the performance of OCRS in the coastal waters of the Mackenzie Delta – Beaufort Sea region, we first tested three available atmospheric corrections (WFR, C2RCC v.2.1, and Polymer 4.12) by comparing in situ measured R_{rs} with satellite-derived R_{rs}. Following this, we tested two CDOM retrieval algorithms (ONNS and gsmA) using the R_{rs} of each of the three tested AC's. Note that only legs 2, 3 and 4 were considered for OCRS evaluation, since the surface of the water was covered in ice during leg 1.

Atmospheric correction

Figure 5.7 shows the match-up comparisons between in situ measured R_{rs} (per steradian; sr^{-1}) and the satellite-derived R_{rs}. The Polymer algorithm provides best performance with the lowest MPE (mean of three wavelengths=18.7%) and the lowest RMSE (mean of three wavelengths=0.0026 sr^{-1}) compared to the other two AC's tested (**Figure 5.7**, **Table 5.1**). The low slope of the regression for the three evaluated wavelengths, especially for 443 and 510 nm, indicates that Polymer is not sensitive enough to changing R_{rs}, leading to an overestimation at lower values and underestimation at higher values, especially at lower

wavelengths. The C2RCC algorithm could retrieve R_{rs} at more stations than the other tested AC's, indicating a higher robustness of this algorithm. The low number of retrieved R_{rs} for WFR and Polymer was caused by flagging values that were outside of validity bounds for the AC algorithm. The red band at 665 nm, which also has the highest R_{rs} range, showed the best performance for all tested AC's.

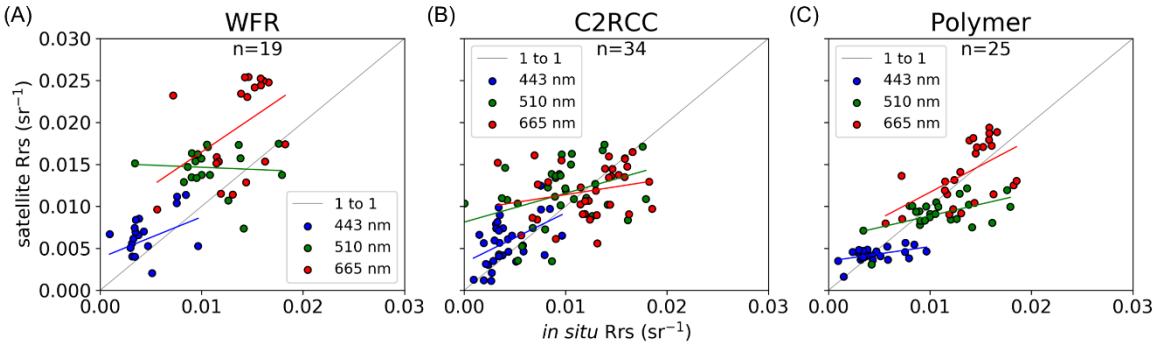

Figure 5.7: Match-up of in situ and satellite R_{rs} of three selected wavelengths in the blue (443 nm), green (510 nm) and red (665 nm) after using the AC's WFR (A), C2RCC (B) and Polymer (C). Only the stations where in situ measurements could be paired with satellite acquisitions (±6 hours of sampling period) were used.

Table 5.1: Performance of different AC at three different wavelengths: match-ups between in situ and satellite R_{rs}.

AC	Slope			r^2			MPE (%)			RMSE (sr^{-1})		
	443 nm	510 nm	665 nm	443 nm	510 nm	665 nm	443 nm	510 nm	665 nm	443 nm	510 nm	665 nm
WFR	0.49	-0.05	0.82	0.27	0.0	0.2	44.1	36.3	35.3	0.0041	0.0056	0.0077
C2RCC	0.59	0.34	0.19	0.21	0.14	0.05	39.6	32.5	16.0	0.0031	0.0048	0.0043
Polymer	0.17	0.28	0.64	0.24	0.29	0.32	25.2	15.6	15.4	0.0019	0.0034	0.0032

Generally, the match-up comparison indicates rather poor performances of all three AC's in the near-shore waters of the Mackenzie Delta - Beaufort Sea region. However, the evaluation of AC's in extremely optically complex waters as in this study is difficult due to at least two factors. First, an evaluation requires a high accuracy of in situ measured R_{rs}, which is challenging to achieve in these waters. This is because subsurface radiometric measurements for the retrieval of R_{rs} require extrapolation of $L_u(z)$ to right below the surface ($z=0^-$). The quality of the estimate at the 0^- m depth strongly depends on whether the layer that was used for the extrapolation is representative for the layer the satellite detects. If multiple water layers with different optical properties are present, it is necessary to restrict the extrapolation to the uppermost water layer. At some locations, only a very thin layer (<50 cm) of turbid river waters overlaid transparent saline waters with distinctly different optical properties. Using small vessels meant that measurements often took place at high tilt angles, reducing the number of data points that were used and resulting in a

weaker regression for the extrapolation of $L_u(z)$ to the water surface. Second, waters within the fluvial-marine transition zone can be highly turbulent and a time difference of even just a few minutes can be sufficient to explain the observed deviation between satellite and in situ R_{rs}. For the match-up analysis, we considered all pixels from satellite images that were acquired within ±6 hours of the sampling timing for in situ measurement. Although no distinct patterns of a time dependency of the match-up performance were observed, the influence of rapidly changing water masses cannot be excluded. Our AC performance test agrees with reported OLCI AC comparisons for coastal waters (Gossn et al., 2019; Mograne et al., 2019; Renosh et al., 2020). Mograne et al. (2019) evaluated five different OLCI AC's (WFR, C2RCC v.2.1 and Polymer v. 4.10, amongst others) for turbid coastal waters. They concluded that C2RCC v.2.1 and Polymer 4.10 performed best, which agrees with our results. The overall satellite-in situ match-up performance of all tested OLCI AC's reported by Mograne et al. (2019) was, however, substantially better. The weaker performance of the match-up results in our study compared to Mograne et al. (2019) could be caused by a higher optical complexity of the waters in our study but also by the uncertainty of the in situ R_{rs} quality. However, to the best of our knowledge, our study presents the first extensive in situ radiometric data that provide insights into the performance of recent atmospheric correction algorithms in optically complex Arctic waters near a large river mouth. Current efforts, devoted to modify AC's in order to provide more robust performances in extremely optically-complex waters (e.g. ACIX (Doxani et al., 2018), Ocean Colour Bright Pixel Correction (Eumetsat)), will further improve OCRS in these waters.

CDOM retrieval performance

In this study, we tested two in-water CDOM retrieval algorithms (gsmA and ONNS) applied to R_{rs} data from the three tested AC's. The results of match-up comparisons with in situ observed CDOM showed that the gsmA retrieval algorithm performed better compared to ONNS, regardless of which AC was used (**Figure 5.8**). The use of gsmA in combination with the Polymer AC resulted in the best match-up performance (slope=0.92, r^2=0.52, MPE=24.1%, RMSE=0.44 m^{-1}). While the CDOM retrieval using gsmA in combination with WFR AC had the next highest performance (slope=0.55, r^2=0.33, MPE=46.8%, RMSE=0.47 m^{-1}), the gsmA retrieval with C2RCC AC resulted in low determination coefficient (r^2=0.07) and higher errors (MPE=108.6%, RMSE=0.75 m^{-1}).

(Matsuoka et al., 2013, 2017) report a similar performance of the gsmA CDOM retrieval using MODIS satellite data in predominantly more northern / offshore Beaufort Sea waters.

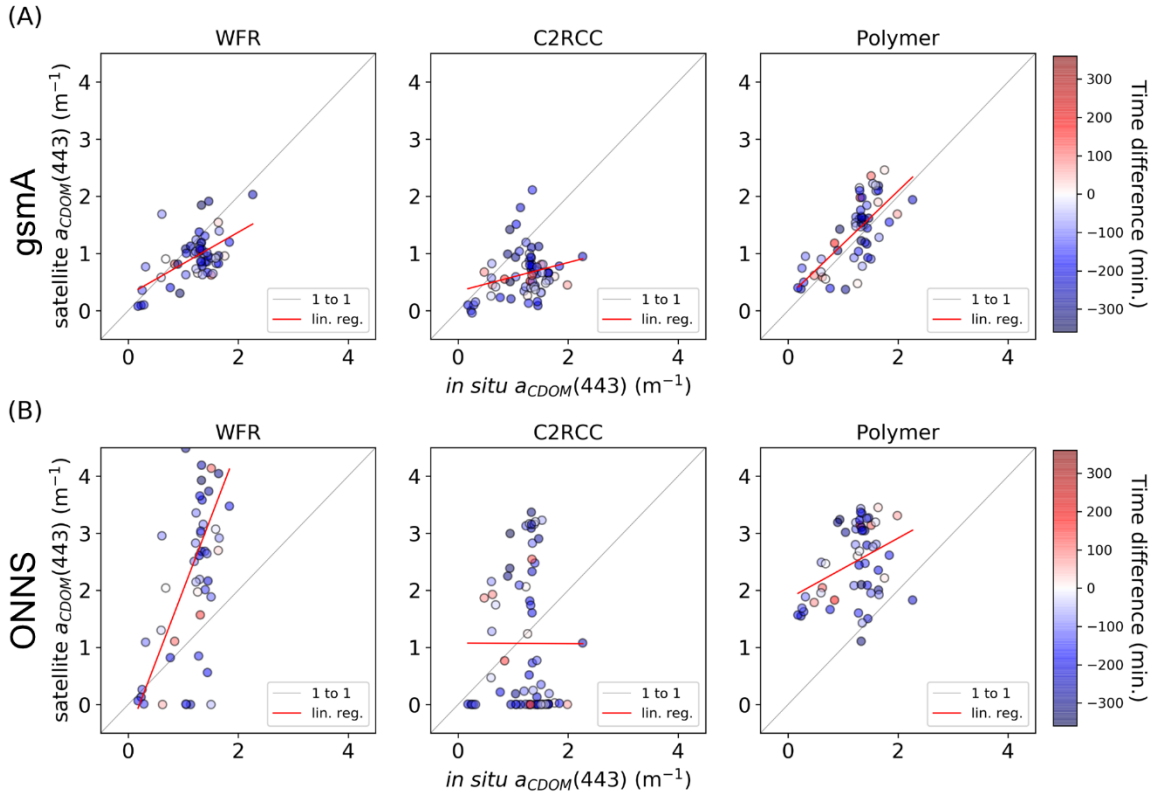

Figure 5.8: Match-up comparison between in situ $a_{CDOM}(443)$ and satellite-derived $a_{CDOM}(443)$ for the three tested AC's and two CDOM retrieval algorithms: (A) gsmA, (B) ONNS. The colourmap is showing the time differences between in situ sampling and satellite acquisition.

CDOM retrieval using the ONNS algorithm in combination with the WFR and C2RCC AC performs poorly (r^2<0.37, MPE>60%, RMSE>1.29). A reason for the poor performance of ONNS with WFR and C2RCC is the fallacious allocation between particle absorption and dissolved absorption. This is likely caused by the problematic separation between particle absorption, mostly non algal particle absorption ($a_{NAP,}$), and CDOM absorption, due to the similar spectral shape (Lee et al., 2006). The ONNS retrieval allocates almost all of the total absorption to the particulate fraction, rather than to the dissolved fraction, leading to the low (almost 0 m^{-1}) $a_{CDOM}(443)$. In combination with the Polymer AC, the absorption allocation problem of the ONNS algorithm was not observed, resulting in slightly better performance (slope=0.53, r^2=0.14, MPE=54.1%, RMSE=1.43 m^{-1}). The gsmA algorithm uses an empirical relationship between a_{NAP} and the backscatter to separate between particle and dissolved absorption.

Table 5.2: Performance statistics of $a_{CDOM}(443)$ retrieval using the three tested AC's and two retrieval algorithms.

AC	Algorithm	Slope	r^2	MPE (%)	RMSE
WFR	ONNS	2.52	0.37	60.1	1.99
	gsmA	0.55	0.33	46.8	0.47
C2RCC	ONNS	0	0	251.9	1.29
	gsmA	0.25	0.07	108.6	0.75
Polymer	ONNS	0.53	0.14	54.1	1.43
	gsmA	0.92	0.52	24.1	0.44

Retrieving DOC concentrations from CDOM

For the retrieval of DOC concentrations based on $a_{CDOM}(443)$, we merged the available in situ data for the Mackenzie Delta - Beaufort Sea region from Osburn et al. (2009) and Matsuoka et al. (2012) and our study and developed a new DOC-CDOM relationship:

$$DOC = 4.4917 * a_{CDOM}(443)^{0.578}. \quad \text{(Equation 5.28)}$$

This relationship includes data from river, coastal and offshore waters of the region and thus enables the retrieval across the fluvial-marine transition zone. **Figure 5.9** shows the match-up between in situ DOC concentrations and the satellite-derived DOC concentrations using the best performing AC and CDOM retrieval (Polymer-gsmA) and the merged DOC-CDOM relationship. The satellite-derived DOC concentrations lay within a 16.6% error (1.11 mg L^{-1}) of the in situ data for the dataset as a whole. The use of a merged cross-domain DOC-CDOM relationship substantially improved the retrieval of DOC concentrations for near-shore waters of the Mackenzie Delta - Beaufort Sea region compared to relationships that were developed from only one water domain.

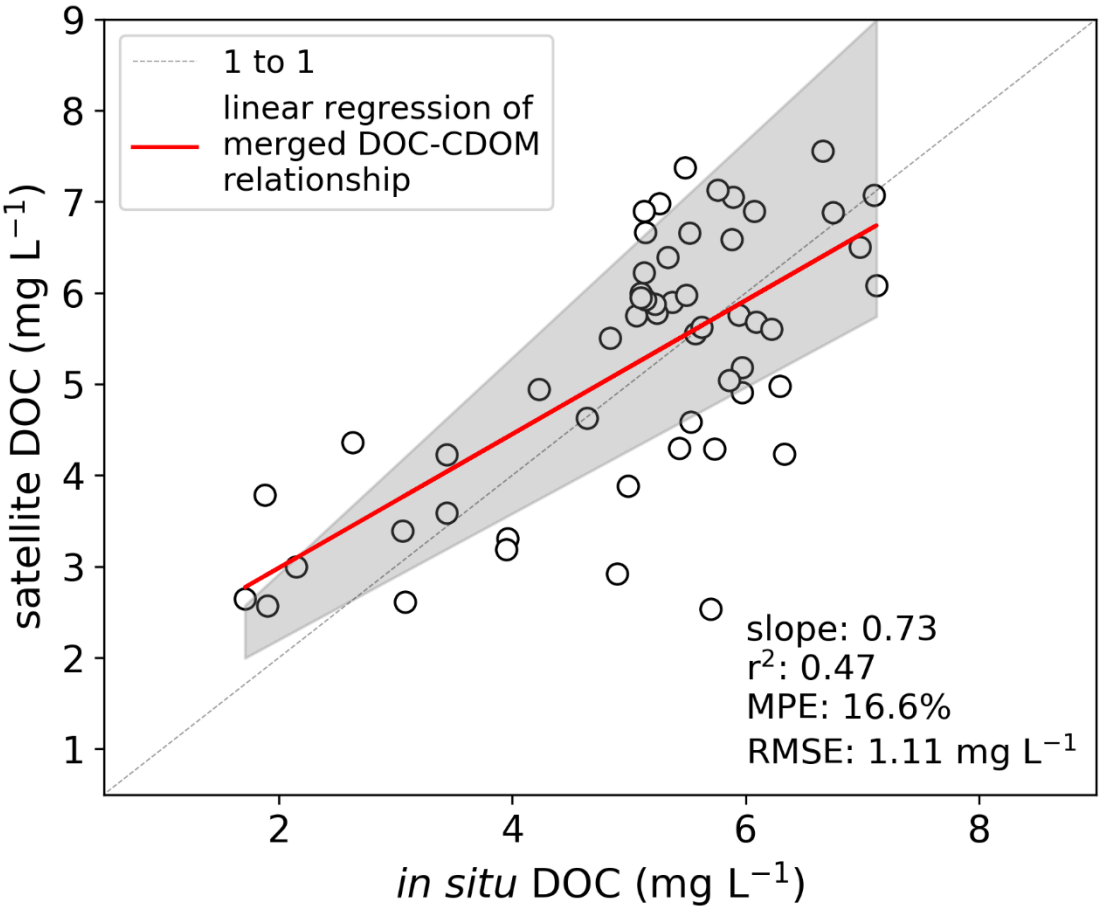

Figure 5.9: Performance of DOC retrieval using Polymer AC in combination with the gsmA CDOM retrieval and a merged DOC-CDOM relationship for the Beaufort Sea. The grey area represents the range of linear regressions using the DOC-CDOM relationships O09, M12 or the one reported from this study (legs 2, 3 and 4, red line **Figure 5.6**)

5.4.4 Synoptic satellite maps of DOC concentrations

We use the results of the match-up analysis for the retrieval of satellite-derived DOC concentrations from $a_{CDOM}(443)$ to map surface water DOC concentrations across the fluvial-marine transition zone of the Mackenzie mouth region. The high temporal resolution of polar orbiting satellites (such as OLCI) provides a powerful tool for synoptic monitoring of river plume propagation and surface water DOC distribution for the entire sea ice free season. **Figure 5.10** shows the surface water DOC concentration for the wider Mackenzie Delta – Beaufort Sea region between June and mid of October using Polymer, gsmA and the merged DOC-CDOM relationship (Equation 5.28).

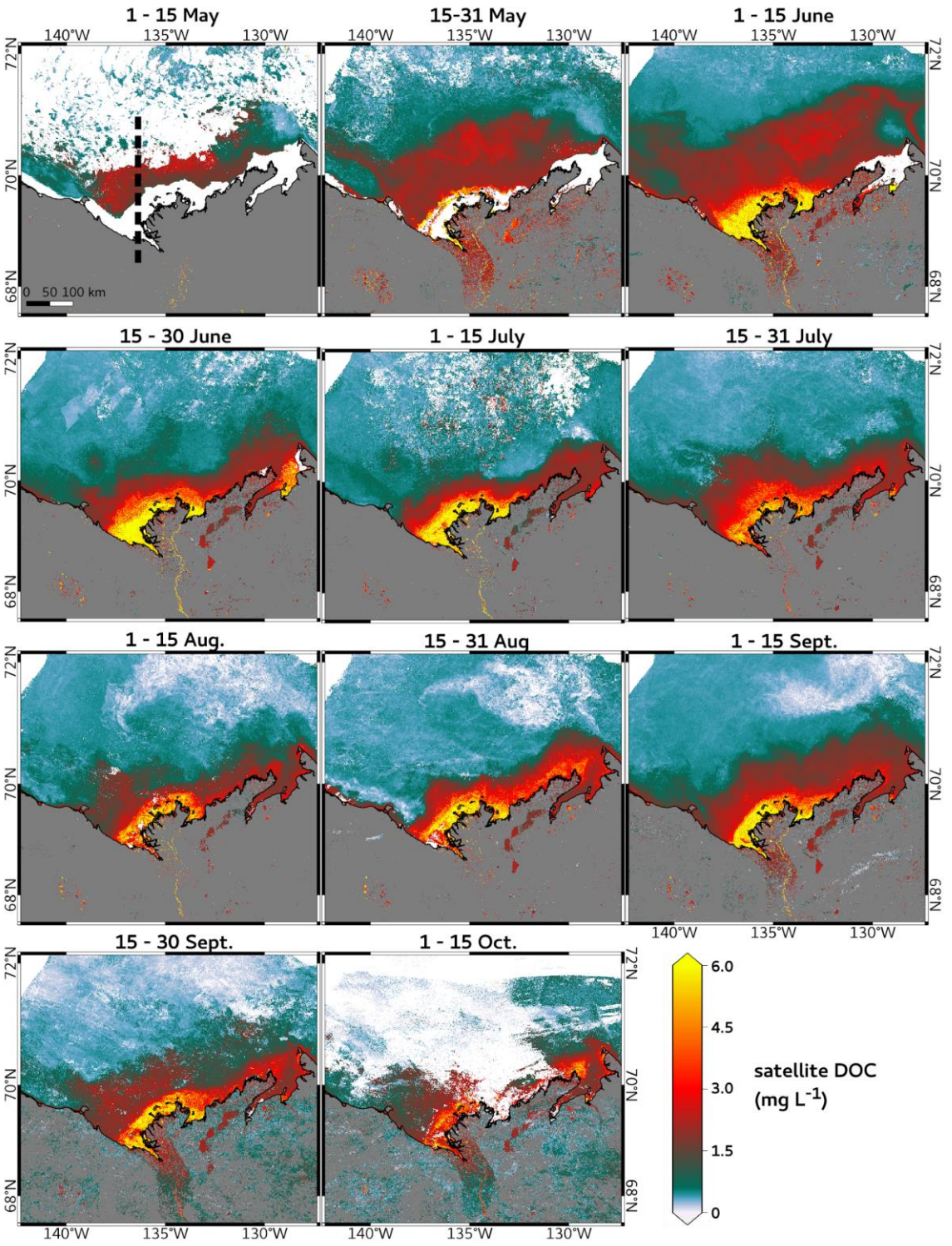

Figure 5.10: Half-month mean surface water DOC concentration of the Mackenzie Delta – Beaufort Sea region. The Polymer AC, in combination with the gsmA CDOM retrieval, was applied to all available S3 OLCI data. DOC concentration was calculated using Equation 5.28. The black line in the upper left map shows the position of the transect described in **Figure 5.11**A.

The maps in **Figure 5.10** show strong variability in the size and maximum concentrations of the Mackenzie River plume throughout the open water season. In the first half of May, sea ice still covered the water surface in the near-shore areas and most of the Beaufort Sea

Shelf. Nevertheless, in the open water area between landfast and pack ice, the onset of the river plume propagation initiated by the river ice breakup was visible. The spatial distribution of the DOC-rich river plume then expanded and was the highest during the first half of June. Besides the farthest northward propagation, waters with high DOC concentrations (>1.5 mg L^{-1}) were transported to the northwest and the northeast. The extent of the plume rapidly decreased in the second half of June, indicating a rapid decrease of DOC from the surface waters. This is likely caused by physical advection of the river water with low-DOC ocean water. Additionally, to some part, a rapid DOC removal is corroborated by other studies that report higher biological and photochemical lability of DOM, which is exported during the spring freshet, compared to DOM that is exported in summer, resulting in its fast degradation (Osburn et al., 2009; Amon et al., 2012; Mann et al., 2012). Later in the year, the size of the plume varied, but stayed smaller than it was after the spring freshet. High concentrations (above 4 mg L^{-1}) were limited to a relatively narrow band around the Mackenzie Delta (<5 km) throughout the whole season. The synoptic views in **Figure 5.10** also reveal the potential influence of coastal erosion leading to higher DOC concentrations along the coastline west of the Mackenzie Delta in the second half of August. Generally, the maps indicate a dominantly eastward transport of the river water. Furthermore, seasonal variation of DOC can even be observed in the river channel, suggesting a potential use of OCRS to assist and complement river sampling programs.

Figure 5.11A shows the DOC concentrations along the 136.4 °W meridian (from 69 °N to 71 °N, black line in **Figure 5.10**) during the open water season from May 1 to October 1, 2019. Variations in DOC along the south-north transect over time demonstrate the impact of Mackenzie runoff (**Figure 5.11**B) on the northward river plume propagation over the Beaufort Sea Shelf. The highest concentrations as well as the farthest northward propagation of DOC-rich waters correspond to the peak of the Mackenzie River water level (as a proxy for discharge). The satellite-derived DOC concentrations of the southernmost part of the transect corroborate the observed in situ seasonal variation with the highest DOC during leg 2, low concentrations during leg 3 and moderate concentrations during leg 4. At the beginning of the open water period, the concentration and propagation of DOC appear to have depended entirely on the Mackenzie River runoff due to the large volume of water that entered the Beaufort Sea at that time. While the DOC concentration near the river mouth later in the year was still strongly associated with the Mackenzie runoff, the extent

of northward plume propagation appeared to vary independently. During the low discharge of the Mackenzie River, other processes, such as ocean currents and winds, likely controlled the propagation of the river plume in the Beaufort Sea.

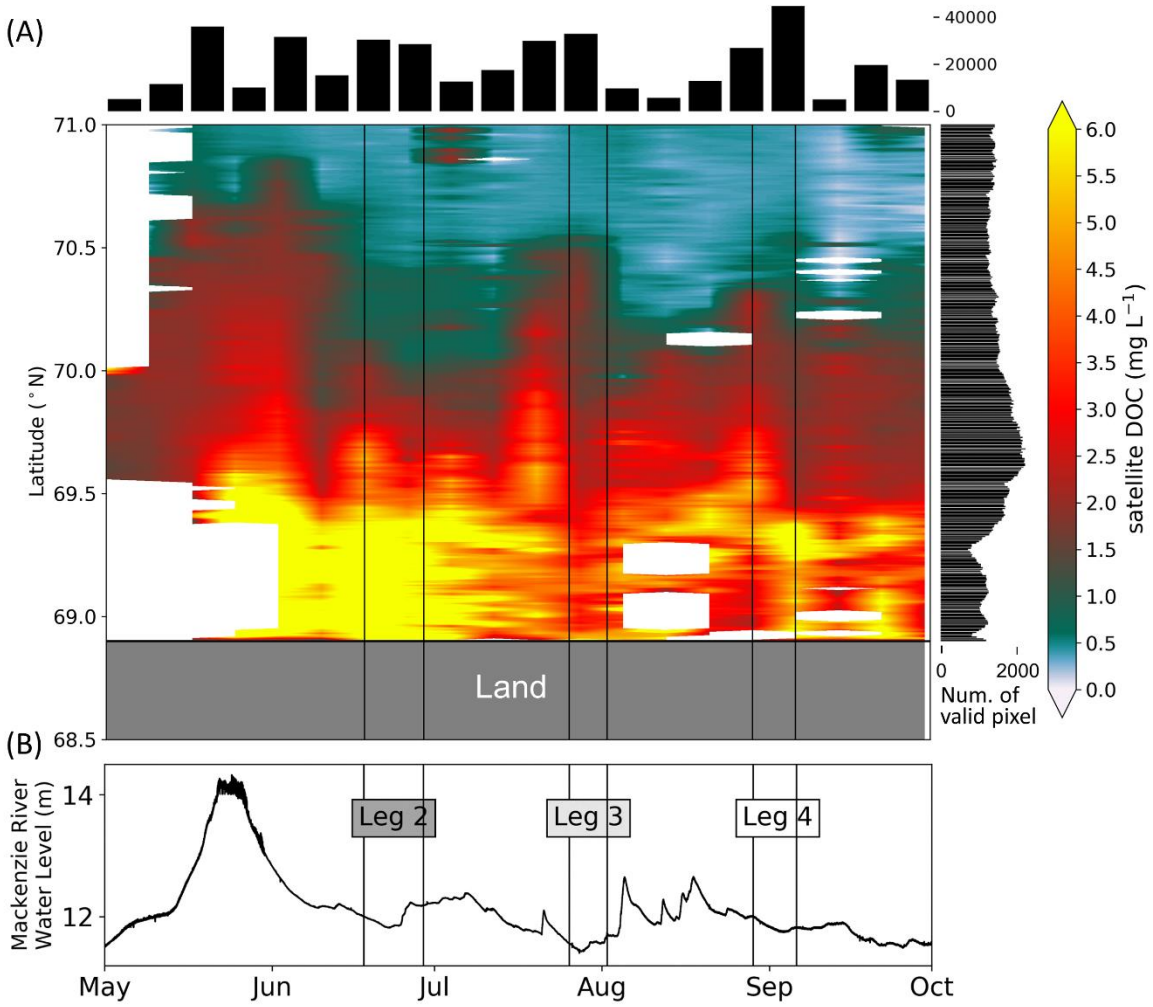

Figure 5.11: (A) DOC concentrations along the 136.4 °W meridian (consisting of 313 x 9 pixels) from 68.5 to 71°N from May to October 2019. All available OLCI acquisitions have been processed with the Polymer AC. CDOM was retrieved using the gsmA algorithm. The DOC concentrations were estimated using the merged DOC-CDOM relationship (Equation 5.28). To account for masked satellite data due to cloud and ice cover, transect medians of eight days were used. The number of valid pixels for each eight day median is displayed in the upper histogram and the number of valid pixels along a latitude grid is shown in the histogram on the right. **Appendix Figure 8** shows the number of observations that were used for each grid point of this figure. (B) shows the provisional water level of the Mackenzie River (East Channel) at Inuvik (Station 10LC002) for May to October 2019 (Water Survey of Canada). Vertical lines show the periods of the expedition legs.

Overall, the applicability of OCRS for this study benefited from exceptionally ice-free and relatively cloud-free conditions over large areas of the Beaufort Sea Shelf, as well as the early northward progression of the pack ice-edge in 2019. The use of OCRS improved the extent of both spatial and temporal monitoring of river plume propagation and the distribution of DOC on the Beaufort Sea Shelf. Furthermore, OCRS places in situ

observations into a wider context, reveals transport pathways and indicates the speed of how rapid DOC concentrations in surface waters of Arctic shelves change.

5.5 Conclusion

This study, we present the results of an extensive sampling program in the Mackenzie River - Beaufort Sea region covering four ~two week periods from before spring until late fall in 2019. The results reveal a strong seasonal variability of the Mackenzie River plume propagation and the associated distribution of terrigenous DOC over the Beaufort Sea Shelf. Ratios of DOC-CDOM (SUVA) show different signatures between winter and summer, suggesting dependence of DOM sources on the season. This consequently also affected the DOC-CDOM relationship which is needed to enable CDOM as a proxy for DOC concentrations. These findings have implications for the retrieval accuracy of DOC via CDOM and suggest that future estimates may need to take this seasonal variability into account.

Assessing the performance of atmospheric corrections in near-shore Arctic coastal waters remains challenging. This is mostly due to difficulties in obtaining accurate in situ radiometric data, which serve as the ground truth for such assessments. Assessing the performance of atmospheric corrections in near-shore Arctic coastal waters remains challenging. Results from this study show that, of the three algorithms tested, the Polymer AC yielded the best performance, allowing us to correct for atmospheric interference with an accuracy of 18.7% (mean percentage error). We also tested two CDOM retrieval algorithms (gsmA and ONNS) by making a comparison between in situ and satellite-derived CDOM measurements. This comparison revealed a satellite-borne CDOM retrieval accuracy of 24.1% (mean percentage error) using the gsmA algorithm. By merging multiple datasets from several studies that cover the complete transition zone from freshwater to marine conditions, we provide a new DOC-CDOM relationship which is applicable to a wider range of optically complex Arctic waters: river, coastal, and offshore. Using this relationship we were able to retrieve DOC concentrations using CDOM data from Sentinel 3 OLCI sensors across the fluvial-marine transition zone over the Beaufort Sea Shelf with an accuracy of 16.6% (mean percentage error).

The use of OCRS greatly extended the in situ observations, that, despite huge logistical efforts, were still limited in spatial and temporal coverage. We demonstrate the performance of OCRS in Arctic waters and its potential to improve our knowledge of the

transport and fate of DOC. To evaluate the performance of OCRS and to identify uncertainties of remotely-sensed DOC concentrations in other river-influenced regions such as the Siberian shelf seas, extensive in situ data collections of radiometric and biogeochemical data from these regions are needed. Continuous in situ data collection and improvements in AC and DOC retrieval should enable an accurate estimation of carbon fluxes from land to the Arctic Ocean on a pan-Arctic scale. The projected decrease in sea ice extent and shortening of the ice-covered period will further increase the applicability of OCRS in the Arctic. Exploiting the existing satellite data from the past ~20 years could reveal potential trends in fluxes of DOC associated with ongoing climate change in the Arctic.

5.6 Funding and acknowledgements

This research has been supported by the EU Horizon 2020 programme (Nunataryuk, grant no. 773421), ArcticNet, Sentinel North, JAXA GCOM-C (Contract number: 19RT000542), and Québec-Océan.

Bennet Juhls was supported by the Geo.X, the Research Network for Geosciences in Berlin and Potsdam (grant no. SO_087_GeoX) and a Sentinel North mobility grant for a research stay in Quebec City (Université Laval).

We thank all participants of the expeditions and persons involved in the logistical support, including M. Béguin, T. Bossé-Demers, C. Guilmette, A. Laberge-Carignan, J. Ferland, M.-H. Forget, É. Leymarie, L. Oziel, L. Tisserand. Also, we thank our local partners in Inuvik, Aklavik and Tuktoyaktuk. A special thanks goes out to our local research assistants: D. O. J. Anikina, M. Dillon, R. Ettagiak, T. Gordon and S. Gruben Jr. We want to express our gratitude to Dustin Whalen (Natural Resources Canada), and Dr. Lisa Bröder (ETH, Zurich), for logistical support prior to and during field work. We would like to thank Gaëlle Mevel for data collection and processing. Further, we thank Martin Hieronymi for the processing with the ONNS algorithm and helpful discussions as well as Michael Angelopoulos and Sofia Antonova for proof reading of this manuscript.

Chapter VI

Synthesis

6 Synthesis and major outcomes

6.1 Scientific contributions

The main aim of this thesis is to improve the existing quantitative and qualitative assessments of carbon fluxes from land to sea and to improve the understanding of their fate on Arctic shelves.

Chapter 3 presents the first results of a new year-round high frequency sampling program near the mouth of the Lena River. The dataset was used to quantify annual DOC fluxes with unique accuracy, setting a baseline for studying biogeochemical changes associated with Arctic warming. Water chemistry analysis revealed that three major water types (melt water, rain water, subsurface water) control seasonal variations in the concentrations of DOM in the Lena River. Furthermore, the seasonality of DOM properties was linked to DOM sources, which were shown to shift from fresh / recently-fixed carbon to older / permafrost-originating carbon, from spring to fall. The Such high frequency sampling method should be applied to other Arctic rivers to improve the monitoring of river export fluxes at the pan-Arctic scale.

Chapter 4 presents the synthesis of a DOM dataset collected during multiple ship- and land-based campaigns between 2007 and 2017 from the fluvial-marine transition zone covering the Lena River, as well as the coastal and offshore shelf waters of the Laptev Sea. This unique large-scale and cross-compartment dataset led to the development of a new relationship between DOC and CDOM, which integrated a wide variety of water types unique to the Arctic region. Testing of a number of different OCRS algorithms revealed weaknesses in their performance beyond a certain range of absorption. Consequently, this resulted in large (>100%) errors for the retrieval of CDOM. The algorithm ONNS, however, allowed the retrieval of CDOM with reasonable accuracy and demonstrated the applicability of OCRS to monitor DOC concentration in the surface waters of the Arctic shelf using the established DOC-CDOM relationship.

Chapter 5 presents a large-scale in situ dataset, collected from spring to fall in the riverine and coastal waters of the Mackenzie River Delta and the Beaufort Sea during several field campaigns conducted between April and September 2019. The dataset defined the seasonal variations of the Mackenzie River plume propagation by tracking DOM at the same locations over time. The characteristics of DOM and its conservative mixing behaviour

were compared to studies from other Arctic shelf regions. Additional comparison of the constructed DOC-CDOM relationship with those from other studies exposed the limitations of such bio-optical models over wide geographic extents. Match-up comparisons between in situ and satellite data were used to identify the combination of (1) atmospheric correction algorithm and (2) CDOM-retrieval algorithm that provided the best performance for the near-shore waters of the Mackenzie Delta - Beaufort Sea region. This combination was used to map CDOM on the Beaufort Sea Shelf for the open-water season, demonstrating the capability of OCRS to monitor DOM-rich river water propagation onto the Arctic shelf and link it to environmental forcing.

As a whole, this thesis analyses the fluxes of terrigenous DOM, as well as its distribution and propagation in two river-influenced regions of the Arctic Ocean: Lena – Laptev Sea (**chapter 3** and **chapter 4**) and Mackenzie Delta – Beaufort Sea (**chapter 5**). The analysis is unique in that it covers a wide range of DOM concentrations from fluvial to marine waters. It demonstrates that rivers induce strong seasonality and control the distribution and fate of DOM on a large spatial scale in both regions. Rapid climate change in the Arctic and, particularly in Siberia, results in hydrological changes including river discharge increase and shifts in river discharge seasonality. The necessity of year-round high frequency monitoring of Arctic rivers to capture these changes and their climate-relevant consequences for the land-to-ocean component was demonstrated. As a result, the sampling program presented in **chapter 3** is still-ongoing to this day in an attempt of generating a long-term monitoring series that may capture climate-driven impacts on carbon cycle.

The combined in situ sampling of DOC and CDOM across a wide range of water types and across compartments showed that the established DOC-CDOM relationship is valid over the entire system of river, coastal and shelf waters. These findings extend the spatial reach of OCRS methodology by allowing the monitoring of DOC propagation from its source to the shelf waters. Moreover, this work shows that the relationship between DOC and CDOM varies as a function of season, region on the shelf, and salinity. Relationships established in previous studies have over- or underestimated DOC by ignoring these dependencies. A comprehensive study of all factors influencing DOC - CDOM relationships will pave the way towards a robust pan-Arctic OCRS quantification of DOC.

6.2 Comparing two Arctic fluvial-marine transition zones

Concentrations of DOC and absorption intensity by CDOM, both measured in situ and estimated from OCRS, differed significantly between the two river-influenced Arctic shelf regions and represent the lower and upper range of reported Arctic River DOM concentrations. In the Lena - Laptev Sea region, DOM concentrations are among the highest reported across the Arctic, while Mackenzie - Beaufort Sea DOM ranges are among the lowest compared to all big Arctic River systems (**Figure 2.3**). This can be explained to some extent by the difference in catchment size between the two rivers with 2.61 x 10^6 km^2 for the Lena River, and 1.78 x 10^6 km^2, for the Mackenzie River. However, the remaining high difference in DOC yields (annual loading normalised to catchment size) (Lena River: ~3 g C m^{-2} yr^{-1}, Mackenzie River: 0.6 g C m^{-2} yr^{-1}; Stedmon et al. (2011)) points towards specific divergence in catchment characteristics. One possible explanation for the lower DOC yield in the Mackenzie River could be the higher proportion of particulate fraction of organic matter compared to the dissolved fraction observed in the Mackenzie River (Stedmon et al., 2011). Another reason could be the presence of the large Great Slave Lake located about half way from the source to the mouth of the Makenzie River, which results in lengthening of water travel time to the potential higher degradation before reaching the Arctic Ocean. There, substantial modification and removal of DOM could result in lower DOM yields arriving at the mouth (Holmes et al., 2012b). River discharge and DOM concentration also determine size and reach of the river plume and the distribution of DOM. While the Lena River plume, delineated by high DOM concentration, can spread over the entire Laptev Sea Shelf (>700 km**, chapter 4, Figure 3.1**) even during low discharge in summer, the Mackenzie river plume propagates, at its very farthest, up to 200 km northwards during the highest discharge right after the spring ice break-up (**chapter 5, Figure 3.5**).

Beyond the specificities in DOM distribution fluxes arising from the differences between Lena and Mackenzie rivers described above, ranges in CDOM absorption were also very different and the OCRS retrieval algorithms performed differently in two regions. While the gsmA algorithm (Matsuoka et al., 2013) showed the best performance with the lower CDOM range (0.25 to 2.25 m^{-1}) in the Mackenzie - Beaufort Sea region, the neural network approach ONNS (Hieronymi et al., 2017) performed best in the higher CDOM range (up to ~8 m^{-1}) in the Lena - Laptev Sea region. One reason for this discrepancy may stem from the classification into multiple optical water types and the use of multiple neural networks

trained for an overall wide range of concentrations by the ONNS algorithm. This appears to allow a more accurate CDOM retrieval in very high-CDOM waters.

6.3 Measuring carbon export fluxes from land to sea in the Arctic

Rising temperatures, increasing river discharge, and mobilization of ancient carbon from thawing permafrost affect the river catchments and the aquatic systems in the Arctic, resulting in a change of carbon flux from land to sea. As the rate of these ongoing changes is increasing, there is a growing imperativeness for the development of accurate in situ and remote sensing sampling strategies that are adapted to accurately predict future changes in carbon export from the rivers to the Arctic Ocean. Previous sampling programs for the Lena River (PARTNERS and ArcticGRO) relied on substantially fewer samples annually (~7 samples yr^{-1}). Load models such as LOADEST (Runkel et al., 2004) interpolate, assuming a correlation between water discharge and DOC concentration, were typically used to compensate for this data deficiency. However, even when multiple seasonal changes in the relationship between water discharge and DOC concentration were considered and multiple relationships were used (Stedmon et al., 2011), linking water discharge to DOC concentration led to an inevitable error and uncertainty in estimates of annual DOC fluxes. This error could exceed expected interannual flux changes that might result during the next decades in a warming Arctic. **Figure 6.1** shows the relationship between water discharge and DOC concentration in the Lena River. The relationship based on the new and the old sampling program is highly variable between seasons and results in unquantified but potentially high errors for load-model derived DOC flux estimates reported by (e.g. Raymond et al., 2007; Stedmon et al., 2011; Holmes et al., 2012b).

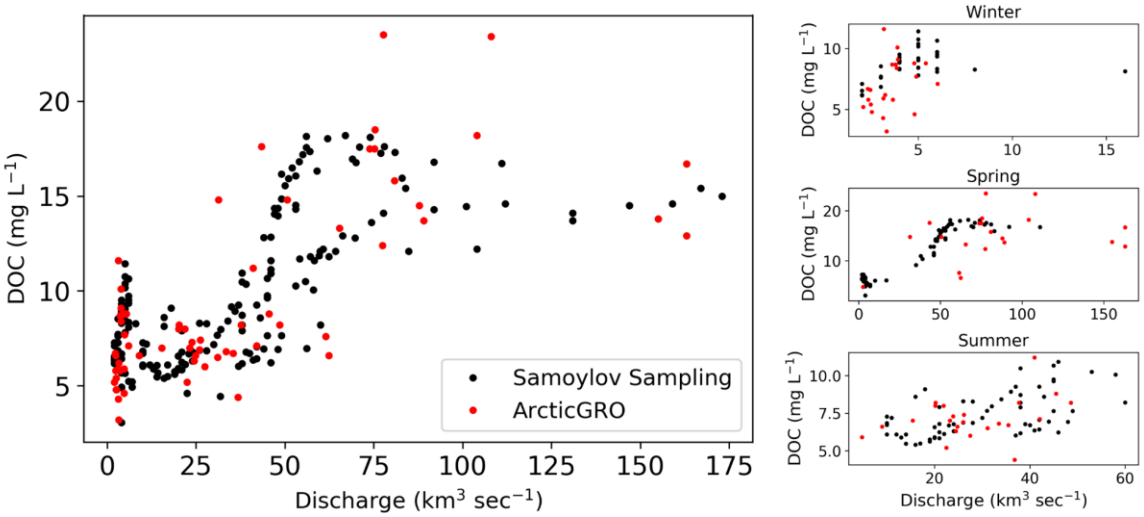

Figure 6.1: All-year relationship between Lena River discharge and DOC concentration, measured during ArcticGRO and the studies presented in **chapter 3** and **chapter 4** (Samoylov sampling) on the left. Right (panels from top to bottom): Observations split into winter (November throughout April), spring (June and July) and summer (August throughout October).

The hypothesis of linking discharge and DOC stemmed from the fact that measured concentrations of DOC varied with the volume of water collected by a river. Thus, the hypothesis implies that river discharge is the main transport of DOC originating from the land surface of the catchment. However, increased DOC mobilization, initiated by permafrost thaw during short summers, would likely not be captured by this relationship, since large amounts of DOC could be released even with low volumes of water. As shown in **chapter 3,** with sufficiently frequent sampling, DOC concentrations can be linearly interpolated between sampling events, without the recourse to discharge-related load-models. A frequent sampling of the major Arctic rivers would, therefore, be an essential step en route to capturing short temporal changes, particularly if they are associated with shifts in hydrological regime and permafrost thaw.

Another crucial improvement in the river water monitoring, which was presented in this study, is the proximity of the sampling to the river mouth. This allowed to capture the biogeochemical properties of the river water, which are actually representative of the water exported to the Laptev Sea. This was not covered in PARTNERS and ArcticGRO programs, which is, for the Lena River, based on a sampling ~700 km upstream. Therefore, DOC flux values, reported in **chapter 3**, are the most accurate export estimates of the Lena River and should be used as a baseline for future studies. Coordinated frequent and continuous sampling of major Arctic Rivers could further improve flux estimates and aid in monitoring climate-related changes within their catchments. Involvement of existing research stations and local residents facilitates sampling throughout the whole year. This

also improves communication between local communities and researchers and stimulate the choice of measured parameters relevant to the local communities.

Additionally, OCRS can complement in situ sampling for the open water period (further discussed in **chapter 6.4.1**). Indeed, monitoring quantitative and qualitative changes of DOM and it sources in Arctic rivers benefits from the inclusion of in situ sampling and analytical measurements, since OCRS holds its own limitations (further discussed in **chapter 6.3)**. With ongoing Arctic warming and accelerating permafrost thaw, higher fractions of DOM originating from old permafrost deposits are expected to be mobilized and exported to the Arctic Ocean. However, the fraction of young DOM, that is drained from the surface of the catchments, currently dominates the overall composition of DOM throughout the year (Wild et al., 2019). This was observed in this and previous studies and is corroborated by the relatively minor changes in SUVA between seasons (**Figure 3.5**, **Figure 5.4** and Stedmon et al. (2011)) and in DOC ages throughout the year observed by Wild et al. (2019). Thus, the discrimination and quantification of the fraction of permafrost-originating DOM within the total pool of DOM remains challenging.

Beyond measuring the amount and quality of DOM export, this thesis demonstrated the possibility to trace river plumes by measuring DOM concentrations in the Laptev and Beaufort Sea shelves. To use DOM concentrations for tracing river water, a dominant or exclusive riverine source of DOM is assumed. This assumption is based on the strong reverse linear relationship between salinity and DOM in the surface waters of Arctic shelves, shown in this thesis (**chapter 4, Figure 4.3** and **chapter 5, Figure 5.5**) and in a number of previous studies (Köhler et al., 2003; Amon and Meon, 2004; Matsuoka et al., 2012; Kaiser et al., 2017a; Pugach et al., 2018). This strong relationship also indicates a conservative mixing behaviour of DOM. Due to the conservative mixing, the concentration of DOM in the surface waters follows the distribution of the river plume itself. This property can be used to directly trace pathways of river water in the Arctic Ocean and to better understand changing freshwater transport patterns linked to climate change (Fichot et al., 2013). The possibility to trace river plume by measuring DOM concentrations in the Laptev and Beaufort Sea shelves is demonstrated in **chapter 4** and **chapter 5**. However, the mixing behaviour of DOM-rich river water is complex, and can feature non-conservative mixing and rapid removal of DOM from Arctic Shelf waters (e.g. Alling et al., 2010; Letscher et al., 2011; Stedmon et al., 2011). These contradictions indicate that the processes of DOM mixing and removal are not straightforward. A variety of processes

can weaken the linear relationship between salinity and DOM (**Figure 6.2**) and should be properly considered.

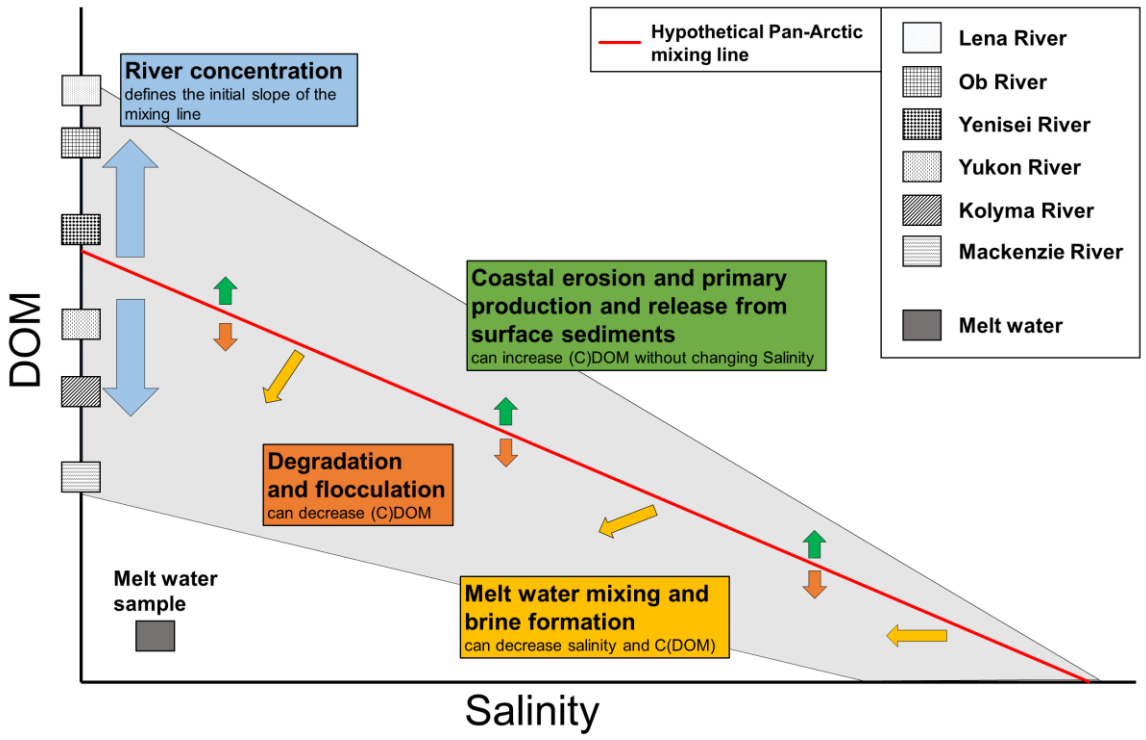

Figure 6.2: Schematic illustration of the factors that affect the relationship between salinity and DOM in Arctic waters.

The strong seasonality of DOM concentration in Arctic rivers (**Figure 3.5**) and the generally large differences in DOM concentration between the Arctic rivers (**Figure 6.2**) define the initial slope of the salinity-DOM mixing line for a particular region, which can then be altered by a number of processes. Melt water and brine formation as well as flocculation and degradation processes can decrease the DOM concentration. Mixing with melt water and brine formations also affect the salinity at the same time. In contrast, coastal erosion, marine production (by e.g. phytoplankton) and OM release from surface sediments can increase the DOM concentration without changing the salinity. Spatial and seasonal variability of these processes makes it difficult to estimate their discrete influence on individual water samples or local scales. Furthermore, some of these processes can counteract each other and to some part cancel out deviations from the mixing line, which can result in a seemingly conservative behaviour. A further complication is an impact of multiple freeze/thaw cycles shelf waters on DOM alteration and its removal with brine formations, the factor which is yet mostly understudied (Hölemann et al.; Granskog et al., 2009). Additionally, riverine DOM lability to degradation is itself prone to seasonal variations (Osburn et al., 2009; Amon et al., 2012; Mann et al., 2012; Kaiser et al., 2017b).

Thus, the number of processes affecting DOM and salinity complicates the study of DOM transport and fate in the Arctic Ocean shelves. For instance, to quantify DOM removal on Arctic shelves, all the processes mentioned above need to be considered and quantified before the impact of a single process can be identified. When using OCRS-retrieved DOM to track river plumes, the potential influences of the suite of processes that affect DOM concentration must be considered. Coastal erosion at the coastline and phytoplankton blooms, producing fresh DOM near the sea ice edge, are two examples of additional DOM sources that are indistinct from the riverine DOM from a remote sensing perspective.

6.4 Challenges related to Arctic coastal waters

Arctic coastal waters are not monitored on a regular basis due to the general remoteness of much of the Arctic and limited access to infrastructure, as well as to the availability of ships, boats, helicopter or other sampling platforms. Logistical efforts and costs for transport and specialized equipment are high and often surpass constraints of time, human resources and expenditure associated with scientific projects. Moreover, span of latent time and shipping conditions between sampling sites and laboratories may be critical to sample quality and viability. Besides the logistical hurdles, the environment itself can be challenging for in situ sampling. The shallow waters of Arctic shelves, and especially of near-shore coastal regions, require boats or ships with a small draft. These are very prone to the storms and waves, making such campaigns prone to failures and reducing a safe operation. Legal restrictions pose another obstacle for working in coastal waters: coastal waters are within the Exclusive Economic Zone (200 nautical miles) or even territorial waters (12 nautical miles) in contrast to the central Arctic Ocean, mandating regional and national permissions for operation. Paying attention to national borders is crucial for planning sampling campaigns.

For the studies included in this thesis, the compromises made and the solutions found along the way were fundamental to the retrieval of datasets and presentation of the results. The extreme challenges that were overcome further highlight the value and uniqueness of the results in this thesis. To collect samples and make instrumental measurements, various platforms for transportation and observation were exploited (**Figure 6.3**). They include small boats and yachts of local residents and private companies (**Figure 6.3**A and B), chartered helicopters for transit but also for aerial sampling during hovering flight (**Figure 6.3**D, G, H and I), small inflatable outboard boats (**Figure 6.3**C), trucks for transport along

frozen river channels (**Figure 6.3**E), and snowmobiles for work on land-fast ice (**Figure 6.3**F).

Figure 6.3: Different sampling platforms that have been used in the field: (A) Yacht, which was used in the Lena River Delta and its surrounding coastal waters up to ~100 km offshore. (B) ~6 m long boat that was used for sampling in extremely shallow areas (<5 m) in Mackenzie Bay (owned and operated by local residents). (C) Use of inflatable boat in the Laptev Sea to reach near-shore zones from a bigger ship. (D) Use of helicopter for transport to land-fast ice on the Beaufort Sea. (E) Transit via ice roads on Mackenzie River channels. (F) Transit on land-fast ice via snowmobiles on Kugmallit Bay (Beaufort Sea). (G) In situ water column profiling from a hovering helicopter. (H) Transit and equipment transport with a helicopter in the central Lena River Delta. (I) Water sampling in the Beaufort Sea from a hovering helicopter.

While the scientific benefits of in situ sampling in Arctic coastal waters are undeniable, the challenges mentioned above remain prohibitive to physical in proprio persona monitoring on a regular basis. Therefore, remote sensing applications such as OCRS are important and indispensable tools and complement to field work. With declining extent and duration of sea ice cover in the Arctic and potentially increasing number of polar orbiting satellites in the future, OCRS will be increasingly valuable for Arctic Ocean monitoring. OCRS can contribute to the estimation of carbon and matter fluxes and to our understanding of freshwater transport in the Arctic Ocean. However, OCRS cannot fully replace in situ observations on the Arctic shelves and in the central Arctic Ocean because satellite data will likely never be as accurate as in situ measurements (Loisel et al., 2013). Furthermore, technical and analytical limitations (e.g. spectral resolution and range) hamper the retrieval of specific parameters associated with the quality of DOM (e.g. SUVA, CDOM slopes).

Ultimately, in situ measurements remain necessary to validate satellite observations (Loisel et al., 2013).

Arctic coastal waters, especially near river mouths, are also specifically challenging for the application of OCRS. Extreme heterogeneity and concentration ranges of water constituents, turbulently moving water (tides, current, fronts) and bubbles due to breaking waves in coastal waters complicate the validation of satellite data highly challenging. Precise temporal matches between in situ and satellite observations are required, which translates to a challenge for in situ sampling. In addition, spatial resolution of many OCRS satellite sensors is too low for an adequate comparison with in situ measurements in coastal waters. Low spatial resolution also impedes the investigation of small-scale processes or small or narrow water bodies such as lakes and rivers with OCRS (**Figure 6.4**). With technical advances, spatial resolutions of satellite sensors are however, expected to improve in future.

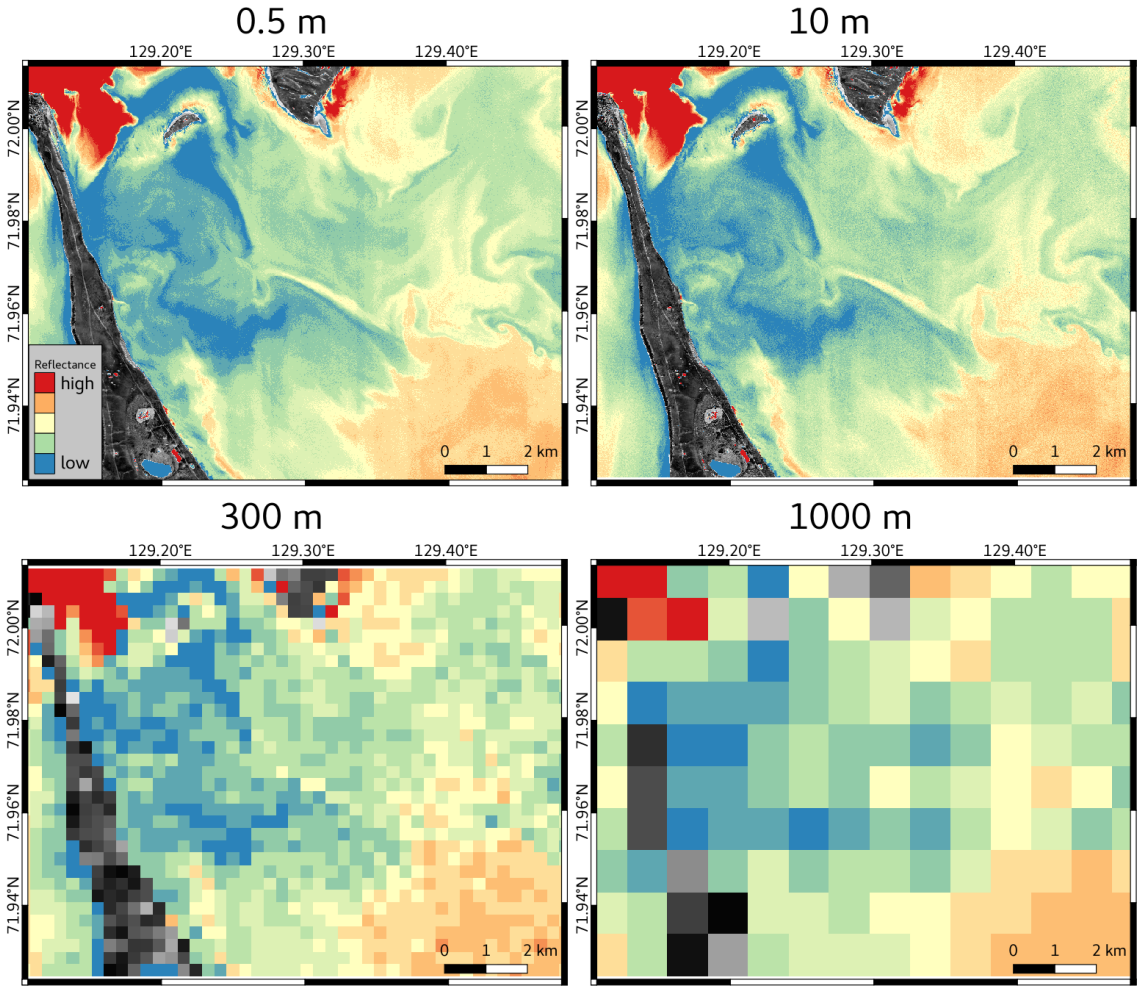

Figure 6.4: Reflectance maps from the red band for four different spatial resolutions using a high-resolution satellite acquisition (WorldView-3) in an area near the Lena River mouth. The image was resampled to four different spatial

resolutions (0.5, 10, 300 and 1000 m) that are typical for OCRS sensors (grey colour is for the land). Small scale features such as eddies and plume fronts become imperceptible at lower resolutions.

6.5 Outlook to future research

6.5.1 Quantifying total organic carbon flux into the Arctic Ocean

Although in the last few decades there has been substantial progress made in improving estimates of the organic matter export fluxes to the Arctic Ocean (Raymond et al., 2007; Stedmon et al., 2011; Holmes et al., 2012b; Juhls et al., 2020), there are still large uncertainties due to the limited amount of observational data available. Reported estimates are mostly limited to the big Arctic rivers that make up about 50% of the pan-Arctic river catchment area. To account for the missing half, reported DOC yields are extrapolated (as DOC flux per area) to unmonitored portions of the watershed under an assumption of homogeneity (Holmes et al., 2012b). However, smaller rivers for which the associated catchments are confined to high latitudes likely differ in their DOC load and yields from the big rivers, which collect and integrate organic matter from catchments extending into the temperate zone. Climate change can be expected to affect these rivers differently in terms of changes to discharge regime, the relative importance of snowmelt and the proportion of old carbon being released by permafrost thaw. Furthermore, infrequent sampling that is restricted to the open water season is likely to miss changes that are due to shifts in the seasonality of discharge and fluvial biogeochemical load (McGuire et al., 2009).

Additionally, the organic carbon fluxes reported in most of the studies listed in **chapter 3**, **Table 3.4**, do not account for the carbon release from coastal erosion or derived from resuspension of the seafloor sediment due to storm-driven wave action. Both processes, however, have been shown to increasingly contribute to the concentration of organic carbon in shallow coastal waters due to ongoing climate change in the Arctic (Fritz et al., 2017; Tanski et al., 2017). An increasing open water periods lead to more intensive coastal erosion and more frequent resuspension events, especially as the open water season encroaches on the fall storm season. Erosion and resuspension are often short-term events and can be easily missed with in situ observations.

OCRS can provide estimates of DOC (Juhls, in prep.; Matsuoka et al., 2017; Juhls et al., 2019) and POC (Doxaran et al., 2012) in Arctic river and river-influenced waters and contribute to an improvement of the flux estimates and an understanding of along-channel

variations. Specific tuning or reparameterization (e.g. Matsuoka et al., 2013) of OCRS retrieval algorithms in combination with a growing dataset of in situ optical data (IOPs of major constituents in combination with radiometric measurements) will further improve the robustness of OCRS in Arctic waters. Future studies should benefit by the fast repeat cycles of OCRS satellites, which can increase the total number of observational data (in situ + satellite-derived observation) throughout the open water period. Due to the synoptic view of satellites, remotely-sensed flux estimates can be extended to the pan-Arctic scale and include relatively small fluvial-marine transition zones that cannot reasonably be studied in detail in situ. Nevertheless, technical restrictions such as spatial resolution limit the use of remote sensing for rivers and streams that are too small to be captured.

6.5.2 On the future of OCRS for Arctic regions

Satellite remote sensing is poised to become an increasingly powerful tool to investigate and monitor changes in remote regions such as the Arctic. During the next years, a number of new satellite missions, specifically developed for the OCRS, will be launched. Future technical development of satellite sensors will improve spatial and spectral resolutions (e.g. Environmental Mapping and Analysis Program (EnMAP) and the Plankton, Aerosol, Cloud, ocean Ecosystem (PACE) mission). The decreasing costs of satellite missions and the use of low-budget nano or cube satellites can increase spatial coverage and revisit times (e.g. HawkEye mission). Turbulent events, such as river ice break-up, the associated discharge peak, and rapid propagation of DOM-rich waters on the Arctic shelves, occur on very short time scales (< 1 week). Increasing observation frequency would be a key improvement to monitor such rapid events.

Increasing effort is being spent on the merging and intercomparing of all the currently available OCRS data. The merge of multi-satellite datasets results in an increased spatial coverage and higher revisit frequency. One example of such an effort is the European Space Agency (ESA) Climate Change Initiative (CCI) for Ocean Colour (https://esa-oceancolour-cci.org/). CCI Ocean Colour is a globally merged Ocean Colour dataset that uses a number of satellite sensors that have been in operation or continue to operate between 1997 and the present. The merged dataset provides long-term global Earth observation archives that can assist immensely in detection trends relevant to climate change in the Arctic regions. In combination with other remote sensing variables, such as land and sea surface temperature

as well as sea ice extent and thickness, future studies will result in a better understanding of key processes and controlling mechanisms of climate change in the Arctic.

References

Aagaard, K., and Carmack, E. C. (1989). The role of sea ice and other fresh water in the Arctic circulation. *J. Geophys. Res.* 94, 14485. doi:10.1029/jc094ic10p14485.

Abbott, B. W., Larouche, J. R., Jones, J. B., Bowden, W. B., and Balser, A. W. (2014). Elevated dissolved organic carbon biodegradability from thawing and collapsing permafrost. *J. Geophys. Res. Biogeosciences* 119, 2049–2063. doi:10.1002/2014JG002678.

Alling, V., Sanchez-Garcia, L., Porcelli, D., Pugach, S., Vonk, J. E., van Dongen, B., et al. (2010). Nonconservative behavior of dissolved organic carbon across the Laptev and East Siberian seas. *Global Biogeochem. Cycles* 24, n/a-n/a. doi:10.1029/2010GB003834.

Amon, R. M. W. (2004). "The Role of Dissolved Organic Matter for the Organic Carbon Cycle in the Arctic Ocean," in *The Organic Carbon Cycle in the Arctic Ocean* (Springer Berlin Heidelberg), 83–99. doi:10.1007/978-3-642-18912-8_4.

Amon, R. M. W., and Meon, B. (2004). The biogeochemistry of dissolved organic matter and nutrients in two large Arctic estuaries and potential implications for our understanding of the Arctic Ocean system. *Mar. Chem.* 92, 311–330. doi:10.1016/j.marchem.2004.06.034.

Amon, R. M. W., Rinehart, A. J., Duan, S., Louchouarn, P., Prokushkin, A., Guggenberger, G., et al. (2012). Dissolved organic matter sources in large Arctic rivers. *Geochim. Cosmochim. Acta* 94, 217–237. doi:10.1016/J.GCA.2012.07.015.

Amon, R. R. M. W., Budéus, G., and Meon, B. (2003). Dissolved organic carbon distribution and origin in the Nordic Seas: Exchanges with the Arctic Oean and the North Atlantic. *J. Geophys. Res. C Ocean.* 108, 14–1. doi:10.1029/2002jc001594.

Anderson, L. G., and Amon, R. M. W. (2015). *DOM in the Arctic Ocean*. Second Edi. Elsevier Inc. doi:10.1016/B978-0-12-405940-5.00014-5.

Angelopoulos, M., Westermann, S., Overduin, P., Faguet, A., Olenchenko, V., Grosse, G., et al. (2019). Heat and Salt Flow in Subsea Permafrost Modeled with CryoGRID2. *J. Geophys. Res. Earth Surf.* 124, 920–937. doi:10.1029/2018JF004823.

Antoine, D., Babin, M., Berthon, J.-F., Bricaud, A., Gentili, B., Loisel, H., et al. (2014). Shedding Light on the Sea: André Morel's Legacy to Optical Oceanography. *Annu. Rev. Mar. Sci* 6, 1–21. doi:10.1146/annurev-marine-010213-135135.

Antoine, D., Hooker, S. B., Bélanger, S., Matsuoka, A., and Babin, M. (2013). Apparent optical properties of the Canadian Beaufort Sea – Part 1: Observational overview and water column relationships. *Biogeosciences* 10, 4493–4509. doi:10.5194/bg-10-4493-2013.

Antoine, D., and Morel, A. (1999). A multiple scattering algorithm for atmospheric correction of remotely sensed ocean colour (MERIS instrument): Principle and implementation for atmospheres carrying various aerosols including absorbing ones. *Int. J. Remote Sens.* 20, 1875–1916. doi:10.1080/014311699212533.

Aré, F. E. (1988). Thermal abrasion of sea coasts (part I). *Polar Geogr. Geol.* 12, 1. doi:10.1080/10889378809377343.

Arrigo, K. R., and Van Dijken, G. L. (2011). Secular trends in Arctic Ocean net primary production. *J. Geophys. Res. Ocean.* 116. doi:10.1029/2011JC007151.

Asmala, E., Bowers, D. G., Autio, R., Kaartokallio, H., and Thomas, D. N. (2014). Qualitative changes of riverine dissolved organic matter at low salinities due to flocculation. *J. Geophys. Res. Biogeosciences* 119, 1919–1933. doi:10.1002/2014JG002722.

Babin, M. (2020). Climate change tweaks Arctic marine ecosystems Nutrient input might enhance productivity in the Arctic Ocean of the future. *Science (80-.).* doi:10.1126/science.abd1231.

Babin, M., Stramski, D., Ferrari, G. M., Claustre, H., Bricaud, A., Obolensky, G., et al. (2003). Variations in the light absorption coefficients of phytoplankton, nonalgal particles, and dissolved organic matter in coastal waters around Europe. *J. Geophys. Res.* 108, 3211. doi:10.1029/2001JC000882.

Bailey, S. W., and Werdell, P. J. (2006). A multi-sensor approach for the on-orbit validation of ocean color satellite data products. doi:10.1016/j.rse.2006.01.015.

Bareiss, J., and Görgen, K. (2005). Spatial and temporal variability of sea ice in the Laptev Sea: Analyses and review of satellite passive-microwave data and model results, 1979 to 2002. *Glob. Planet. Change* 48, 28–54. doi:10.1016/j.gloplacha.2004.12.004.

Bauch, D., Hölemann, J. A., Nikulina, A., Wegner, C., Janout, M. A., Timokhov, L. A., et al. (2013). Correlation of river water and local sea-ice melting on the Laptev Sea shelf (Siberian Arctic). *J. Geophys. Res. Ocean.* 118, 550–561. doi:10.1002/jgrc.20076.

Bauer, J. E., Cai, W. J., Raymond, P. A., Bianchi, T. S., Hopkinson, C. S., and Regnier, P. A. G. (2013). The changing carbon cycle of the coastal ocean. *Nature* 504, 61–70. doi:10.1038/nature12857.

Bélanger, S., Carrascal-Leal, C., Jaegler, T., Larouche, P., and Galbraith, P. (2017). Assessment of radiometric data from a buoy in the St. Lawrence estuary. *J. Atmos. Ocean. Technol.* 34, 877–896. doi:10.1175/JTECH-D-16-0176.1.

Bélanger, S., Xie, H., Krotkov, N., Larouche, P., Vincent, W. F., and Babin, M. (2006). Photomineralization of terrigenous dissolved organic matter in Arctic coastal waters from 1979 to 2003: Interannual variability and implications of climate change. *Global Biogeochem. Cycles* 20. doi:10.1029/2006GB002708.

Benner, R., Benitez-Nelson, B., Kaiser, K., and Amon, R. M. W. (2004). Export of young terrigenous dissolved organic carbon from rivers to the Arctic Ocean. *Geophys. Res. Lett.* 31. doi:10.1029/2003gl019251.

Benner, R., and Kaiser, K. (2011). Biological and photochemical transformations of amino acids and lignin phenols in riverine dissolved organic matter. *Biogeochemistry* 102, 209–222. doi:10.1007/s10533-010-9435-4.

Bintanja, R., and Selten, F. M. (2014). Future increases in Arctic precipitation linked to local evaporation and sea-ice retreat. *Nature* 509, 479–482. doi:10.1038/nature13259.

Biskaborn, B. K., Smith, S. L., Noetzli, J., Matthes, H., Vieira, G., Streletskiy, D. A., et al. (2019). Permafrost is warming at a global scale. *Nat. Commun.* 10, 1–11. doi:10.1038/s41467-018-08240-4.

Bonne, J.-L., Meyer, H., Behrens, M., Boike, J., Kipfstuhl, S., Rabe, B., et al. (2020). Moisture origin as a driver of temporal variabilities of the water vapour isotopic composition in the Lena River Delta, Siberia. *Atmos. Chem. Phys. Discuss.* in review. doi:10.5194/acp-2019-942.

Børsheim, K. Y., and Myklestad, S. M. (1997). Dynamics of DOC in the Norwegian sea inferred from monthly profiles collected during 3 years at 66°N, 2°E. *Deep. Res. Part I Oceanogr. Res. Pap.* 44, 593–601. doi:10.1016/S0967-0637(96)00106-9.

Boss, C. B., and Fredeen, K. J. (1997). *Concepts, Instrumentation, and Techniques in Inductively Coupled Plasma Optical Emission Spectrometry*. Perkin Elmer.

Bricaud, A., Mejia, C., Blondeau-Patissier, D., Claustre, H., Crepon, M., and Thiria, S. (2007). Retrieval of pigment concentrations and size structure of algal populations from their absorption spectra using multilayered perceptrons. *Appl. Opt.* 46, 1251–1260. doi:10.1364/AO.46.001251.

Bricaud, A., Morel, A., and André, J. M. (1987). Spatial/temporal variability of algal

biomass and potential productivity in the Mauritanian upwelling zone, as estimated from CZCS data. *Adv. Sp. Res.* 7, 53–62. doi:10.1016/0273-1177(87)90164-5.

Bricaud, A., Morel, A., and Prieur, L. (1981). Absorption by dissolved organic matter of the sea (yellow substance) in the UV and visible domains1. *Limnol. Oceanogr.* 26, 43–53. doi:10.4319/lo.1981.26.1.0043.

Brockmann, C., Doerffer, R., Peters, M., Stelzer, K., Embacher, S., and Ruescas, A. (2016). Evolution of the C2RCC Neural Network for Sentinel 2 and 3 for the Retrieval of Ocean Color Products in Normal and Extreme Optically Complex Waters. *Living Planet Symp.* Vol. 740. Available at: http://brockmann.urracreative.com/wp-content/uploads/2017/11/sco1_12brockmann.pdf [Accessed February 1, 2018].

Bröder, L., Andersson, A., Tesi, T., Semiletov, I., and Gustafsson, Ö. (2019). Quantifying Degradative Loss of Terrigenous Organic Carbon in Surface Sediments Across the Laptev and East Siberian Sea. *Global Biogeochem. Cycles* 33, 85–99. doi:10.1029/2018GB005967.

Bröder, L., Tesi, T., Andersson, A., Semiletov, I., and Gustafsson, Ö. (2018). Bounding cross-shelf transport time and degradation in Siberian-Arctic land-ocean carbon transfer. *Nat. Commun.* 9, 1–8. doi:10.1038/s41467-018-03192-1.

Bröder, L., Tesi, T., Salvadó, J. A., Semiletov, I. P., Dudarev, O. V., and Gustafsson, Ö. (2016). Fate of terrigenous organic matter across the Laptev Sea from the mouth of the Lena River to the deep sea of the Arctic interior. *Biogeosciences* 13, 5003–5019. doi:10.5194/bg-13-5003-2016.

Brüchert, V., Bröder, L., Sawicka, J. E., Tesi, T., Joye, S. P., Sun, X., et al. (2018). Carbon mineralization in Laptev and East Siberian sea shelf and slope sediment. *Biogeosciences* 15, 471–490. doi:10.5194/bg-15-471-2018.

Butman, D., Raymond, P. A., Butler, K., and Aiken, G. (2012). Relationships between Δ 14 C and the molecular quality of dissolved organic carbon in rivers draining to the coast from the conterminous United States. *Global Biogeochem. Cycles* 26. doi:10.1029/2012GB004361.

Camill, P. (2005). Permafrost Thaw Accelerates in Boreal Peatlands During Late-20th Century Climate Warming. *Clim. Change* 68, 135–152. doi:10.1007/s10584-005-4785-y.

Carder, K. L., Steward, R. G., Harvey, G. R., and Ortner, P. B. (1989). Marine humic and fulvic acids : Their efEcts on remote sensing of ocean chlorophyll. *Science (80-.).* 34, 68–81.

Carmack, E., and Aagaard, K. (1973). On the deep water of the Greenland Sea. *Deep. Res. Oceanogr. Abstr.* 20, 687–715. doi:10.1016/0011-7471(73)90086-7.

Cauwet, G. (2002). "DOM in the coastal zone," in *Biogeochemistry of Marine Dissolved Organic Matter*, eds. D. A. In: Hansell and C. A. (Eds. . Carlson, 579–609.

Cauwet, G., and Sidorov, I. (1996). The biogeochemistry of Lena River: organic carbon and nutrients distribution. *Mar. Chem.* 53, 211–227. doi:10.1016/0304-4203(95)00090-9.

Chan, F. T., Stanislawczyk, K., Sneekes, A. C., Dvoretsky, A., Gollasch, S., Minchin, D., et al. (2019). Climate change opens new frontiers for marine species in the Arctic: Current trends and future invasion risks. *Glob. Chang. Biol.* 25, 25–38. doi:10.1111/gcb.14469.

Charette, M. A., Kipp, L. E., Jensen, L. T., Dabrowski, J. S., Whitmore, L. M., Fitzsimmons, J. N., et al. (2020). The Transpolar Drift as a Source of Riverine and Shelf-Derived Trace Elements to the Central Arctic Ocean. *J. Geophys. Res. Ocean.* 125. doi:10.1029/2019jc015920.

Charkin, A. N., Dudarev, O. V., Semiletov, I. P., Kruhmalev, A. V., Vonk, J. E., Sánchez-

García, L., et al. (2011). Seasonal and interannual variability of sedimentation and organic matter distribution in the Buor-Khaya Gulf: the primary recipient of input from Lena River and coastal erosion in the southeast Laptev Sea. *Biogeosciences* 8, 2581–2594. doi:10.5194/bg-8-2581-2011.

Clarke, R. A., and Gascard, J.-C. (1983). The Formation of Labrador Sea Water. Part I: Large-Scale Processes. American Meteorological Society doi:10.1175/1520-0485(1983)013<1764:TFOLSW>2.0.CO;2.

Coch, C., Juhls, B., Lamoureux, S. F., Lafrenière, M. J., Fritz, M., Heim, B., et al. (2019). Comparisons of dissolved organic matter and its optical characteristics in small low and high Arctic catchments. *Biogeosciences* 16, 4535–4553. doi:10.5194/bg-16-4535-2019.

Cooper, L. W., Benner, R., McClelland, J. W., Peterson, B. J., Holmes, R. M., Raymond, P. A., et al. (2005). Linkages among runoff, dissolved organic carbon, and the stable oxygen isotope composition of seawater and other water mass indicators in the Arctic Ocean. *J. Geophys. Res. Biogeosciences* 110. doi:10.1029/2005JG000031.

Cooper, L. W., Mcclelland, J. W., Holmes, R. M., Raymond, P. A., Gibson, J. J., Guay, C. K., et al. (2008). Flow-weighted values of runoff tracers (d 18 O, DOC, Ba, alkalinity) from the six largest Arctic rivers. doi:10.1029/2008GL035007.

Copernicus Open Access Hub *Available online:*, https://scihub.copernicus.eu/.

D'Alimonte, D., Kajiyama, T., and Saptawijaya, A. (2016). Ocean Color Remote Sensing of Atypical Marine Optical Cases. *IEEE Trans. Geosci. Remote Sens.* 54, 6574–6586. doi:10.1109/TGRS.2016.2587106.

D'Alimonte, D., and Zibordi, G. (2003). Phytoplankton determination in an optically complex coastal region using a multilayer perceptron neural network. *IEEE Trans. Geosci. Remote Sens.* 41, 2861–2868. doi:10.1109/TGRS.2003.817682.

Davis, J., and Benner, R. (2005). Seasonal trends in the abundance, composition and bioavailability of particulate and dissolved organic matter in the Chukchi/Beaufort Seas and western Canada Basin. *Deep. Res. Part II Top. Stud. Oceanogr.* 52, 3396–3410. doi:10.1016/j.dsr2.2005.09.006.

Defoin-Platel, M., and Chami, M. (2007). How ambiguous is the inverse problem of ocean color in coastal waters? *J. Geophys. Res.* 112, C03004. doi:10.1029/2006JC003847.

Del Vecchio, R., and Blough, N. V (2002). Photobleaching of chromophoric dissolved organic matter in natural waters: kinetics and modeling. *Mar. Chem.* 78, 231–253. doi:10.1016/S0304-4203(02)00036-1.

Delwart, S., Preusker, R., Bourg, L., Santer, R., Ramon, D., and Fischer, J. (2007). MERIS in-flight spectral calibration. *Int. J. Remote Sens.* 28, 479–496. doi:10.1080/01431160600821119.

Dittmar, T., and Kattner, G. (2003). The biogeochemistry of the river and shelf ecosystem of the Arctic Ocean: a review. *Mar. Chem.* 83, 103–120. doi:10.1016/S0304-4203(03)00105-1.

Dmitrenko, I. A., Kirillov, S. A., Tremblay, L. B., Kassens, H., Anisimov, O. A., Lavrov, S. A., et al. (2011). Recent changes in shelf hydrography in the Siberian Arctic: Potential for subsea permafrost instability. *J. Geophys. Res. Ocean.* 116. doi:10.1029/2011JC007218.

Dmitrenko, I., Golovin, P., Gribanov, V., and Kassens, H. (1999). "Oceanographic Causes for Transarctic Ice Transport of River Discharge," in *Land-Ocean Systems in the Siberian Arctic* (Springer Berlin Heidelberg), 73–92. doi:10.1007/978-3-642-60134-7_9.

Doerffer, R., and Schiller, H. (2007). The MERIS Case 2 water algorithm. *Int. J. Remote Sens.* 28, 517–535. doi:10.1080/01431160600821127.

Doxani, G., Vermote, E., Roger, J.-C., Gascon, F., Adriaensen, S., Frantz, D., et al. (2018). Atmospheric Correction Inter-Comparison Exercise. *Remote Sens.* 10, 352. doi:10.3390/rs10020352.

Doxaran, D., Ehn, J., Bélanger, S., Matsuoka, A., Hooker, S., and Babin, M. (2012). Optical characterisation of suspended particles in the Mackenzie River plume (Canadian Arctic Ocean) and implications for ocean colour remote sensing. *Biogeosciences* 9, 3213–3229. doi:10.5194/bg-9-3213-2012.

Droppo, I. G., Jeffries, D., Jaskot, C., and Backus, S. (1998). The prevalence of freshwater flocculation in cold regions: A case study from the Mackenzie River Delta, Northwest Territories, Canada. *Arctic* 51, 155–164. doi:10.14430/arctic1056.

Dubinenkov, I., Flerus, R., Schmitt-Kopplin, P., Kattner, G., and Koch, B. P. (2015). Origin-specific molecular signatures of dissolved organic matter in the Lena Delta. *Biogeochemistry* 123, 1–14. doi:10.1007/s10533-014-0049-0.

Emmerton, C. A., Lesack, L. F. W., and Vincent, W. F. (2008). Mackenzie River nutrient delivery to the Arctic Ocean and effects of the Mackenzie Delta during open water conditions. *Global Biogeochem. Cycles* 22. doi:10.1029/2006GB002856.

Engbrodt, R., and Kattner, G. (2005). On the biogeochemistry of dissolved carbohydrates in the Greenland Sea (Arctic). *Org. Geochem.* 36, 937–948. doi:10.1016/j.orggeochem.2004.12.007.

Eulenburg, A., Juhls, B., and Hölemann, J. A. (2019). Surface water Dissolved Organic Matter (DOC, CDOM) in the Lena River (2014). *PANGAEA*. doi:10.1594/PANGAEA.898711.

Fahrbach, E., Meincke, J., Østerhus, S., Rohardt, G., Schauer, U., Tverberg, V., et al. (2001). Direct measurements of volume transports through Fram Strait. *Polar Res.* 20, 217–224. doi:10.1111/j.1751-8369.2001.tb00059.x.

Farquharson, L. M., Mann, D. H., Swanson, D. K., Jones, B. M., Buzard, R. M., and Jordan, J. W. (2018). Temporal and spatial variability in coastline response to declining sea-ice in northwest Alaska. *Mar. Geol.* 404, 71–83. doi:10.1016/j.margeo.2018.07.007.

Fasching, C., Behounek, B., Singer, G. A., and Battin, T. J. (2015). Microbial degradation of terrigenous dissolved organic matter and potential consequences for carbon cycling in brown-water streams. *Sci. Rep.* 4, 4981. doi:10.1038/srep04981.

Fedorova, I., Chetverova, A., Bolshiyanov, D., Makarov, A., Boike, J., Heim, B., et al. (2015). Lena Delta hydrology and geochemistry: long-term hydrological data and recent field observations. *Biogeosciences* 12, 345–363. doi:10.5194/bg-12-345-2015.

Fichot, C. G., and Benner, R. (2011). A novel method to estimate DOC concentrations from CDOM absorption coefficients in coastal waters. *Geophys. Res. Lett.* 38. doi:10.1029/2010GL046152.

Fichot, C. G., and Benner, R. (2012). The spectral slope coefficient of chromophoric dissolved organic matter (S 275-295) as a tracer of terrigenous dissolved organic carbon in river-influenced ocean margins. *Limnol. Oceanogr.* 57, 1453–1466. doi:10.4319/lo.2012.57.5.1453.

Fichot, C. G., and Benner, R. (2014). The fate of terrigenous dissolved organic carbon in a river-influenced ocean margin. *Global Biogeochem. Cycles* 28, 300–318. doi:10.1002/2013GB004670.

Fichot, C. G., Kaiser, K., Hooker, S. B., Amon, R. M. W., Babin, M., Bélanger, S., et al. (2013). Pan-Arctic distributions of continental runoff in the Arctic Ocean. *Sci. Rep.* 3, 1053. doi:10.1038/srep01053.

Fischer, J., and Grassl, H. (1984). Radiative transfer in an atmosphere–ocean system: an azimuthally dependent matrix-operator approach. *Appl. Opt.* 23, 1032. doi:10.1364/ao.23.001032.

Forest, A., Coupel, P., Else, B., Nahavandian, S., Lansard, B., Raimbault, P., et al. (2014). Synoptic evaluation of carbon cycling in the Beaufort Sea during summer: Contrasting river inputs, ecosystem metabolism and air-sea CO2 fluxes. *Biogeosciences* 11, 2827–2856. doi:10.5194/bg-11-2827-2014.

Franz, B. A., Bailey, S. W., Werdell, P. J., and McClain, C. R. (2007). Sensor-independent approach to the vicarious calibration of satellite ocean color radiometry. *Appl. Opt.* 46, 5068–5082. doi:10.1364/AO.46.005068.

Freeman, C., Evans, C. D., Monteith, D. T., Reynolds, B., and Fenner, N. (2001). Export of organic carbon from peat soils. *Nature* 412, 785–785. doi:10.1038/35090628.

Frey, K. E., and McClelland, J. W. (2009). Impacts of permafrost degradation on arctic river biogeochemistry. *Hydrol. Process.* 23, 169–182. doi:10.1002/hyp.7196.

Frey, K. E., and Smith, L. C. (2005). Amplified carbon release from vast West Siberian peatlands by 2100. *Geophys. Res. Lett.* 32, L09401. doi:10.1029/2004GL022025.

Fritz, M., Vonk, J. E., and Lantuit, H. (2017). Collapsing Arctic coastlines. *Nat. Clim. Chang.* 7, 6–7. doi:10.1038/nclimate3188.

Gonçalves-Araujo, R., Rabe, B., Peeken, I., and Bracher, A. (2018). High colored dissolved organic matter (CDOM) absorption in surface waters of the central-eastern Arctic Ocean: Implications for biogeochemistry and ocean color algorithms. *PLoS One* 13, e0190838. doi:10.1371/journal.pone.0190838.

Gonçalves-Araujo, R., Stedmon, C. A., Heim, B., Dubinenkov, I., Kraberg, A., Moiseev, D., et al. (2015). From Fresh to Marine Waters: Characterization and Fate of Dissolved Organic Matter in the Lena River Delta Region, Siberia. *Front. Mar. Sci.* 2, 108. doi:10.3389/fmars.2015.00108.

Gordeev, V. V., and Kravchishina, M. D. (2009). "River flux of dissolved organic carbon (DOC) and particulate organic carbon (POC) to the Arctic Ocean: what are the consequences of the global changes?," in *Influence of Climate Change on the Changing Arctic and Sub-Arctic Conditions* (Dordrecht: Springer Netherlands), 145–160. doi:10.1007/978-1-4020-9460-6_11.

Gordeev, V. V., Martin, J. M., Sidorov, I. S., and Sidorova, M. V. (1996). A reassessment of the Eurasian river input of water, sediment, major elements, and nutrients to the Arctic Ocean. *Am. J. Sci.* 296, 664–691. doi:10.2475/ajs.296.6.664.

Gordon, H. R. (1973). Simple Calculation of the Diffuse Reflectance of the Ocean. *Appl. Opt.* 12, 2803. doi:10.1364/ao.12.002803.

Gordon, H. R., Brown, O. B., Evans, R. H., Brown, J. W., Smith, R. C., Baker, K. S., et al. (1988). A semianalytic radiance model of ocean color. *J. Geophys. Res. Atmos.* 93, 10909–10924. doi:10.1029/JD093ID09P10909.

Gordon, H. R., and Clark, D. K. (1981). Clear water radiances for atmospheric correction of coastal zone color scanner imagery. *Appl. Opt.* 20, 4175. doi:10.1364/ao.20.004175.

Gorham, E. (1991). Northern peatlands: role in the carbon cycle and probable responses to climatic warming. *Ecol. Appl.* 1, 182–195. doi:10.2307/1941811.

Gossn, J., Ruddick, K., and Dogliotti, A. (2019). Atmospheric Correction of OLCI Imagery over Extremely Turbid Waters Based on the Red, NIR and 1016 nm Bands and a New Baseline Residual Technique. *Remote Sens.* 11, 220. doi:10.3390/rs11030220.

Granskog, M. A., Macdonald, R. W., Kuzyk, Z. Z. A., Senneville, S., Mundy, C.-J., Barber, D. G., et al. (2009). Coastal conduit in southwestern Hudson Bay (Canada) in summer: Rapid transit of freshwater and significant loss of colored dissolved organic matter. *J. Geophys. Res.* 114. doi:10.1029/2009jc005270.

Granskog, M. A., Stedmon, C. A., Dodd, P. A., Amon, R. M. W., Pavlov, A. K., de Steur, L., et al. (2012). Characteristics of colored dissolved organic matter (CDOM) in the

Arctic outflow in the Fram Strait: Assessing the changes and fate of terrigenous CDOM in the Arctic Ocean. *J. Geophys. Res. Ocean.* 117. doi:10.1029/2012JC008075.

GRDC (2020). Major River Basins of the World / Global Runoff Data Centre, GRDC.

Green, S. A., and Blough, N. V. (1994). Optical absorption and fluorescence properties of chromophoric dissolved organic matter in natural waters. *Limnol. Oceanogr.* 39, 1903–1916. doi:10.4319/lo.1994.39.8.1903.

Griffin, C. G., Mcclelland, J. W., Frey, K. E., Fiske, G., and Holmes, R. M. (2018). Quantifying CDOM and DOC in major Arctic rivers during ice-free conditions using Landsat TM and ETM+ data. *Remote Sens. Environ.* 209, 395–409. doi:10.1016/j.rse.2018.02.060.

Grosse, G. (2013). Distribution of Late Pleistocene Ice-Rich Syngenetic Permafrost of the Yedoma Suite in East and Central Siberia, Russia. US Geological Survey Open File Report

Guay, C. K. H., Falkner, K. K., Muench, R. D., Mensch, M., Frank, M., and Bayer, R. (2001). Wind-driven transport pathways for Eurasian Arctic river discharge. *J. Geophys. Res. Ocean.* 106, 11469–11480. doi:10.1029/2000jc000261.

Günther, F., Overduin, P. P., Baranskaya, A., Opel, T., and Grigoriev, M. N. (2013). Observing Muostakh Island disappear: erosion of a ground-ice-rich coast in response to summer warming and sea ice reduction on the East Siberian shelf. *Cryosph. Discuss.* 7, 4101–4176. doi:10.5194/tcd-7-4101-2013.

Günther, F., Overduin, P. P., Yakshina, I. A., Opel, T., Baranskaya, A. V., and Grigoriev, M. N. (2015). Observing Muostakh disappear: permafrost thaw subsidence and erosion of a ground-ice-rich island in response to arctic summer warming and sea ice reduction. *Cryosph.* 9, 151–178. doi:10.5194/tc-9-151-2015.

Guo, W., Stedmon, C. A., Han, Y., Wu, F., Yu, X., and Hu, M. (2007). The conservative and non-conservative behavior of chromophoric dissolved organic matter in Chinese estuarine waters. *Mar. Chem.* 107, 357–366. doi:10.1016/J.MARCHEM.2007.03.006.

Hansell, D. A., Kadko, D., and Bates, N. R. (2004). Degradation of Terrigenous Dissolved Organic Carbon in the Western Arctic Ocean. *Science (80-.).* 304, 858–861. doi:10.1126/science.1096175.

Hansen, A. M., Kraus, T. E. C., Pellerin, B. A., Fleck, J. A., Downing, B. D., and Bergamaschi, B. A. (2016). Optical properties of dissolved organic matter (DOM): Effects of biological and photolytic degradation. *Limnol. Oceanogr.* 61, 1015–1032. doi:10.1002/lno.10270.

He, M., Hu, Y., Chen, N., Wang, D., Huang, J., and Stamnes, K. (2019). High cloud coverage over melted areas dominates the impact of clouds on the albedo feedback in the Arctic. *Sci. Rep.* 9, 1–11. doi:10.1038/s41598-019-44155-w.

Heim, B., Abramova, E., Doerffer, R., Günther, F., Hölemann, J., Kraberg, A., et al. (2014). Ocean colour remote sensing in the southern Laptev Sea: evaluation and applications. *Biogeosciences* 11, 4191–4210. doi:10.5194/bg-11-4191-2014.

Helms, J. R., Mao, J., Stubbins, A., Schmidt-Rohr, K., Spencer, R. G. M., Hernes, P. J., et al. (2014). Loss of optical and molecular indicators of terrigenous dissolved organic matter during long-term photobleaching. *Aquat. Sci.* 76, 353–373. doi:10.1007/s00027-014-0340-0.

Helms, J. R., Stubbins, A., Ritchie, J. D., Minor, E. C., Kieber, D. J., and Mopper, K. (2008). Absorption spectral slopes and slope ratios as indicators of molecular weight, source, and photobleaching of chromophoric dissolved organic matter. *Limnol. Oceanogr.* 53, 955–969. doi:10.4319/lo.2008.53.3.0955.

Hieronymi, M. (2019). Spectral band adaptation of ocean color sensors for applicability of

the multi-water biogeo-optical algorithm ONNS. *Opt. Express* 27, A707. doi:10.1364/OE.27.00A707.

Hieronymi, M., Müller, D., and Doerffer, R. (2017). The OLCI Neural Network Swarm (ONNS): A Bio-Geo-Optical Algorithm for Open Ocean and Coastal Waters. *Front. Mar. Sci.* 4, 140. doi:10.3389/fmars.2017.00140.

Hill, V. J. (2008). Impacts of chromophoric dissolved organic material on surface ocean heating in the Chukchi Sea. *J. Geophys. Res.* 113, C07024. doi:10.1029/2007JC004119.

Hölemann, J. A., Juhls, B., Bauch, D., Koch, B., Janout, M., and Heim, B. The importance of fast ice formation and melt for the distribution of terrestrial dissolved organic matter in Siberian Arctic shelf seas (in preparation).

Holmes, R. M., Coe, M. T., Fiske, G. J., Gurtovaya, T., McClelland, J. W., Shiklomanov, A. I., et al. (2012a). "Climate Change Impacts on the Hydrology and Biogeochemistry of Arctic Rivers," in *Climatic Change and Global Warming of Inland Waters* (Chichester, UK: John Wiley & Sons, Ltd), 1–26. doi:10.1002/9781118470596.ch1.

Holmes, R. M., McClelland, J. W., Peterson, B. J., Tank, S. E., Bulygina, E., Eglinton, T. I., et al. (2012b). Seasonal and Annual Fluxes of Nutrients and Organic Matter from Large Rivers to the Arctic Ocean and Surrounding Seas. *Estuaries and Coasts* 35, 369–382. doi:10.1007/s12237-011-9386-6.

Holmes, R. M., McClelland, J. W., Raymond, P. A., Frazer, B. B., Peterson, B. J., and Stieglitz, M. (2008). Lability of DOC transported by Alaskan rivers to the Arctic Ocean. *Geophys. Res. Lett.* 35, L03402. doi:10.1029/2007GL032837.

Holmes, R. M., McClelland, J. W., Tank, S. E., Spencer, R. G. M., and Shiklomanov, A. I. (2018a). ArcticGRO Absorbance Dataset. *https://www.arcticgreatrivers.org/data* Absorbance.

Holmes, R. M., McClelland, J. W., Tank, S. E., Spencer, R. G. M., and Shiklomanov, A. I. (2018b). ArcticGRO Water Quality Dataset. *https://www.arcticgreatrivers.org/data* Quality.

Holmes, R. M., Shiklomanov, A. I., Suslova, A., Tretiakov, M., McClelland, J. W., Spencer, R. G. M., et al. (2018c). "River Discharge," in *in Arctic Report Card 2018* Available at: https://arctic.noaa.gov/Report-Card/Report-Card-2018.

Hooker, S. B., Morrow, J. H., and Matsuoka, A. (2013). Apparent optical properties of the Canadian Beaufort Sea - Part 2: The 1% and 1 cm perspective in deriving and validating AOP data products. *Biogeosciences* 10, 4511–4527. doi:10.5194/bg-10-4511-2013.

Hovis, W. A., Clark, D. K., Anderson, F., Austin, R. W., Wilson, W. H., Baker, E. T., et al. (1980). Nimbus-7 coastal zone color scanner: System description and initial imagery. *Science (80-.).* 210, 60–63. doi:10.1126/science.210.4465.60.

Hu, C., Feng, L., Lee, Z., Davis, C. O., Mannino, A., McClain, C. R., et al. (2012). Dynamic range and sensitivity requirements of satellite ocean color sensors: learning from the past. *Appl. Opt.* 51, 6045. doi:10.1364/AO.51.006045.

Hu, L., Zhang, X., Xiong, Y., and He, M.-X. (2019). Calibration of the LISST-VSF to derive the volume scattering functions in clear waters. *Opt. Express* 27, A1188. doi:10.1364/oe.27.0a1188.

Huang, J., Wu, M., Cui, T., and Yang, F. (2019). Quantifying DOC and Its Controlling Factors in Major Arctic Rivers during Ice-Free Conditions using Sentinel-2 Data. *Remote Sens.* 11, 2904. doi:10.3390/rs11242904.

Hugelius, G., Strauss, J., Zubrzycki, S., Harden, J. W., Schuur, E. A. G., Ping, C.-L., et al. (2014). Estimated stocks of circumpolar permafrost carbon with quantified uncertainty ranges and identified data gaps. *Biogeosciences* 11, 6573–6593.

doi:10.5194/bg-11-6573-2014.

Jamet, C., Loisel, H., and Dessailly, D. (2012). Retrieval of the spectral diffuse attenuation coefficient K d (λ) in open and coastal ocean waters using a neural network inversion. *J. Geophys. Res. Ocean.* 117. doi:10.1029/2012jc008076.

Jerlov, N. G. (1953). Influence of Suspended and Dissolved Matter on the Transparency of Sea Water. *Tellus* 5, 59–65. doi:10.3402/tellusa.v5i1.8562.

Jerlov, N. G. (1969). "Optical Oceanography," in *Optical Oceanography Elsevier*, 156–161.

Jollymore, A., Johnson, M. S., and Hawthorne, I. (2012). Submersible UV-Vis Spectroscopy for Quantifying Streamwater Organic Carbon Dynamics: Implementation and Challenges before and after Forest Harvest in a Headwater Stream. *Sensors* 12, 3798–3813. doi:10.3390/s120403798.

Jones, B. M., Arp, C. D., Jorgenson, M. T., Hinkel, K. M., Schmutz, J. A., and Flint, P. L. (2009). Increase in the rate and uniformity of coastline erosion in Arctic Alaska. *Geophys. Res. Lett.* 36. doi:10.1029/2008GL036205.

Juhls, B. Seasonal dynamics of dissolved organic matter of the Mackenzie Delta, Canadian Arctic waters: implications for ocean color remote sensing (in preparation).

Juhls, B., Overduin, P. P., Hölemann, J., Hieronymi, M., Matsuoka, A., Heim, B., et al. (2019). Dissolved organic matter at the fluvial-marine transition in the Laptev Sea using in situ data and ocean colour remote sensing. *Biogeosciences* 16. doi:10.5194/bg-16-2693-2019.

Juhls, B., Stedmon, C. A., Morgenstern, A., Meyer, H., Hölemann, J., Heim, B., et al. (2020). Identifying Drivers of Seasonality in Lena River Biogeochemistry and Dissolved Organic Matter Fluxes. *Front. Environ. Sci.* 8, 53. doi:10.3389/fenvs.2020.00053.

Kaiser, K., Benner, R., and Amon, R. M. W. (2017a). The fate of terrigenous dissolved organic carbon on the Eurasian shelves and export to the North Atlantic. *J. Geophys. Res. Ocean.* 122.1, 4–22. doi:10.1002/2016JC012380.

Kaiser, K., Canedo-Oropeza, M., McMahon, R., and Amon, R. M. W. (2017b). Origins and transformations of dissolved organic matter in large Arctic rivers. *Sci. Rep.* 7, 13064. doi:10.1038/s41598-017-12729-1.

Kalle, K. (1937). Nährstoff-Untersuchungen als hydrographisches Hilfsmittel zur Unterscheidung von Wasserkör- pern. *Annl. Hydrogr. Berl.*, 65, 1–18.

Kattner, G., Lobbes, J. ., Fitznar, H. ., Engbrodt, R., Nöthig, E.-M., and Lara, R. . (1999). Tracing dissolved organic substances and nutrients from the Lena River through Laptev Sea (Arctic). *Mar. Chem.* 65, 25–39. doi:10.1016/S0304-4203(99)00008-0.

Keuper, F., Bodegom, P. M., Dorrepaal, E., Weedon, J. T., Hal, J., Logtestijn, R. S. P., et al. (2012). A frozen feast: thawing permafrost increases plant-available nitrogen in subarctic peatlands. *Glob. Chang. Biol.* 18, 1998–2007. doi:10.1111/j.1365-2486.2012.02663.x.

Kicklighter, D. W., Hayes, D. J., McClelland, J. W., Peterson, B. J., McGuire, A. D., and Melillo, J. M. (2013). Insights and issues with simulating terrestrial DOC loading of Arctic river networks. *Ecol. Appl.* 23, 1817–1836. doi:10.1890/11-1050.1.

Köhler, H., Meon, B., Gordeev, V., Spitzy, A., and Amon, R. M. W. (2003). "Dissolved organic matter (DOM) in the estuaries of Ob and Yenisei and the adjacent Kara Sea, Russia," in *Siberian river run-off in the Kara Sea: Characterisation, Quantification, Variability and Environmental Significance*, eds. R. Stein, K. Fahl, D. K. Fütterer, E. M. Galimov, and O. Y. Stepanets (Amsterdam), 281–306.

Krumpen, T., Belter, H. J., Boetius, A., Damm, E., Haas, C., Hendricks, S., et al. (2019). Arctic warming interrupts the Transpolar Drift and affects long-range transport of sea

ice and ice-rafted matter. *Sci. Rep.* 9, 1–9. doi:10.1038/s41598-019-41456-y.

Lasareva, E. V., Parfenova, A. M., Romankevich, E. A., Lobus, N. V., and Drozdova, A. N. (2019). Organic Matter and Mineral Interactions Modulate Flocculation Across Arctic River Mixing Zones. *J. Geophys. Res. Biogeosciences* 124, 1651–1664. doi:10.1029/2019JG005026.

Le Fouest, V., Babin, M., and Tremblay, J.-É. (2013). The fate of riverine nutrients on Arctic shelves. *Biogeosciences* 10, 3661–3677. doi:10.5194/bg-10-3661-2013.

Lebo, S. E., Gargulak, J. D., and McNally, T. J. (2001). "Lignin," in *Kirk-Othmer Encyclopedia of Chemical Technology* (Hoboken, NJ, USA: John Wiley & Sons, Inc.). doi:10.1002/0471238961.12090714120914.a01.pub2.

Lee, Z., Arnone, R., Babin, M., Barnard, A. H., Boss, E., Cannizzaro, J. P., et al. (2006). *Reports of the International Ocean-Colour Coordinating Group Remote Sensing of Inherent Optical Properties: Fundamentals, Tests of Algorithms, and Applications*. , ed. V. Stuart Available at: http://www.ioccg.org [Accessed July 27, 2020].

Lee, Z., Carder, K. L., and Arnone, R. A. (2002). Deriving inherent optical properties from water color: a multiband quasi-analytical algorithm for optically deep waters. *Appl. Opt.* 41, 5755. doi:10.1364/ao.41.005755.

Lefering, I., Röttgers, R., Utschig, C., and McKee, D. (2017). Uncertainty budgets for liquid waveguide CDOM absorption measurements. *Appl. Opt.* 56, 6357. doi:10.1364/ao.56.006357.

Letscher, R. T., Hansell, D. A., and Kadko, D. (2011). Rapid removal of terrigenous dissolved organic carbon over the Eurasian shelves of the Arctic Ocean. *Mar. Chem.* 123, 78–87. doi:10.1016/j.marchem.2010.10.002.

Lewis, K. M., van Dijken, G. L., and Arrigo, K. R. (2020). Changes in phytoplankton concentration now drive increased Arctic Ocean primary production. *Science (80-.).* 369, 198–202. doi:10.1126/science.aay8380.

Liu, B., Yang, D., Ye, B., and Berezovskaya, S. (2005). Long-term open-water season stream temperature variations and changes over Lena River Basin in Siberia. *Glob. Planet. Change* 48, 96–111. doi:10.1016/J.GLOPLACHA.2004.12.007.

Lobbes, J. M., Fitznar, H. P., and Kattner, G. (2000). Biogeochemical characteristics of dissolved and particulate organic matter in Russian rivers entering the Arctic Ocean. *Geochim. Cosmochim. Acta* 64, 2973–2983. doi:10.1016/S0016-7037(00)00409-9.

Loisel, H., Vantrepotte, V., Jamet, C., and Ngoc Dat, D. (2013). "Challenges and New Advances in Ocean Color Remote Sensing of Coastal Waters," in *Topics in Oceanography* (InTech). doi:10.5772/56414.

Lu, X., Hu, Y., Trepte, C., Zeng, S., and Churnside, J. H. (2014). Ocean subsurface studies with the CALIPSO spaceborne lidar. *J. Geophys. Res. Ocean.* 119, 4305–4317. doi:10.1002/2014JC009970.

Ludwig, W., Amiotte Suchet, P., and Probst, J.-L. (1996). "River discharges of carbon to the world's oceans: determining local inputs of alkalinity and of dissolved and particulate organic carbon," in *Sciences de la terre et des planètes (Comptes rendus de l'Académie des sciences)*, 1007–1014. Available at: https://oatao.univ-toulouse.fr/3498/ [Accessed June 12, 2020].

Lundberg, L., and Haugan, P. M. (1996). A Nordic Seas-Arctic Ocean carbon budget from volume flows and inorganic carbon data. *Global Biogeochem. Cycles* 10, 493–510. doi:10.1029/96GB00359.

MacGilchrist, G. A., Naveira Garabato, A. C., Tsubouchi, T., Bacon, S., Torres-Valdés, S., and Azetsu-Scott, K. (2014). The Arctic Ocean carbon sink. *Deep. Res. Part I Oceanogr. Res. Pap.* 86, 39–55. doi:10.1016/j.dsr.2014.01.002.

Makarewicz, A., Kowalczuk, P., Sagan, S., Granskog, M. A., Pavlov, A. K., Zdun, A., et

al. (2018). Characteristics of chromophoric and fluorescent dissolved organic matter in the Nordic Seas. *Ocean Sci* 14, 543–562. doi:10.5194/os-14-543-2018.

Mann, P. J., Davydova, A., Zimov, N., Spencer, R. G. M., Davydov, S., Bulygina, E., et al. (2012). Controls on the composition and lability of dissolved organic matter in Siberia's Kolyma River basin. *J. Geophys. Res. Biogeosciences* 117. doi:10.1029/2011JG001798.

Mann, P. J., Spencer, R. G. M., Hernes, P. J., Six, J., Aiken, G. R., Tank, S. E., et al. (2016). Pan-Arctic Trends in Terrestrial Dissolved Organic Matter from Optical Measurements. *Front. Earth Sci.* 4, 25. doi:10.3389/feart.2016.00025.

Mannino, A., Novak, M. G., Nelson, N. B., Belz, M., Berthon, J.-F., Blough, N. V, et al. (2019). "Measurement protocol of absorption by chromophoric dissolved organic matter (CDOM) and other dissolved materials," in *Inherent Optical Property Measurements and Protocols: Absorption Coefficient*, eds. A. Mannino and M. G. Novak (Dartmouth, NS, Canada: IOCCG Ocean Optics and Biogeochemistry Protocols for Satellite Ocean Colour Sensor Validation). Available at: http://www.ioccg.org [Accessed July 16, 2020].

Mannino, A., Russ, M. E., and Hooker, S. B. (2008). Algorithm development and validation for satellite-derived distributions of DOC and CDOM in the U.S. Middle Atlantic Bight. *J. Geophys. Res. Ocean.* 113. doi:10.1029/2007JC004493.

Maritorena, S., Siegel, D. A., and Peterson, A. R. (2002). Optimization of a semianalytical ocean color model for global-scale applications. *Appl. Opt.* 41, 2705. doi:10.1364/AO.41.002705.

Massicotte, P., Asmala, E., Stedmon, C., and Markager, S. (2017). Global distribution of dissolved organic matter along the aquatic continuum: Across rivers, lakes and oceans. *Sci. Total Environ.* 609, 180–191. doi:10.1016/J.SCITOTENV.2017.07.076.

Mathis, J. T., Hansell, D. A., Kadko, D., Bates, N. R., and Cooper, L. W. (2007). Determining net dissolved organic carbon production in the hydrographically complex western Arctic Ocean. *Limnol. Oceanogr.* 52, 1789–1799. doi:10.4319/lo.2007.52.5.1789.

Matsuoka, A., Babin, M., and Devred, E. C. (2016). A new algorithm for discriminating water sources from space: A case study for the southern Beaufort Sea using MODIS ocean color and SMOS salinity data. *Remote Sens. Environ.* 184, 124–138. doi:10.1016/J.RSE.2016.05.006.

Matsuoka, A., Boss, E., Babin, M., Karp-Boss, L., Hafez, M., Chekalyuk, A., et al. (2017). Pan-Arctic optical characteristics of colored dissolved organic matter: Tracing dissolved organic carbon in changing Arctic waters using satellite ocean color data. *Remote Sens. Environ.* 200, 89–101. doi:10.1016/J.RSE.2017.08.009.

Matsuoka, A., Bricaud, A., Benner, R., Para, J., Sempéré, R., Prieur, L., et al. (2012). Tracing the transport of colored dissolved organic matter in water masses of the Southern Beaufort Sea: relationship with hydrographic characteristics. *Biogeosciences* 9, 925–940. doi:10.5194/bg-9-925-2012.

Matsuoka, A., Hill, V., Huot, Y., Babin, M., and Bricaud, A. (2011). Seasonal variability in the light absorption properties of western Arctic waters: Parameterization of the individual components of absorption for ocean color applications. *J. Geophys. Res.* 116, C02007. doi:10.1029/2009JC005594.

Matsuoka, A., Hooker, S. B., Bricaud, A., Gentili, B., and Babin, M. (2013). Estimating absorption coefficients of colored dissolved organic matter (CDOM) using a semi-analytical algorithm for southern Beaufort Sea waters: application to deriving concentrations of dissolved organic carbon from space. *Biogeosciences* 10, 917–927. doi:10.5194/bg-10-917-2013.

Matsuoka, A., Ortega-Retuerta, E., Bricaud, A., and Babin, M. (2015). Characteristics of colored dissolved organic matter (CDOM) in the Western Arctic Ocean: Relationships with microbial activities. *Deep Sea Res. Part II Top. Stud. Oceanogr.* 118, 44–52. doi:10.1016/J.DSR2.2015.02.012.

Mauritzen, C. (2012). Oceanography: Arctic freshwater. *Nat. Geosci.* 5, 162–164. doi:10.1038/ngeo1409.

McClelland, J. W., Déry, S. J., Peterson, B. J., Holmes, R. M., and Wood, E. F. (2006). A pan-arctic evaluation of changes in river discharge during the latter half of the 20th century. *Geophys. Res. Lett.* 33, L06715. doi:10.1029/2006GL025753.

McClelland, J. W., Holmes, R. M., Dunton, K. H., and Macdonald, R. W. (2012). The Arctic Ocean Estuary. *Estuaries and Coasts* 35, 353–368. doi:10.1007/s12237-010-9357-3.

McGuire, A. D., Anderson, L. G., Christensen, T. R., Scott, D., Laodong, G., Hayes, D. J., et al. (2009). Sensitivity of the carbon cycle in the Arctic to climate change. *Ecol. Monogr.* 79, 523–555. doi:10.1890/08-2025.1.

Meyer, H., Schönicke, L., Wand, U., Hubberten, H. W., and Friedrichsen, H. (2000). Isotope studies of hydrogen and oxygen in ground ice - Experiences with the equilibration technique. *Isotopes Environ. Health Stud.* 36, 133–149. doi:10.1080/10256010008032939.

Mobley, C. D. (1999). Estimation of the remote-sensing reflectance from above-surface measurements. *Appl. Opt.* 38, 7442. doi:10.1364/AO.38.007442.

Mobley, C. D., Gentili, B., Gordon, H. R., Jin, Z., Kattawar, G. W., Morel, A., et al. (1993). Comparison of numerical models for computing underwater light fields. *Appl. Opt.* 32, 7484. doi:10.1364/ao.32.007484.

Mobley, C. D., Stramski, D., Bissett, W. P., and Boss, E. (2004). Optical modeling of ocean waters: is the Case 1-Case 2 classification still useful? *Oceanography* 17, 60–67. doi:10.5670/oceanog.2004.48.

Mograne, M., Jamet, C., Loisel, H., Vantrepotte, V., Mériaux, X., and Cauvin, A. (2019). Evaluation of Five Atmospheric Correction Algorithms over French Optically-Complex Waters for the Sentinel-3A OLCI Ocean Color Sensor. *Remote Sens.* 11, 668. doi:10.3390/rs11060668.

Morel, A., and Prieur, L. (1977). Analysis of variations in ocean color1. *Limnol. Oceanogr.* 22, 709–722. doi:10.4319/lo.1977.22.4.0709.

Morison, J., Kwok, R., Peralta-Ferriz, C., Alkire, M., Rigor, I., Andersen, R., et al. (2012). Changing Arctic Ocean freshwater pathways. *Nature* 481, 66–70. doi:10.1038/nature10705.

Morrow, J. H., Hooker, S. B., Booth, C. R., Bernhard, G., Lind, R. N., and Brown, J. W. (2010). Advances in Measuring the Apparent Optical Properties (AOPs) of Optically Complex Waters. Available at: http://www.sti.nasa.gov/STI-homepage.html [Accessed July 16, 2020].

Neff, J. C., Finlay, J. C., Zimov, S. A., Davydov, S. P., Carrasco, J. J., Schuur, E. A. G., et al. (2006). Seasonal changes in the age and structure of dissolved organic carbon in Siberian rivers and streams. *Geophys. Res. Lett.* 33, L23401. doi:10.1029/2006GL028222.

Nelson, N. B., Carlson, C. A., and Steinberg, D. K. (2004). Production of chromophoric dissolved organic matter by Sargasso Sea microbes. doi:10.1016/j.marchem.2004.02.017.

Nelson, N. B., and Siegel, D. A. (2002). "Chromophoric DOM in the Open Ocean," in *Biogeochemistry of Marine Dissolved Organic Matter* (Elsevier), 547–578. doi:10.1016/B978-012323841-2/50013-0.

Nelson, N. B., Siegel, D. A., Carlson, C. A., Swan, C., Smethie, W. M., and Khatiwala, S. (2007). Hydrography of chromophoric dissolved organic matter in the North Atlantic. *Deep Sea Res. Part I Oceanogr. Res. Pap.* 54, 710–731. doi:10.1016/J.DSR.2007.02.006.

Niederdrenk, A. L., Sein, D. V., and Mikolajewicz, U. (2016). Interannual variability of the Arctic freshwater cycle in the second half of the twentieth century in a regionally coupled climate model. *Clim. Dyn.* 47, 3883–3900. doi:10.1007/s00382-016-3047-1.

O'Donnell, J. A., Aiken, G. R., Walvoord, M. A., Raymond, P. A., Butler, K. D., Dornblaser, M. M., et al. (2014). Using dissolved organic matter age and composition to detect permafrost thaw in boreal watersheds of interior Alaska. *J. Geophys. Res. Biogeosciences* 119, 2155–2170. doi:10.1002/2014JG002695.

Obu, J., Westermann, S., Bartsch, A., Berdnikov, N., Christiansen, H. H., Dashtseren, A., et al. (2019). Northern Hemisphere permafrost map based on TTOP modelling for 2000–2016 at 1 km2 scale. *Earth-Science Rev.* 193, 299–316. doi:10.1016/j.earscirev.2019.04.023.

Opsahl, S., and Benner, R. (1997). Distribution and cycling of terrigenous dissolved organic matter in the ocean. *Nature* 386, 480–482. doi:10.1038/386480a0.

Opsahl, S., Benner, R., and Amon, R. M. W. (1999). Major flux of terrigenous dissolved organic matter through the Arctic Ocean. *Limnol. Oceanogr.* 44, 2017–2023. doi:10.4319/lo.1999.44.8.2017.

Örek, H., Doerffer, R., Röttgers, R., Boersma, M., and Wiltshire, K. H. (2013). Contribution to a bio-optical model for remote sensing of Lena River water. *Biogeosciences* 10, 7081–7094. doi:10.5194/bg-10-7081-2013.

Osburn, C. L., Retamal, L., and Vincent, W. F. (2009). Photoreactivity of chromophoric dissolved organic matter transported by the Mackenzie River to the Beaufort Sea. *Mar. Chem.* 115, 10–20. doi:10.1016/j.marchem.2009.05.003.

Overduin, P. P., Schneider von Deimling, T., Miesner, F., Grigoriev, M. N., Ruppel, C., Vasiliev, A., et al. (2019). Submarine Permafrost Map in the Arctic Modeled Using 1-D Transient Heat Flux (SuPerMAP). *J. Geophys. Res. Ocean.* 124. doi:10.1029/2018JC014675.

Overeem, I., Anderson, R. S., Wobus, C. W., Clow, G. D., Urban, F. E., and Matell, N. (2011). Sea ice loss enhances wave action at the Arctic coast. *Geophys. Res. Lett.* 38. doi:10.1029/2011GL048681.

Park, H., Yoshikawa, Y., Oshima, K., Kim, Y., Ngo-Duc, T., Kimball, J. S., et al. (2016). Quantification of Warming Climate-Induced Changes in Terrestrial Arctic River Ice Thickness and Phenology. *J. Clim.* 29, 1733–1754. doi:10.1175/JCLI-D-15-0569.1.

Pavelsky, T. M., and Zarnetske, J. P. (2017). Rapid decline in river icings detected in Arctic Alaska: Implications for a changing hydrologic cycle and river ecosystems. *Geophys. Res. Lett.* 44, 3228–3235. doi:10.1002/2016GL072397.

Pegau, W. S. (2002). Inherent optical properties of the central Arctic surface waters. *J. Geophys. Res. C Ocean.* 107. doi:10.1029/2000jc000382.

Peterson, B. J. (2002). Increasing River Discharge to the Arctic Ocean. *Science (80-.).* 298, 2171–2173. doi:10.1126/science.1077445.

Peterson, B. J., McClelland, J., Curry, R., Holmes, R. M., Walsh, J. E., and Aagaard, K. (2006). Trajectory shifts in the arctic and subarctic freshwater cycle. *Science (80-.).* 313, 1061–1066. doi:10.1126/science.1122593.

Petzold, T. J., Duntley, S. Q., and Nierenberg, W. A. (1972). Volume Scattering Functions for Selected Ocean Waters.

Plaza, C., Pegoraro, E., Bracho, R., Celis, G., Crummer, K. G., Hutchings, J. A., et al. (2019). Direct observation of permafrost degradation and rapid soil carbon loss in

tundra. *Nat. Geosci.* 12, 627–631. doi:10.1038/s41561-019-0387-6.

Polyakov, I. V., Alekseev, G. V., Bekryaev, R. V., Bhatt, U., Colony, R. L., Johnson, M. A., et al. (2002). Observationally based assessment of polar amplification of global warming. *Geophys. Res. Lett.* 29, 25–1. doi:10.1029/2001GL011111.

Porter, C., Morin, P., Howat, I., Noh, M.-J., Bates, B., Peterman, K., et al. (2018). ArcticDEM. *Harvard Dataverse* V1. doi:https://doi.org/10.7910/DVN/OHHUKH.

Pugach, S. P., Pipko, I. I., Shakhova, N. E., Shirshin, E. A., Perminova, I. V., Gustafsson, Ö., et al. (2018). Dissolved organic matter and its optical characteristics in the Laptev and East Siberian seas: Spatial distribution and interannual variability. *Ocean Sci.* doi:10.5194/os-14-87-2018.

Rawlins, M. A., Steele, M., Holland, M. M., Adam, J. C., Cherry, J. E., Francis, J. A., et al. (2010). Analysis of the Arctic System for Freshwater Cycle Intensification: Observations and Expectations. *J. Clim.* 23, 5715–5737. doi:10.1175/2010JCLI3421.1.

Raymond, P. A., McClelland, J. W., Holmes, R. M., Zhulidov, A. V., Mull, K., Peterson, B. J., et al. (2007). Flux and age of dissolved organic carbon exported to the Arctic Ocean: A carbon isotopic study of the five largest arctic rivers. *Global Biogeochem. Cycles* 21. doi:10.1029/2007GB002934.

Renosh, P. R., Doxaran, D., De Keukelaere, L., and Gossn, J. I. (2020). Evaluation of atmospheric correction algorithms for sentinel-2-MSI and sentinel-3-OLCI in highly turbid estuarine waters. *Remote Sens.* 12, 1285. doi:10.3390/RS12081285.

Retamal, L., Bonilla, S., and Vincent, W. F. (2008). Optical gradients and phytoplankton production in the Mackenzie River and the coastal Beaufort Sea. *Polar Biol.* 31, 363–379. doi:10.1007/s00300-007-0365-0.

Richter-Menge, J., Druckenmiller, M. L., and Jeffries, M. (2019). Eds., 2019: Arctic Report Card 2019. Available at: https://www.arctic.noaa.gov/Report-Card.

Riedel, A., Michel, C., Gosselin, M., and LeBlanc, B. (2008). Winter-spring dynamics in sea-ice carbon cycling in the coastal Arctic Ocean. *J. Mar. Syst.* 74, 918–932. doi:10.1016/j.jmarsys.2008.01.003.

Runkel, R. L., Crawford, C. G., and Cohn, T. A. (2004). "Load Estimator (LOADEST): A FORTRAN Program for Estimating Constituent Loads in Streams and Rivers," in *Techniques and Methods Book 4*, Chapter A5, 69 . Available at: http://www.usgs.gov/ [Accessed January 22, 2020].

Schlosser, P., Bauch, D., Fairbanks, R., and Bönisch, G. (1994). Arctic river-runoff: mean residence time on the shelves and in the halocline. *Deep. Res. Part I* 41, 1053–1068. doi:10.1016/0967-0637(94)90018-3.

Schroeder, T., and Schaale, M. (2005). MERIS Case-2 Water Properties Processor, Version 1.0.1, Institute for Space Sciences, Freie Universität Berlin (FUB). *http://www.brockmann-consult.de/beam/software/plugins/FUB-WeWWater-1.0.1.zip*.

Schulien, J. A., Behrenfeld, M. J., Hair, J. W., Hostetler, C. A., and Twardowski, M. S. (2017). Vertically- resolved phytoplankton carbon and net primary production from a high spectral resolution lidar. *Opt. Express* 25, 13577. doi:10.1364/oe.25.013577.

Schuur, E. A. G., McGuire, A. D., Schädel, C., Grosse, G., Harden, J. W., Hayes, D. J., et al. (2015). Climate change and the permafrost carbon feedback. *Nature* 520, 171–179. doi:10.1038/nature14338.

Schuur, E. A. G., Vogel, J. G., Crummer, K. G., Lee, H., Sickman, J. O., and Osterkamp, T. E. (2009). The effect of permafrost thaw on old carbon release and net carbon exchange from tundra. *Nature* 459, 556–559. doi:10.1038/nature08031.

Schweiger, A. J. (2004). Changes in seasonal cloud cover over the Arctic seas from satellite and surface observations. *Geophys. Res. Lett.* 31, n/a-n/a.

doi:10.1029/2004GL020067.

Screen, J. A., and Francis, J. A. (2016). Contribution of sea-ice loss to Arctic amplification is regulated by Pacific Ocean decadal variability. *Nat. Clim. Chang.* 6, 856–860. doi:10.1038/nclimate3011.

Scully, N. M., and Miller, W. L. (2000). Spatial and temporal dynamics of colored dissolved organic matter in the north water polynya. *Geophys. Res. Lett.* 27, 1009–1011. doi:10.1029/1999gl007002.

Semiletov, I. P., Shakhova, N. E., Pipko, I. I., Pugach, S. P., Charkin, A. N., Dudarev, O. V., et al. (2013). Space–time dynamics of carbon and environmental parameters related to carbon dioxide emissions in the Buor-Khaya Bay and adjacent part of the Laptev Sea. *Biogeosciences* 10, 5977–5996. doi:10.5194/bg-10-5977-2013.

Serreze, M. C., Barrett, A. P., Slater, A. G., Woodgate, R. A., Aagaard, K., Lammers, R. B., et al. (2006). The large-scale freshwater cycle of the Arctic. *J. Geophys. Res. Ocean.* 111. doi:10.1029/2005JC003424.

Serreze, M. C., and Barry, R. G. (2011). Processes and impacts of Arctic amplification: A research synthesis. *Glob. Planet. Change* 77, 85–96. doi:10.1016/j.gloplacha.2011.03.004.

Shen, Y., Fichot, C. G., and Benner, R. (2012). Dissolved organic matter composition and bioavailability reflect ecosystem productivity in the Western Arctic Ocean. *Biogeosciences* 9, 4993–5005. doi:10.5194/bg-9-4993-2012.

Shiklomanov, A. I. (2010). Observed and naturalized discharge data for large Siberian rivers. Available at: http://www.r-arcticnet.sr.unh.edu/ObservedAndNaturalizedDischarge-Website/.

Shiklomanov, A. I., Holmes, R. M., McClelland, J. W., Tank, S. E., and Spencer., R. G. M. (2018). ArcticGRO Discharge Dataset. *Arct. Gt. Rivers Obs.* Discharge.

Shiklomanov, A. I., and Lammers, R. B. (2009). Record Russian river discharge in 2007 and the limits of analysis. *Environ. Res. Lett.* 4. doi:10.1088/1748-9326/4/4/045015.

Shiklomanov, A. I., and Lammers, R. B. (2014). River ice responses to a warming Arctic - Recent evidence from Russian rivers. *Environ. Res. Lett.* 9. doi:10.1088/1748-9326/9/3/035008.

Siegel, D. A., Wang, M., Maritorena, S., and Robinson, W. (2000). Atmospheric correction of satellite ocean color imagery: the black pixel assumption. *Appl. Opt.* 39, 3582. doi:10.1364/ao.39.003582.

Slade, W. H., and Boss, E. S. (2006). Calibrated near-forward volume scattering function obtained from the LISST particle sizer. *Opt. Express* 14, 3602. doi:10.1364/oe.14.003602.

Smith, L. C., and Pavelsky, T. M. (2008). Estimation of river discharge, propagation speed, and hydraulic geometry from space: Lena River, Siberia. *Water Resour. Res.* 44, 1–11. doi:10.1029/2007WR006133.

Smith, R. E. H., Gosselin, M., Kudoh, S., Robineau, B., and Taguchi, S. (1997). DOC and its relationship to algae in bottom ice communities. *J. Mar. Syst.* 11, 71–80. doi:10.1016/S0924-7963(96)00029-2.

Soppa, M. A., Pefanis, V., Hellmann, S., Losa, S. N., Hölemann, J., Martynov, F., et al. (2019). Assessing the Influence of Water Constituents on the Radiative Heating of Laptev Sea Shelf Waters. *Front. Mar. Sci.* 6, 221. doi:10.3389/fmars.2019.00221.

Spencer, R. G. M., Aiken, G. R., Butler, K. D., Dornblaser, M. M., Striegl, R. G., and Hernes, P. J. (2009). Utilizing chromophoric dissolved organic matter measurements to derive export and reactivity of dissolved organic carbon exported to the Arctic Ocean: A case study of the Yukon River, Alaska. *Geophys. Res. Lett.* 36, L06401. doi:10.1029/2008GL036831.

Spors, S. (2018). Stable Water Isotope Characteristics of Recent Precipitation from Tiksi and Samoylov Island – Calibration of a Geoscientific Proxy for Northern Siberia.

Spreen, G., Kwok, R., and Menemenlis, D. (2011). Trends in Arctic sea ice drift and role of wind forcing: 1992-2009. *Geophys. Res. Lett.* 38. doi:10.1029/2011GL048970.

Stedmon, C. A., Amon, R. M. W., Rinehart, A. J., and Walker, S. A. (2011). The supply and characteristics of colored dissolved organic matter (CDOM) in the Arctic Ocean: Pan Arctic trends and differences. *Mar. Chem.* 124, 108–118. doi:10.1016/J.MARCHEM.2010.12.007.

Stedmon, C. A., and Bro, R. (2008). Characterizing dissolved organic matter fluorescence with parallel factor analysis: A tutorial. *Limnol. Oceanogr. Methods* 6, 572–579. doi:10.4319/lom.2008.6.572.

Stedmon, C. A., Granskog, M. A., and Dodd, P. A. (2015). An approach to estimate the freshwater contribution from glacial melt and precipitation in East Greenland shelf waters using colored dissolved organic matter (CDOM). *J. Geophys. Res. Ocean.* 120, 1107–1117. doi:10.1002/2014JC010501.

Stedmon, C. A., and Markager, S. (2001). The optics of chromophoric dissolved organic matter (CDOM) in the Greenland Sea: An algorithm for differentiation between marine and terrestrially derived organic matter. *Limnol. Oceanogr.* 46, 2087–2093. doi:10.4319/lo.2001.46.8.2087.

Stedmon, C. A., Markager, S., and Bro, R. (2003). Tracing dissolved organic matter in aquatic environments using a new approach to fluorescence spectroscopy. *Mar. Chem.* 82, 239–254. doi:10.1016/S0304-4203(03)00072-0.

Stedmon, C. A., and Nelson, N. B. (2015). "The Optical Properties of DOM in the Ocean," in *Biogeochemistry of Marine Dissolved Organic Matter: Second Edition* (Elsevier Inc.), 481–508. doi:10.1016/B978-0-12-405940-5.00010-8.

Stein, R., Macdonald, R. W., Naidu, A. S., Yunker, M. B., Gobeil, C., Cooper, L. W., et al. (2004). "Organic Carbon in Arctic Ocean Sediments: Sources, Variability, Burial, and Paleoenvironmental Significance," in *The Organic Carbon Cycle in the Arctic Ocean* (Springer Berlin Heidelberg), 169–314. doi:10.1007/978-3-642-18912-8_7.

Steinmetz, F., Deschamps, P.-Y., and Ramon, D. (2011). Atmospheric correction in presence of sun glint: application to MERIS. *Opt. Express* 19, 9783. doi:10.1364/oe.19.009783.

Striegl, R. G., Dornblaser, M. M., Aiken, G. R., Wickland, K. P., and Raymond, P. A. (2007). Carbon export and cycling by the Yukon, Tanana, and Porcupine rivers, Alaska, 2001-2005. *Water Resour. Res.* 43. doi:10.1029/2006WR005201.

Stroeve, J., and Notz, D. (2018). Changing state of Arctic sea ice across all seasons. *Environ. Res. Lett.* 13. doi:10.1088/1748-9326/aade56.

Sugimoto, A., and Maximov, T. C. (2012). Study on Hydrological Processes in Lena River Basin using Stable Isotope Ratios of River Water (IAEA-TECDOC--1673). *Monit. Isot. Rivers Creat. Glob. Netw. Isot. Rivers*, 41.

Sydor, M., Gould, R. W., Arnone, R. A., Haltrin, V. I., and Goode, W. (2004). Uniqueness in remote sensing of the inherent optical properties of ocean water. *Appl. Opt.* 43, 2156–2162. doi:10.1364/AO.43.002156.

Syed, T. H., Famiglietti, J. S., Zlotnicki, V., and Rodell, M. (2007). Contemporary estimates of Pan-Arctic freshwater discharge from GRACE and reanalysis. *Geophys. Res. Lett.* 34, L19404. doi:10.1029/2007GL031254.

Tanaka, K., Takesue, N., Nishioka, J., Kondo, Y., Ooki, A., Kuma, K., et al. (2016). The conservative behavior of dissolved organic carbon in surface waters of the southern Chukchi Sea, Arctic Ocean, during early summer. *Sci. Rep.* 6, 1–10. doi:10.1038/srep34123.

Tananaev, N. I., Makarieva, O. M., and Lebedeva, L. S. (2016). Trends in annual and extreme flows in the Lena River basin, Northern Eurasia. *Geophys. Res. Lett.* 43, 10,764-10,772. doi:10.1002/2016GL070796.

Tank, S. E., Striegl, R. G., McClelland, J. W., and Kokelj, S. V. (2016). Multi-decadal increases in dissolved organic carbon and alkalinity flux from the Mackenzie drainage basin to the Arctic Ocean. *Environ. Res. Lett.* 11. doi:10.1088/1748-9326/11/5/054015.

Tanski, G., Couture, N., Lantuit, H., Eulenburg, A., and Fritz, M. (2016). Eroding permafrost coasts release low amounts of dissolved organic carbon (DOC) from ground ice into the nearshore zone of the Arctic Ocean. *Global Biogeochem. Cycles* 30, 1054–1068. doi:10.1002/2015GB005337.

Tanski, G., Lantuit, H., Ruttor, S., Knoblauch, C., Radosavljevic, B., Strauss, J., et al. (2017). Transformation of terrestrial organic matter along thermokarst-affected permafrost coasts in the Arctic. *Sci. Total Environ.* 581–582, 434–447. doi:10.1016/j.scitotenv.2016.12.152.

Tarnocai, C., Canadell, J. G., Schuur, E. A. G., Kuhry, P., Mazhitova, G., and Zimov, S. (2009). Soil organic carbon pools in the northern circumpolar permafrost region. *Global Biogeochem. Cycles* 23. doi:10.1029/2008GB003327.

Thibodeau, B., Bauch, D., Kassens, H., and Timokhov, L. A. (2014). Interannual variations in river water content and distribution over the Laptev Sea between 2007 and 2011: The Arctic Dipole connection. *Geophys. Res. Lett.* 41, 7237–7244. doi:10.1002/2014GL061814.

Turetsky, M. R., Abbott, B. W., Jones, M. C., Walter Anthony, K., Olefeldt, D., Schuur, E. A. G., et al. (2019). Permafrost collapse is accelerating carbon release. *Nature* 569, 32–34. doi:10.1038/d41586-019-01313-4.

Vallières, C., Retamal, L., Ramlal, P., Osburn, C. L., and Vincent, W. F. (2008). Bacterial production and microbial food web structure in a large arctic river and the coastal Arctic Ocean. *J. Mar. Syst.* 74, 756–773. doi:10.1016/j.jmarsys.2007.12.002.

van Huissteden, J. (2020). "Permafrost Carbon Quantities and Fluxes," in *Thawing Permafrost* (Cham: Springer International Publishing), 179–274. doi:10.1007/978-3-030-31379-1_4.

Vantrepotte, V., Danhiez, F.-P., Loisel, H., Ouillon, S., Mériaux, X., Cauvin, A., et al. (2015). CDOM-DOC relationship in contrasted coastal waters: implication for DOC retrieval from ocean color remote sensing observation. *Opt. Express* 23, 33. doi:10.1364/OE.23.000033.

Velicogna, I., Tong, J., Zhang, T., and Kimball, J. S. (2012). Increasing subsurface water storage in discontinuous permafrost areas of the Lena River basin, Eurasia, detected from GRACE. *Geophys. Res. Lett.* 39. doi:10.1029/2012GL051623.

Vetrov, A. A., Romankevich, E. A., Vetrov, A. A., and Romankevich, E. A. (2004). "Horizontal Carbon Fluxes in the Land-Sea System," in *Carbon Cycle in the Russian Arctic Seas* (Springer Berlin Heidelberg), 201–227. doi:10.1007/978-3-662-06208-1_5.

Vonk, J. E., Sanchez-Garca, L., Van Dongen, B. E., Alling, V., Kosmach, D., Charkin, A., et al. (2012). Activation of old carbon by erosion of coastal and subsea permafrost in Arctic Siberia. *Nature* 489, 137–140. doi:10.1038/nature11392.

Vonk, J. E., Tank, S. E., and Walvoord, M. A. (2019). Integrating hydrology and biogeochemistry across frozen landscapes. *Nat. Commun.* 10, 1–4. doi:10.1038/s41467-019-13361-5.

Walker, S. A., Amon, R. M. W., and Stedmon, C. A. (2013). Variations in high-latitude riverine fluorescent dissolved organic matter: A comparison of large Arctic rivers. *J.*

Geophys. Res. Biogeosciences 118, 1689–1702. doi:10.1002/2013JG002320.

Walker, S. A., Amon, R. M. W., Stedmon, C., Duan, S., and Louchouarn, P. (2009). The use of PARAFAC modeling to trace terrestrial dissolved organic matter and fingerprint water masses in coastal Canadian Arctic surface waters. *J. Geophys. Res.* 114, G00F06. doi:10.1029/2009JG000990.

Wang, M. (2002). The Rayleigh lookup tables for the SeaWiFS data processing: Accounting for the effects of ocean surface roughness. *Int. J. Remote Sens.* 23, 2693–2702. doi:10.1080/01431160110115591.

Wang, M., and Bailey, S. W. (2001). Correction of sun glint contamination on the SeaWiFS ocean and atmosphere products. *Appl. Opt.* 40, 4790. doi:10.1364/ao.40.004790.

Wang, M., and Overland, J. E. (2009). A sea ice free summer Arctic within 30 years? *Geophys. Res. Lett.* 36. doi:10.1029/2009GL037820.

Wang, M., and Overland, J. E. (2012). A sea ice free summer Arctic within 30 years: An update from CMIP5 models. *Geophys. Res. Lett.* 39. doi:10.1029/2012GL052868.

Wegner, C., Bauch, D., Hölemann, J. A., Janout, M. A., Heim, B., Novikhin, A., et al. (2013). Interannual variability of surface and bottom sediment transport on the Laptev Sea shelf during summer. *Biogeosciences* 10, 1117–1129. doi:10.5194/bg-10-1117-2013.

Weishaar, J. L., Aiken, G. R., Bergamaschi, B. A., Fram, M. S., Roger, F., and Mopper, K. (2003). Evaluation of Specific Ultraviolet Absorbance as an Indicator of the Chemical Composition and Reactivity of Dissolved Organic Carbon. doi:10.1021/ES030360X.

Weiss, J. (2001). *Ionenchromatographie*. Wiley doi:10.1002/9783527625031.

Werdell, P. J., McKinna, L. I. W., Boss, E., Ackleson, S. G., Craig, S. E., Gregg, W. W., et al. (2018). An overview of approaches and challenges for retrieving marine inherent optical properties from ocean color remote sensing. *Prog. Oceanogr.* 160, 186–212. doi:10.1016/j.pocean.2018.01.001.

Wild, B., Andersson, A., Bröder, L., Vonk, J., Hugelius, G., McClelland, J. W., et al. (2019). Rivers across the Siberian Arctic unearth the patterns of carbon release from thawing permafrost. *Proc. Natl. Acad. Sci. U. S. A.* 116, 10280–10285. doi:10.1073/pnas.1811797116.

Woo, M.-K. (1986). Permafrost hydrology in North America Permafrost Hydrology in North America. *AtmosphereOcean* 24:3, 201–234. doi:10.1080/07055900.1986.9649248.

Yang, D., Kane, D. L., Hinzman, L. D., Zhang, X., Zhang, T., and Ye, H. (2002). Siberian Lena River hydrologic regime and recent change. *J. Geophys. Res. Atmos.* 107, ACL 14-1-ACL 14-10. doi:10.1029/2002JD002542.

Yang, D., Marsh, P., and Shaoqing Ge, & (2013). Cold and Mountain Region Hydrological Systems Under Climate Change. IAHS Publ Available at: http://www.usgs.gov/ [Accessed December 16, 2019].

Yang, D., Shi, X., and Marsh, P. (2015). Variability and extreme of Mackenzie River daily discharge during 1973-2011. *Quat. Int.* 380–381, 159–168. doi:10.1016/j.quaint.2014.09.023.

Yang, D., Zhao, Y., Armstrong, R., Robinson, D., and Brodzik, M.-J. (2007). Streamflow response to seasonal snow cover mass changes over large Siberian watersheds. *J. Geophys. Res.* 112, F02S22. doi:10.1029/2006JF000518.

Ye, B., Yang, D., and Kane, D. L. (2003). Changes in Lena River streamflow hydrology: Human impacts versus natural variations. *Water Resour. Res.* 39. doi:10.1029/2003WR001991.

Yoder, J. A., McClain, C. R., Blanton, J. O., and Oeymay, L.-Y. (1987). Spatial scales in CZCS-chlorophyll imagery of the southeastern U.S. continental shelf1. *Limnol.*

Oceanogr. 32, 929–941. doi:10.4319/lo.1987.32.4.0929.

Zhang, X., Huot, Y., Gray, D. J., Weidemann, A., and Rhea, W. J. (2013). Climate of the Past Geoscientific Instrumentation Methods and Data Systems Biogeochemical origins of particles obtained from the inversion of the volume scattering function and spectral absorption in coastal waters. *Biogeosciences* 10, 6029–6043. doi:10.5194/bg-10-6029-2013.

Zibordi, G., Voss, K. J., Johnson, B. C., and Mueller, J. L. (2019). IOCCG Ocean Optics and Biogeochemistry Protocols for Satellite Ocean Colour Sensor Validation. *IOCCG Protoc. Ser.* 3. doi:10.25607/OBP-691.

Acknowledgements

First, I would particularly like to thank Paul Overduin. The excellent guidance you provided on scientific and career but also on personal matters quickly became indispensable for me during my PhD. Thank you for your patience, endlessly emitting motivation, and your constant support! I also would like to thank Prof. Jürgen Fischer for providing me the opportunity to work under his supervision at the Institute for Space Science (WEW) and for his help in realizing my PhD project. I want to thank my colleagues at WEW for the everyday nice working atmosphere, good coffee, and fruitful discussions. In addition, many thanks go to Prof. Guido Grosse and the AWI Permafrost section for the logistical and financial support of the extensive fieldwork, but also for providing a second scientific home for my PhD project. I thank Antje Eulenburg for the extensive lab-work and endless lab-specific discussions. I am thankful to Birgit Heim for her support, especially in the initialization of my project and her inexhaustible drive to connect people. Speaking of inexhaustible – thanks, Michael Angelopoulos, for becoming an inexhaustibly motivating and complimenting friend! I am grateful to Prof. Marcel Babin and the Takuvik Lab members for hosting me for half a year in Québec City. I thank all participants of the Mackenzie Expeditions and especially my fieldwork buddies Laurent Oziel and Guislain Bécu. Thank you, Atsushi Matsuoka for your invaluable help during my PhD. Your great work was an inspiration for my thesis. During our time in Québec City, we (Sonya and I) became friends with the wonderful Martine Lizotte. Thank you for everything you did for us to make it an unforgettable summer. I also acknowledge the support and helpful discussions with Colin Stedmon (DTU), Martin Hieronymi (HZG), and Rafael Gonçalves-Araujo (DTU). Special thanks go to Jens Hölemann (AWI) and Markus Janout (AWI) for the scientific discussions and the ongoing long-term support since the start of my bachelor's studies. Further, I want to thank my colleagues Vasily Povazhnyi, Antonina Chetverova and Lyudmila Korolyeva at the Otto Schmidt Laboratory in Saint Petersburg and many more Russian partners and colleagues without whom my work would not be possible.

Additional thanks for proof-reading, discussions and suggestions for this thesis goes to Paul Overduin, Martine Lizotte, Sofia Antonova, Anna Irrgang, Michael Angelopoulos, and Frederieke Miesner. Big thanks goes out to my wife, all my friends and colleagues, who supported me all the time.

Further, I would like to thank all members of the Geo.X Young Academy, the Geo.X steering committee, and coordinators. The research for this work was supported by the Geo.X, the Research Network for Geosciences in Berlin and Potsdam (grant no. SO_087_GeoX).

Appendix

Appendix A

Difference in DOC and a_{CDOM} using different instruments, filter types and pore sizes

During the additional sampling program in July 2018, DOC and CDOM absorption (a_{CDOM}) samples were filtered through 4 different filter types and filter pore sizes: (1) 0.22 µm CA, (2) 0.45 µm CA, (3) 0.7 µm GF/F and (4) 0.8 µm CA. CDOM absorbance was measured at OSL (SPECORD 200 spectrophotometer, Analytik Jena) and additionally measured right after filtration on Samoylov Island using a AC-s (WET Labs).

There are a number of protocols for measuring a_{CDOM} in inland water with high DOM concentrations and high particulate load. For instance, different filter types and pore sizes are used to separate the dissolved organic matter fraction from the total organic matter including absorbing particles and pigments. Too small filter pore sizes trend to clog too fast and filtration of enough volume is difficult. Thus, for the monitoring program, we chose a 0.45 µm Cellulose Acetate (CA) filter. To evaluate differences between different filter pore sizes and their materials, we used four different filter for each sample during the high frequency sampling period in July (**Table 4.2**). The results show consistent but small differences in $a_{CDOM}(443)$ (**Appendix Figure 1**). The mean difference between 0.45 µm CA filter and 0.22 µm CA was 2.98% for the 22 samples. Between 0.45 µm CA and 0.7 GF/F we observed a mean difference of 2.16%. Between the a_{CDOM} measurements using a AC-s and 0.22 µm CA filter and a spectrophotometer (Specord) and also 0.22 µm CA filter we observed a mean difference of 2.56%.

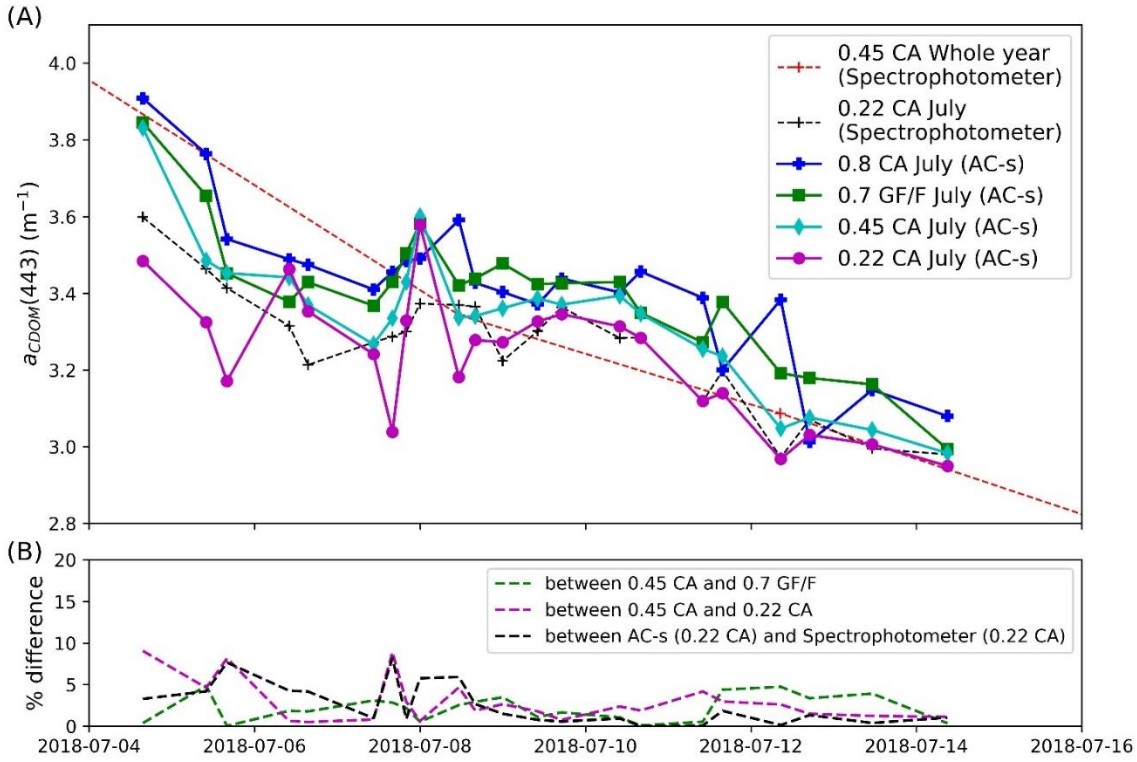

Appendix Figure 1: (A) Comparison of $a_{CDOM}(443)$ measured with different instruments, filter types and pore sizes. (B) Percentage differences.

In addition to filter tests for $a_{CDOM}(443)$, we also tested the difference for DOC concentration between 0.45 µm CA filter (which we use in the whole-year sampling) and 0.7 µm GF/F filter (**Appendix Figure 2**). The mean absolute difference between DOC concentrations of both tested filters is 0.232 mg L^{-1} (2.51%).

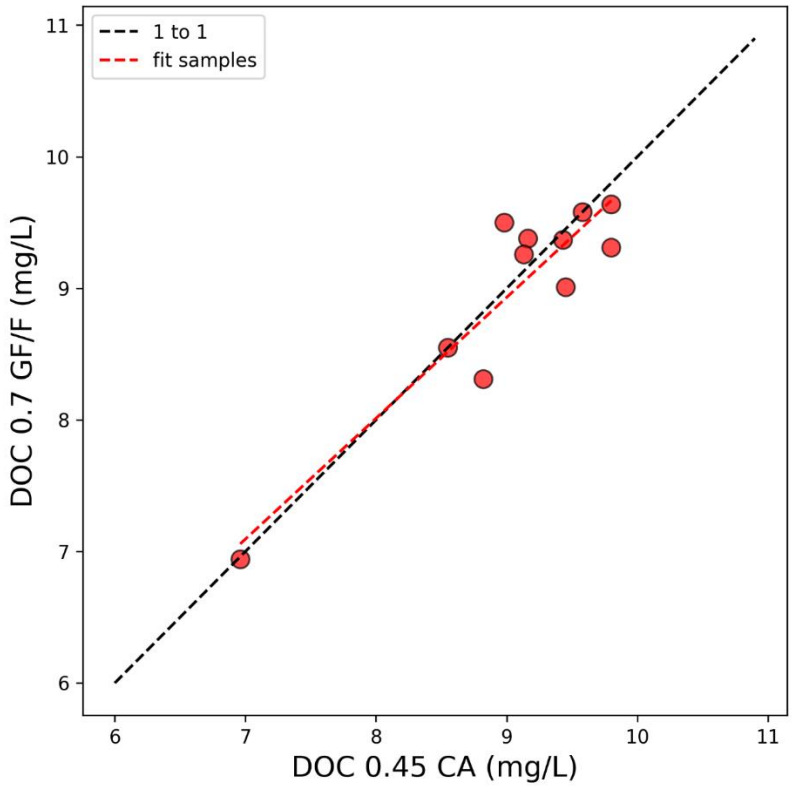

Appendix Figure 2: Comparison between DOC concentration using two different filter type and pore sizes.

Principal Component Analysis (PCA) of biogeochemical parameter

Appendix Table 1: Percentage of variability that is explained by each component.

Component	% of variability explained
Component 1	97.97545
Component 2	1.809842
Component 3	0.185318
Component 4	0.019407
Component 5	0.003892
Component 6	0.002956
Component 7	0.001691
Component 8	0.000701
Component 9	0.000398
Component 10	0.000175
Component 11	0.000113
Component 12	4.24E-05
Component 13	1.06E-05
Component 14	2.97E-08

Major ions

Major dissolved species concentrations in the Lena River vary seasonally. **Appendix Figure 3** shows concentrations normalized to the annual range of concentrations. Missing data points are samples with concentrations below the detection limit, except for the data break in all parameters in the beginning of October, when sampling was interrupted. Some anion concentrations (F^-, Cl^- $SO4^{2-}$) dip strongly for one sample only, which probably results from sampling problems, since this change in concentration is not reflected in other measured parameters; these values should be discarded.

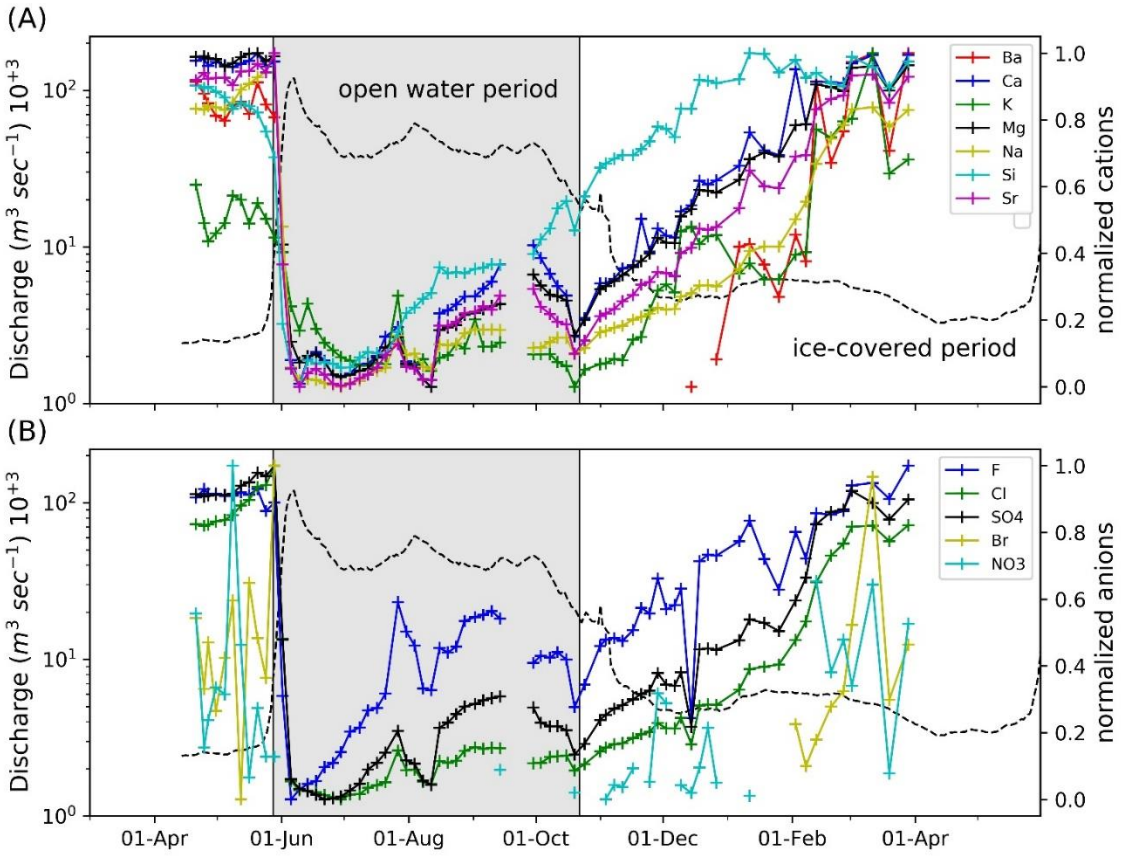

Appendix Figure 3: Normalized major ions concentration. Al (<100 µg/L), Fe (<100 µg/L), Mn (<20 µg/L) and P (<0.1 mg/L) are below detection limit.

Biogeochemistry of Lena River ice

To get an insight about how much DOM is stored in the river ice during winter, we drilled an ice core in the end of winter 2018 (May 4, 2018). The total ice thickness was 144 cm and the snow cover was 36 cm. Lena River water EC below ice was 453 µS/cm. The ice core consisted of 5 pieces. At each end, we removed one samples due to signs of contamination (peaks of DOM and high EC). Generally, DOC and $a_{CDOM}(254)$ in the ice

core is low. Mean DOC concentration is 1.04 mg L^{-1} and mean $a_{CDOM}(254)$ is 0.96 m^{-1}. No clear trend from top to bottom could be observed.

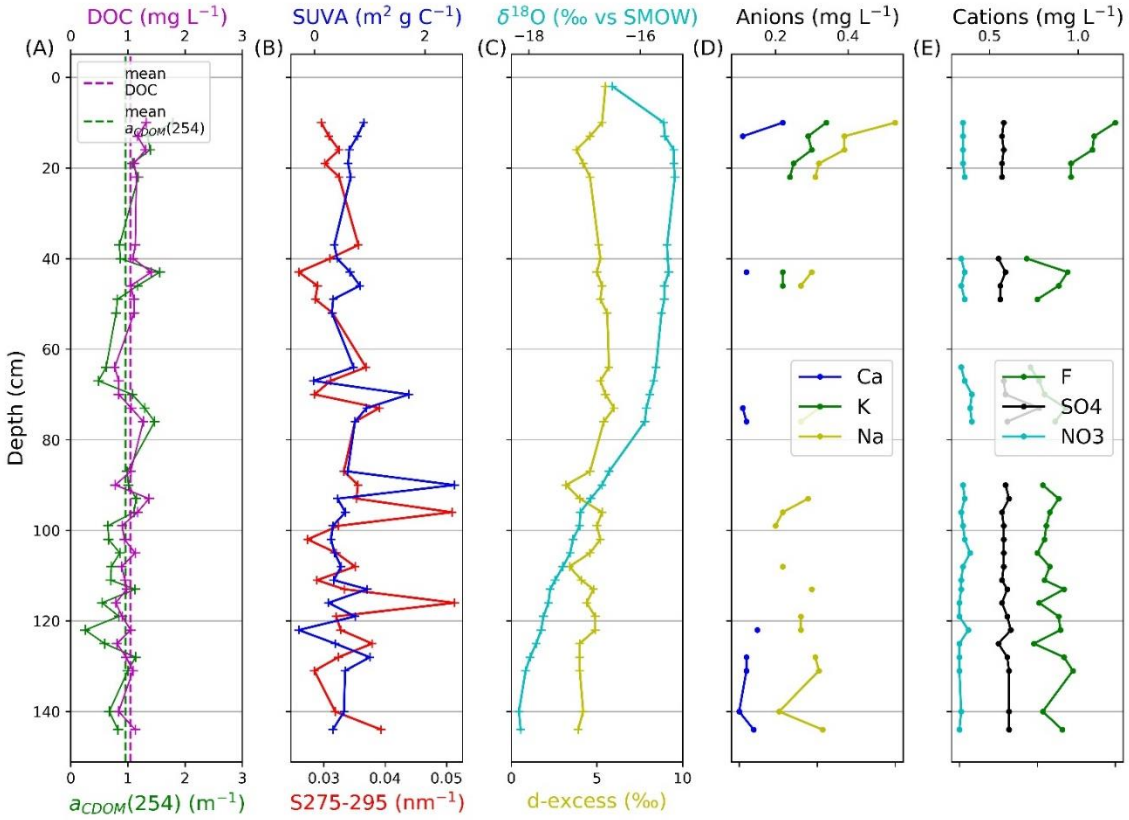

Appendix Figure 4: Ice Core taken in May 2018 showing in (A) DOC, $a_{CDOM}(254)$, optical DOM properties (B), stable water isotopes (C), and major ions (D, E).

Seasonal DOC flux comparisons

Following Raymond et al. (2007), percent spring thaw DOC flux is defined here as the 2-month period preceding the point on the hydrograph when 50% of maximum flow is hit (June 2, 2018 to August 2, 2018). The percent spring thaw DOC flux of 53.2% (3.62 Tg C) for 2018 is low compared to 54% (2.84 Tg C) in 2004 and 70% (4.47 Tg C) in 2005. When divide the year into spring (May to June, 2 month), summer (July to October) and winter (Nov. to April), we see a dominant flux in during summer (48%) compared to spring (41%) and winter (11%) (**Appendix Figure 5**). The percentage flux of spring and summer as well as the percent spring DOC flux is very variable between different years. Both, Raymond et al. (2007) and Stedmon et al. (2011) report a dominant flux in spring rather than during summer as observed in this study. Reasons for the variability of seasonal fluxes between years can be changing discharge and DOC concentrations but also timing of spring ice break-up and duration of the peak discharge can contribute to the variations. Another factor

is the potential error of daily DOC concentration calculated by statistical models connecting the discharge and DOC concentration as used in many studies (i.e. Holmes et al., 2012; Raymond et al., 2007; Stedmon et al., 2011). These models are applied to overcome the lack of measurements throughout the whole year. The winter flux varies only between 9 and 11% when comparing different studies.

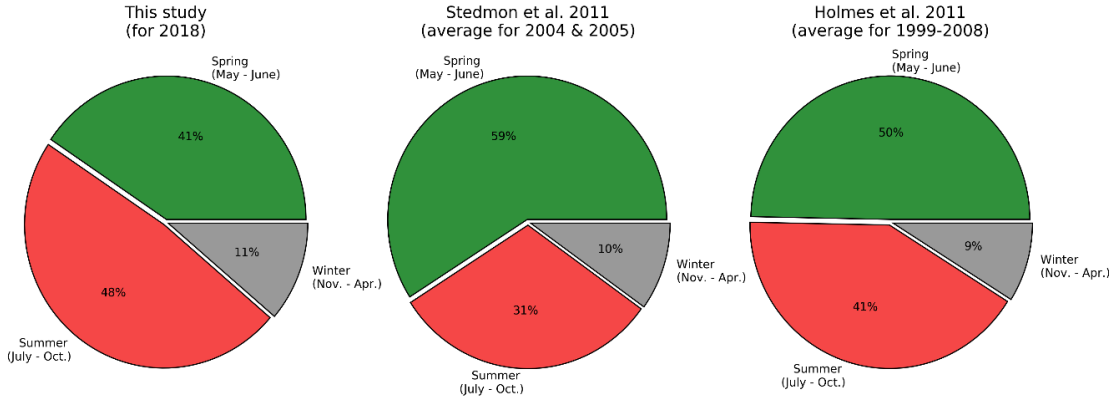

Appendix Figure 5: Percentage season fluxes (spring, summer and winter) of this study (for year 2018) compared to reported averaged values for 2004 to 2005 (Stedmon et al., 2011) and 1999 to 2008 (Holmes et al., 2012).

Appendix B

Appendix Table 2: Coefficients selected wavelengths for $a_{CDOM}(\lambda)$ using the equation $b * a_{CDOM}(\lambda)^c$.

λ of $a_{CDOM}(\lambda)$)	**b**	**c**
254	20.9462548427	0.8483590018983822
350	97.4272121688	0.7260394049434391
375	136.577758485	0.715114349676763
440	322.902097112	0.6667788739998305
443	333.695151626	0.6640204313768572

The regression between DOC and $a_{CDOM}(\lambda)$ was performed for a number of selected wavelengths (λ) to enable comparisons with other studies. **Appendix Table 2** shows regression coefficients dependent on wavelengths.

Performance of all tested OCRS algorithms are shown in **Appendix Figure 6**. Whereas ONNS and C2X provide reasonable results close to the 1 to 1 line compared to in situ data, other algorithms (C2R, C2RCC, FUB/WeW) underestimate $a_{CDOM}(\lambda)^{sat}$ strongly.

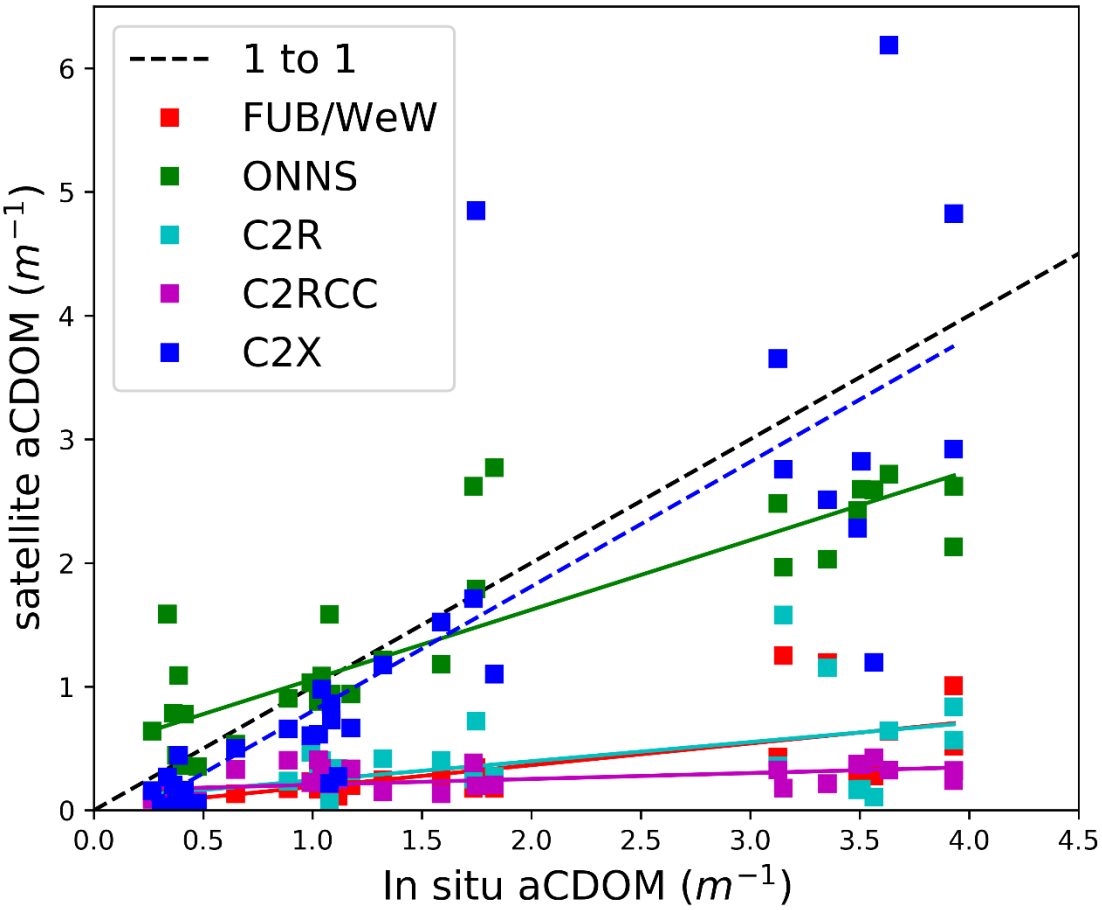

Appendix Figure 6: Comparison of in situ $a_{CDOM}(443)$ or $a_{CDOM}(440)$ with $a_{CDOM}(\lambda)^{sat}$ from different OCRS algorithms.

The percentage membership of each pixel is then used to calculate a weighted sum of different neural networks trained for different OWTs. **Appendix Figure 7** shows the OWTs of the processed scenes from **Figure 4.6** and **Figure 4.7**. It is visible that Lena River plume in the coastal waters was classified as OWT 1 (see 1 in **Appendix Figure 7**) which indicates optically complex, extreme absorbing and high scattering water. The plume between the Lena Delta and the New Siberian Island is characterized by OWT 5 (see 2 in **Appendix Figure 7**a & b), which indicated a mixture of high absorbing and scattering waters. The Lena River water plume with generally case 2, optically complex waters is sharply delineated to the west, where different water types occur (see 3 in **Appendix Figure 7**& b). Waters west of this plume were classified as OWT 11 displaying Case 1 waters (generally optically deep waters) waters with a small fraction of absorbing waters.

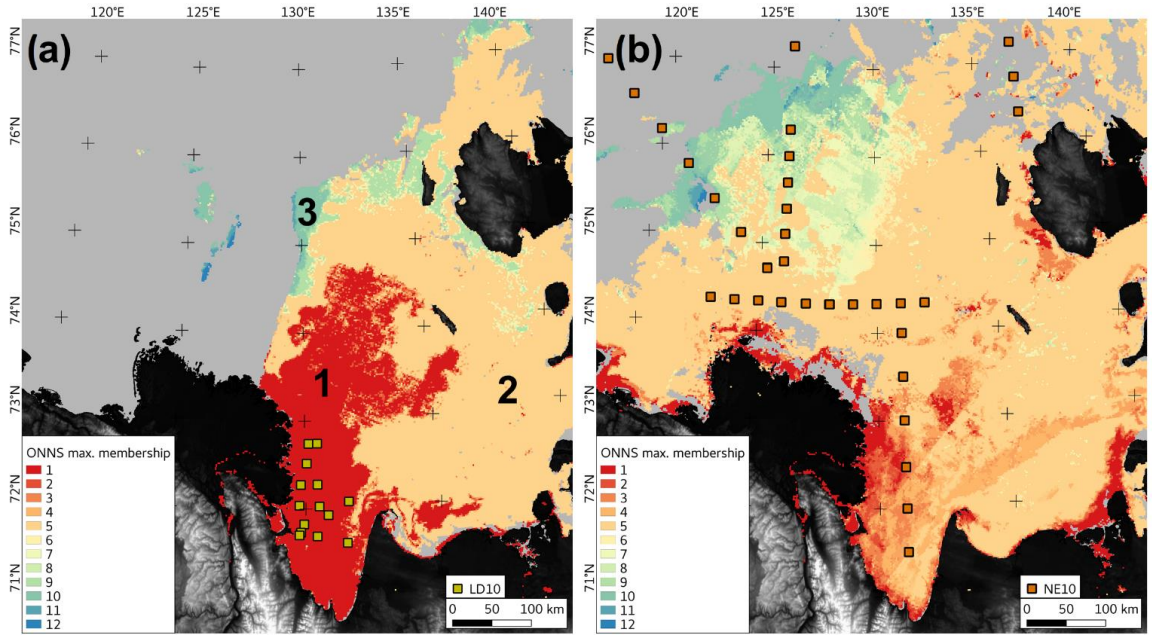

Appendix Figure 7: Optical water types from ONNS fuzzy logic classification for (a) average of August 3, 2010 to August 5, 2010 and (b) average of September 7, 2010 and September 18, 2010 to September 20, 2010.

Appendix C

Flags used for different atmospheric corrections

Appendix Table 3: List of flags that were used to mask invalid pixel for satellite data extraction.

AC	Flags
WFR	**Pixels excluded that were flagged with:**
	WQSF_lsb_LAND
	WQSF_lsb_CLOUD_AMBIGUOUS
	WQSF_lsb_CLOUD_MARGIN
	WQSF_lsb_AC_FAIL
	WQSF_lsb_HISOLZEN
	WQSF_lsb_LOWRW
	WQSF_msb_ANNOT_TAU06
C2RCC v.2	**Pixels excluded that were flagged with:**
	quality_flags_bright
	quality_flags_land
	quality_flags_invalid
Polymer	**Only pixels included that were flagged with:**
	1024 (Case 2)
	0 (no flag).

Number of observations for Transect time series (Figure 5.11)

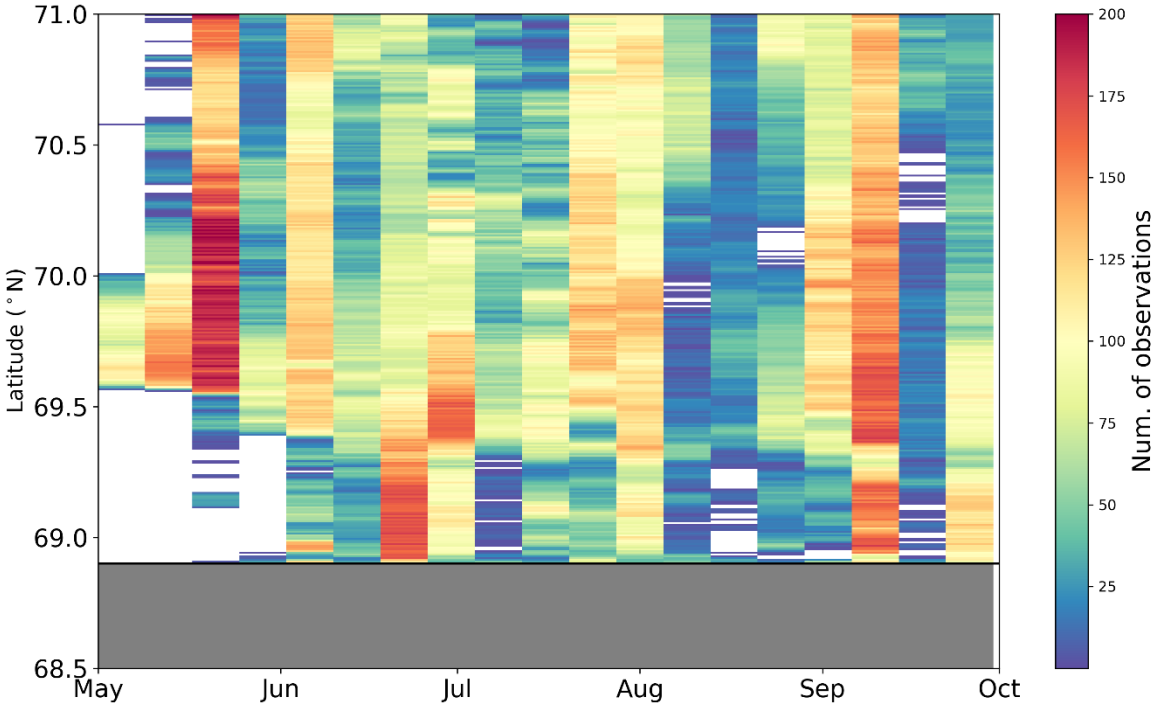

Appendix Figure 8: Number of observations (sum of nine pixel transect width) for each grid point of the extracted transect along 136.4 °W.